UNIVERSIDAD DE CONCEPCIÓN

FACULTAD DE INGENIERÍA AGRÍCOLA

ÍNDICES DE VEGETACIÓN PARA ANÁLISIS HIDROLÓGICOS Y ESTUDIO DE DINÁMICAS VEGETACIONALES

KAMILA IGNACIA TOBAR PONCE

HABILITACIÓN PROFESIONAL PRESENTADA A LA FACULTAD DE INGENIERÍA AGRÍCOLA DE LA UNIVERSIDAD DE CONCEPCIÓN, PARA OPTAR AL TÍTULO DE INGENIERO AMBIENTAL

CHILLÁN-CHILE

2024

ÍNDICES DE VEGETACIÓN PARA ANÁLISIS HIDROLÓGICOS Y ESTUDIO DE DINÁMICAS VEGETACIONALES

Aprobado por:

Sebastián Krogh Navarro
Ingeniero Civil, Ph. D. _____
Profesor Asociado Profesor Guía

Mario Lillo Saavedra
Ingeniero Eléctrico Ph. D. _____
Profesor Titular Profesor Asesor

Nicole Uslar Valle
Ingeniero Civil Agrícola, Ph. D. _____
Profesor Asociado Profesor Asesor

José Luis Arumí Ribera
Ingeniero Civil, Ph. D. _____
Profesor Titular Director de Departamento

María Eugenia González Rodríguez
Ingeniero Agrónomo, Ph. D. _____
Profesor Asociado Decana

ÍNDICE DE MATERIAS

ÍNDICE DE TABLAS

En el texto

En el Anexo

ÍNDICE DE FIGURAS

ÍNDICE DE ECUACIONES

ÍNDICES DE VEGETACIÓN PARA ANÁLISIS HIDROLÓGICOS Y ESTUDIO DE DINÁMICAS VEGETACIONALES

VEGETATION INDICES FOR HYDROLOGICAL ANALYSES AND VEGETATION DYNAMICS STUDIES

Palabras claves: Índices de vegetación, teledetección, ecohidrología, evapotranspiración.

RESUMEN

Una forma de evaluar la respuesta de los ecosistemas forestales ante cambios ambientales asociados al cambio climático es a través de la utilización de índices de vegetación. El objetivo de este estudio es analizar las características de los índices de vegetación utilizados en técnicas de percepción remota y su aplicabilidad en dinámicas hidrológicas, mediante una revisión bibliográfica. Se revisaron de artículos tipo *review*, para luego generar una base de datos de artículos que estudiaran los índices de vegetación con herramientas de teledetección, analizándolos con la inteligencia artificial Chat GPT-4o. Posteriormente, se realizó una nueva búsqueda de artículos que aplicaran los índices de vegetación en estudios de modelación hidrológica y se analizaron. Se obtuvo que los índices más utilizados en estudios científicos son el NDVI, LAI, SAVI y EVI, cada uno con ventajas y limitaciones específicas, y su elección depende de las características del área de estudio y si requiere

de correcciones atmosféricas o del suelo, entre otros. La escala de aplicación de estos índices de vegetación depende de la resolución espacial, temporal y espectral de sensores satelitales como Landsat, Sentinel y MODIS, o de UAVs que ofrecen mayor resolución espacial. Esto permite cuantificar las dinámicas vegetacionales y mejorar la estimación de evapotranspiración, reduciendo las incertidumbres asociadas a modelación hidrológica. A escala local, la utilización de dendrómetros, mediante la medición del crecimiento del tronco de árboles, complementa esta información y permite una estimación de la evapotranspiración más robusta. Sin embargo, la integración de teledetección y dendrómetros con parámetros hidrológicos de montaña como la acumulación y el derretimiento de nieve es un desafío poco explorado y que ofrece un potencial relevante para investigaciones futuras en Los Andes Chilenos.

VEGETATION INDICES FOR HYDROLOGICAL ANALYSES AND VEGETATION DYNAMICS STUDIES

Keywords: Vegetation index, remote sensing, ecohydrology, evapotranspiration.

ABSTRACT

Vegetation indices can be used to evaluate the response of forest ecosystems to environmental changes associated with climate change. The objective of this study is to analyze the characteristics of the vegetation indices used in remote sensing techniques and their applicability in hydrological dynamics, through a bibliographic review. First, review articles were reviewed, to generate a database of articles that studied vegetation indices with remote sensing tools, analyzing them with Chat GPT-4o artificial intelligence. Subsequently, a new search for articles that applied vegetation indices in hydrological modeling studies was carried out and analyzed. It was found that the most used indices in scientific studies are NDVI, LAI, SAVI and EVI, each with specific advantages and limitations. Their choice depends on the characteristics of the study area and whether it requires atmospheric or soil corrections, among other considerations. The scale of application of these vegetation indices depends on the spatial, temporal and spectral resolution of satellite sensors such as Landsat, Sentinel and MODIS, or UAVs that offer greater spatial resolution. This information allows us to better understand vegetation dynamics, improving

our estimates of evapotranspiration, and overall reducing the uncertainty in hydrological modeling. At a local scale, the use of dendrometers that measure the growth of tree trunks, complements this information and improving the estimation of evapotranspiration. However, the integration of remote sensing and dendrometers, and their relationship with key mountain hydrological processes such as snow accumulation and melt, is an underexplored challenge that offers relevant potential for future research in the Chilean Andes.

1. INTRODUCCIÓN

Los recursos hídricos son un elemento fundamental para el desarrollo humano, productivo y natural, por lo que es imprescindible su gestión sustentable (Henríquez, 2020). Sin embargo, al igual que otros recursos naturales, el agua se ha visto amenazada por el crecimiento demográfico, desarrollo económico y cambio climático (Koncagüil et al., 2020; Montenegro, 2022; ODEPA, 2016), causando en el curso de los últimos 100 años que se haya perdido entre un 50% y 70% de los humedales naturales en todo el mundo (Naciones Unidas, 2019), cuyo término incluye zonas pantanosas, ríos, lagos y por ende, las napas subterráneas y disponibilidad hídrica se ven afectadas con esta pérdida.

Esta escasez de agua prolongada ha generado sequías, las cuales son uno de los eventos climáticos extremos más complejos y peligrosos que se ha intensificado con el cambio climático (Lloyd-Hughes, 2014). Lo anterior ha afectado negativamente a los bosques, con impactos que varían significativamente entre distintos biomas y especies de árboles (Algarra, 2024; Gazol et al., 2018; Miranda et al., 2020; Walther et al., 2002), puesto que la disminución de las precipitaciones provocan una serie de consecuencias en cadena para la vegetación al afectar la disponibilidad hídrica asociada a la escorrentía, la humedad del suelo, caudal, entre otros (Ukkola et al., 2016; Zeng, 2018). Por lo tanto, el acceso al agua por parte de los árboles se ve limitado, afectando su desarrollo y productividad (Lozano-Parra, 2015; Rodriguez-Iturbe et al., 2007), ya que este recurso es el principal componente

de sus tejidos, transporta los nutrientes y provee la fuerza mecánica que promueve el crecimiento de las células y tejidos de sus hojas, tallos y raíces (Medina & Orlov, 2021; Sellés & Ferreyra, 2000).

Además, los ecosistemas forestales interaccionan con el recurso hídrico a través del ciclo hidrológico en dos procesos. El primero, es aquel en que el árbol mediante su sistema radical absorbe el agua y la evapora a través de las estomas de la hoja, denominado transpiración. El segundo, corresponde a la intercepción del agua lluvia o nieve por las superficies de las hojas, ramas y troncos y su posterior evaporación o sublimación. De este modo, el conjunto de la transpiración y evaporación, conforman el proceso conocido como evapotranspiración, el cual es fundamental para la regulación energética e hídrica de estos ecosistemas (Pizarro et al., 2019).

En términos generales, la vegetación responde a la falta de agua disminuyendo su evapotranspiración y la tasa de asimilación neta de carbono, a través del cierre de sus estomas y, de manera crucial, disminuyendo su crecimiento (Gazol et al., 2018; Miranda et al., 2020). Por lo tanto, la sequía prolongada puede provocar disfunciones en la fisiología de los árboles debido a la falta de agua, lo que causa alteraciones estructurales como la caída de hojas y brotes (Miranda et al., 2020; Rood et al., 2000), la muerte regresiva del dosel (conjunto de hojas y ramas), un aumento en la eficiencia del uso del agua (Grossiord et al., 2014; Miranda et al., 2020) e incluso, en casos extremos, los árboles pueden morir por falla hidráulica cuando su capacidad

de captación y transporte del agua ha sido gravemente dañado (Anderegg et al., 2013; Miranda et al., 2020).

Una forma de evaluar la respuesta de los ecosistemas forestales ante estos cambios ambientales asociados al cambio climático es a través de la utilización de índices de vegetación obtenidos mediante técnicas de percepción remota (Estay et al., 2023; Miranda et al., 2020), los cuales se basan en la relación existente entre una alta absorción de energía por la vegetación en el rango rojo del espectro y una alta reflectividad en el infrarrojo cercano, proporcionando un parámetro fisiológico asociado a la abundancia de la clorofila en las hojas de los árboles, capacidad de fotosíntesis y potencial de crecimiento de los individuos (Miranda et al., 2020; Running et al., 2004). Es decir, los índices de vegetación responden a cambios fisiológicos expresados en los ecosistemas forestales, por lo que se constituyen como herramientas esenciales para medir los efectos a medio plazo del cambio climático y evaluar el impacto de eventos climáticos específicos, como las sequías en la vegetación (Barbosa & Asner, 2017; Miranda et al., 2020).

Lo anterior, se ha evidenciado en la zona centro-sur de Chile, donde a causa de la sequía existente desde el año 2010 (Garreaud et al., 2017) y/o por eventos de calor extremo (Robledo, 2021), los bosques mediterráneos han sufrido la desecación de sus órganos foliares, provocando un pardeamiento foliar y una disminución en la reflectancia de la banda infrarroja cercana del espectro, asociado al Índice de Vegetación de Diferencia Normalizada (NDVI),

con una tendencia lineal decreciente (Robledo, 2021). Así mismo, en la temporada en que ocurren los eventos de calor extremo (estival) los árboles agudizan el proceso de evapotranspiración, y de no existir disponibilidad de humedad en el suelo, esto resulta en estrés hídrico del ecosistema y el pardeamiento foliar de los árboles (Robledo, 2021).

En específico, entre los años 2010 y 2017, los bosques de la precordillera andina de la zona central de Chile, tuvieron un efecto negativo en su productividad y cobertura de dosel, disminuyendo su NDVI y oscureciendo la vegetación de la zona. Sin embargo, ciertas comunidades forestales ubicadas en valles pronunciados y laderas empinadas tuvieron una consecuencia menor en la tasa de oscurecimiento, debido a que este tipo de topografía permite que exista un mayor Índice de Humedad Topográfica (TWI) y una menor cantidad de radiación solar que en las laderas orientadas al norte (Miranda et al., 2020). También, se han identificado patrones contraintuitivos en relación con el NDVI, como aquel en el que una reducción significativa en las precipitaciones se asocia con una menor tasa de disminución del NDVI. Este fenómeno respalda la teoría de que algunas áreas de ecosistemas forestales pueden estar alcanzando un punto crítico en su capacidad de resistir la escasez de precipitaciones. Lo que ha conllevado a los árboles a reacondicionar el uso de los recursos y funcionamiento de su estructura y composición, tal como, aumentar la caída de hojas para disminuir la pérdida de agua por la

evapotranspiración y disminuir su productividad para poder sobrevivir (Miranda et al., 2020).

El NDVI es solo uno de los muchos índices de vegetación utilizados en la teledetección, ya que las aplicaciones de esta técnica están determinadas por diversas misiones espaciales multiespectrales, que proporcionan datos cuantitativos y cualitativos que reducen la complejidad del trabajo de campo y el tiempo necesario para los estudios sobre la superficie terrestre (Andivia et al., 2024). Sin embargo, se ha demostrado que los datos obtenidos de las diferentes bandas espectrales tienen limitaciones para representar las propiedades y condiciones biofísicas de la vegetación. Para corregir estas limitaciones, se han desarrollado diversas combinaciones de bandas espectrales, dando lugar a una variedad de índices de vegetación (Andivia et al., 2024), pero ¿Cuáles y de qué constan los más utilizados?, ¿Cuáles son las principales ventajas y desventajas de cada uno de ellos? y, ¿Cuáles se utilizan para realizar análisis hidrológicos asociados a las dinámicas vegetacionales?, son preguntas que valen la pena realizarse. Para responderlas y comprender las diferencias entre los principales índices de vegetación, es de interés realizar un análisis bibliográfico que identifique y evalúe los índices de vegetación más utilizados, y que los asocie con las dinámicas hidrológicas.

2. OBJETIVOS

2.1. Objetivo general

Analizar las características de los índices de vegetación utilizados en técnicas de percepción remota y su aplicabilidad en análisis hidrológicos y dinámicas vegetacionales, mediante una revisión bibliográfica y análisis crítico.

2.2. Objetivos específicos

- Desarrollar base de datos que incluya los principales índices de vegetación utilizados en análisis de percepción remota.
- Evaluar las ventajas y desventajas de los índices de vegetación más utilizados.
- Realizar un catastro y análisis crítico de estudios que utilicen estos índices de vegetación para análisis hidrológicos.

3. MARCO TEÓRICO

3.1. Flujo de trabajo

Esta revisión bibliográfica sobre herramientas de teledetección respecto a índices de vegetación (IV) y su aplicación en dinámicas hidrológicas se desarrollará siguiendo los pasos resumidos en el diagrama de flujo mostrado en la Figura 1, cuyo desarrollo es especificado en los ítems posteriores.

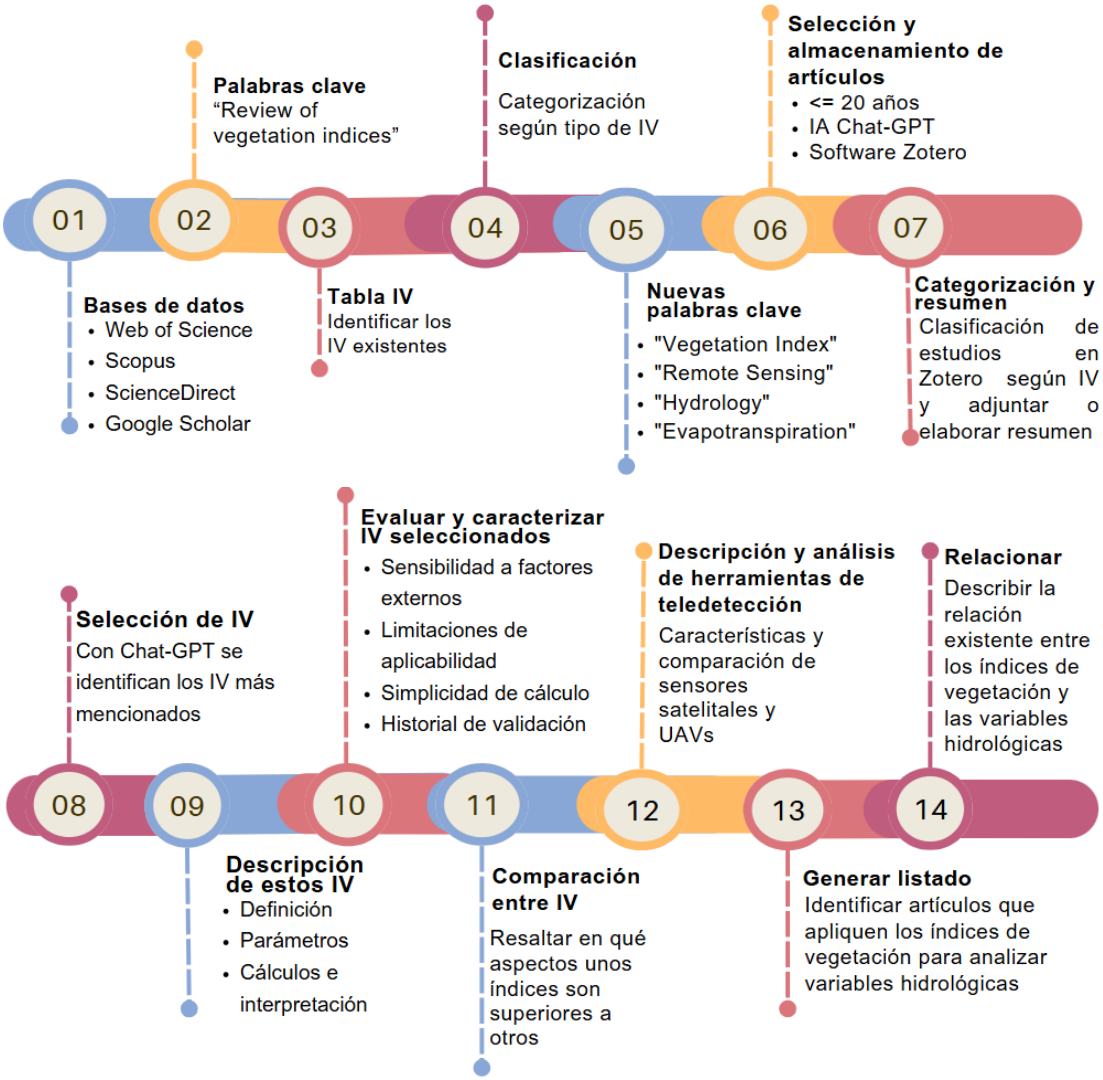

Figura 1. Diagrama de flujo de trabajo para el desarrollo de la revisión bibliográfica. Fuente: Elaboración propia.

3.2. Identificación de índices de vegetación

El primer paso de este estudio consiste en llevar a cabo una revisión de artículos científicos de tipo *review* sobre índices espectrales de vegetación disponibles en bases de datos académicas como Web of Science (WoS), Scopus, ScienceDirect y Google Scholar (Vidican et al., 2023). Esta revisión incluye estudios claves, como el trabajo de Bannari et al., (1995), así como otros estudios relevantes que proporcionen un panorama integral del estado del arte en esta materia, cuya información se recopila y resume en la Tabla A1 del ítem 7.1. del Anexo. Así, a partir de los *reviews* analizados, se definieron clasificaciones de los índices de vegetación según sus bandas y aplicaciones, como se muestra en la Figura 2 y en el ítem 3.3.

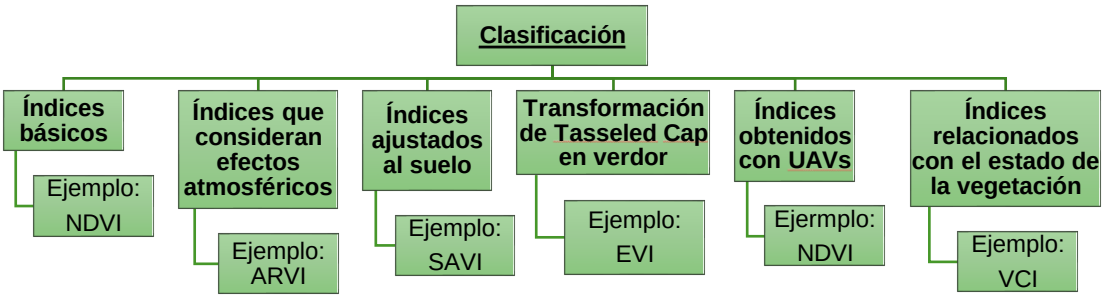

Figura 2. Clasificación de índices de vegetación.

3.3. Clasificación de índices de vegetación

3.3.1. Índices de vegetación básicos

Indicadores que se sustentan principalmente en la relación existente entre la reflectancia de la banda roja (R) e infrarroja (NIR). Estos constituyen algunos

de los primeros índices de vegetación desarrollados (Xue & Su, 2017) y entre ellos se encuentran:

a) RVI: Índice de Relación de la Vegetación, el cual se basa en el principio de que las hojas absorben más luz R que NIR, cuya fórmula de obtención es la Ecuación 1.

$$RVI = \frac{R}{NIR} \quad [1]$$

Así, el RVI se utiliza en la estimación y monitoreo de biomasa verde, especialmente en áreas de alta densidad de cobertura vegetal, debido a su alta sensibilidad a la vegetación y su buena correlación con la biomasa de las plantas. Sin embargo, en coberturas vegetales por debajo del 50%, el RVI presenta una elevada sensibilidad a efectos atmosféricos, lo que debilita su capacidad para representar de manera precisa la biomasa (Xue & Su, 2017).

b) DVI: Índice de Vegetación Diferencial que posee una alta sensibilidad a los cambios en el suelo y se utiliza para monitorear el entorno ecológico de la vegetación, el cual se calcula con la Ecuación 2 (Xue & Su, 2017).

$$DVI = \frac{NIR}{R} \quad [2]$$

c) PVI*:* Índice de Vegetación Perpendicular, el cual filtra los efectos del fondo del suelo eficientemente, siendo también menos sensible a los efectos atmosféricos y se utiliza principalmente para cuantificar el rendimiento de

pasto y/o contenido de clorofila, estimación del Índice de Área Foliar (LAI) y la identificación y clasificación de la vegetación. Sin embargo, PVI es sensible al brillo y reflectividad del suelo, sobre todo cuando existe una baja cobertura de vegetación (Xue & Su, 2017). Este índice se puede calcular con la Ecuación 3.

$$PVI = (DN_{NIR} - b)\, cos\, \theta - DN_R \cdot sin\, \theta \quad [3]$$

Donde: DN_{NIR} y DN_R corresponden a valores de luminancia, o bien conocidos como números digitales, de la radiación reflejada NIR y R, respectivamente; b es la intersección de la línea base del suelo y el eje vertical de la reflectividad NIR; y θ corresponde al ángulo entre el eje horizontal de la reflectividad R y la línea base del suelo (Xue & Su, 2017).

d) NDVI*:* Índice de Vegetación de Diferencia Normalizada se calcula mediante un procedimiento de normalización y es sensible a la vegetación verde incluso para zonas con poca densidad. Sin embargo, es demasiado sensible a los efectos del brillo y color del suelo, condiciones atmosféricas, nubes y sus sombras y sombras de hojas. Se estima a través de la Ecuación 4 (Xue & Su, 2017).

$$NDVI = \frac{NIR-R}{NIR+R} \quad [4]$$

3.3.2. Índices de vegetación que consideran efectos atmosféricos

Consideran las distorsiones causadas por la atmósfera al analizar imágenes de teledetección, ajustando o corrigiendo los efectos de la dispersión de luz y la absorción, para mejorar la precisión de las mediciones de la vegetación (Xue & Su, 2017), siendo algunos ejemplos:

a) ARVI: Índice de Vegetación Atmosféricamente Resistente que se basa en el principio en que la atmósfera afecta significativamente a R en comparación con el NIR, por lo que se incluyó la diferencia entre la banda azul (B) y R, asociada a la reflectividad relacionada con la dispersión molecular y absorción gaseosa para correcciones de aerosoles y ozono. Se calcula a través de la Ecuación 5 (Xue & Su, 2017).

$$ARVI = \frac{NIR-(B-R)}{NIR+(B-R)} \quad [5]$$

b) IAVI: Índice de Vegetación de Interferencia Atmosférica que proviene del ARVI, pero que logra disminuir el efecto de la atmósfera entre 0.4% y 3.7%, en comparación con el NDVI que en las mismas condiciones presenta un error entre 14% y 31%. Se obtiene mediante la Ecuación 6 (Xue & Su, 2017).

$$IAVI = \frac{NIR-(R-\gamma(B-R))}{NIR+(R-\gamma(B-R))} \quad [6]$$

Donde: γ es un factor de corrección diseñado para reducir el efecto de la dispersión atmosférica en la banda B y su influencia sobre la banda R.

3.3.3. Índices de vegetación ajustados al suelo

Este tipo de índices tiene el objetivo de corregir el efecto del brillo del suelo en áreas donde la vegetación es escasa o dispersa modificando los índices de vegetación convencionales (Xue & Su, 2017). Entre ellos se encuentran:

a) SAVI: Índice de Vegetación Ajustado al Suelo que tiene por objetivo mejorar la sensibilidad del NDVI a los fondos del suelo y se utiliza generalmente en áreas de alta densidad y cobertura de dosel, el cual se puede obtener con la Ecuación 7 (Xue & Su, 2017).

$$SAVI = \frac{(NIR-R)(1+L)}{(NIR+R+L)} \quad [7]$$

Donde: L es el índice de acondicionamiento del suelo, que mejora la sensibilidad del NDVI.

A partir de este índice se generaron nuevas versiones (SAVI2, SAVI3 y SAVI4) basados en las consideraciones teóricas de los efectos de los suelos húmedos y secos, los cuales reducen el efecto del brillo del suelo de fondo, al tener en cuenta el efecto de la variación del ángulo de incidencia solar y los cambios en la estructura física del suelo (Xue & Su, 2017).

b) MSAVI: Índice de Vegetación Ajustado al Suelo Modificado se utiliza para reducir la influencia del suelo desnudo sobre el SAVI, el cual se obtiene con la Ecuación 8 (Xue & Su, 2017).

$$MSAVI = 0.5 \cdot \{2R_{800} + 1 - \sqrt{(2R_{800} + 1)^2 - 8(R_{800} - R_{670})}\} \quad [8]$$

Donde: R_{800} es la reflectancia en la banda NIR, centrada alrededor de los 800 nm; R_{670} corresponde a la reflectancia en R, centrada alrededor de los 670 nm.

c) MSAVI2: Índice de Vegetación Ajustado al Suelo Secundario Modificado que proviene del SAVI pero posee un cálculo más simple y se utiliza en el análisis del crecimiento de las plantas, desertificación, rendimiento de pastizales, LAI, materia orgánica del suelo y erosión. Se calcula a través de la Ecuación 9 (Xue & Su, 2017).

$$MSAVI2 = 0.5 \cdot \{2NIR + 1 - \sqrt{(2NIR + 1)^2 - 8(NIR - R)}\} \quad [9]$$

d) OSAVI: Índice de Vegetación Ajustado al Suelo Optimizado proveniente de los demás índices mencionados y elimina la influencia del fondo del suelo de manera efectiva, pero se utiliza para la estimación de biomasa aérea, contenido de nitrógeno de las hojas y clorofila, entre otros. Se obtiene a través de la Ecuación 10 (Xue & Su, 2017).

$$OSAVI = \frac{NIR - R}{NIR + R + X} \quad [10]$$

Donde: X es un factor de corrección que se introduce para reducir la influencia del fondo del suelo en el cálculo del índice.

3.3.4. Transformación de *Tasseled Cap* en Verdor de Índices de Vegetación

La transformación *Tasseled Cap* (TCT) es una técnica utilizada en teledetección para reducir los datos multiespectrales en tres componentes claves: brillo, verdor y humedad, siendo su objetivo principal procesar y simplificar las imágenes satelitales, comúnmente derivadas de Landsat (Nijun et al., 2024). Algunos de los índices de vegetación que aplican esta técnica son:

a) SBI y GVI: Índice de Brillo del Suelo y Índice de Vegetación Verde, respectivamente, se utilizan para evaluar el comportamiento de la vegetación y el suelo desnudo, pero ignora la interacción y los efectos de la atmósfera, suelo y vegetación. Se calcula a través de la Ecuación 11 y 12 (Xue & Su, 2017).

$$SBI = +0.433MSS_4 - 0.632MSS_5 + 0.586MSS_6 + 0.264MSS_7 \quad [11]$$

$$GVI = -0.290MSS_4 - 0.562MSS_5 + 0.600MSS_6 + 0.491MSS_7 \quad [12]$$

Donde: MSS_4, MSS_5, MSS_6 y MSS_7 hacen referencia a las bandas espectrales captadas por el sensor Multispectral Scanner (MSS), que se utilizaba en los primeros satélites de observación de la Tierra, como Landsat 1 a Landsat 3.

b) YVI: Índice de Vegetación Amarilla que ignora la interacción y los efectos de la atmósfera, suelo y vegetación. Se obtiene con la Ecuación 13 (Xue & Su, 2017).

$$YVI = -0.829MSS_4 - 0.522MSS_5 + 0.039MSS_6 + 0.149MSS_7 \quad [13]$$

c) ASBI y AGVI: Índice de Brillo del Suelo Ajustado e Índice de Vegetación Verde Ajustado son índices provenientes de SBI y GVI, y se obtienen con las Ecuaciones 14 y 15 (Xue & Su, 2017).

$$ASBI = 2.0\,YVI \quad [14]$$

$$AGVI = GVI - (1 - 0.018\,GVI)YVI - \frac{NSI}{2} \quad [15]$$

Donde: NSI corresponde al Índice Normalizado del Suelo que se obtiene con la Ecuación 16, cuyo parámetro BIRS se asocia a la banda correspondiente al infrarrojo de onda corta y BIRC es la banda del infrarrojo cercano.

$$NSI = \frac{BIRS - BIRC}{BIRS + BIRC} \quad [16]$$

d) MSBI, MGVI y MYVI: Índice de Brillo del Suelo de Misra, Índice de Vegetación Verde de Misra e Índice de Vegetación Amarilla de Misra son creados a base de los índices anteriores, considerando un análisis de componentes principales de imágenes satelitales y factores múltiples. Se pueden obtener a través de las Ecuaciones 17, 18 y 19 (Xue & Su, 2017).

$$MSBI = +0.406MSS_4 - 0.60MSS_5 + 0.645MSS_6 + 0.243MSS_7 \quad [17]$$

$$MGVI = -0.3860MSS_4 - 0.53MSS_5 + 0.535MSS_6 + 0.532MSS_7 \quad [18]$$

$$MYVI = 0.723MSS_4 - 0.597MSS_5 + 0.206MSS_6 + 0.278MSS_7 \quad [19]$$

e) EVI: Índice de Vegetación Mejorado, introduce un mecanismo de retroalimentación mediante la construcción de parámetros para corregir simultáneamente los efectos atmosféricos (G) y del suelo (L) a partir del NDVI, incluyendo también coeficientes de corrección (C1 y C2). Se calcula a través de la Ecuación 20 (Xue & Su, 2017).

$$EVI = G\frac{NIR - RED}{NIR + C1\ RED - C2\ BLUE + L} \quad [20]$$

3.3.5. Índices de vegetación basados en teledetección con Sistema Aéreo No Tripulado (UAVs) en la región del espectro visible

Se enfocan en el uso de drones o UAVs para capturar datos de vegetación utilizando bandas de luz visible, principalmente en los espectros rojo, verde y azul, pudiendo proporcionar imágenes de alta resolución y detalle (Xue & Su, 2017). Algunos ejemplos son:

a) NDVI: Índice de Vegetación de Diferencia Normalizada obtenido a través de UAVs, el cual se calcula a través de la reflectancia a 800 nm y 680 nm, como se muestra en la Ecuación 21 (Xue & Su, 2017).

$$NDVI = \frac{R_{800} - R_{680}}{R_{800} + R_{680}} \quad [21]$$

b) VDVI: Índice de Vegetación de Diferencia de Banda Visible, que se basa en utilizar la banda verde (G) en lugar de la banda NIR, teniendo una precisión superior al 90%. Se obtiene a través de la Ecuación 22 (Xue & Su, 2017).

$$VDVI = \frac{2 \cdot G - R - B}{2 \cdot G + R + B} \quad [22]$$

3.3.6. Índices de vegetación relacionados con el estado de la vegetación

Constan de evaluar y monitorear la salud, vigor y condición general de la vegetación. Estos índices miden características clave como el verdor, la densidad y la actividad fotosintética de las plantas para determinar su estado (Xue & Su, 2017), algunos de ellos son:

a) WDRVI: Índice de Vegetación de Amplio Rango Dinámico, el cual mejora el rango del NDVI al aplicar un parámetro (α) de ponderación a la reflectancia NIR, cuyo valor es 1 cuando existe baja densidad de vegetación y 0.1 cuando existe alta densidad. Su fórmula se muestra en la Ecuación 23 (Xue & Su, 2017).

$$WDRVI = \frac{\alpha NIR - R}{\alpha NIR + R} \quad [23]$$

b) CARI: Índice de Proporción de Absorción de Clorofila mide el nivel de absorción a 670 nm y lo relaciona con el peak de reflexión a 700 nm y 550 nm, como se observa en la Ecuación 24 (Xue & Su, 2017).

$$CARI = \frac{|((R_{700}-R_{500})/150)\cdot 670+R_{670}+(R_{550}-(a\cdot 550))|}{(((R_{700}-R_{500})/150)^2+1)^{0.5}} * \frac{R_{700}}{R_{670}} \quad [24]$$

c) MCARI: Índice de Proporción de Absorción de Clorofila Modificado es más sensible a las concentraciones de clorofila en las hojas que CARI, y se obtiene con la Ecuación 25 (Xue & Su, 2017).

$$MCARI = \frac{1.5\,[2.5(R_{800}-R_{670})-1.3(R_{800}-R_{550})]}{\sqrt{(2R_{800}+1)^2-(6R_{800}-5R_{670})-0.5}} \quad [25]$$

d) CWSI: Índice de Estrés Hídrico de los Cultivos, obtiene un valor que está dado por la temperatura de las hojas del dosel completamente iluminadas por el sol (Tcanopy), por la temperatura de las hojas del dosel completamente iluminadas por el sol cuando el cultivo no está estresado por el agua (Tnws) y cuando está severamente estresado (Tdry). Se calcula a través de la Ecuación 26 (Xue & Su, 2017).

$$CWSI = \frac{Tcanopy-Tnws}{Tdry-Tnws} \quad [26]$$

e) PRI: Índice de Reflectancia Fotoquímica se basa en el estrés hídrico y se aplica a la detección de síntomas de enfermedades. Se obtiene a través de la Ecuación 27, que es una diferencia normalizada de reflectividad a 531 nm y 570 nm (Xue & Su, 2017).

$$PRI = \frac{R_{531} - R_{570}}{R_{531} + R_{570}} \quad [27]$$

f) VCI: El índice de Condición de la Vegetación permite identificar las variaciones temporales y espaciales de las condiciones de la vegetación asociadas al estrés por déficit de precipitaciones (Zambrano et al., 2016). Relaciona las condiciones de sequía de la vegetación a través del NDVI actual ($NDVI_j$), mínimo ($NDVI_{min}$) y máximo ($NDVI_{max}$) para un periodo de tiempo determinado. Se obtiene con la Ecuación 28 (Xue & Su, 2017).

$$VCI_j = \frac{(NDVI_j - NDVI_{min})}{(NDVI_{max} - NDVI_{min})} \quad [28]$$

3.4. Descripción de índices de vegetación más utilizados

Posteriormente, la búsqueda en bases de datos se afina, ampliando el espectro para incluir tanto artículos nacionales como internacionales, así como tesis de pregrado y posgrado. Esta segunda fase se centra en los *reviews* analizados y en estudios que contengan alguna de las siguientes palabras clave: "Vegetation Index", "Remote Sensing", "Hydrology" y "Evapotranspiration", priorizando publicaciones de los últimos 20 años, es decir, desde 2004 hasta 2024. La literatura obtenida se procesa a través de la herramienta de inteligencia artificial (IA) Chat-GPT 4o, que permite realizar un análisis preliminar del contenido de los artículos, facilitando la exclusión de estudios que no cumplan con los criterios establecidos, como la ausencia de

aplicaciones directas a dinámicas vegetacionales o la falta de pertinencia con las palabras clave seleccionadas. Tras aplicar los criterios de selección, se generó una base de datos que contenía 144 artículos asociados a distintos índices de vegetación, los cuales fueron almacenados y organizados en el software de gestión bibliográfica Zotero, lo que optimizó su búsqueda y consulta dentro de la base de datos generada.

A partir de lo anterior, preliminarmente se obtuvo la Figura 3 correspondiente a una nube de palabras clave utilizando la base de datos generada y su análisis con la IA Chat-GPT cuya identificación se realizó a través de títulos, palabras clave y resúmenes de cada artículo, cuyo detalle se presenta en el ítem 7.2. del Anexo.

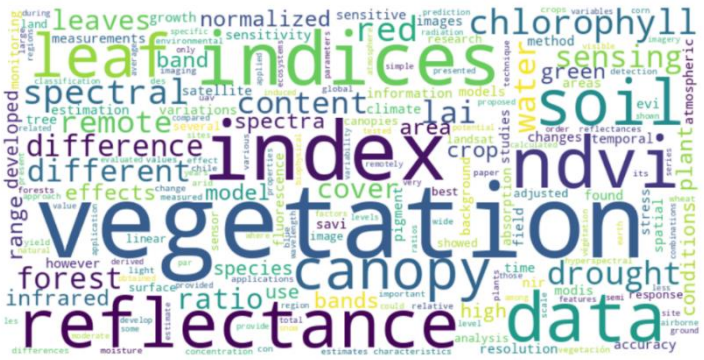

Figura 3. Nube de palabras clave realizada con Chat-GPT a partir de la base de datos generada.

En la Figura 3, se puede observar que las palabras de mayor frecuencia utilizadas en los artículos analizados son *vegetation, index* e *indices*, *reflectance, NDVI*, *soil,* l*eaf* y *data.*

Luego, con el objetivo de enfocar el análisis en los índices de vegetación más utilizados según la literatura revisada, se solicitó a Chat-GPT identificarlos a partir de los títulos y resúmenes de cada artículo, logrando distinguir los 10 más mencionados, los cuales son presentados en la Figura 4.

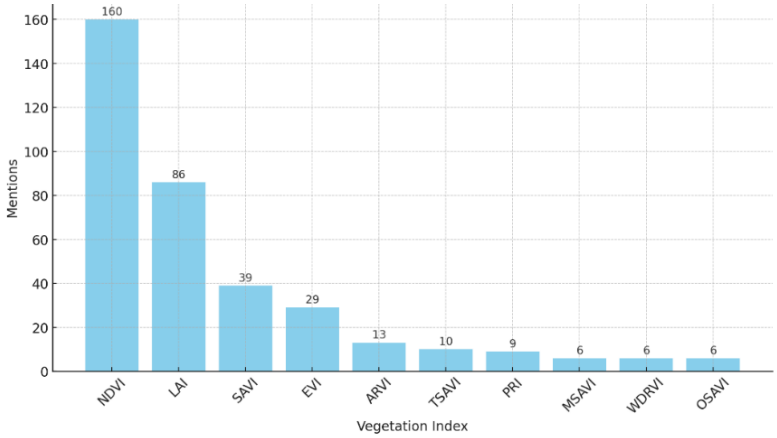

Figura 4. Índices de vegetación más mencionados en la base de datos generada identificados con Chat-GPT.

En la Figura 4 se muestran los 10 índices de vegetación más mencionados y recurrentes en la base de datos generada, que corresponden al NDVI, LAI o bien conocido también por sus siglas IAF, SAVI, EVI, TSAVI, PRI, MSAVI, WDRVI y OSAVI. De los índices anteriores se seleccionaron los primeros 4 más mencionados, los cuales se describen a continuación.

a) NDVI

El Índice de Vegetación de Diferencia Normalizada (NDVI) fue uno de los primeros productos analíticos derivados de la teledetección que simplifica la interpretación de imágenes espectrales complejas respecto a la vegetación

(Huang et al., 2021) y es el índice de vegetación más utilizado para representar las propiedades biofísicas del dosel vegetal (Jiang et al., 2006; Jin & Baofeng, 2017). Los parámetros para su cálculo se basan en la radiación infrarroja cercana menos la radiación roja dividida por la radiación infrarroja cercana más la radiación roja, como se observa en la Ecuación 4 (Huang et al., 2021).

Los valores de NDVI varían entre -1 y +1, los cuales generalmente son negativos para cuerpos de agua, cercano a cero para rocas, arenas u hormigón, y positivos para la vegetación, que incluyen bosques, pastos, arbustos y cultivos (Huang et al., 2021; Jones & Vaughan, 2010). Lo anterior, se debe a que las clorofilas a y b de las hojas verdes absorben fuertemente la radiación R, con una absorción máxima cercana a los 690 nm, mientras que las paredes celulares dispersan fuertemente la luz en NIR de aproximadamente 850 nm. Así, la vegetación densa tiene un NDVI alto, el suelo posee un NDVI bajo pero positivo y el agua tiene un valor negativo debido a su alta absorción de NIR (Glenn et al., 2008). Un ejemplo de una imagen satelital para NDVI es la Figura 5.

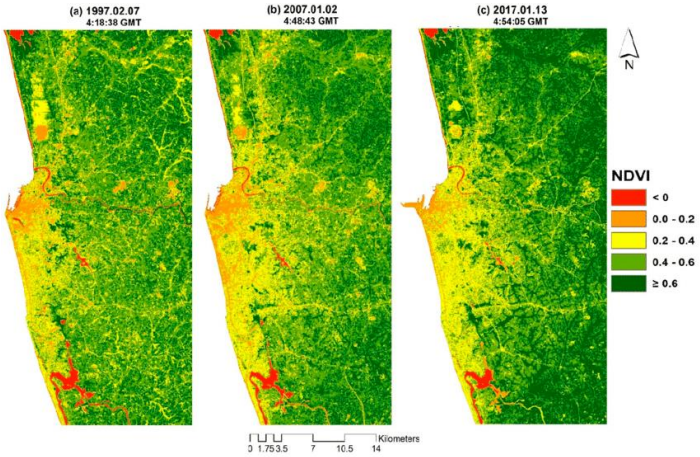

Figura 5. Mapas del NDVI del Área Metropolitana de Colombo, Sri Lanka. (a) 1997; (b) 2007; y (c) 2017. Fuente: Ranagalage et al., 2017.

b) LAI

El índice de área foliar (LAI) es una variable clave utilizada por los fisiólogos y modeladores de cultivos para comprender y pronosticar los procesos biofísicos de crecimiento y rendimiento de los doseles forestales y de los cultivos, así como para estimar la cobertura del follaje (Haboudane et al., 2004). El método indirecto más utilizado para la estimación del LAI se basa en imágenes de satélite y consiste en asociarlo con características espectrales e índices de vegetación (Nafarrate-Hecht et al., 2018). El LAI se obtiene a través de la Ecuación 29.

$$LAI = \frac{Área\ total\ de\ hojas\ en\ el\ dosel}{Área\ de\ suelo} \quad [29]$$

Generalmente, LAI presenta valores iguales o superiores a 0. Los valores más bajos corresponden a zonas con baja densidad de dosel, lo cual indica una menor capacidad de fotosíntesis. Mientras que, los valores más altos están

relacionados con una alta densidad de dosel, lo que implica una mayor biomasa y, en consecuencia, una mayor capacidad fotosintética en el área analizada (Haboudane et al., 2004). Un ejemplo de la visualización de LAI con imágenes satelitales es la Figura 6.

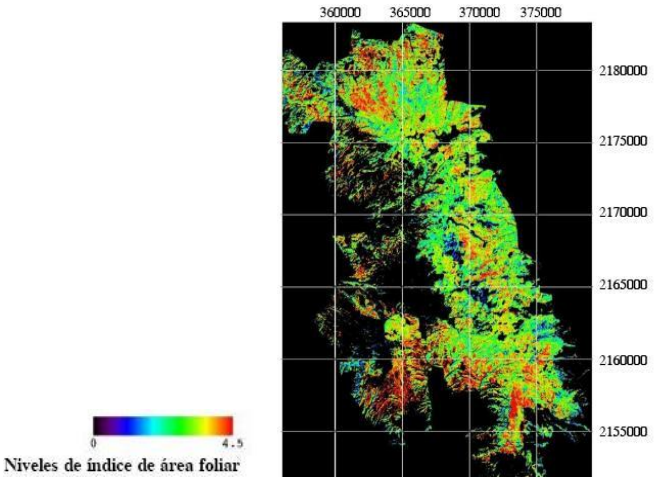

Figura 6. Parte del mapa de LAI de la reserva de la Mariposa Monarca en México en el año 2001. Fuente: Velasco López et al., 2010.

c) SAVI

El Índice de Vegetación Ajustado al Suelo (SAVI) pretende describir adecuadamente la relación entre el suelo y la vegetación a través de la mitigación del impacto del brillo en el suelo asociado al color, humedad y variabilidad del suelo (Huete, 1988; Jiang et al., 2008). Lo anterior, se logra al añadir un factor a la Ecuación 4, como se muestra en la Ecuación 7.

Donde: L corresponde a un factor de ajuste del suelo (Jiang et al., 2008), cuyos valores son ajustables al tipo de vegetación, es decir, cuando existe una mayor densidad L es igual a 0,25, una densidad intermedia L es igual a 0,5 y para

una baja densidad se debe utilizar un valor de 1 (Huete, 1988; Sudhanshu et al., 2010) e incluso, cuando el L es igual a 0, el SAVI es igual al NDVI (Jin & Baofeng, 2017; Paredes, 2018). Los resultados del SAVI se presentan en el mismo rango que el NDVI, entre -1 y +1, con su mismo significado (Paredes, 2018). Un ejemplo del SAVI observado en imágenes satelitales es la Figura 7.

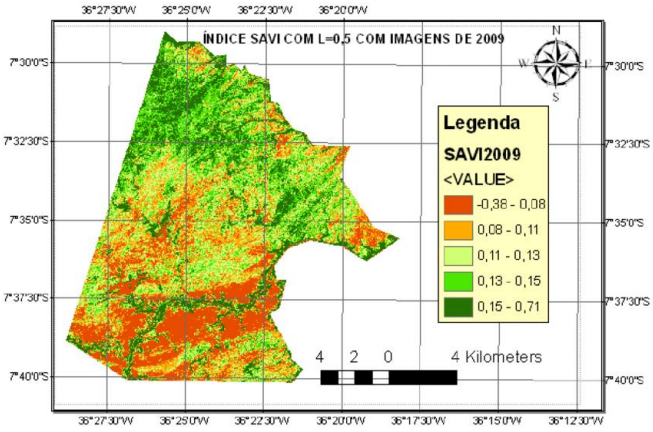

Figura 7. Mapa de SAVI del municipio de São Domingos do Cariri-PB, Brasil, con factor de ajuste del suelo igual a 0,5. Fuente: Ribeiro et al., 2016.

d) EVI

El Índice de Vegetación Mejorado (EVI) se desarrolló para incorporar la retroalimentación que no estaba presente en el NDVI, lo cual permite corregir el ajuste del fondo y mitigar las influencias atmosféricas (Matsushita et al., 2007; Paredes, 2018) asociadas a la absorción de Rayleigh y ozono (Jiang et al., 2008). Lo anterior, se logra a través de la incorporación de constantes, factores y la banda B a la Ecuación 4, como se muestra en la Ecuación 20.

Donde: NIR, R y B son la reflectancia en las longitudes de onda infrarroja cercana (0,7-1,1 µm), roja (0,6-0,7 µm) y azul (0,45-0,52 µm), respectivamente (Huete et al., 1994, 1997; Paredes, 2018), cuya diferencia entre las reflectancias azul y roja puede estimar la influencia atmosférica (Didan & Munoz, s. f.). C1 y C2 son coeficientes de corrección para la dispersión de aerosoles en R a través de B, cuyos valores utilizados son 6 y 7,5, respectivamente. L es el factor de ajuste del suelo y dosel, cuyo valor se considera igual a 1. G es un factor de cambio cuyo valor es igual a 2,5 (Huete et al., 1994, 1997; Paredes, 2018). El EVI al ser una versión modificada del NDVI, también posee resultados en el rango de -1 y +1, y es un índice global para el monitoreo de la actividad fotosintética terrestre (Paredes, 2018). Un ejemplo de la visualización el EVI con imágenes satelitales es la Figura 8.

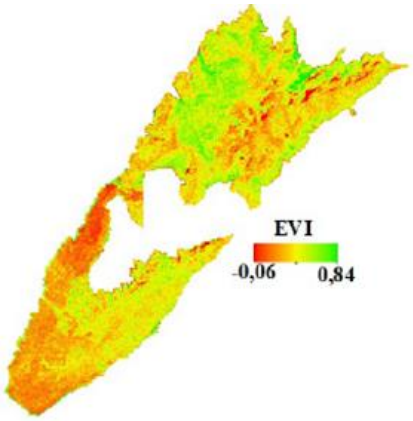

Figura 8. EVI determinado para la época seca (febrero) en bosques del Santuario de Fauna y Flora Iguaque en Boyacá, Colombia. Fuente: Perea-Ardila et al., 2021.

3.5. Análisis de índices de vegetación seleccionados

El NDVI es ampliamente utilizado en estudios sobre la evaluación de la vegetación a escala regional y global (Jin & Baofeng, 2017), debido a su vinculación con diversas propiedades biofísicas del dosel, tales como con el LAI, la fracción de radiación fotosintéticamente activa absorbida, la producción primaria neta, la biomasa, la concentración de clorofila, la cobertura vegetal y el estrés hídrico en las plantas (Asrar et al., 1984; Chávez et al., 2016; Dutrieux et al., 2015; Gitelson, 2004; Holben, 1986; Pastor et al., 2015; Sellers, 1985; Tian et al., 2017; Tucker et al., 1986; Vicente-Serrano et al., 2016; Zhu & Liu, 2015). Por lo anterior, el NDVI resulta útil para identificar distintos tipos de vegetación, como sabanas, bosques densos, campos agrícolas y no forestales, diferenciar entre bosques perennes y estacionales, analizar series temporales, monitorear la vegetación, detectar cambios en el uso del suelo, evaluar el estado de los cultivos y estudiar fenómenos como la sequía (Huang et al., 2021; Pettorelli et al., 2005).

Sin embargo, la estructura sin retroalimentación de la ecuación del NDVI la hace susceptible a errores e incertidumbre sobre las condiciones variables (Matsushita et al., 2007) asociadas a efectos del brillo y color del suelo, la atmósfera, nubes y su sombra, como también la sombra del dosel de las hojas, por lo que requiere de calibración para mejorarlo (Jin & Baofeng, 2017). Lo anterior, puede verse reflejado en que el NDVI sobreestima el porcentaje de cubierta vegetal al inicio de la temporada de crecimiento y tiende a

subestimarla a finales de esta. Por lo tanto, se recomienda utilizar el NDVI a mediados de temporada, donde los cultivos o bosques están en crecimiento activo (Bannari et al., 1995; Paredes, 2018).

Por otro lado, si bien el LAI permite evaluar la densidad del dosel de vegetación y su capacidad de absorción de luz y fotosíntesis, entre otras funciones, su predicción a partir de datos de teledetección enfrenta dos desafíos principales: (1) los índices de vegetación tienden a alcanzar un nivel de saturación de forma asintótica cuando el LAI supera valores entre 2 y 5, dependiendo del índice específico utilizado; (2) no existe una relación única entre el LAI y un índice de vegetación en particular, sino más bien diversas relaciones que dependen del contenido de clorofila y/o de otras características del dosel (Haboudane et al., 2004).

El SAVI, por su parte, si bien utiliza las mismas bandas espectrales que el NDVI, sus ecuaciones son bastantes similares y sus resultados se presentan en el mismo rango entre -1 y +1, ambos índices de vegetación no son equivalentes. Esto se debe a que responden de manera distinta a las condiciones de vegetación en diferentes lugares, se ven afectados de manera distinta ante las condiciones de topografía, y el ruido o interferencia del LAI en ambos índices de vegetación varían según las estaciones del año. De ese modo, es recomendable utilizar el SAVI para el análisis de regiones con vegetación escasa y se debe ajustar debidamente el coeficiente L (Ecuación

7) para obtener valores representativos de la superficie vegetal (Rodríguez-Moreno & Bullock, 2013).

El EVI se desarrolló para incorporar la retroalimentación que no estaba presente en el NDVI, a través de los factores L y G (Ecuación 20), teniendo mayor sensibilidad en las regiones de alta biomasa y mejor capacidad para monitorear la vegetación en estas zonas (Matsushita et al., 2007). Puesto que este índice de vegetación es más funcional en la reflectancia NIR que en la absorción R (Ecuación 20) y, por lo tanto, no se satura tan rápidamente como el NDVI en vegetación densa (Glenn et al., 2008). Así, el EVI se ha aplicado en estudios fenológicos demostrando que está altamente correlacionado con la fotosíntesis, productividad y la evapotranspiración (Glenn et al., 2008), con lo que es posible generar series temporales y detectar las etapas de desarrollo de la vegetación, como el momento de inicio de crecimiento, la longitud de la producción de hojas, el período constante y el inicio de la senescencia de las hojas (Houborg et al., 2007).

Sin embargo, el EVI tiene como deficiencia que no toma en cuenta el efecto topográfico, el cual está asociado a la variación en la radiancia debida a cambios en la orientación de una superficie, de horizontal a inclinada, en respuesta a la fuente de luz y la posición del sensor satelital. Además, los efectos topográficos en las partes visible e infrarroja cercana del espectro solar son comparables, lo que permite que puedan ser eliminados o reducidos cuando los índices de vegetación se expresan como proporciones de bandas,

como lo es el caso del EVI con el factor de ajuste del suelo y dosel (coeficiente L en la Ecuación 20) en su denominador (Matsushita et al., 2007). Por lo tanto, es recomendable utilizarlo en zonas con alta densidad de vegetación, es decir, con abundante clorofila, pero con una topografía mínima (Glenn et al., 2008; Matsushita et al., 2007).

Así, la Tabla 1, resume el análisis de los índices de vegetación seleccionados.

Tabla 1. Ventajas y desventajas de los índices de vegetación seleccionados.

Índices de vegetación	**Ventajas**	**Desventajas**
NDVI	Ampliamente utilizado para evaluar y monitorear vegetación, detectar cambios en el uso del suelo y estudiar fenómenos como la sequía a escala regional y global.	Susceptible a errores e incertidumbres por condiciones variables, como brillo del suelo, atmósfera y sombras. Sobrestima la vegetación al inicio de la temporada y la subestima al final.
LAI	Evalúa densidad del dosel y capacidad de fotosíntesis, asociado con la absorción de radiación solar y otras funciones del dosel.	No hay una relación única con los índices de vegetación, depende del contenido de clorofila y otras características.
SAVI	Recomendado para áreas con vegetación escasa, ya que ajusta los efectos del brillo y color del suelo.	Afectado por la topografía y el ruido del LAI, según la estación del año. Requiere ajuste del coeficiente L para obtener resultados precisos.
EVI	Mayor sensibilidad en regiones de alta biomasa. No se satura rápidamente en vegetación densa. Altamente correlacionado con la fotosíntesis y productividad. Útil para series temporales y monitoreo fenológico.	No toma en cuenta el efecto topográfico, lo que puede afectar su precisión en terrenos inclinados. Recomendable solo en áreas con alta densidad de vegetación y mínima topografía.

Fuente: Elaboración propia.

3.6. Descripción de sensores remotos

Los sensores remotos ofrecen la capacidad de observar un objeto sin estar en contacto con el mismo y durante las últimas décadas las investigaciones en sensores remotos y su aplicación se han incrementado gracias a la disponibilidad de imágenes satelitales de alta resolución y al uso de vehículos aéreos no tripulados (UAVs por sus siglas en inglés) que generan información base para distintos análisis (Guzman-Alvarez et al., 2022).

3.6.1. Sensores satelitales

Los sensores satelitales capturan datos multiespectrales que permiten generar índices de vegetación y así, cuantificar y monitorear el estado de la vegetación (Almalki et al., 2022), siendo los principales sensores satelitales utilizados años atrás y en la actualidad los presentados en la Tabla 2, cuyas respectivas longitudes de banda se encuentran especificadas en la Tabla A2, ítem 7.3. del Anexo.

Tabla 2. Sensores satelitales multiespectrales comúnmente utilizados.

Sensores satelitales	Bandas	Resolución		Periodo	Acceso a datos
		Temporal (días)	Espacial (m)		
Landsat MSS	4	180	80	1972-1992	https://earthexplorer.usgs.gov/
TM Landsat	7	16	30, 120	1982-presente	https://earthexplorer.usgs.gov/
ETM+ Landsat	8	16	30, 15, 60	2003-presente	https://earthexplorer.usgs.gov/

Continuación tabla anterior.

Landsat OLI	11	16	30, 15	2013-presente	https://earthexplorer.usgs.gov/
Sentinel-1	Banda C	12	5	2014-presente: 1A 2016-presente: 1B	https://scihub.copernicus.eu/
Sentinel-2	13	5	60, 10, 20	2015-presente: 2A 2017-presente: 2B	https://scihub.copernicus.eu/
MODIS	36	1-2	250, 500, 1000	2000-presente: Terra 2002-presente: Aqua	https://earthexplorer.usgs.gov/ https://search.earthdata.nasa.gov/
AVHRR	5	1	1100-5000	1980-presente	https://earthexplorer.usgs.gov/
IKONOS	5	1-2	4	1999-2015	https://earth.esa.int/
MERIS	15	3	300	2002-2012	https://earth.esa.int/
QuickBird	5	1-3,5	2.4	2001-presente	https://earth.esa.int/
Rapid Eye	5	5.5	5	2008-2020	https://earth.esa.int/
SPOT	4	26	10, 20	1986-2913	https://earth.esa.int/
Worldwiew-2	8	1	<1	2014-presente	https://earth.esa.int/

Fuente: Almalki et al., 2022.

A partir de la Tabla 2, se pueden observar los sensores satelitales más utilizados durante el transcurso de los años, siendo a su vez, clasificados como de baja/media resolución espacial aquellos que poseen pixeles mayores a 10 m, mientras que una resolución alta son aquellos igual o menores a 10 m (Almalki et al., 2022). Otro factor por analizar es la resolución temporal, siendo en este caso, MODIS, VHRR, QuickBird y Worldview-2, los que tienen una resolución temporal alta (menor a 7 días), mientras que se considera una resolución temporal media aquella mayor a la semanal, como los sensores Landsat, que muestran cambios bimensuales (Almalki et al., 2022). Además, la resolución espectral, es otro factor de análisis, que corresponde al número de bandas de longitud de onda, ya que cada banda espectral detecta de forma única una característica particular en la superficie de la Tierra al enfocar su espectro electromagnético en un rango específico, tales como pancromátricas, de color visible como azul, verde y rojo, e infrarrojas. Si tiene 5 o menos bandas es de resolución espectral baja, pero si tiene mayor a 5 tiene resolución media/alta. En el caso del sensor Landsat-8, este contiene 11 bandas para cada imagen (resolución media/alta), mientras que el QuickBird contiene sólo 5, es decir, resolución baja (Almalki et al., 2022).

Los sensores satelitales multiespectrales, como los de las series Landsat y AVHRR, destacan por su amplia cobertura temporal, lo que los convierte en fuentes clave para analizar los cambios en la cobertura vegetal ocurridos durante los últimos 40 años. Landsat, en particular, ofrece una resolución

espacial media y ha estado operando de manera continua desde 1972, lo que proporciona un extenso archivo de imágenes históricas. Mientras que algunos sensores más recientes, como Worldview-2, lanzado en 2014, presentan un período de cobertura considerablemente más corto, lo que limita su capacidad para detectar cambios en la cobertura vegetal a lo largo del tiempo. En la mayoría de los casos, los satélites de alta resolución, como Sentinel-1, QuickBird, y Rapid Eye, fueron lanzados en los últimos 20 años, lo que también reduce su aplicabilidad para estudios de largo plazo sobre cambios en la vegetación (Almalki et al., 2022).

También, vale mencionar, que si bien algunos de los sensores en satélites lanzados más recientemente tienen una alta resolución espacial y temporal, son herramientas de pago, por lo tanto, el acceso a la información de índices de vegetación es limitada, tales como IKONOS, MERIS (*Medium Resolution Imaging Spectrometer*), Quickbrid, Rapid Eye, SPOT y World View 2 (WV2). Sin embargo, todas las generaciones de Landsat mencionadas, Sentinel-1 y 2, MODIS y AVHRR (*Advanced Very High Resolution Radiometer*) son gratuitos y permiten la utilización de los datos de forma más transversal para estudios científicos (Almalki et al., 2022).

Un sensor satelital que proporciona una combinación de buenas resoluciones espaciales, temporales y es gratuito es el ECOSTRESS (Experimento de Radiómetro Térmico a Bordo del Espacio ECOsystem), el cual se lanzó en el 2018 y sigue vigente hasta el presente, midiendo en 5 longitudes de banda la

radiación infrarroja y una banda extra (sexta) para geolocalización y detección de nubes, teniendo una frecuencia de retorno entre 1 y 5 días, y resolución espacial de 70 m aproximadamente (Fisher et al., 2020). Aunque ECOSTRESS tiene potencial para recolectar imágenes en todas las regiones entre 52°N y -52°S, la revisita efectiva depende de una combinación de prioridades científicas, trayectorias orbitales y limitaciones atmosféricas, lo que hace que ciertas regiones reciban mayor atención que otras (Fisher et al., 2020).

3.6.2. Sensores montados en UAVs

La teledetección también es realizada utilizando variados UAVs, los cuales tienen tipos de clasificaciones, siendo una de ellas por tamaño y diseño, detallada en la Figura 9 (Sabour et al., 2023).

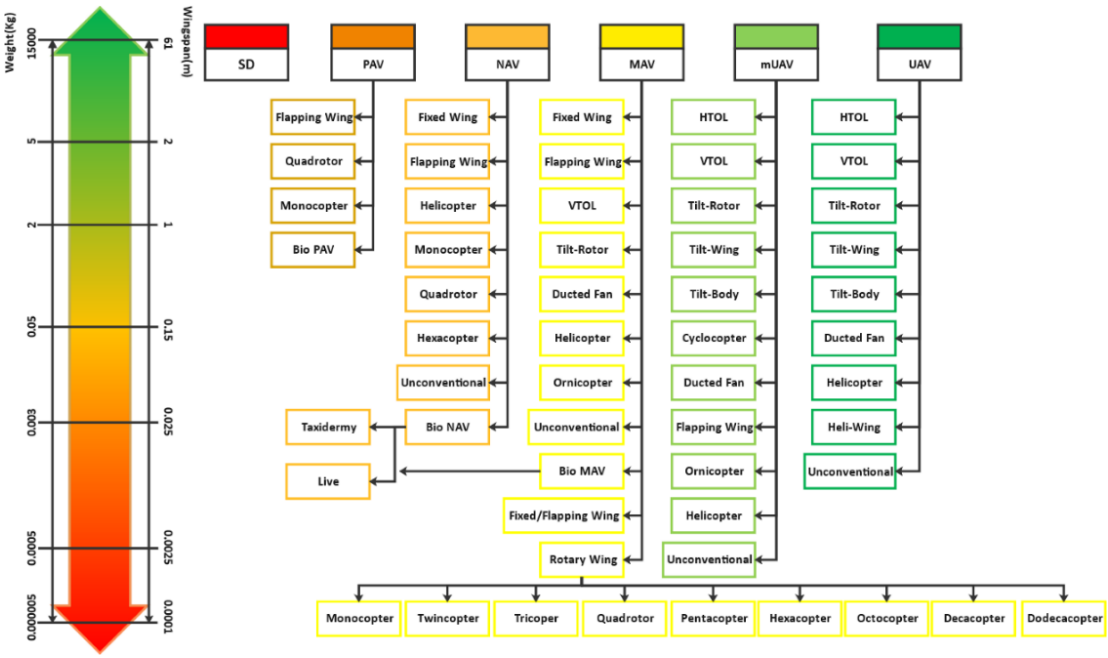

Figura 9. Clasificación de UAVs considerando espectro de peso y diseño. Fuente: Sabour et al., 2023.

Un ejemplo de los UAVs multirrotores o que cuentan con múltiples hélices son los helicópteros (que poseen 2 hélices) y cuadricópteros (con 4 hélices), entre otros, y son especialmente utilizados en aplicaciones de fotografía, grabación y monitoreo, debido a su estabilidad y facilidad de maniobra en espacios reducidos (Figura 10.a y 10.b). Otro ejemplo son los UAVs de ala fija, que tienen un diseño similar al de un avión y son ideales para vuelos de largo alcance, mapeos, monitoreo de grandes áreas y observación a gran escala (Figura 10.c). O bien, los UAVs híbridos, que combinan las ventajas de los vehículos de ala fija y los multirrotores, realizando vuelos de largo alcance, así como despegues y aterrizajes verticales, entre otros modelos (Sabour et al., 2023).

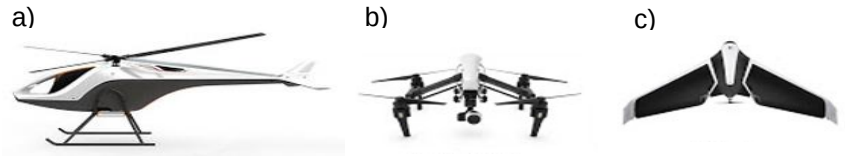

Figura 10. a) UAV helicóptero. b) UAV cuadricóptero. c) UAV ala fija. Fuente: Academia de Drones Chile, 2017.

Así, los UAVs han impulsado nuevas fuentes de datos para mejorar la caracterización de las métricas de la vegetación, ya que ofrecen imágenes de muy alta resolución espacial que generalmente son del orden de centímetros por píxel, y permiten superar algunas de las limitaciones comunes en la teledetección satelital tradicional, como la baja resolución y la interferencia de nubes (Tian et al., 2017). Así, se pueden obtener distintos índices de vegetación, tales como el NDVI, a partir de imágenes multiespectrales

capturadas por UAVs en diferentes longitudes de onda, generalmente en el espectro visible y el infrarrojo cercano, las cuales demostraron ser superiores a las imágenes satelitales en la capacidad de distinguir entre vegetación y fondo, lo que mejora significativamente la precisión de las mediciones, como por ejemplo del LAI, especialmente en ambientes complejos con varios tipos de vegetación y suelos heterogéneos. Además, los UAVs brindan flexibilidad para ajustar parámetros clave, como la altura de vuelo, los ángulos de visión y la superposición de imágenes, permitiendo una adaptabilidad y precisión mayores en las aplicaciones de teledetección (Tian et al., 2017). Entre los tipos de sensores que pueden montarse en UAVs se incluyen cámaras de color verdadero (RGB), multiespectrales, hiperespectrales, LiDAR (*Light Detection and Ranging*), de microondas y térmicas, todos capaces de captar datos a resoluciones espaciales muy altas y en períodos de adquisición adaptables. Lo anterior, contrasta con los satélites tradicionales que, aunque pueden capturar grandes áreas, enfrentan problemas de revisita limitada y menor resolución espacial para estudios locales y de precisión, afectando el mapeo con índices de vegetación y los resultados de estudios detallados de vegetación (Tian et al., 2017).

Un ejemplo de imágenes obtenidas con UAVs son aquellas capturadas en los tres canales básicos de color: rojo (R), verde (G) y azul (B), o bien llamadas RGB, las cuales presentan en este caso una resolución espacial de 1 cm en la Figura 11. En cambio, la Figura 12 muestra la diferencia de resolución en el

análisis de NDVI entre imágenes satelitales, como las capturadas por el satélite WorldView-2, y las obtenidas por UAVs con cámaras RGB.

Figura 11. Parte de imagen RGB de UAV con resolución espacial de 1 cm. Fuente: Tian et al., 2017.

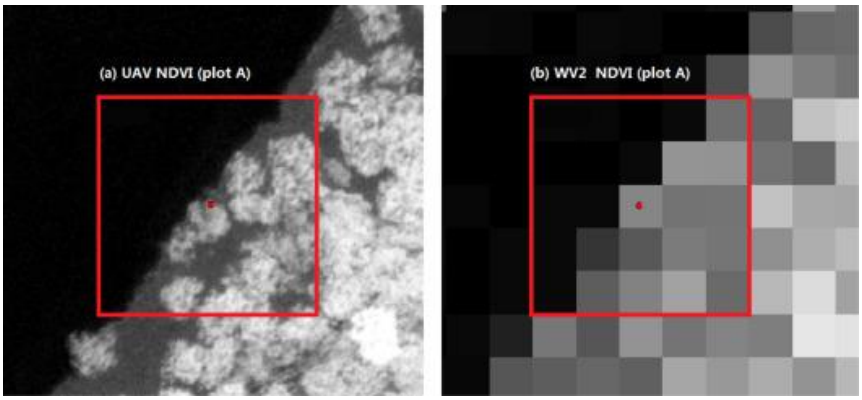

Figura 12. Comparación del NDVI a nivel de píxel de (a) UAV con RGB y (b) satélite World View 2. Fuente: Tian et al., 2017.

3.7. Análisis de estudios hidrológicos asociados al uso de índices de vegetación seleccionados

A partir de una nueva búsqueda en bases de datos académicas como Web of Science, Scopus, ScienceDirect y Google Scholar, utilizando las palabras

clave “*Indices of vegetation*”, “*Hydrology*”, “*Hydrological Modeling*”, “*Uncertainty*” y “*Water balance*”, se recopilaron estudios claves en donde se utilizan índices de vegetación para disminuir la incertidumbre asociada a la selección de parámetros en estudios de modelación hidrológica, los cuales se presentan en la Tabla 3.

Tabla 3. Artículos que incorporan índices de vegetación para disminuir la incertidumbre asociada a la selección de parámetros en estudios de modelación hidrológica.

Título	Cita	Enlace
Enhancing ecohydrological simulation with improved dynamic vegetation growth module in SWAT	An et al., 2024	https://www.sciencedirect.com/science/article/abs/pii/S0022169424014380
Informing the SWAT model with remote sensing detected vegetation phenology for improved modeling of ecohydrological processes	Chen et al., 2023	https://www.sciencedirect.com/science/article/pii/S0022169422013877
Comparing the ability of different remotely sensed evapotranspiration products in enhancing hydrological model performance and reducing prediction uncertainty	Taia et al., 2023	https://www.sciencedirect.com/science/article/pii/S1574954123003813
Multivariate assimilation of satellite-based leaf area index and ground-based river streamflow for hydrological modelling of irrigated watersheds using SWAT+	Mohammadi Igder et al., 2022	https://www.sciencedirect.com/science/article/pii/S002216942200587X?casa_token=xkRaljtqMT4AAAAA:3BlCOS0jpC8JB4FTOHXM27W0NLHvUJzlrcnU2aZbtcX6g1qNY8Qbw3VavatYe0zqcnb6ziMH
Satellite-Based Evapotranspiration in Hydrological Model Calibration	Jiang et al., 2020	https://www.mdpi.com/2072-4292/12/3/428

Continuación tabla anterior.

Multi-site calibration and validation of SWAT with satellite-based evapotranspiration in a data-sparse catchment in southwestern Nigeria	Odusanya et al., 2019	https://hess.copernicus.org/articles/23/1113/2019/
Modeling boreal forest evapotranspiration and water balance at stand and catchment scales: a spatial approach	Launiainen et al., 2019	https://hess.copernicus.org/articles/23/3457/2019/hess-23-3457-2019.html
Combining satellite data and appropriate objective functions for improved spatial pattern performance of a distributed hydrologic model	Demirel et al., 2018	https://hess.copernicus.org/articles/22/1299/2018/
Hydrologic model predictability improves with spatially explicit calibration using remotely sensed evapotranspiration and biophysical parameters	Rajib et al., 2018	https://www.sciencedirect.com/science/article/pii/S0022169418307856
Using tree ring data as a proxy for transpiration to reduce predictive uncertainty of a model simulating groundwater–surface water–vegetation interactions	Schilling et al., 2014	https://www.sciencedirect.com/science/article/pii/S0022169414006969?casa_token=ULsvmVft1gIAAAAA:84bcVSqTIIgZdMZjmrxDNHkwLJ2fwA6Jv8939E_oR6-Hwokn0I2OjdKabGTwrT3cfqGpapEb
Influences of Leaf Area Index estimations on water balance modeling in a Mediterranean semi-arid basin	Gigante et al., 2009	https://nhess.copernicus.org/articles/9/979/2009/
Calibration of a distributed hydrological model based on satellite evapotranspiration	Immerzeel & Droogers, 2008	https://www.sciencedirect.com/science/article/pii/S0022169407006944?casa_token=-z3kTTFzojAAAAAA:lVtWe_UcBrl2tYDEBrKizVStj1ZByEmk7HgSsf4doacps9YEq7jvX-NhABjpI0RyjcPhp8qd

Continuación tabla anterior.

Use of remotely sensed precipitation and leaf area index in a distributed hydrological model	Andersen et al., 2002	https://www.sciencedirect.com/science/article/pii/S0022169402000046X?casa_token=pDznFuSarBUAAAAA:LCTO85YgDTCN0GnK3skN07X1ZE2x_fIgm1hILarNdA_Dof6sYpFjeiqNa_-BFtpuFISCe34A

En la Tabla 3, se presentan artículos que asocian los índices de vegetación obtenidos con teledetección satelital con la mejora de calibración de modelos hidrológicos. El modelo *Soil and Water Assessment Tool* (SWAT) ha sido el más utilizado en los artículos revisados para simular procesos ecohidrológicos como el caudal y la evapotranspiración (ET) bajo diferentes condiciones climáticas y de uso del suelo (An et al., 2024; Chen et al., 2023; Immerzeel & Droogers, 2008; Mohammadi et al., 2022; Odusanya et al., 2019; Rajib et al., 2018; Taia et al., 2023). Sin embargo, una de las principales limitaciones del SWAT, radica en su deficiente representación de la dinámica de la vegetación, atribuida al uso de un modelo teórico y simplista para describir su crecimiento y desarrollo (Chen et al., 2023).

Otros modelos utilizados, que buscan representar de manera más precisa el papel de la vegetación, es el *Variable Infiltration Capacity* (VIC), basado en principios físicos, el cual realiza una calibración espacialmente distribuida utilizando la ET detectada remotamente (Jiang et al., 2020). También, se destaca el marco SpaFHy, que consta de tres modelos: uno asociado al dosel, que incluye la ecuación de Penman-Monteith para estimar la ET; otro para el

balance hídrico de la capa superficial del suelo; y un tercero denominado TOPMODEL, utilizado para modelar la zona saturada del suelo (Launiainen et al., 2019). Además, se utiliza un modelo hidrológico distribuido de mesoescala (mHM) para simular el caudal y la ET real a partir de teledetección y patrones espaciales observados, lo que contribuye a mejorar el balance hídrico (Demirel et al., 2018). Otro modelo destacado es el basado en procesos DREAM, el cual considera una parametrización distribuida e incluye NDVI y LAI para las estimaciones y cierre del balance hídrico (Gigante et al., 2009). El modelo MIKE SHE utiliza la precipitación y el LAI detectado remotamente para realizar una modelación hidrológica espacialmente distribuida (Andersen et al., 2002). Finalmente, el modelo Hydro-GeoSphere simula interacciones entre aguas subterráneas, aguas superficiales y vegetación, mediante el uso de datos del crecimiento de anillos de árboles como indicador de la transpiración en el conjunto de datos de calibración (Schilling et al., 2014).

Así, los autores han determinado principalmente valores de LAI y ET real a partir de imágenes satelitales. En algunos casos, también se ha utilizado teledetección para obtener el NDVI, con el fin de incorporarlo en la estimación del LAI (Gigante et al., 2009). Se ha demostrado que la introducción del LAI detectado remotamente mejora la simulación de hidrogramas en comparación con el uso de datos predefinidos, gracias a la variabilidad interanual que incorpora (Andersen et al., 2002). Además, genera cambios significativos en

las proporciones relativas de los componentes de la ET real, como la evaporación del dosel, la evaporación del suelo y la transpiración (Andersen et al., 2002). Así, el uso de datos de ET real obtenidos mediante teledetección en la calibración puede mejorar significativamente la precisión y confiabilidad de las predicciones del modelo (Taia et al., 2023). Mientras que la incorporación del LAI, por lo menos en el modelo SWAT, ha resultado en un aumento de la eficiencia de Nash-Sutcliffe (NSE), pasando de −0,18 a 0,87 y acercándose notablemente a una predicción perfecta, cuyo valor es 1 (An et al., 2024).

Además, la combinación de índices de vegetación con datos de caudal medido permite mejorar la precisión de los modelos hidrológicos y reducir la incertidumbre en la modelación (Mohammadi-Igder et al., 2022; Taia et al., 2023). Uno de los resultados clave de estos estudios es que el crecimiento dinámico de la vegetación puede aumentar la ET, lo que a su vez disminuye el caudal y el rendimiento hídrico. Por lo tanto, integrar este parámetro es esencial para tener un cierre adecuado del balance hídrico (An et al., 2024).

Los satélites más utilizados para la obtención de parámetros para los modelos anteriormente mencionados son Landsat (Chen et al., 2023), Sentinel (Mohammadi-Igder et al., 2022) y, principalmente, MODIS (Chen et al., 2023; Immerzeel & Droogers, 2008; Jiang et al., 2020; Launiainen et al., 2019; Odusanya et al., 2019; Rajib et al., 2018; Taia et al., 2023). Sin embargo, también se han utilizados satélites menos comunes, como lo son el Meteosat

(Andersen et al., 2002), el NOAA-AVHRR (Gigante et al., 2009), el Gravity Recovery and Climate Experiment (GRACE) (Demirel et al., 2018) y el Global Land Surface Satellite (GLASS) (An et al., 2024). Siendo el principal desafío asociado a la preferencia del satélite MODIS que, aunque ofrece una alta resolución temporal, su resolución espacial es baja, con píxeles de 250, 500 y 1000 m (Almalki et al., 2022). Esto limita su utilidad en estudios locales, ya que no puede representar de manera adecuada las condiciones de la superficie en áreas específicas o de menor escala, siendo más apropiado para investigaciones a nivel regional.

Una forma de reducir la incertidumbre en la estimación de la ET a escala local dentro del balance hídrico es mediante mediciones en terreno. Por ejemplo, el uso de dendrómetros permite medir la transpiración de los árboles a través del crecimiento de su tronco, identificando períodos de latencia y reactivación del crecimiento a resoluciones de micrómetros. Este enfoque parte del supuesto de que el crecimiento de los anillos es cero si la transpiración también lo es, ya que la producción de biomasa está estrechamente vinculada a la fotosíntesis, la cual requiere un cierto nivel de transpiración (Schilling et al., 2014).

En Chile, estas aplicaciones se han utilizado para analizar cómo las fluctuaciones de temperatura y precipitación afectan el crecimiento de bosques y plantaciones en distintas zonas climáticas, así como para el monitoreo de especies nativas (Salinas et al., 2019) y cultivos (Fernández & Claudia, 2005).

Sin embargo, no se han encontrado estudios que combinen herramientas como la teledetección y la dendrocronología para reducir la incertidumbre en los parámetros de ET dentro del balance hídrico.

4. CONCLUSIONES

Los índices de vegetación más utilizados son el NDVI, LAI, SAVI y EVI, y corresponden a herramientas clave para monitorear la vegetación y cambios en el uso del suelo. Cada índice tiene aplicaciones específicas y limitaciones: NDVI es versátil para fenómenos globales, pero sensible al brillo del suelo y la atmósfera; LAI mide densidad del dosel, aunque no tiene una relación única con los otros índices; SAVI ajusta efectos del suelo en áreas de baja cobertura vegetal, pero requiere calibración; y EVI, adecuado para alta biomasa, es menos preciso en terrenos complejos debido a la topografía.

La integración de estos índices, como NDVI y LAI, permite representar de manera más precisa la vegetación y su influencia en procesos hidrológicos, como la evapotranspiración. Estas herramientas son fundamentales en estudios ecohidrológicos, ya que mejoran la calibración de parámetros y reducen la incertidumbre en la modelación hidrológica, facilitando un cierre más efectivo del balance hídrico. La teledetección, por su parte, ofrece una opción viable para la obtención de estos datos a gran escala, aunque su resolución espacial puede no ser la más adecuada para estudios en escalas pequeñas, siendo recomendable en esta última situación la utilización de UAVs. También, a escala local, el uso de dendrómetros es valioso, ya que permite cuantificar con precisión los procesos de crecimiento de los anillos de los árboles en terreno, proporcionando información clave para estimar la

evapotranspiración y reducir la incertidumbre asociada a su medición, y estimación a través de la implementación de modelo hidrológicos.

En Chile, si bien se han desarrollado aplicaciones independientes de teledetección y dendrómetros, aún no se ha estudiado su combinación ni la relación existente entre las dinámicas de acumulación y derretimiento de nieve y los procesos de activación y latencia de la vegetación en bosques cordilleranos de Los Andes. Esta ausencia de investigaciones representa una brecha de conocimiento significativa e insta a explorar cómo la integración de ambas herramientas podría optimizar la modelación hidrológica en estos ecosistemas de montaña.

5. NOMENCLATURA

AGVI	Índice de Vegetación Verde Ajustado.
ARVI	Índice de Vegetación Atmosféricamente Resistente.
ASBI	Índice de Brillo del Suelo Ajustado.
B	Banda azul.
CARI	Índice de Proporción de Absorción de Clorofila.
CWSI	Índice de Estrés Hídrico de los Cultivos.
DVI	Índice de Vegetación Diferencial.
ET	Evapotranspiración.
EVI	Índice de Vegetación Mejorado.
G	Banda verde
GVI	Índice de Vegetación Verde.
IAVI	Índice de Vegetación de Interferencia Atmosférica.
IV	Índices de vegetación.
LAI	Índice de Área Foliar.
MCARI	Índice de Proporción de Absorción de Clorofila Modificado.
MGVI	Índice de Brillo del Suelo de Misra 2.
MSAVI	Índice de Vegetación Ajustado al Suelo Modificado.
MSAVI2	Índice de Vegetación Ajustado al Suelo Secundario Modificado.
MSBI	Índice de Brillo del Suelo de Misra.
MYVI	Índice de Brillo del Suelo de Misra 3.

NDVI	Índice de Vegetación de Diferencia Normalizada.
NIR	Banda infrarroja.
NSI	Índice Normalizado del Suelo.
OSAVI	Índice de Vegetación Ajustado al Suelo Optimizado.
PRI	Índice de reflectancia fotoquímica se basa en el estrés hídrico.
PVI	Índice de Vegetación Perpendicular.
R	Banda roja.
RVI	Índice de Relación de la Vegetación.
SAVI	Índice de Vegetación Ajustado al Suelo.
SBI	Índice de Brillo del Suelo.
UAV	Vehículo Aéreo No Tripulado.
VCI	Índice de Condición de la Vegetación.
VDVI	Índice de Vegetación de Diferencia de Banda Visible.
WDRVI	Índice de Vegetación de Amplio Rango Dinámico.
YVI	Índice de Vegetación Amarilla.

6. BIBLIOGRAFÍA

Academia de Drones Chile. (2017). *Pilotaje de drones | conductor de drones*. Academia de Drones de Chile. https://www.academiadronchile.cl/estos-los-diferentes-tipos-drones-existen-mercado/

Algarra, J. (2024). *Avances en la gestión integral de flora en montaña mediterránea: Seguimiento, efecto de la nieve y desarrollo de la dimensión social*. https://digibug.ugr.es/handle/10481/93115

Almalki, R., Khaki, M., Saco, P. M., & Rodriguez, J. F. (2022). Monitoring and Mapping Vegetation Cover Changes in Arid and Semi-Arid Areas Using Remote Sensing Technology: A Review. *Remote Sensing*, *14*(20), Article 20. https://doi.org/10.3390/rs14205143

An, S., Wu, Y., Liang, W., Zhang, G., Chen, J., Liu, S., Zhao, F., Qiu, L., & Yin, X. (2024). Enhancing ecohydrological simulation with improved dynamic vegetation growth module in SWAT. *Journal of Hydrology*, *644*, 132042. https://doi.org/10.1016/j.jhydrol.2024.132042

Anderegg, L., Anderegg, W., & Berry, J. (2013). Not all droughts are created equal: Translating meteorological drought into woody plant mortality. *Tree physiology*, *33*. https://doi.org/10.1093/treephys/tpt044

Andersen, J., Dybkjaer, G., Jensen, K. H., Refsgaard, J. C., & Rasmussen, K. (2002). Use of remotely sensed precipitation and leaf area index in a distributed hydrological model. *Journal of Hydrology*, *264*(1), 34–50. https://doi.org/10.1016/S0022-1694(02)00046-X

Andivia, E., Arenas-Castro, S., Ariza, A., Arthus, R., Cachinero, A., Camarero, J., Fernández, P., García, B., Giménez, F., & Guerrero, J. (2024). *Una revisión sencilla del análisis de patrón de puntos aplicado a la ecología forestal* (p. 562). https://www.researchgate.net/profile/Ricardo-Enrique-Hernandez-Lambrano/publication/382495599_Una_revision_sencilla_del_analisis_de_patron_de_puntos_aplicado_a_la_ecologia_forestal/links/66a0b7455919b66c9f683f41/Una-revision-sencilla-del-analisis-de-patron-de-puntos-aplicado-a-la-ecologia-forestal.pdf#page=171

Ashburn, P. (1979). *The vegetative index number and crop identification*. https://ntrs.nasa.gov/citations/19800007243

Asrar, G., Fuchs, M., Kanemasu, E. T., & Hatfield, J. L. (1984). Estimating Absorbed Photosynthetic Radiation and Leaf Area Index from Spectral Reflectance in Wheat. *Agronomy Journal*, *76*(2), 300–306. https://doi.org/10.2134/agronj1984.00021962007600020029x

Badhwar, G. (1981). *The use of parameters to separate and identify spring small grains*. https://scholar.google.es/scholar?hl=es&as_sdt=0%2C5&q=Badhwar%2C+G.+D.+%281981%29+The+Use+of+Parameters+to+Separate+and+Identify+Spring+Small+Grains.+Quarterly+Technical+Interchange+Meeting%2C+NASA-JSC%2C+Houston%2C+TX%2C+USA.&btnG=

Bannari, A. (1994). High spatial and spectral resolution remote sensing for the management of the urban environment. *First Int. Airborne Remote Sensing Conference and Exhibition, Strasburg, France*, *0*, 247–260.

Bannari, A., Asalhi, H., & Teillet, P. M. (2002). Transformed difference vegetation index (TDVI) for vegetation cover mapping. *IEEE International Geoscience and Remote Sensing Symposium*, *5*, 3053–3055 vol.5. https://doi.org/10.1109/IGARSS.2002.1026867

Bannari, A., Morin, D., Bonn, F., & Huete, A. (1995). A review of vegetation indices. *Remote Sensing Reviews*, *13*(1–2), 95–120. https://doi.org/10.1080/02757259509532298

Barbosa, J. M., & Asner, G. P. (2017). Effects of long-term rainfall decline on the structure and functioning of Hawaiian forests. *Environmental Research Letters*, *12*(9), 094002. https://doi.org/10.1088/1748-9326/aa7ee4

Baret, F. (1989). TSAVI: A vegetation index which minimizes soil brightness effects on LAI and APAR estimation. *12th Canadian Symp. on Remote Sensing and IGARSS '90, Vancouver, Canada, 10-14 July 1989*. https://cir.nii.ac.jp/crid/1573668926152004224

Baret, F., & Guyot, G. (1991). Potentials and limits of vegetation indices for LAI and APAR assessment. *Remote Sensing of Environment*, *35*(2), 161–173. https://doi.org/10.1016/0034-4257(91)90009-U

Birth, G., & McVey, G. (1968). Measuring the Color of Growing Turf with a Reflectance Spectrophotometer. *Agronomy Journal*, *60*(6), 640–643. https://doi.org/10.2134/agronj1968.00021962006000060016x

Blackburn, G. A. (1998). Quantifying Chlorophylls and Caroteniods at Leaf and Canopy Scales: An Evaluation of Some Hyperspectral Approaches. *Remote Sensing of Environment*, *66*(3), 273–285. https://doi.org/10.1016/S0034-4257(98)00059-5

Broge, N. H., & Leblanc, E. (2001). Comparing prediction power and stability of broadband and hyperspectral vegetation indices for estimation of green leaf area index and canopy chlorophyll density. *Remote Sensing of Environment*, *76*(2), 156–172. https://doi.org/10.1016/S0034-4257(00)00197-8

Buschmann, C., & Nagel, E. (1993). In vivo spectroscopy and internal optics of leaves as basis for remote sensing of vegetation. *International Journal of Remote Sensing*, *14*(4), 711–722. https://doi.org/10.1080/01431169308904370

Chappelle, E., Kim, M., & McMurtrey, J. (1992). Ratio analysis of reflectance spectra (RARS): An algorithm for the remote estimation of the concentrations of chlorophyll A, chlorophyll B, and carotenoids in soybean leaves. *Remote Sensing of Environment*, *39*(3), 239–247. https://doi.org/10.1016/0034-4257(92)90089-3

Chávez, R. O., Clevers, J. G. P. W., Decuyper, M., de Bruin, S., & Herold, M. (2016). 50 años de extracción de agua en la cuenca de la Pampa del

Tamarugal: ¿Pueden los árboles *de Prosopis tamarugo* sobrevivir en el hiperárido desierto de Atacama (norte de Chile)? *Journal of Arid Environments*, *124*, 292–303. https://doi.org/10.1016/j.jaridenv.2015.09.007

Chen, J. (1996). Evaluation of Vegetation Indices and a Modified Simple Ratio for Boreal Applications. *Canadian Journal of Remote Sensing*, *22*(3), 229–242. https://doi.org/10.1080/07038992.1996.10855178

Chen, S., Fu, Y. H., Wu, Z., Hao, F., Hao, Z., Guo, Y., Geng, X., Li, X., Zhang, X., Tang, J., Singh, V. P., & Zhang, X. (2023). Informing the SWAT model with remote sensing detected vegetation phenology for improved modeling of ecohydrological processes. *Journal of Hydrology*, *616*, 128817. https://doi.org/10.1016/j.jhydrol.2022.128817

Clevers, J. (1986). *The application of a vegetation index in correcting the infrared reflectance for soil background.* https://research.wur.nl/en/publications/the-application-of-a-vegetation-index-in-correcting-the-infrared-

Courel, M.-F., Chamard, Ph. C., Guenegou, M. C., Lerhun, J., Levasseur, J., & Togola, M. (1991). Utilisation des bandes spectrales du vert et du rouge pour une meilleure évaluation des formations végétales actives. *Congrès AUPELF-UREF*. https://hal.science/hal-00327879

Crippen, R. (1990). Calculating the vegetation index faster. *Remote Sensing of Environment*, *34*(1), 71–73. https://doi.org/10.1016/0034-4257(90)90085-Z

Datt, B. (1998). Remote Sensing of Chlorophyll a, Chlorophyll b, Chlorophyll a+b and Total Carotenoid Content in Eucalyptus Leaves. *Remote Sensing of Environment*, *66*(2), 111–121. https://doi.org/10.1016/S0034-4257(98)00046-7

Datt, B. (1999a). A New Reflectance Index for Remote Sensing of Chlorophyll Content in Higher Plants: Tests using *Eucalyptus* Leaves. *Journal of Plant Physiology*, *154*(1), 30–36. https://doi.org/10.1016/S0176-1617(99)80314-9

Datt, B. (1999b). Visible/near infrared reflectance and chlorophyll content in Eucalyptus leaves. *International Journal of Remote Sensing*, *20*(14), 2741–2759. https://doi.org/10.1080/014311699211778

Daughtry, C. S. T. (2001). Discriminating Crop Residues from Soil by Shortwave Infrared Reflectance. *Agronomy Journal*, *93*(1), 125–131. https://doi.org/10.2134/agronj2001.931125x

Daughtry, C. S. T., Walthall, C., Kim, M. S., de Colstoun, E. B., & McMurtrey, J. E. (2000). Estimating Corn Leaf Chlorophyll Concentration from Leaf and Canopy Reflectance. *Remote Sensing of Environment*, *74*(2), 229–239. https://doi.org/10.1016/S0034-4257(00)00113-9

Demetriades-Shah, T., Steven, M., & Clark, J. (1990). High resolution derivative spectra in remote sensing. *Remote Sensing of Environment*, *33*(1), 55–64. https://doi.org/10.1016/0034-4257(90)90055-Q

Demirel, M. C., Mai, J., Mendiguren, G., Koch, J., Samaniego, L., & Stisen, S. (2018). Combining satellite data and appropriate objective functions for

improved spatial pattern performance of a distributed hydrologic model. *Hydrology and Earth System Sciences*, *22*(2), 1299–1315. https://doi.org/10.5194/hess-22-1299-2018

Didan, K., & Munoz, A. B. (s. f.). *MODIS Vegetation Index User's Guide (MOD13 Series)*. https://modis-land.gsfc.nasa.gov/pdf/MOD13_User_Guide_V61.pdf

Dutrieux, L. P., Verbesselt, J., Kooistra, L., & Herold, M. (2015). Monitoring forest cover loss using multiple data streams, a case study of a tropical dry forest in Bolivia. *ISPRS Journal of Photogrammetry and Remote Sensing*, *107*, 112–125. https://doi.org/10.1016/j.isprsjprs.2015.03.015

Elvidge, C. D., & Chen, Z. (1995). Comparison of broad-band and narrow-band red and near-infrared vegetation indices. *Remote Sensing of Environment*, *54*(1), 38–48. https://doi.org/10.1016/0034-4257(95)00132-K

Emery, W., & Camps, A. (2017). *Advanced Very High Resolution Radiometer—An overview*. https://www.sciencedirect.com/topics/earth-and-planetary-sciences/advanced-very-high-resolution-radiometer

EOS Data Analytics. (2021a). *Sentinel 1: Imágenes satelitales, descripción general y características*. https://eos.com/find-satellite/sentinel-1/

EOS Data Analytics. (2021b). *Sentinel-2: Imágenes satelitales, descripción general y características*. https://eos.com/find-satellite/sentinel-2/

Escadafal, R., & Huete, A. (1991). Etude des propriétés spectrales des sols arides appliquée à l'amélioration des indices de végétation obtenus par

télédétection. *Etude des propriétés spectrales des sols arides appliquée à l'amélioration des indices de végétation obtenus par télédétection*, *312*(11), 1385–1391.

Estay, S., Chávez, R., Lastra, J., Rocco, R., Gutiérrez, Á., & Decuyper, M. (2023). *Serie temporal MODIS revela nuevos registros máximos de área defoliada por Ormiscodes amphimone en bosques caducifolios de Nothofagus, sur de Chile*. https://www.mdpi.com/2072-4292/15/14/3538

Fernández, S., & Claudia, M. (2005). *Uso del dendrómetro para determinar estado hídrico en vides cv. Cabernet Sauvignon*. https://hdl.handle.net/20.500.14001/56832

Fisher, J. B., Lee, B., Purdy, A. J., Halverson, G. H., Dohlen, M. B., Cawse-Nicholson, K., Wang, A., Anderson, R. G., Aragon, B., Arain, M. A., Baldocchi, D. D., Baker, J. M., Barral, H., Bernacchi, C. J., Bernhofer, C., Biraud, S. C., Bohrer, G., Brunsell, N., Cappelaere, B., … Hook, S. (2020). ECOSTRESS: NASA's Next Generation Mission to Measure Evapotranspiration From the International Space Station. *Water Resources Research*, *56*(4), e2019WR026058. https://doi.org/10.1029/2019WR026058

Gamon, J., Peñuelas, J., & Field, C. B. (1992). A narrow-waveband spectral index that tracks diurnal changes in photosynthetic efficiency. *Remote Sensing of Environment*, *41*(1), 35–44. https://doi.org/10.1016/0034-4257(92)90059-S

Gamon, J., & Surfus, J. (1999). Assessing leaf pigment content and activity with a reflectometer. *The New Phytologist*, *143*(1), 105–117. https://doi.org/10.1046/j.1469-8137.1999.00424.x

Garreaud, R., Alvarez-Garreton, C., Barichivich, J., Boisier, J. P., Christie, D., Galleguillos, M., LeQuesne, C., McPhee, J., & Zambrano-Bigiarini, M. (2017). The 2010–2015 megadrought in central Chile: Impacts on regional hydroclimate and vegetation. *Hydrology and Earth System Sciences*, *21*(12), 6307–6327. https://doi.org/10.5194/hess-21-6307-2017

Gazol, A., Camarero, J. J., Vicente-Serrano, S. M., Sánchez-Salguero, R., Gutiérrez, E., de Luis, M., Sangüesa-Barreda, G., Novak, K., Rozas, V., Tíscar, P. A., Linares, J. C., Martín-Hernández, N., Martínez del Castillo, E., Ribas, M., García-González, I., Silla, F., Camisón, A., Génova, M., Olano, J. M., … Galván, J. D. (2018). Forest resilience to drought varies across biomes. *Global Change Biology*, *24*(5), 2143–2158. https://doi.org/10.1111/gcb.14082

Gigante, V., Iacobellis, V., Manfreda, S., Milella, P., & Portoghese, I. (2009). Influences of Leaf Area Index estimations on water balance modeling in a Mediterranean semi-arid basin. *Natural Hazards and Earth System Sciences*, *9*(3), 979–991. https://doi.org/10.5194/nhess-9-979-2009

Gillian, J. (s.f.a). *IKONOS*. https://www.landscapetoolbox.org/remote-sensor-types/ikonos/

Gillian, J. (s.f.b). *Quickbird*. https://www.landscapetoolbox.org/remote-sensor-types/quickbird/

Giovos, R., Tassopoulos, D., Kalivas, D., Lougkos, N., & Priovolou, A. (2021). Remote Sensing Vegetation Indices in Viticulture: A Critical Review. *Agriculture*, *11*(5), Article 5. https://doi.org/10.3390/agriculture11050457

Gitelson, A. A. (2004). Wide Dynamic Range Vegetation Index for Remote Quantification of Biophysical Characteristics of Vegetation. *Journal of Plant Physiology*, *161*(2), 165–173. https://doi.org/10.1078/0176-1617-01176

Gitelson, A. A., Kaufman, Y. J., Stark, R., & Rundquist, D. (2002). Novel algorithms for remote estimation of vegetation fraction. *Remote Sensing of Environment*, *80*(1), 76–87. https://doi.org/10.1016/S0034-4257(01)00289-9

Gitelson, A., Keydan, G., & Merzlyak, M. (2006). Three-band model for noninvasive estimation of chlorophyll, carotenoids, and anthocyanin contents in higher plant leaves. *Geophysical Research Letters*, *33*(11). https://doi.org/10.1029/2006GL026457

Gitelson, A., & Merzlyak, M. (1996). Signature Analysis of Leaf Reflectance Spectra: Algorithm Development for Remote Sensing of Chlorophyll. *Journal of Plant Physiology*, *148*(3), 494–500. https://doi.org/10.1016/S0176-1617(96)80284-7

Gitelson, A., Merzlyak, M., & Chivkunova, O. (2001). Optical Properties and Nondestructive Estimation of Anthocyanin Content in Plant Leaves. *Photochemistry and Photobiology*, *74*(1), 38–45. https://doi.org/10.1562/0031-8655(2001)0740038OPANEO2.0.CO2

Glenn, E. P., Huete, A. R., Nagler, P. L., & Nelson, S. G. (2008). Relationship Between Remotely-sensed Vegetation Indices, Canopy Attributes and Plant Physiological Processes: What Vegetation Indices Can and Cannot Tell Us About the Landscape. *Sensors*, *8*(4), Article 4. https://doi.org/10.3390/s8042136

Goel, N., & Qin, W. (1994). Influences of canopy architecture on relationships between various vegetation indices and LAI and Fpar: A computer simulation. *Remote Sensing Reviews*, *10*(4), 309–347. https://doi.org/10.1080/02757259409532252

Grossiord, C., Granier, A., Ratcliffe, S., Bouriaud, O., Bruelheide, H., Chećko, E., Forrester, D. I., Dawud, S. M., Finér, L., Pollastrini, M., Scherer-Lorenzen, M., Valladares, F., Bonal, D., & Gessler, A. (2014). Tree diversity does not always improve resistance of forest ecosystems to drought. *Proceedings of the National Academy of Sciences*, *111*(41), 14812–14815. https://doi.org/10.1073/pnas.1411970111

Guzman-Alvarez, J. A., González-Zuñiga, M., Sandoval Fernandez, J. A., & Calvo-Alvarado, J. C. (2022). Uso de sensores remotos en la agricultura: Aplicaciones en el cultivo del banano. *Agronomía Mesoamericana*, 48279. https://doi.org/10.15517/am.v33i3.48279

Haboudane, D., Miller, J. R., Pattey, E., Zarco-Tejada, P. J., & Strachan, I. B. (2004). Hyperspectral vegetation indices and novel algorithms for predicting green LAI of crop canopies: Modeling and validation in the context of precision agriculture. *Remote Sensing of Environment*, *90*(3), 337–352. https://doi.org/10.1016/j.rse.2003.12.013

Haboudane, D., Miller, J. R., Tremblay, N., Zarco-Tejada, P. J., & Dextraze, L. (2002). Integrated narrow-band vegetation indices for prediction of crop chlorophyll content for application to precision agriculture. *Remote Sensing of Environment*, *81*(2), 416–426. https://doi.org/10.1016/S0034-4257(02)00018-4

Hay, C., Kuretz, C., Odenweller, J., Scheffner, E., & Wood, B. (1979). *Development of AI procedures for dealing with the effects of episodal events on crop temporal spectral response*. https://ntrs.nasa.gov/api/citations/19800024310/downloads/19800024310.pdf

Henríquez, J. R. (2020). *Análisis de algunos componentes de la gestión y la gobernanza del recurso hídrico en la microcuenca El Manzanar, comuna de Curacautín, Región de La Araucanía, Chile.* https://repositorio.catie.ac.cr/handle/11554/9726

Holben, B. (1986). Characteristics of maximum-value composite images from temporal AVHRR data. *International Journal of Remote Sensing*, *7*(11), 1417–1434. https://doi.org/10.1080/01431168608948945

Houborg, R., Soegaard, H., & Boegh, E. (2007). Combining vegetation index and model inversion methods for the extraction of key vegetation biophysical parameters using Terra and Aqua MODIS reflectance data. *Remote Sensing of Environment*, *106*(1), 39–58. https://doi.org/10.1016/j.rse.2006.07.016

Huang, S., Tang, L., Hupy, J. P., Wang, Y., & Shao, G. (2021). A commentary review on the use of normalized difference vegetation index (NDVI) in the era of popular remote sensing. *Journal of Forestry Research*, *32*(1), 1–6. https://doi.org/10.1007/s11676-020-01155-1

Huete, A. (1988a). A soil-adjusted vegetation index (SAVI). *Remote Sensing of Environment*, *25*(3), 295–309. https://doi.org/10.1016/0034-4257(88)90106-X

Huete, A. (1988b). A soil-adjusted vegetation index (SAVI). *Remote Sensing of Environment*, *25*(3), 295–309. https://doi.org/10.1016/0034-4257(88)90106-X

Huete, A., Didan, K., Miura, T., Rodriguez, E. P., Gao, X., & Ferreira, L. G. (2002). Overview of the radiometric and biophysical performance of the MODIS vegetation indices. *Remote Sensing of Environment*, *83*(1), 195–213. https://doi.org/10.1016/S0034-4257(02)00096-2

Huete, A., Justice, C., & Liu, H. (1994). Development of vegetation and soil indices for MODIS-EOS. *Remote Sensing of Environment*, *49*(3), 224–234. https://doi.org/10.1016/0034-4257(94)90018-3

Huete, A., Liu, H. Q., Batchily, K., & van Leeuwen, W. (1997). A comparison of vegetation indices over a global set of TM images for EOS-MODIS. *Remote Sensing of Environment*, *59*(3), 440–451. https://doi.org/10.1016/S0034-4257(96)00112-5

Hunt, E., & Rock, B. (1989). Detection of changes in leaf water content using Near- and Middle-Infrared reflectances. *Remote Sensing of Environment*, *30*(1), 43–54. https://doi.org/10.1016/0034-4257(89)90046-1

Idso, S., Jackson, R., Pinter, P., Reginato, R., & Hatfield, J. (1981). Normalizing the stress-degree-day parameter for environmental variability. *Agricultural Meteorology*, *24*, 45–55. https://doi.org/10.1016/0002-1571(81)90032-7

Immerzeel, W. W., & Droogers, P. (2008). Calibration of a distributed hydrological model based on satellite evapotranspiration. *Journal of Hydrology*, *349*(3), 411–424. https://doi.org/10.1016/j.jhydrol.2007.11.017

Jackson, R. D., Slater, P. N., & Pinter, P. J. (1983). Discrimination of growth and water stress in wheat by various vegetation indices through clear and turbid atmospheres. *Remote Sensing of Environment*, *13*(3), 187–208. https://doi.org/10.1016/0034-4257(83)90039-1

Jackson, R., Pinter, P., Paul, J., Reginato, R., Robert, J., & Idso, S. (1980). *Hand-held radiometry: A set of notes developed for use at the Workshop*

of Hand-held radiometry—NASA Technical Reports Server (NTRS). https://ntrs.nasa.gov/citations/19810019958

Jiang, L., Wu, H., Tao, J., Kimball, J., Alferi, L., & Chen, X. (2020). *Satellite-Based Evapotranspiration in Hydrological Model Calibration*. https://www.mdpi.com/2072-4292/12/3/428

Jiang, Z., Huete, A. R., Chen, J., Chen, Y., Li, J., Yan, G., & Zhang, X. (2006). Analysis of NDVI and scaled difference vegetation index retrievals of vegetation fraction. *Remote Sensing of Environment*, *101*(3), 366–378. https://doi.org/10.1016/j.rse.2006.01.003

Jiang, Z., Huete, A. R., Didan, K., & Miura, T. (2008). Development of a two-band enhanced vegetation index without a blue band. *Remote Sensing of Environment*, *112*(10), 3833–3845. https://doi.org/10.1016/j.rse.2008.06.006

Jin, X., & Baofeng, S. de. (2017). Significant Remote Sensing Vegetation Indices: A Review of Developments and Applications. *Journal of Sensors*, *2017*(1), 1353691. https://doi.org/10.1155/2017/1353691

Jones, H. G., & Vaughan, R. A. (2010). *Remote Sensing of Vegetation: Principles, Techniques, and Applications*. OUP Oxford. https://books.google.es/books?hl=es&lr=&id=sTmcAQAAQBAJ&oi=fnd&pg=PR5&dq=Jones+HG,+Vaughan+RA+(2010)+Remote+sensing+of+vegetation:+principles,+techniques,+and+applications.+Oxford+University+Press,+New+York,+p+353&ots=0gWI8EhY4X&sig=E5ej42Y5QA_abs1tqnqazl14EV4#v=onepage&q&f=false

Jordan, C. (1969). Derivation of Leaf-Area Index from Quality of Light on the Forest Floor. *Ecology*, *50*(4), 663–666. https://doi.org/10.2307/1936256

Kaufman, Y. J., & Tanre, D. (1992). *Atmospherically resistant vegetation index (ARVI) for EOS-MODIS | IEEE Journals & Magazine | IEEE Xplore*. https://ieeexplore.ieee.org/abstract/document/134076

Kauth, R., & Thomas, G. (1976). *A Graphic Description of the Spectral-Temporal Development of Agricultural Crops as Seen by LANDSAT*. https://docs.lib.purdue.edu/cgi/viewcontent.cgi?article=1160&context=lars_symp

Kim, M. S., Daughtry, C. S. T., Chappelle, E. W., Mcmurtrey, J. E., & Walthall, C. L. (1994, enero 1). *The Use of High Spectral Resolution Bands for Estimating Absorbed Photosynthetically Active Radiation (A Par)*. https://ntrs.nasa.gov/citations/19950010604

Kogan, F. (1995). Application of vegetation index and brightness temperature for drought detection. *Advances in Space Research*, *15*(11), 91–100. https://doi.org/10.1016/0273-1177(95)00079-T

Koncagüil, E., Tran, M., & Connor, R. (2020). *Informe mundial de las Naciones Unidas sobre el desarrollo de los recursos hídricos 2020: Agua y cambio climático, datos y cifras*. UNESCO Digital Library. https://unesdoc.unesco.org/ark:/48223/pf0000372876_spa

Launiainen, S., Guan, M., Salmivaara, A., & Kieloaho, A.-J. (2019). Modeling boreal forest evapotranspiration and water balance at stand and catchment scales: A spatial approach. *Hydrology and Earth System*

Sciences, *23*(8), 3457–3480. https://doi.org/10.5194/hess-23-3457-2019

Li, F., Miao, Y., Feng, G., Yuan, F., Yue, S., Gao, X., Liu, Y., Liu, B., Ustin, S. L., & Chen, X. (2014). Improving estimation of summer maize nitrogen status with red edge-based spectral vegetation indices. *Field Crops Research*, *157*, 111–123. https://doi.org/10.1016/j.fcr.2013.12.018

Lichtenthaler, H., Lang, M., Sowinska, M., Heisel, F., & Miehé, J. A. (1996). Detection of Vegetation Stress Via a New High Resolution Fluorescence Imaging System. *Journal of Plant Physiology*, *148*(5), 599–612. https://doi.org/10.1016/S0176-1617(96)80081-2

Lloyd-Hughes, B. (2014). The impracticality of a universal drought definition. *Theoretical and Applied Climatology*, *117*(3), 607–611. https://doi.org/10.1007/s00704-013-1025-7

Louhaichi, M., Borman, M., & Johnson, D. (2001). Spatially Located Platform and Aerial Photography for Documentation of Grazing Impacts on Wheat. *Geocarto International*, *16*(1), 65–70. https://doi.org/10.1080/10106040108542184

Lozano-Parra. (2015). *Dinámica del Agua Edáfica en Dehesas y su Relación con el Clima y la Vegetación*. https://dehesa.unex.es/flexpaper/template.html?path=https://dehesa.unex.es/bitstream/10662/2820/1/TDUEX_2015_Lozano_Parra.pdf#page=1

Mahlein, A., Rumpf, T., Welke, P., Dehne, H.-W., Plümer, L., Steiner, U., & Oerke, E.-C. (2013). Development of spectral indices for detecting and identifying plant diseases. *Remote Sensing of Environment*, *128*, 21–30. https://doi.org/10.1016/j.rse.2012.09.019

Matsushita, B., Yang, W., Chen, J., Onda, Y., & Qiu, G. (2007). Sensitivity of the Enhanced Vegetation Index (EVI) and Normalized Difference Vegetation Index (NDVI) to Topographic Effects: A Case Study in High-density Cypress Forest. *Sensors*, *7*(11), Article 11. https://doi.org/10.3390/s7112636

McFeeters, S. (1996). The use of the Normalized Difference Water Index (NDWI) in the delineation of open water features. *International Journal of Remote Sensing*, *17*(7), 1425–1432. https://doi.org/10.1080/01431169608948714

McMurtrey, J., Chappelle, E., Kim, M., Meisinger, J., & Corp, L. (1994). Distinguishing nitrogen fertilization levels in field corn (Zea mays L.) with actively induced fluorescence and passive reflectance measurements. *Remote Sensing of Environment*, *47*(1), 36–44. https://doi.org/10.1016/0034-4257(94)90125-2

McNairn, H., & Protz, R. (1993). Mapping Corn Residue Cover on Agricultural Fields in Oxford County, Ontario, Using Thematic Mapper. *Canadian Journal of Remote Sensing*, *19*(2), 152–159. https://doi.org/10.1080/07038992.1993.10874543

Medina, A., & Orlov, D. (2021, julio 8). *El "reino" de los árboles*. https://desdelapatagonia.uncoma.edu.ar/index.php/el-reino-de-los-arboles/

Merzlyak, M., Gitelson, A., Chivkunova, O., & Rakitin, V. (1999). Non-destructive optical detection of pigment changes during leaf senescence and fruit ripening. *Physiologia Plantarum*, *106*(1), 135–141. https://doi.org/10.1034/j.1399-3054.1999.106119.x

Meyer, G., Hindman, T., & Laksmi, K. (1999). Machine vision detection parameters for plant species identification. *Precision Agriculture and Biological Quality*, *3543*, 327–335. https://doi.org/10.1117/12.336896

Miranda, A., Lara, A., Altamirano, A., Di Bella, C., González, M. E., & Julio Camarero, J. (2020). Forest browning trends in response to drought in a highly threatened mediterranean landscape of South America. *Ecological Indicators*, *115*, 106401. https://doi.org/10.1016/j.ecolind.2020.106401

Misra, P. (1977). *Kauth-Thomas brightness and greenness axes*. https://cir.nii.ac.jp/crid/1572543024797184896

Mohammadi, O., Alizadeh, H., Mojaradi, B., & Bayat, M. (2022). Multivariate assimilation of satellite-based leaf area index and ground-based river streamflow for hydrological modelling of irrigated watersheds using SWAT+. *Journal of Hydrology*, *610*, 128012. https://doi.org/10.1016/j.jhydrol.2022.128012

Montenegro, F. (2022). *Gestión Integral de Recursos Hídricos en la Escasez de Agua de los Pobladores de El Melón en Chile*. https://repositorio.upn.edu.pe/bitstream/handle/11537/33112/Montenegro%20Saavedra%20Francisco%20Gabriel.pdf?sequence=3&isAllowed=y

Musick, H., & Pelletier, R. (1988). Response to soil moisture of spectral indexes derived from bidirectional reflectance in thematic mapper wavebands. *Remote Sensing of Environment*, *25*(2), 167–184. https://doi.org/10.1016/0034-4257(88)90099-5

Naciones Unidas. (2019). *Informe de los Objetivos de Desarrollo Sostenible 2019*. https://unstats.un.org/sdgs/report/2019/The-Sustainable-Development-Goals-Report-2019_Spanish.pdf

Nafarrate-Hecht, A. C., Dupuy-Rada, J. M., George-Chacon, S. P., Hernández-Stefanoni, J. L., Nafarrate-Hecht, A. C., Dupuy-Rada, J. M., George-Chacon, S. P., & Hernández-Stefanoni, J. L. (2018). Modelización y mapeo estacional del índice de área foliar en un bosque tropical seco usando imágenes de satélite de alta resolución. *Madera y bosques*, *24*(3). https://doi.org/10.21829/myb.2018.2431666

NASA Earth Data. (s.f.a). *ECOSTRESS*. ECOSTRESS. https://ecostress.jpl.nasa.gov/instrument

NASA Earth Data. (s.f.b). *MODIS Overview*. https://lpdaac.usgs.gov/data/get-started-data/collection-overview/missions/modis-overview/

Neto, J. (2004). Un enfoque combinado de computación estadística y soft para la clasificación sobre y mapeo de especies de malezas en sistemas de labranza mínima. *Recolección ETD para la Universidad de Nebraska-Lincoln*, 1–170.

Nijun, J., Changyong, D., Yunwei, T., Galdies, C., Yan, L., & Haifeng, D. (2024). Derivation of tasseled cap transformation coefficients for SDGSAT-1 Multispectral Imager at-sensor reflectance data. *International Journal of Digital Earth*, *17*(1), 2413885. https://doi.org/10.1080/17538947.2024.2413885

ODEPA. (2016). *El cambio climático y los recursos hídricos de Chile*. Opia.CL: Observatorio para la Innovación Agraria, Agroalimentaria y Forestal. https://opia.fia.cl/601/w3-article-91835.html

Odusanya, A. E., Mehdi, B., Schürz, C., Oke, A. O., Awokola, O. S., Awomeso, J. A., Adejuwon, J. O., & Schulz, K. (2019). Multi-site calibration and validation of SWAT with satellite-based evapotranspiration in a data-sparse catchment in southwestern Nigeria. *Hydrology and Earth System Sciences*, *23*(2), 1113–1144. https://doi.org/10.5194/hess-23-1113-2019

Paredes, M. (2018). *Uso de índices de vegetación del sensor MODIS-TERRA en la estimación de biomasa aerea de pajonales altoandinos*. https://repositorio.lamolina.edu.pe/bitstream/handle/20.500.12996/3351/paredes-choccemiguel-enrique.pdf?sequence=1&isAllowed=y

Pastor, J., Atkinson, P., Jadunandan, T., & Rioja, R. (2015). *Remote Sensing | Free Full-Text | Spatiotemporal Variation in Mangrove Chlorophyll Concentration Using Landsat 8*. https://www.mdpi.com/2072-4292/7/11/14530

Pearson, R., & Miller, L. (1972). *Remote mapping of standing crop biomass for estimation of the productivity of the shortgrass prairie, Pawnee National Grasslands, Colorado.* https://www.cabidigitallibrary.org/doi/full/10.5555/19740715986

Perea-Ardila, M. A., Andrade-Castañeda, H. J., & Segura-Madrigal, M. A. (2021). Estimación de Biomasa Aérea y Carbono con Teledetección en Bosques Alto-Andinos de Boyacá, Colombia. Estudio de caso: Santuario de Fauna y Flora Iguaque. *Revista Cartográfica*, *102*, Article 102. https://doi.org/10.35424/rcarto.i102.821

Perry, C., & Lautenschalager. (1984). *Functional equivalence of spectral vegetation indices—ScienceDirect*. https://www.sciencedirect.com/science/article/pii/0034425784900130

Pettorelli, N., Vik, J. O., Mysterud, A., Gaillard, J.-M., Tucker, C. J., & Stenseth, N. Chr. (2005). Using the satellite-derived NDVI to assess ecological responses to environmental change. *Trends in Ecology & Evolution*, *20*(9), 503–510. https://doi.org/10.1016/j.tree.2005.05.011

Pinty, B., & Verstraete, M. (1992). *GEMI: a non-linear index to monitor global vegetation from satellites*. https://link.springer.com/article/10.1007/bf00031911

Pizarro, R., Sangüesa, C., Vallejos, C., Mendoza, R., Pino, J., Berríos, Á., Ibáñez, A., Castillo, B., Bernal, A., García, P., Arumí, J. L., & Iroumé, A. (2019). *Antecedentes de la relación masa forestal y disponibilidad hídrica en Chile*. https://unesdoc.unesco.org/ark:/48223/pf0000370891.locale=en

Plummer, S. (1994). *The angular vegetation index: An atmospherically resistant index for the second along track scanning radiometer (ATSR-2)*. https://cir.nii.ac.jp/crid/1570854174936916736

Qi, J., Chehbouni, A., Huete, A. R., Kerr, Y. H., & Sorooshian, S. (1994). A modified soil adjusted vegetation index. *Remote Sensing of Environment*, *48*(2), 119–126. https://doi.org/10.1016/0034-4257(94)90134-1

Rajib, A., Evenson, G. R., Golden, H. E., & Lane, C. R. (2018). Hydrologic model predictability improves with spatially explicit calibration using remotely sensed evapotranspiration and biophysical parameters. *Journal of Hydrology*, *567*, 668–683. https://doi.org/10.1016/j.jhydrol.2018.10.024

Ranagalage, M., Estoque, R., & Murayama, Y. (2017). An Urban Heat Island Study of the Colombo Metropolitan Area, Sri Lanka, Based on Landsat Data (1997–2017). *International Journal of Geo-Information*, *6*, 17. https://doi.org/10.3390/ijgi6070189

Ribeiro, G., Silva, J., & Silva, J. (2016). Adjusted Vegetation Index to Solo (SAVI): State of the art and its potential. *Revista Brasileira de Geografia Física*, *9*. https://doi.org/10.5935/1984-2295.20160144

Richardson, A., & Weigand, C. (1977). *Distinguishing Vegetation from Soil Background Information*. https://www.asprs.org/wp-content/uploads/pers/1977journal/dec/1977_dec_1541-1552.pdf

Robledo, A. (2021). *Análisis del fenómeno de pardeamiento foliar y su relación con el proceso de evapotranspiración durante los eventos extremos de calor del periodo estival 2019-2020 en el Parque Nacional Río Clarillo*. https://repositorio.uchile.cl/handle/2250/186618

Rodriguez-Iturbe, I., D'Odorico, P., Laio, F., Ridolfi, L., & Tamea, S. (2007). Challenges in humid land ecohydrology: Interactions of water table and unsaturated zone with climate, soil, and vegetation. *Water Resources Research*, *43*(9). https://doi.org/10.1029/2007WR006073

Rodríguez-Moreno, V. M., & Bullock, S. H. (2013). Comparación espacial y temporal de índices de la vegetación para verdor y humedad y aplicación para estimar LAI en el Desierto Sonorense. *Revista mexicana de ciencias agrícolas*, *4*(4), 611–623.

Rondeaux, G., Steven, M., & Baret, F. (1996). Optimization of soil-adjusted vegetation indices. *Remote Sensing of Environment*, *55*(2), 95–107. https://doi.org/10.1016/0034-4257(95)00186-7

Rood, S. B., Patiño, S., Coombs, K., & Tyree, M. T. (2000). Branch sacrifice: Cavitation-associated drought adaptation of riparian cottonwoods. *Trees*, *14*(5), 248–257. https://doi.org/10.1007/s004680050010

Roujean, J.-L., & Breon, F.-M. (1995). Estimating PAR absorbed by vegetation from bidirectional reflectance measurements. *Remote Sensing of Environment*, *51*(3), 375–384. https://doi.org/10.1016/0034-4257(94)00114-3

Rouse, J. W., Haas, R. H., Deering, D. W., Schell, J. A., & Harlan, J. C. (1974). *Monitoring the Vernal Advancement and Retrogradation (Green Wave Effect) of Natural Vegetation* (E75-10354). https://ntrs.nasa.gov/citations/19750020419

Running, S. W., Nemani, R. R., Heinsch, F. A., Zhao, M., Reeves, M., & Hashimoto, H. (2004). A Continuous Satellite-Derived Measure of Global Terrestrial Primary Production. *BioScience*, *54*(6), 547–560. https://doi.org/10.1641/0006-3568(2004)054[0547:ACSMOG]2.0.CO;2

Sabour, M. H., Jafary, P., & Nematiyan, S. (2023). Applications and classifications of unmanned aerial vehicles: A literature review with focus on multi-rotors. *The Aeronautical Journal*, *127*(1309), 466–490. https://doi.org/10.1017/aer.2022.75

Salinas, J., Riquelme Espergue, F., Acuña Aroca, B., & Uribe M., A. (2019). *Crecimiento de renovales de Lenga (Nothofagus pumilio (Poepp. & Endl.) Krasser) en el sur austral de Chile*. https://bibliotecadigital.infor.cl/

Satellite Imaging Corporation. (2022). *RapidEye Satellite Sensor*. https://www.satimagingcorp.com/satellite-sensors/other-satellite-sensors/rapideye/

Schilling, O. S., Doherty, J., Kinzelbach, W., Wang, H., Yang, P. N., & Brunner, P. (2014). Using tree ring data as a proxy for transpiration to reduce predictive uncertainty of a model simulating groundwater–surface water–vegetation interactions. *Journal of Hydrology*, *519*, 2258–2271. https://doi.org/10.1016/j.jhydrol.2014.08.063

Sellers, P. (1985). Canopy reflectance, photosynthesis and transpiration. *International Journal of Remote Sensing*, *6*(8), 1335–1372. https://doi.org/10.1080/01431168508948283

Sellés, G., & Ferreyra, R. (2000). *El agua. Por qué es tan importante para las plantas*. https://biblioteca.inia.cl/handle/20.500.14001/5747

Serrano, L., Peñuelas, J., & Ustin, S. L. (2002). Remote sensing of nitrogen and lignin in Mediterranean vegetation from AVIRIS data: Decomposing biochemical from structural signals. *Remote Sensing of Environment*, *81*(2), 355–364. https://doi.org/10.1016/S0034-4257(02)00011-1

Servicio Geológico de Estados Unidos. (2024). *¿Cuáles son las designaciones de banda de los satélites Landsat?* https://www.usgs.gov/faqs/what-are-band-designations-landsat-satellites

Smith, R., Adams, J., Stephens, D., & Hick, P. T. (1995). Forecasting wheat yield in a Mediterranean-type environment from the NOAA satellite.

Australian Journal of Agricultural Research, *46*(1), 113–125. https://doi.org/10.1071/ar9950113

Sripada, R., Heiniger, R., White, J., & Weisz, R. (2005). Aerial Color Infrared Photography for Determining Late-Season Nitrogen Requirements in Corn. *Agronomy Journal*, *97*(5), 1443–1451. https://doi.org/10.2134/agronj2004.0314

Sudhanshu, P., Ames, D. P., & Panigrahi, S. (2010). Application of Vegetation Indices for Agricultural Crop Yield Prediction Using Neural Network Techniques. *Remote Sensing*, *2*(3), Article 3. https://doi.org/10.3390/rs2030673

Taia, S., Scozzari, A., Erraioui, L., Kili, M., Mridekh, A., Haida, S., Chao, J., & El Mansouri, B. (2023). Comparing the ability of different remotely sensed evapotranspiration products in enhancing hydrological model performance and reducing prediction uncertainty. *Ecological Informatics*, *78*, 102352. https://doi.org/10.1016/j.ecoinf.2023.102352

The European Space Agency. (s.f.a). *MERIS Overview*. https://earth.esa.int/eogateway/instruments/meris/description

The European Space Agency. (s.f.b). *SPOT 5*. https://earth.esa.int/eogateway/missions/spot-5

The European Space Agency. (s.f.c). *WorldView-2*. https://earth.esa.int/eogateway/missions/worldview-2

Tian, J., Wang, L., Li, X., Gong, H., Shi, C., Zhong, R., & Liu, X. (2017). Comparison of UAV and WorldView-2 imagery for mapping leaf area

index of mangrove forest. *International Journal of Applied Earth Observation and Geoinformation*, *61*, 22–31. https://doi.org/10.1016/j.jag.2017.05.002

Tucker, C. (1979). Red and photographic infrared linear combinations for monitoring vegetation. *Remote Sensing of Environment*, *8*(2), 127–150. https://doi.org/10.1016/0034-4257(79)90013-0

Tucker, C., Fung, I. Y., Keeling, C. D., & Gammon, R. H. (1986). Relationship between atmospheric CO2 variations and a satellite-derived vegetation index. *Nature*, *319*(6050), 195–199. https://doi.org/10.1038/319195a0

Ukkola, A. M., Prentice, I. C., Keenan, T. F., van Dijk, A. I. J. M., Viney, N. R., Myneni, R. B., & Bi, J. (2016). Reduced streamflow in water-stressed climates consistent with CO2 effects on vegetation. *Nature Climate Change*, *6*(1), 75–78. https://doi.org/10.1038/nclimate2831

Velasco López, S., Champo, O., España, M. L., & Baret, F. (2010). *Estimación del índice de área foliar en la Reserva de la Biósfera Mariposa Monarca*. https://www.scielo.org.mx/scielo.php?script=sci_arttext&pid=S0187-73802010000200010

Verrelst, J., Schaepman, M. E., Koetz, B., & Kneubühler, M. (2008). Angular sensitivity analysis of vegetation indices derived from CHRIS/PROBA data. *Remote Sensing of Environment*, *112*(5), 2341–2353. https://doi.org/10.1016/j.rse.2007.11.001

Vicente-Serrano, S. M., Camarero, J. J., Olano, J. M., Martín-Hernández, N., Peña-Gallardo, M., Tomás-Burguera, M., Gazol, A., Azorin-Molina, C.,

Bhuyan, U., & El Kenawy, A. (2016). Diverse relationships between forest growth and the Normalized Difference Vegetation Index at a global scale. *Remote Sensing of Environment*, *187*, 14–29. https://doi.org/10.1016/j.rse.2016.10.001

Vidican, R., Mălinaș, A., Ranta, O., Moldovan, C., Marian, O., Ghețe, A., Ghișe, C. R., Popovici, F., & Cătunescu, G. M. (2023). Using Remote Sensing Vegetation Indices for the Discrimination and Monitoring of Agricultural Crops: A Critical Review. *Agronomy*, *13*(12), Article 12. https://doi.org/10.3390/agronomy13123040

Vogelmann, J., Rock, B., & Moss, D. (1993). *Red edge spectral measurements from sugar maple leaves: International Journal of Remote Sensing: Vol 14, No 8*. https://www.tandfonline.com/doi/abs/10.1080/01431169308953986

Walther, G.-R., Post, E., Convey, P., Menzel, A., Parmesan, C., Beebee, T. J. C., Fromentin, J.-M., Hoegh-Guldberg, O., & Bairlein, F. (2002). Ecological responses to recent climate change. *Nature*, *416*(6879), 389–395. https://doi.org/10.1038/416389a

Wang, L., & Qu, J. J. (2007). NMDI: A normalized multi-band drought index for monitoring soil and vegetation moisture with satellite remote sensing. *Geophysical Research Letters*, *34*(20). https://doi.org/10.1029/2007GL031021

Wang, X., Wang, M., Wang, S., & Wu, Y. (2015). *Extracción de información de vegetación basada en teledetección UAV en banda de luz visible.*

https://d.wanfangdata.com.cn/periodical/ChlQZXJpb2RpY2FsQ0hJTmV3UzIwMjQwNzA0Eg9ueWdjeGIyMDE1MDUwMjIaCGx6enA3ZDJl

Weng, Q. (2011). *Advances in Environmental Remote Sensing: Sensors, Algorithms, and Applications*. CRC Press.

Woebbecke, D., Meyer, G., Von Bargen, K., & Mortensen, D. (1995). Color indices for weed identification under various soil, residue, and lighting conditions. *Transactions of the American Society of Agricultural Engineers*, *38*(1), 259–269. Scopus.

Wolf, A. (2012). Using WorldView-2 Vis-NIR multispectral imagery to support land mapping and feature extraction using normalized difference index ratios. *Algorithms and Technologies for Multispectral, Hyperspectral, and Ultraspectral Imagery XVIII*, *8390*, 188–195. https://doi.org/10.1117/12.917717

Xue, J., & Su, B. (2017a). Significant Remote Sensing Vegetation Indices: A Review of Developments and Applications. *Journal of Sensors*, *2017*(1), 1353691. https://doi.org/10.1155/2017/1353691

Xue, J., & Su, B. (2017b). Significant Remote Sensing Vegetation Indices: A Review of Developments and Applications. *Journal of Sensors*, *2017*(1), 1353691. https://doi.org/10.1155/2017/1353691

Yang, Z., Willis, P., & Mueller, R. (2008). *IMPACT OF BAND-RATIO ENHANCED AWIFS IMAGE TO CROP CLASSIFICATION ACCURACY*. https://www.asprs.org/a/publications/proceedings/pecora17/0041.pdf

Yazdani, R., Derenyi, E., & Ryerson, R. (1982). *Vegetation change detection in an agricultural area- A simple approach for use with geo-data base*. https://scholar.google.es/scholar?hl=es&as_sdt=0%2C5&q=Yazdani%2C+R.%2C+Ryerson%2C+A.+R.+and+Derenyi%2C+E.+%281981%29+Vegetation+change+detection+in+an+area%E2%80%94a+simple+approach+for+use+with+geo-data+base.+Proceedings+of+the+7th+Canadian+Symposium+on+Remote+Sensing%2C+Winnipeg%2C+Manitoba%2C+Canada%2C+88-92&btnG=

Zambrano, F., Lillo-Saavedra, M., Verbist, K., & Lagos, O. (2016). *Sixteen years of agricultural drought assessment of the bio bio in Chile using a 250 m resolution vegetation condition index (VCI)*.

Zarco-Tejada, P. J., Berjón, A., López-Lozano, R., Miller, J. R., Martín, P., Cachorro, V., González, M. R., & de Frutos, A. (2005). Assessing vineyard condition with hyperspectral indices: Leaf and canopy reflectance simulation in a row-structured discontinuous canopy. *Remote Sensing of Environment*, *99*(3), 271–287. https://doi.org/10.1016/j.rse.2005.09.002

Zarco-Tejada, P. J., González-Dugo, V., & Berni, J. A. J. (2012). Fluorescence, temperature and narrow-band indices acquired from a UAV platform for water stress detection using a micro-hyperspectral imager and a thermal camera. *Remote Sensing of Environment*, *117*, 322–337. https://doi.org/10.1016/j.rse.2011.10.007

Zeng, Z. (2018). *Impact of Earth Greening on the Terrestrial Water Cycle*. https://journals.ametsoc.org/view/journals/clim/31/7/jcli-d-17-0236.1.xml

Zhang, B., Wu, D., Zhang, L., Jiao, Q., & Li, Q. (2012). Application of hyperspectral remote sensing for environment monitoring in mining areas. *Environmental Earth Sciences*, *65*(3), 649–658. https://doi.org/10.1007/s12665-011-1112-y

Zhang, R., Rao, N., & Liao, K. (1996). *Approach for a Vegetation Index Resistant to Atmospheric Effect*. https://www.jipb.net/EN/abstract/abstract23925.shtml

Zhang, Y., Meng, Q., Wu, J., & Zhao, F. (2011). *Investigación sobre inversión del índice de vegetación ambiental y del índice de área foliar basada en datos CCD de satélites ambientales*. https://my.wanfangdata.com.cn/auth/user/alllogin.do?service=https%3a%2f%2foss.wanfangdata.com.cn%2fwww%2f%25E5%259F%25BA%25E4%25BA%258E%25E7%258E%25AF%25E5%25A2%2583%25E6%2598%259FCCD%25E6%2595%25B0%25E6%258D%25AE%25E7%259A%2584%25E7%258E%25AF%25E5%25A2%2583%25E6%25A4%258D%25E8%25A2%25AB%25E6%258C%2587%25E6%2595%25B0%25E5%258F%258A%25E5%258F%25B6%25E9%259D%25A2%25E7%25A7%25AF%25E6%258C%2587%25E6%2595%25B0%25E5%258F%258D%25E6%25BC%2594%25E7%25A0%2594%25E7%

25A9%25B6.ashx%3fisread%3dtrue%26type%3dperio%26resourceId%3dgpxygpfx201110043

Zhu, X., & Liu, D. (2015). Improving forest aboveground biomass estimation using seasonal Landsat NDVI time-series. *ISPRS Journal of Photogrammetry and Remote Sensing*, *102*, 222–231. https://doi.org/10.1016/j.isprsjprs.2014.08.014

7. ANEXO

7.1. Índices de vegetación identificados a partir de los *reviews* estudiados.

Tabla A 1. Índices de vegetación, junto con sus abreviaciones, fórmulas y fuentes, identificados a partir de los reviews analizados.

Índice	Abreviación	Fórmula	Autor y año	Cita
Simple Green Index	SGI	$\frac{NIR}{R}$	Birth & McVey, 1968	Xue & Su, 2017
Simple Ratio	SR	$\frac{R_{800}}{R_{670}}$; $\frac{\rho}{\rho_{RED}}$	Jordan, 1969	Xue & Su, 2017; Giovos et al., 2021; Glenn et al., 2008
Ratio Vegetation-Index	RVI	$\frac{R}{NIR}$	Pearson & Miller, 1972; Birth & McVey, 1968	Bannari et al., 1995; Xue & Su, 2017; Giovos et al., 2021

Continuación tabla anterior.

Vegetation Index Number	VIN	$\frac{NIR}{R}$	Pearson & Miller, 1972	Bannari et al., 1995
Normalized Difference Vegetation Index	NDVI	$\frac{(NIR - R)}{(NIR + R)}$	Rouse et al., 1974	Bannari et al., 1995; Xue & Su, 2017; Giovos et al., 2021; Glenn et al., 2008
Transformed Vegetation Index	TVI	$\sqrt{NDVI + 0.5}$	Rouse et al., 1974	Bannari et al., 1995
Transformed Vegetation Index	TVI	$\sqrt{NDVI + 0.5\,L}$	Rouse et al., 1974	Xue & Su, 2017
Green Vegetation Index	GVI	$(-0.283MSS4 - 0.660MSS5 + 0.577MSS6 + 0.388MSS7)$	Kauth & Thomas, 1976	Bannari et al., 1995; Xue & Su, 2017
Soil Brightness Index	SBI	$(0.332MSS4 + 0.603MSS5 + O.675MSS6 + 0.262MSS7)$	Kauth & Thomas, 1976	Bannari et al., 1995

Continuación tabla anterior.

Soil Brightness Index	SBI	$(-0.283MSS4 - 0.66MSS5 + 0.577MSS6 + 0.388MSS7)$	Kauth & Thomas, 1976	Xue & Su, 2017
Yellow Vegetation Index	YVI	$(-0.899MSS4 + 0.428MSS5 + 0.076MSS6 - 0.041MSS7)$	Kauth & Thomas, 1976	Bannari et al., 1995
Non Such Index	NSI	$(-0.016MSS4 + 0.131MSS5 - 0.425MSS6 + 0.882MSS7)$	Kauth & Thomas, 1976	Bannari et al., 1995
Yellow Vegetation Index	YVI	$(-0.283MSS4 - 0.66MSS5 + 0.577MSS6 + 0.388MSS7)$	Kauth & Thomas, 1976	Xue & Su, 2017
Soil Background Line	SBL	$(MSS7 - 2.4MSS5)$	Richardson & Weigand, 1977	Bannari et al., 1995; Xue & Su, 2017
Differenced Vegetation Index	DVI	$(2.4MSS7 - MSS5)$	Richardson & Weigand, 1977	Bannari et al., 1995; Xue & Su, 2017
Misra Soil Brightness Index	MSBI	$(0.406MSS4 + 0.600MSS5 + 0.645MSS6 + 0.243MSS7)$	Misra, 1977	Bannari et al., 1995; Xue & Su, 2017

Continuación tabla anterior.

Misra Green Vegetation Index	MGVI	$(-0.386MSS4 - 0.530MSS5 + 0.535MSS6 + 0.532MSS7)$	Misra, 1977	Bannari et al., 1995; Xue & Su, 2017
Misra Yellow Vegetation Index	MYVI	$(0.723MSS4 - 0.597MSS5 + 0.206MSS6 - 0.278MSS7)$	Misra, 1977	Bannari et al., 1995; Xue & Su, 2017
Misra Non Such Index	MNSI	$(0.404MSS4 - 0.039MSS5 - 0.505MSS6 + 0.762MSS7)$	Misra, 1977	Bannari et al., 1995; Xue & Su, 2017
Perpendicular Vegetation Index	PVI	$\sqrt{(\rho_{sol} - \rho_{veg})_R^2 + (\rho_{sol} - \rho_{veg})_{NIR}^2}$ $(DN_{NIR} - b)\cos\theta - DN_R \cdot \sin\theta$	Richardson & Weigand, 1977	Bannari et al., 1995; Xue & Su, 2017
Ashburn Vegetation Index	AVI	$(2.0MSS7 - MSS5)$	Ashburn, 1979	Bannari et al., 1995; Xue & Su, 2017
Greenness Above Bare Soil	GRABS	$(GVI - 0.09178SBI + 5.58959)$	Hay et al., 1979	Bannari et al., 1995; Xue & Su, 2017

Continuación tabla anterior.

Normalized Difference Green/Red Index	NGRDI	$\frac{(Green - Red)}{(Green + Red)}$	Tucker, 1979	Xue & Su, 2017
Perpendicular Vegetation Index	PVI	$\frac{(NIR - aR - b)}{\sqrt{a^2 + 1}}$	Jackson et al., 1980	Bannari et al., 1995; Xue & Su, 2017
Multi-Temporal Vegetation Index	MTVI	$(NDVI(date\ 2)\ -\ NDVI(date\ 1))$	Yazdani et al., 1982	Bannari et al., 1995; Giovos et al., 2021
Greenness Vegetation and Soil Brightness	GVSB	$\frac{GVI}{SBI}$	Badhwar, 1981	Bannari et al., 1995; Xue & Su, 2017
Crop water stress index	CWSI	$\frac{((T_c - T_a) - (T_c - T_a)_{ll})}{((T_c - T_a)_{ul} - (T_c - T_a)_{ll})}$	Idso et al., 1981	Xue & Su, 2017
Adjusted Soil Brightness Index	ASBI	$(2.0\ YVI)$	Jackson et al., 1983	Bannari et al., 1995; Xue & Su, 2017

Continuación tabla anterior.

Adjusted Green Vegetation Index	AGVI	$GVI - (1 + 0.018GVI)YVI - \frac{NSI}{2}$	Jackson et al., 1983	Bannari et al., 1995; Xue & Su, 2017
Transformed Vegetation Index	TVI	$\frac{(NDVI + 0.5)}{\lvert NDVI + 0.5\rvert}\sqrt{\lvert NDVI + 0.5\rvert}$	Perry & Lautensch alager, 1984	Bannari et al., 1995
Differenced Vegetation Index	DVI	$(NIR - R)$	Clevers, 1986	Bannari et al., 1995
Soil Adjusted Vegetation Index	SAVI	$\frac{(NIR - R)}{(NIR + R + L)}(1 + L)$	Huete, 1988	Bannari et al., 1995
Soil Adjusted Vegetation Index	SAVI	$\frac{(NIR - G)}{(NIR + G + L)} + (1 + L)$	Huete, 1988	Xue & Su, 2017
	II	$\frac{TM_5}{TM_7}$	Musick & Pelletier, 1988	Xue & Su, 2017
Transformed SAVI	TSAVI	$\frac{[a(NIR - aR - b)]}{(R + aNIR - ab)}$	Baret, 1989	Bannari et al., 1995; Xue & Su, 2017

Continuación tabla anterior.

Moisture Stress Index	MSI	$\frac{\rho_{1599}}{\rho_{819}}$	Hunt & Rock, 1989	Xue & Su, 2017
	DVI	$\int_{\lambda_1}^{\lambda_1}\left(\frac{d_\rho}{d_\lambda}\right)d_\lambda$	Demetriades-Shah et al., 1990	Xue & Su, 2017
Infrared Percentage Vegetation Index	IPVI	$\frac{TM_4}{TM_4+TM_3}$	Crippen, 1990	Xue & Su, 2017
Normalized Difference Greenness Index	NDGI	$\frac{(G-R)}{(G+R)}$	Courel et al., 1991	Bannari et al., 1995; Xue & Su, 2017
Redness Index	RI	$\frac{(R-G)}{(R+G)}$	Escadafal & Huete, 1991	Bannari et al., 1995; Xue & Su, 2017
Transformed SAVI	ATSAVI	$\frac{[a(NIR-aR-b)]}{[R+aNIR-ab+X(1+a^2)]}$	Baret & Guyot, 1991	Bannari et al., 1995; Xue & Su, 2017

Continuación tabla anterior.

Atmospherically Resistant Vegetation Index	ARVI	$\frac{(NIR - RB)}{(NIR + RB)}$ $RB = R - \gamma(B - R)$	Kaufman & Tanre, 1992	Bannari et al., 1995; Xue & Su, 2017
Global Environment Monitoring Index	GEMI	$\eta(1 - 0.25\eta) - \frac{(R - 0.125)}{(1 - R)}$ $\eta = \frac{[2(NIR^2 - R^2) + 1.5NIR + 0.5R]}{(NIR + R + 0.5)}$	Pinty & Verstraete, 1992	Bannari et al., 1995; Xue & Su, 2017
Physiological Reflectance Index	PRI	$\frac{(R_{531} - R_{570})}{(R_{531} + R_{570})}$	Gamon et al., 1992	Xue & Su, 2017; Giovos et al., 2021
Simple Ratio 5	SR5	$\frac{R_{675}}{R_{700}\, R_{650}}$	Chappelle et al., 1992	Xue & Su, 2017
Normalized Difference Index	NDI	$\frac{(NIR - MIR)}{(NIR + MIR)}$	McNairn & Protz, 1993	Bannari et al., 1995; Xue & Su, 2017
	DI1	$R_{800} - R_{550}$	Buschmann & Nagel, 1993	Xue & Su, 2017

Continuación tabla anterior.

Simple Ratio 2	SR2	$\frac{R_{800}}{R_{550}}$	Buschman n & Nagel, 1993	Xue & Su, 2017
Normalized Difference Index 3	NDI3	$\frac{(R_{734} - R_{747})}{(R_{715} - R_{726})}$	Vogelman n et al., 1993	Xue & Su, 2017
Simple Ratio 4	SR4	$\frac{R_{740}}{R_{720}}$	Vogelman n et al., 1993	Xue & Su, 2017
	VREI1	$\frac{R_{740}}{R_{720}}$	Vogelman n et al., 1993	Xue & Su, 2017
	VREI2	$\frac{(R_{734} - R_{747})}{(R_{715} - R_{726})}$	Vogelman n et al., 1993	Xue & Su, 2017
Simple Ratio 3	SR3	$\frac{R_{700}}{R_{670}}$	McMurtrey et al., 1994	Xue & Su, 2017
Transformed Soil Atmospherical ly Resistant Vegetation Index	TSARVI	$\frac{[a_{rb}(NIR - a_{rb}rb - b_{rb})]}{[RB + a_{rb}NIR - a_{rb}b_{rb} + X(1 + a_{rb}^2)]}$	Bannari, 1994	Bannari et al., 1995; Xue & Su, 2017

Continuación tabla anterior.

Modified SAVI	MSAVI	$\frac{2NIR + 1 - \sqrt{(2NIR + 1)^2 - 8(NIR - R)}}{2}$	Qi et al., 1994	Bannari et al., 1995
Modified SAVI	MSAVI	$0.5\ \{2R_{800} + 1 - SQRT[(2R_{800} + 1)^2 - 8(R_{800} - R_{670})]\ \}$	Qi et al., 1994	Xue & Su, 2017
Angular Vegetation Index	AVI	$tan^{-1}\left\{\frac{\lambda_3 - \lambda_2}{\lambda_2}[NIR - R]^{-1}\right\} + tan^{-1}\left\{\frac{\lambda_2 - \lambda_1}{\lambda_2}[G - R]^{-1}\right\}$	Plummer, 1994	Bannari et al., 1995; Xue & Su, 2017
Chlorophyll Absorption Ratio Index	CARI	$CAR\left(\frac{R_{700}}{R_{670}}\right)$	Kim et al., 1994	Xue & Su, 2017
Non-Linear Index	NLI	$\frac{(NIR^2 - Red)}{(NIR^2 + Red)}$	Goel & Qin, 1994	Xue & Su, 2017
Renormalized Difference Vegetation Index	RDVI	$\frac{(R_{800} - R_{670})}{[SQRT(R_{800} + R_{670})]}$	Roujean & Breon, 1995	Xue & Su, 2017
	RDVI	$\sqrt{NDIVI * DVI}$	Roujean & Breon, 1995	Xue & Su, 2017

Continuación tabla anterior.

First-order derivate green vegetation index derived using zero baseline	1DZ-DGVI	$\sum_{\lambda_1}^{\lambda_n} \lvert\rho'(\lambda_i)\rvert \Delta\lambda_i$	Elvidge & Chen, 1995	Xue & Su, 2017
Second-order derivate green vegetation index derived using zero baseline	2DZ-DGVI	$\sum_{\lambda_1}^{\lambda_n} \lvert\rho''(\lambda_i)\rvert \Delta\lambda_i$	Elvidge & Chen, 1995	Xue & Su, 2017
Excess Green	ExG	$2\ \rho_{green}\ \rho_{red}\ \rho_{blue}$	Woebbecke et al., 1995	Xue & Su, 2017; Giovos et al., 2021
Greenness index	G	$\frac{R_{400}}{R_{677}}$	Smith et al., 1995	Xue & Su, 2017
Vegetation Condition Index	VCI	$\frac{(NDVI_i - NDVI_{min})}{(NDVI_{max} - NDVI_{min})}$	Kogan, 1995	Xue & Su, 2017

Continuación tabla anterior.

Vegetation Health Index	VHI	$a\,VCI + (1-a)\,TCI$	Kogan, 1995	Xue & Su, 2017
Normalized Difference Water Index	NDWI	$\frac{Green - NIR}{Green + NIR}$	McFeeters, 1996	Xue & Su, 2017
Lichtenthaler Index	LIC 3	$\frac{R_{400}}{R_{740}}$	Lichtenthaler et al., 1996	Xue & Su, 2017
Normalized Difference Vegetation Index	NDVI	$\frac{R_{800} - R_{680}}{R_{800} + R_{680}}$	Lichtenthaler et al., 1996	Xue & Su, 2017
Atmospheric Effect Resistant Vegetation Index	IAVI	$\frac{\{\rho_{nir} - [\rho_r - \gamma(\rho_b - \rho_r)]\}}{\{\rho_{nir} + [\rho_r - \gamma(\rho_b - \rho_r)]\}}$	Zhang et al., 1996	Xue & Su, 2017
Modified SAVI 2	GM1	$\frac{R_{750}}{R_{550}}$	Gitelson & Merzlyak, 1996	Xue & Su, 2017
Modified Simple Ratio Optimization SAVI	GM2	$\frac{R_{750}}{R_{700}}$	Gitelson & Merzlyak, 1996	Xue & Su, 2017

Continuación tabla anterior.

Modified Simple Ratio Optimization SAVI 2	MSAVI2	$0.5\ [\ (2\ NIR + 1) - \sqrt{(2NIR + 1)^2 - 8(NIR - R)}]$	Chen, 1996	Xue & Su, 2017
	MSR	$\frac{[\left(\frac{R_{800}}{R_{670}}\right) - 1]}{[SQRT(R_{800}/R_{670} + 1)]}$	Chen, 1996	Xue & Su, 2017
	OSAVI	$\frac{(1 + 0.16)(R_{800} - R_{670})}{(R_{800} + R_{670} + 0.61)}$	Rondeaux et al., 1996	Xue & Su, 2017
Pigment-Specific Normalized Difference	PSNDa	$\frac{R_{800} - R_{680}}{R_{800} + R_{680}}$	Blackburn, 1998	Xue & Su, 2017
	PSNDb	$\frac{R_{800} - R_{635}}{R_{800} + R_{635}}$	Blackburn, 1998	Xue & Su, 2017
	PSNDc	$\frac{R_{800} - R_{470}}{R_{800} + R_{470}}$	Blackburn, 1998	Xue & Su, 2017
Pigment-Specific Simple Ratio	PSSRa	$\frac{R_{800}}{R_{680}}$	Blackburn, 1998	Xue & Su, 2017

Continuación tabla anterior.

	PSSRb	$\frac{R_{800}}{R_{635}}$	Blackburn, 1998	Xue & Su, 2017
	PSSRc	$\frac{R_{800}}{R_{470}}$	Blackburn, 1998	Xue & Su, 2017
	SR7	$\frac{R_{860}}{R_{550}\,R_{708}}$	Datt, 1998	Xue & Su, 2017
Normalized Difference Index 1	NDI1	$\frac{(R_{780}-R_{710})}{(R_{780}-R_{680})}$	Datt, 1999	Xue & Su, 2017
Normalized Difference Index 2	NDI2	$\frac{(R_{850}-R_{710})}{(R_{850}-R_{680})}$	Datt, 1999	Xue & Su, 2017
	MRENDVI	$\frac{(\rho_{750}-\rho_{705})}{(\rho_{750}+\rho_{705}-2\,\rho_{445})}$	Datt, 1999	Xue & Su, 2017
	MRESR	$\frac{(\rho_{750}-\rho_{445})}{(\rho_{705}-\rho_{445})}$	Datt, 1999	Xue & Su, 2017

Continuación tabla anterior.

	RGRI	$\frac{\sum_{i=500}^{690} R_I}{\sum_{i=500}^{599} R_J}$	Gamon & Surfus, 1999	Xue & Su, 2017
Plant Senescence Reflectance Index	PSRI	$\frac{(R_{680} - R_{500})}{R_{750}}$	Merzlyak et al., 1999	Xue & Su, 2017
Excess Red	ExR	$1.3\ R\ G$	Meyer et al., 1999	Giovos et al., 2021
Modified Chlorophyll Absorption Ratio Index	MCARI	$[(R_{700} - R_{670}) - 0.2(R_{700} - R_{550})]\left(\frac{R_{700}}{R_{670}}\right)$	Daughtry et al., 2000	Xue & Su, 2017; Giovos et al., 2021
Anth Reflectance Index	ARI	$[R_{550}^{-1} - R_{700}^{-1}]$	Gitelson et al., 2001	Xue & Su, 2017
	ARI2	$R_{NIR}[R_{550}^{-1} - R_{700}^{-1}]$	Gitelson et al., 2001	Xue & Su, 2017

Continuación tabla anterior.

Green Leaf Index	GLI	$\frac{2R_g - R_r - R_b}{2R_g + R_r + R_b}$	Louhaichi et al., 2001	Xue & Su, 2017
Green Normalized Difference Vegetation Index	GNDVI	$\frac{\rho_{NIR} - \rho_G}{\rho_{NIR} + \rho_G}$	Louhaichi et al., 2001	Xue & Su, 2017; Giovos et al., 2021
Cellulose Absorption Index	CAI	$0.5(R_2 + R_{2.2}) - R_{2.1}$	Daughtry, 2001	Xue & Su, 2017
Continuum-Removed Chlorophyll Well Eepth	CRCWD	$1 - \rho_{min}^{r}$	Broge & Leblanc, 2001	Xue & Su, 2017
Simple Ratio 6	SR6	$\frac{R_{672}}{R_{550}\, R_{708}}$	Haboudane et al., 2002	Xue & Su, 2017
Structure Intensive Pigment Index	SIPI	$\frac{(R_{800} - R_{445})}{(R_{800} - R_{680})}$	Haboudane et al., 2002	Xue & Su, 2017
Transformed Chlorophyll Absorption in Reflectance Index	TCARI	$3\,[((R_{700} - R_{670}) - 0.2\,((R_{700} - R_{550})\left(\frac{R_{700}}{R_{670}}\right)]$	Haboudane et al., 2002	Xue & Su, 2017

Continuación tabla anterior.

Normalized Difference Nitrogen Index	NDNI	$\frac{[\log\left(\frac{1}{\rho_{1510}}\right) - \log\left(\frac{1}{\rho_{1680}}\right)]}{[\log\left(\frac{1}{\rho_{1510}}\right) + \log\left(\frac{1}{\rho_{1680}}\right)]}$	Serrano et al., 2002	Xue & Su, 2017
Normalized Difference Lignin Index	NDLI	$\frac{[\log\left(\frac{1}{\rho_{1754}}\right) - \log\left(\frac{1}{\rho_{1680}}\right)]}{[\log\left(\frac{1}{\rho_{1754}}\right) + \log\left(\frac{1}{\rho_{1680}}\right)]}$	Serrano et al., 2002	Xue & Su, 2017
Enhanced Vegetation Index Transformed Difference Gegetation Index	EVI	$\frac{[(TM_4 - TM_3)(1+L)]}{(TM_4 - C_1 TM_3 + C_2 TM + L)}$ $G\frac{NIR\ -\ RED}{NIR\ +\ C1\,RED\ -\ C2\,BLUE\ +\ L}$	Huete et al., 2002	Xue & Su, 2017; Glenn et al., 2008
	TDVI	$\sqrt{0.5 + \left(\frac{NIR - Red}{NIR + Red}\right)}$	Bannari et al., 2002	Xue & Su, 2017
Visible Atmospherically Resistant Index Modified Chlorophyll Absorption Ratio Index	VARI	$(Green - Red)(Green + Red - Blue)$	Gitelson et al., 2002	Xue & Su, 2017

Continuación tabla anterior.

	MCARI	$0.5\,[120\,(R_{750}-R_{550})-200(R_{670}-R_{550})]$	Haboudane et al., 2004	Xue & Su, 2017; Giovos et al., 2021
Modified Triangular Vegetation Index	MTVI	$1.2\,[1.2\,((R_{800}-R_{550})-2.5((R_{670}-R_{550})]$	Haboudane et al., 2004	Xue & Su, 2017; Giovos et al., 2021
Modified Triangular Vegetation Index 2	MTVI2	$\frac{1.5\,[1.2\,((R_{800}-R_{550})-2.5((R_{670}-R_{550})]}{\sqrt{(2\,R_{800}+1)^2-(6\,R_{800}-5\,\sqrt{R_{670}})-0.5}}$	Haboudane et al., 2004	Xue & Su, 2017
Wide Dynamic Range Vegetation Index	WDRVI	$\frac{(\alpha\,\rho_{NIR}-\rho_{RED})}{(\alpha\,\rho_{NIR}+\rho_{RED})}$	Gitelson, 2004	Xue & Su, 2017
Excess Green and Red Green and Blue Index	ExGR	$ExG-ExR$	Neto, 2004	Giovos et al., 2021
	BGI1	$\frac{R_{400}}{R_{550}}$	Zarco-Tejada et al., 2005	Xue & Su, 2017

Continuación tabla anterior.

	BGI2	$\frac{R_{450}}{R_{550}}$	Zarco-Tejada et al., 2005	Xue & Su, 2017
Zarco and Miller	ZM	$\frac{R_{750}}{R_{710}}$	Zarco-Tejada et al., 2005	Xue & Su, 2017
Green Difference Vegetation Index	GDVI	$NIR - Green$	Sripada et al., 2005	Xue & Su, 2017
Green Ratio Vegetation Index	GRVI	$\frac{NIR}{Green}$	Sripada et al., 2005	Xue & Su, 2017
Carotenoids and Chlorophyll Reflectance Index	CRI500	$\frac{1/R_{515}}{1/R_{550}}$	Gitelson et al., 2006	Xue & Su, 2017
	CRI700	$\frac{1/R_{515}}{1/R_{700}}$	Gitelson et al., 2006	Xue & Su, 2017
Ratio Analysis of Reflectance Spectra	RARS	$\frac{R_{746}}{R_{513}}$	Gitelson et al., 2006; Chappelle et al., 1992	Xue & Su, 2017

Continuación tabla anterior.

Normalized Multi-band Drought Index Water Band Index	NMDI	$\frac{[\rho_{860} - (\rho_{1640-}\rho_{1230})]}{[\rho_{860} + (\rho_{1640-}\rho_{1230})]}$	Wang & Qu, 2007	Xue & Su, 2017
	WBI	$\frac{R_{970}}{R_{900}}$	Wang & Qu, 2007	Xue & Su, 2017
Modifies Nonlinear Vegetation Index (NLI)	MNLI	$\frac{[(NIR^2 - Red)(1 + L)]}{(NIR^2 + Red + L)}$	Yang et al., 2008	Xue & Su, 2017
	NGBDI	$\frac{(Green - Red)}{(Green + Blue)}$	Verrelst et al., 2008	Xue & Su, 2017
HJ Satellite Vegetation Index	HJVI	$\frac{[2(\rho_{NIR} - \rho_{RED})]}{(\rho_{NIR} + 6\rho_{RED} - 7.5\rho_{BLUE} + 1)}$	Zhang et al., 2011	Xue & Su, 2017
	SDr	$\sum_N \rho'(\lambda_i)$	Weng, 2011	Xue & Su, 2017

Continuación tabla anterior.

Blue and Red Index	BRI1	$\frac{R_{400}}{R_{690}}$	Zarco-Tejada et al., 2012	Xue & Su, 2017
	BRI2	$\frac{R_{450}}{R_{690}}$	Zarco-Tejada et al., 2012	Xue & Su, 2017
Green and NIR Index	GARI	$\frac{\{NIR - [Green - \gamma(Blue - Red)]\}}{\{NIR + [Green - \gamma(Blue - Red)]\}}$	Zhang et al., 2012	Xue & Su, 2017
WorldView-Vegetation Index	WV-VI	$\frac{(NIR2 - Red)}{(NIR2 + Red)}$	Wolf, 2012	Xue & Su, 2017
Health-Index	HI	$\frac{(R_{534} - R_{698})}{(R_{534} + R_{698})} - 0.5\, R_{704}$	Mahlein et al., 2013	Xue & Su, 2017
Canopy Chlorophyll Content Index	CCCI	$\frac{(NDRE - NDRE_{min})}{(NDRE_{max} - NDRE_{min})}$	Li et al., 2014	Xue & Su, 2017
Visible Band Difference Vegetation Index	VDVI	$\frac{(2\,\rho_{GREEN} - \rho_{RED} - \rho_{BLUE})}{(2\,\rho_{GREEN} + \rho_{RED} + \rho_{BLUE})}$	Wang et al., 2015	Xue & Su, 2017

7.2. Base de datos de los artículos sobre índices de vegetación ingresada a Chat-GPT.

Para realizar el análisis de los artículos se ingresó a Chat-GPT una base de datos .bib con el *promt* “extraer datos de títulos, palabras clave, autor, año de publicación y resumen de cada estudio”, a partir de lo cual se obtuvo lo siguiente presentado en formato .txt.

@article{gitelson_wide_2004,

title = {Wide {Dynamic} {Range} {Vegetation} {Index} for {Remote} {Quantification} of {Biophysical} {Characteristics} of {Vegetation}},

volume = {161},

issn = {0176-1617},

url = {https://www.sciencedirect.com/science/article/pii/S0176161704705726},

doi = {10.1078/0176-1617-01176},

abstract = {El Índice de Vegetación de Diferencia Normalizada (NDVI) se usa ampliamente para monitorear, analizar y mapear distribuciones temporales y espaciales de características fisiológicas y biofísicas de la vegetación. Está bien documentado que el NDVI se acerca a la saturación asintóticamente en condiciones de biomasa aérea de moderada a alta. Mientras que la reflectancia en la región roja (ρred) muestra una respuesta casi plana una vez que el índice de área foliar (LAI) excede 2, la reflectancia

en el infrarrojo cercano (NIR) (ρNIR) continúa respondiendo significativamente a cambios en la densidad de vegetación de moderada a alta (LAI de 2 a 6) en cultivos. Sin embargo, esta mayor sensibilidad del ρNIR tiene poco efecto sobre los valores de NDVI una vez que el ρNIR supera el 30 \%. En este artículo se propuso una modificación simple del NDVI. El índice de vegetación de amplio rango dinámico, WDRVI = (a * ρNIR-ρred)/(a * ρNIR+ρred), donde el coeficiente de ponderación a tiene un valor de 0,1 a 0,2, aumenta la correlación con la fracción de vegetación al linealizar la relación para el trigo típico. , soya y maíz. La sensibilidad del WDRVI al LAI moderado a alto (entre 2 y 6) fue al menos tres veces mayor que la del NDVI. Al mejorar el rango dinámico mientras se utilizan las mismas bandas que el NDVI, el WDRVI permite una caracterización más sólida de las características fisiológicas y fenológicas del cultivo. Aunque este índice necesita una evaluación adicional, la relación lineal con la fracción de vegetación y una sensibilidad mucho mayor al cambio en el LAI serán especialmente valiosas para la agricultura de precisión y el monitoreo del estado de la vegetación en condiciones de densidad moderada a alta. Se prevé que el nuevo índice complementará el NDVI y otros índices de vegetación que se basan en las bandas espectrales roja y NIR.},

number = {2},

urldate = {2024-08-27},

journal = {Journal of Plant Physiology},

author = {Gitelson, Anatoly A.},

month = jan,

year = {2004},

keywords = {leaf area index, reflectance, remote estimation, vegetation fraction, vegetation index},

pages = {165--173},

file = {ScienceDirect Snapshot:files/244/S0176161704705726.html:text/html},

}

@article{huang_commentary_2021,

title = {A commentary review on the use of normalized difference vegetation index ({NDVI}) in the era of popular remote sensing},

volume = {32},

issn = {1993-0607},

url = {https://doi.org/10.1007/s11676-020-01155-1},

doi = {10.1007/s11676-020-01155-1},

abstract = {The Normalized Difference Vegetation Index (NDVI), one of the earliest remote sensing analytical products used to simplify the complexities of multi-spectral imagery, is now the most popular index used for vegetation assessment. This popularity and widespread use relate to how an NDVI can be calculated with any multispectral sensor with a visible and a near-IR band. Increasingly low costs and weights of multispectral sensors mean they can be mounted on satellite, aerial, and increasingly—Unmanned Aerial

Systems (UAS). While studies have found that the NDVI is effective for expressing vegetation status and quantified vegetation attributes, its widespread use and popularity, especially in UAS applications, carry inherent risks of misuse with end users who received little to no remote sensing education. This article summarizes the progress of NDVI acquisition, highlights the areas of NDVI application, and addresses the critical problems and considerations in using NDVI. Detailed discussion mainly covers three aspects: atmospheric effect, saturation phenomenon, and sensor factors. The use of NDVI can be highly effective as long as its limitations and capabilities are understood. This consideration is particularly important to the UAS user community.},

language = {en},

number = {1},

urldate = {2024-08-27},

journal = {Journal of Forestry Research},

author = {Huang, Sha and Tang, Lina and Hupy, Joseph P. and Wang, Yang and Shao, Guofan},

month = feb,

year = {2021},

keywords = {Calibración, Efecto atmosférico, Fenómeno de saturación, Índice de volatilidad de nitrógeno (NDVI), Infrarrojo cercano, Multiespectral, Teledetección con drones, UAS},

pages = {1--6},

file = {Texto completo:files/246/Huang et al. - 2021 - A commentary review on the use of normalized diffe.pdf:application/pdf},

}

@article{didan_modis_nodate,

title = {{MODIS} {Vegetation} {Index} {User}'s {Guide} ({MOD13} {Series})},

url = {https://modis-land.gsfc.nasa.gov/pdf/MOD13_User_Guide_V61.pdf},

abstract = {One of the primary interests of the Earth Observing System (EOS) program is to study the quantity

and role of terrestrial vegetation in large-scale global processes with the goal of understanding

howtheEarth functionsas a system. This requires an understanding of the global distribution of

vegetation types as well as their biophysical and structural properties and spatial/temporal

variations. Vegetation Indices (VI) are robust, empirical measures of vegetation activity at the land

surface. They are designed to enhance the vegetation reflected signal from measured spectral

responses by combining two (or more) wavebands, often in the red (0.6 - 0.7 µm) and NIR

wavelengths (0.7-1.1 µm)regions.},

language = {en},

author = {Didan, Kamel and Munoz, Armando Barreto},

file = {Didan y Munoz - MODIS Vegetation Index User's Guide (MOD13 Series).pdf:files/247/Didan y Munoz - MODIS Vegetation Index User's Guide (MOD13 Series).pdf:application/pdf},

}

@article{jin_significant_2017,

title = {Significant {Remote} {Sensing} {Vegetation} {Indices}: {A} {Review} of {Developments} and {Applications}},

volume = {2017},

copyright = {Copyright © 2017 Jinru Xue and Baofeng Su.},

issn = {1687-7268},

shorttitle = {Significant {Remote} {Sensing} {Vegetation} {Indices}},

url = {https://onlinelibrary.wiley.com/doi/abs/10.1155/2017/1353691},

doi = {10.1155/2017/1353691},

abstract = {Los índices de vegetación (IV) obtenidos a partir de marquesinas basadas en sensores remotos son algoritmos bastante simples y efectivos para evaluaciones cuantitativas y cualitativas de la cobertura vegetal, el vigor y la dinámica de crecimiento, entre otras aplicaciones. Estos índices se han implementado ampliamente en aplicaciones RS utilizando diferentes plataformas aéreas y satelitales con avances recientes que utilizan

vehículos aéreos no tripulados (UAV). Hasta la fecha, no existe una expresión matemática unificada que defina todos los VI debido a la complejidad de las diferentes combinaciones de espectros de luz, instrumentación, plataformas y resoluciones utilizadas. Por lo tanto, se han desarrollado y probado algoritmos personalizados en una variedad de aplicaciones de acuerdo con expresiones matemáticas específicas que combinan la radiación de luz visible, principalmente la región del espectro verde, de la vegetación, y espectros no visibles para obtener cuantificaciones indirectas de la superficie de la vegetación. En las aplicaciones del mundo real, los VI de optimización generalmente se adaptan a los requisitos específicos de la aplicación junto con herramientas y metodologías de validación apropiadas en el terreno. El presente estudio presenta las características espectrales de la vegetación y resume el desarrollo de los VI y las ventajas y desventajas de los diferentes índices desarrollados. Este artículo revisa más de 100 VI, discutiendo su aplicabilidad específica y representatividad de acuerdo con la vegetación de interés, el entorno y la precisión de la implementación. Como era de esperar, la investigación y el desarrollo de VI, que se basan en plataformas hiperespectrales y UAV, tendrían una amplia aplicabilidad en diferentes áreas.},

language = {en},

number = {1},

urldate = {2024-09-08},

journal = {Journal of Sensors},

author = {Jin, Xue and Baofeng, Suministros de},

year = {2017},

note = {_eprint: https://onlinelibrary.wiley.com/doi/pdf/10.1155/2017/1353691},

pages = {1353691},

file = {Full Text PDF:files/274/Xue y Su - 2017 - Significant Remote Sensing Vegetation Indices A R.pdf:application/pdf;Snapshot:files/275/1353691.html:text/html},

}

@book{rouse_third_1974,

title = {Third {Earth} {Resources} {Technology} {Satellite}-1 {Symposium}: {Section} {A}-{B}. {Technical} presentations},

shorttitle = {Third {Earth} {Resources} {Technology} {Satellite}-1 {Symposium}},

abstract = {The Third Symposium on Significant Results Obtained from the first Earth Resources Technology Satellite (ERTS-1) was held from December 10-14, 1973 at the Statler Hilton Hotel in Washington, D.C. The Symposium was sponsored by the National Aeronautics and Space Administration, Goddard Space Flight Center. The structure of this Symposium was similar to the one held from March 5-9, 1973. The Opening Plenary Session on Monday morning contained two papers of general interest to the entire audience, one on the status of the ERTS-1 system and a report on the

Canadian ERTS program. The next two and one-half days were devoted to contributed papers in the various disciplines presented during three parallel sessions. These papers are contained in Volume I of the Proceedings.

The Thursday Summary Session, as before, was designed to highlight and summarize the significant results from the first three days and also to present some typical examples of the applications of ERTS data for solving resources management problems at the national, state and local levels. This Session was highlighted by an introductory address by Dr. James C. Fletcher, NASA Administrator, and by a keynote address by Dr. John C. Whitaker, Under Secretary of the Interior, U.S. Department of the Interior. The presentations from this session are contained in Volume II of the Proceedings.

Volume II contains the Discipline Summary Reports. These are based on a report produced from a two-week long set of extensive interviews with the individual ERTS-1 Principal Investigators. This set of interviews was held between March 5 and the Third ERTS Symposium. The interviews were organized and directed by Dr. Robert P. Saunders of the ERTS Program Office at the Johnson Space Center and were held at the Goddard Space Flight Center from October 22 to November 2, 1973. The Discipline Summary Reports were written by Working Groups in each of the disciplines which convened on Friday, December 14. These Working Groups were chaired by the respective discipline session chairmen and were composed of selected

specialists within the various disciplines. Opinions and recommendations expressed in these reports are those of the panel members and do not necessarily reflect an official position of NASA},

language = {en},

publisher = {Scientific and Technical Information Office, National Aeronautics and Space Administration},

author = {Rouse, J. and Haas, Jr. and Schell, J. and Deering, D.},

year = {1974},

note = {Google-Books-ID: cl42FB2_UEcC},

}

@article{asrar_estimating_1984,

title = {Estimating {Absorbed} {Photosynthetic} {Radiation} and {Leaf} {Area} {Index} from {Spectral} {Reflectance} in {Wheat}},

volume = {76},

copyright = {© American Society of Agronomy},

issn = {1435-0645},

url = {https://onlinelibrary.wiley.com/doi/abs/10.2134/agronj1984.00021962007600020029x},

doi = {10.2134/agronj1984.00021962007600020029x},

abstract = {Some plant growth models require estimates of leaf area and absorbed radiation for simulating evapotranspiration and photosynthesis.

Previous studies indicated that spectral reflectance, absorption of photosynthetically active radiation (PAR), and leaf area index (LAI) are interrelated. The objective of this study was to establish a procedure by which spectral reflectance can be used to simultaneously estimate PAR absorption and LAI. A method is presented for estimating the quantity of absorbed PAR by wheat (Triticum aestivumL.) plants and their LAI based on the normalized difference (ND), transformation of the near infrared (ρn= 800 to 1100 nm) and red (ρr= 600 to 700 nm) canopy reflectances. The results, from a theoretical analysis and field measurements, indicated that ND correlates with the fraction of PAR absorbed by wheat canopies. Bare soil reflectance and scattering of near infrared radiation by foliage elements were the major factors that influenced the relation between ND and PAR absorption. The estimated PAR absorption values, based on the ND, and four classes of assumed leaf angles (45°, 60°, 75°, and spherical), were used to indirectly evaluate LAI of wheat for three different geographical locations. The standard deviation on mean predicted to measured LAI's for the three locations varied from 0.5 to 0.9 for a range of 0 to 6 LAI. The method is considerably less sensitive in predicting LAI above 6.0 since the sensitivity of ND to changes in LAI becomes small ({\textless}0.01), due to small changes in canopy reflectance.},

language = {en},

number = {2},

urldate = {2024-09-08},

journal = {Agronomy Journal},

author = {Asrar, G. and Fuchs, M. and Kanemasu, E. T. and Hatfield, J. L.},

year = {1984},

note = {_eprint: https://onlinelibrary.wiley.com/doi/pdf/10.2134/agronj1984.00021962007600020029x},

keywords = {Remote sensing, Light interception, Normalized difference},

pages = {300--306},

file = {Snapshot:files/284/agronj1984.html:text/html},

}

@article{holben_characteristics_1986,

title = {Characteristics of maximum-value composite images from temporal {AVHRR} data},

volume = {7},

issn = {0143-1161},

url = {https://doi.org/10.1080/01431168608948945},

doi = {10.1080/01431168608948945},

abstract = {Red and near-infrared satellite data from the Advanced Very High Resolution Radiometer sensor have been processed over several days and combined to produce spatially continuous cloud-free imagery over large areas with sufficient temporal resolution to study green-vegetation dynamics. The technique minimizes cloud contamination, reduces directional reflectance

and off-nadir viewing effects, minimizes sun-angle and shadow effects, and minimizes aerosol and water-vapour effects. The improvement is highly dependent on the state of the atmosphere, surface-cover type, and the viewing and illumination geometry of the sun, target and sensor. An example from southern Africa showed an increase of 40 per cent from individual image values to the final composite image. Limitations' associated with the technique are discussed, and recommendations are given to improve this approach},

number = {11},

urldate = {2024-09-08},

journal = {International Journal of Remote Sensing},

author = {Holben, Brent},

month = nov,

year = {1986},

note = {Publisher: Taylor \& Francis
_eprint: https://doi.org/10.1080/01431168608948945},

pages = {1417--1434},

}

@article{sellers_canopy_1985,

title = {Canopy reflectance, photosynthesis and transpiration},

volume = {6},

issn = {0143-1161},

url = {https://doi.org/10.1080/01431168508948283},

doi = {10.1080/01431168508948283},

abstract = {A two-stream approximation model of radiative transfer is used to calculate values of hemispheric canopy reflectance in the visible and near-infrared wavelength intervals. Simple leaf models of photosynthesis and stomatal resistance are integrated over leaf orientation and canopy depth to obtain estimates of canopy photosynthesis and bulk stomatal or canopy resistance. The ratio of near-infrared and visible reflectances is predicted to be a near linear indicator of minimum canopy resistance and photosynthetic capacity but a poor predictor of leaf area index or biomass.},

number = {8},

urldate = {2024-09-08},

journal = {International Journal of Remote Sensing},

author = {Sellers, P},

month = aug,

year = {1985},

note = {Publisher: Taylor \& Francis
_eprint: https://doi.org/10.1080/01431168508948283},

pages = {1335--1372},

file = {Full Text PDF:files/287/SELLERS - 1985 - Canopy reflectance, photosynthesis and transpirati.pdf:application/pdf},

}

@article{tucker_relationship_1986,

title = {Relationship between atmospheric {CO2} variations and a satellite-derived vegetation index},

volume = {319},

copyright = {1986 Springer Nature Limited},

issn = {1476-4687},

url = {https://www.nature.com/articles/319195a0},

doi = {10.1038/319195a0},

abstract = {Estimates derived from satellite data of photosynthetically active radiation absorbed by terrestrial vegetation correlate with atmospheric carbon dioxide concentrations measured at surface recording stations, suggesting that satellite data can be used to estimate terrestrial photosynthesis.},

language = {en},

number = {6050},

urldate = {2024-09-08},

journal = {Nature},

author = {Tucker, C and Fung, I. Y. and Keeling, C. D. and Gammon, R. H.},

month = jan,

year = {1986},

note = {Publisher: Nature Publishing Group},

keywords = {Humanities and Social Sciences, multidisciplinary, Science},

pages = {195--199},
}

@misc{kaufman_atmospherically_1992,
title = {Atmospherically resistant vegetation index ({ARVI}) for {EOS}-{MODIS} {\textbar} {IEEE} {Journals} \& {Magazine} {\textbar} {IEEE} {Xplore}},
url = {https://ieeexplore.ieee.org/abstract/document/134076},
abstract = {An atmospherically resistant vegetation index (ARVI) is proposed and developed for remote sensing of vegetation from the Earth Observing System (EOS) MODIS sensor. The same index can be used for remote sensing from Landsat TM and the EOS-HIRIS sensor. The index takes advantage of the presence of the blue channel (0.47.+or-0.01 mu m) in the MODIS sensor, in addition to the red (0.66+or-0.025 mu m) and the near-IR (0.865+or-0.02 mu m) channels that compose the present normalized difference vegetation index (NDVI). The resistance of the ARVI to atmospheric effects (in comparison to the NDVI) is accomplished by a self-correction process for the atmospheric effect on the red channel, using the difference in the radiance between the blue and the red channels to correct the radiance in the red channel. Simulations using radiative transfer computations on arithmetic and natural surface spectra, for various atmospheric conditions, show that ARVI has a similar dynamic range to the NDVI, but is, on average, four times less sensitive to atmospheric effects than the NDVI},
urldate = {2024-09-08},

author = {Kaufman, Y.J. and Tanre, D.},

year = {1992},

file = {Atmospherically resistant vegetation index (ARVI) for EOS-MODIS | IEEE Journals & Magazine | IEEE Xplore:files/290/134076.html:text/html},

}

@article{huete_soil-adjusted_1988,

title = {A soil-adjusted vegetation index ({SAVI})},

volume = {25},

issn = {0034-4257},

url = {https://www.sciencedirect.com/science/article/pii/003442578890106X},

doi = {10.1016/0034-4257(88)90106-X},

abstract = {A transformation technique is presented to minimize soil brightness influences from spectral vegetation indices involving red and near-infrared (NIR) wavelengths. Graphically, the transformation involves a shifting of the origin of reflectance spectra plotted in NIR-red wavelength space to account for first-order soil-vegetation interactions and differential red and NIR flux extinction through vegetated canopies. For cotton (Gossypium hirsutum L. var DPI-70) and range grass (Eragrosticslehmanniana Nees) canopies, underlain with different soil backgrounds, the transformation nearly eliminated soil-induced variations in vegetation indices. A physical basis for the soil-

adjusted vegetation index (SAVI) is subsequently presented. The SAVI was found to be an important step toward the establishment of simple °lobal" that can describe dynamic soil-vegetation systems from remotely sensed data.},

number = {3},

urldate = {2024-09-08},

journal = {Remote Sensing of Environment},

author = {Huete, A.},

month = aug,

year = {1988},

pages = {295--309},

file = {ScienceDirect Snapshot:files/292/003442578890106X.html:text/html},

}

@inproceedings{baret_tsavi_1989,

title = {{TSAVI}: {A} vegetation index which minimizes soil brightness effects on {LAI} and {APAR} estimation},

volume = {3},

shorttitle = {{TSAVI}},

doi = {10.1109/IGARSS.1989.576128},

abstract = {Soil optical properties affect the spectral response of crop canopies and induce noise onto the relationships between reflectance data and crop characteristics, such as leaf area index (LAI) or absorbed

photosynthetically active radiation (APAR). Different combinations of red and near-infrared bands have been proposed, but these still suffered from a high sensitivity to soil brightness. As ideal vegetation index does not exist, an improved vegetation index, the transformed soil adjusted vegetation index (TSAVI) is described. The SAIL model has been used to simulate, in different conditions, the relationship between TSAVI and LAI or APAR. Experimental data recorded on wheat crops during the growing season are in good agreement with previous theoretical results.},

author = {Baret, Frederic and Guyot, G. and Major, David},

month = aug,

year = {1989},

pages = {1355--1358},

file = {Full Text PDF:files/294/Frederic et al. - 1989 - TSAVI A vegetation index which minimizes soil bri.pdf:application/pdf},

}

@book{jones_remote_2010,

title = {Remote {Sensing} of {Vegetation}: {Principles}, {Techniques}, and {Applications}},

isbn = {978-0-19-920779-4},

shorttitle = {Remote {Sensing} of {Vegetation}},

url = {https://books.google.es/books?hl=es&lr=&id=sTmcAQAAQBAJ&oi=fnd&pg=

PR5&dq=Jones+HG,+Vaughan+RA+(2010)+Remote+sensing+of+vegetation:+principles,+techniques,+and+applications.+Oxford+University+Press,+New+York,+p+353&ots=0gWI8EhY4X&sig=E5ej42Y5QA_abs1tqnqazl14EV4#v=onepage&q&f=false},

abstract = {Remote sensing is becoming an increasingly important tool for agriculturalists, ecologists, and land managers for the study of Earth's agricultural and natural vegetation, and can be applied to further our understanding of key environmental issues, including climate change and ecosystem management. This timely introduction offers an accessible yet rigorous treatment of the basics of remote sensing at all scales, illustrating its practical application to the study of vegetation. Despite a quantitative approach, the advanced mathematics and complex models common in modern remote sensing literature is demystified through clear explanations that emphasise the key underlying principles, and the core physical aspects are explained in the biological context of vegetation and its adaptation to its specific environment. Various techniques and instruments are addressed, making this a valuable source of reference, and the advantages and disadvantages of these are further illustrated through worked examples and case studies. · Rigorous physical and mathematical principles presented in a way readily understood by those without a strong mathematical background · Boxes throughout summarize key information and concepts · The student is directed to carefully chosen further reading articles, allowing them to explore key topics in more detail Online Resource Centre The Online Resource Centre to accompany

Remote Sensing of Vegetation features: For Students: · Links to useful websites For lecturers: · Figures from the book in electronic format, ready to download},

language = {en},

publisher = {OUP Oxford},

author = {Jones, Hamlyn G. and Vaughan, Robin A.},

month = jul,

year = {2010},

note = {Google-Books-ID: sTmcAQAAQBAJ},

keywords = {Gardening / Vegetables, Nature / Plants / General, Science / Earth Sciences / Geography, Science / Life Sciences / Biology, Science / Life Sciences / Ecology, Science / Space Science / Astronomy, Technology \& Engineering / Remote Sensing \& Geographic Information Systems},

}

@article{jiang_analysis_2006,

title = {Analysis of {NDVI} and scaled difference vegetation index retrievals of vegetation fraction},

volume = {101},

issn = {0034-4257},

url = {https://www.sciencedirect.com/science/article/pii/S0034425706000290},

doi = {10.1016/j.rse.2006.01.003},

abstract = {The normalized difference vegetation index (NDVI) is the most widely used vegetation index for retrieval of vegetation canopy biophysical properties. Several studies have investigated the spatial scale dependencies of NDVI and the relationship between NDVI and fractional vegetation cover, but without any consensus on the two issues. The objectives of this paper are to analyze the spatial scale dependencies of NDVI and to analyze the relationship between NDVI and fractional vegetation cover at different resolutions based on linear spectral mixing models. Our results show strong spatial scale dependencies of NDVI over heterogeneous surfaces, indicating that NDVI values at different resolutions may not be comparable. The nonlinearity of NDVI over partially vegetated surfaces becomes prominent with darker soil backgrounds and with presence of shadow. Thus, the NDVI may not be suitable to infer vegetation fraction because of its nonlinearity and scale effects. We found that the scaled difference vegetation index (SDVI), a scale-invariant index based on linear spectral mixing of red and near-infrared reflectances, is a more suitable and robust approach for retrieval of vegetation fraction with remote sensing data, particularly over heterogeneous surfaces. The proposed method was validated with experimental field data, but further validation at the satellite level would be needed.},

number = {3},

urldate = {2024-09-09},

journal = {Remote Sensing of Environment},

author = {Jiang, Zhangyan and Huete, Alfredo R. and Chen, Jin and Chen, Yunhao and Li, Jing and Yan, Guangjian and Zhang, Xiaoyu},

month = apr,

year = {2006},

keywords = {NDVI, Scale effect of NDVI, SDVI, Vegetation fraction retrieval},

pages = {366--378},

file = {ScienceDirect Snapshot:files/303/S0034425706000290.html:text/html},

}

@article{glenn_relationship_2008,

title = {Relationship {Between} {Remotely}-sensed {Vegetation} {Indices}, {Canopy} {Attributes} and {Plant} {Physiological} {Processes}: {What} {Vegetation} {Indices} {Can} and {Cannot} {Tell} {Us} {About} the {Landscape}},

volume = {8},

copyright = {http://creativecommons.org/licenses/by/3.0/},

issn = {1424-8220},

shorttitle = {Relationship {Between} {Remotely}-sensed {Vegetation} {Indices}, {Canopy} {Attributes} and {Plant} {Physiological} {Processes}},

url = {https://www.mdpi.com/1424-8220/8/4/2136},

doi = {10.3390/s8042136},

abstract = {Vegetation indices (VIs) are among the oldest tools in remote sensing studies. Although many variations exist, most of them ratio the reflection of light in the red and NIR sections of the spectrum to separate the landscape into water, soil, and vegetation. Theoretical analyses and field studies have shown that VIs are near-linearly related to photosynthetically active radiation absorbed by a plant canopy, and therefore to light-dependent physiological processes, such as photosynthesis, occurring in the upper canopy. Practical studies have used time-series VIs to measure primary production and evapotranspiration, but these are limited in accuracy to that of the data used in ground truthing or calibrating the models used. VIs are also used to estimate a wide variety of other canopy attributes that are used in Soil-Vegetation-Atmosphere Transfer (SVAT), Surface Energy Balance (SEB), and Global Climate Models (GCM). These attributes include fractional vegetation cover, leaf area index, roughness lengths for turbulent transfer, emissivity and albedo. However, VIs often exhibit only moderate, non-linear relationships to these canopy attributes, compromising the accuracy of the models. We use case studies to illustrate the use and misuse of VIs, and argue for using VIs most simply as a measurement of canopy light absorption rather than as a surrogate for detailed features of canopy architecture. Used this way, VIs are compatible with "Big Leaf" SVAT and GCMs that assume that canopy carbon and moisture fluxes have the same relative response to the environment as any single leaf, simplifying the task of modeling complex landscapes.},

language = {en},

number = {4},

urldate = {2024-09-09},

journal = {Sensors},

author = {Glenn, Edward P. and Huete, Alfredo R. and Nagler, Pamela L. and Nelson, Stephen G.},

month = apr,

year = {2008},

note = {Number: 4
Publisher: Molecular Diversity Preservation International},

keywords = {NDVI, Evapotranspiration, EVI, Primary Production, Remote Sensing},

pages = {2136--2160},

file = {Full Text PDF:files/305/Glenn et al. - 2008 - Relationship Between Remotely-sensed Vegetation In.pdf:application/pdf},

}

@article{tian_comparison_2017,

title = {Comparison of {UAV} and {WorldView}-2 imagery for mapping leaf area index of mangrove forest},

volume = {61},

issn = {1569-8432},

url = {https://www.sciencedirect.com/science/article/pii/S0303243417300983},

doi = {10.1016/j.jag.2017.05.002},

abstract = {Unmanned Aerial Vehicle (UAV) remote sensing has opened the door to new sources of data to effectively characterize vegetation metrics at very high spatial resolution and at flexible revisit frequencies. Successful estimation of the leaf area index (LAI) in precision agriculture with a UAV image has been reported in several studies. However, in most forests, the challenges associated with the interference from a complex background and a variety of vegetation species have hindered research using UAV images. To the best of our knowledge, very few studies have mapped the forest LAI with a UAV image. In addition, the drawbacks and advantages of estimating the forest LAI with UAV and satellite images at high spatial resolution remain a knowledge gap in existing literature. Therefore, this paper aims to map LAI in a mangrove forest with a complex background and a variety of vegetation species using a UAV image and compare it with a WorldView-2 image (WV2). In this study, three representative NDVIs, average NDVI (AvNDVI), vegetated specific NDVI (VsNDVI), and scaled NDVI (ScNDVI), were acquired with UAV and WV2 to predict the plot level (10×10m) LAI. The results showed that AvNDVI achieved the highest accuracy for WV2 (R2=0.778, RMSE=0.424), whereas ScNDVI obtained the optimal accuracy for UAV (R2=0.817, RMSE=0.423). In addition, an overall comparison results of the WV2 and UAV derived LAIs indicated that UAV obtained a better accuracy than WV2 in the plots that were covered with homogeneous mangrove species or in the low LAI plots, which was because UAV can effectively eliminate the influence from the background and the

vegetation species owing to its high spatial resolution. However, WV2 obtained a slightly higher accuracy than UAV in the plots covered with a variety of mangrove species, which was because the UAV sensor provides a negative spectral response function(SRF) than WV2 in terms of the mangrove LAI estimation.},

urldate = {2024-09-09},

journal = {International Journal of Applied Earth Observation and Geoinformation},

author = {Tian, Jinyan and Wang, Le and Li, Xiaojuan and Gong, Huili and Shi, Chen and Zhong, Ruofei and Liu, Xiaomeng},

month = sep,

year = {2017},

keywords = {NDVI, UAV, Background and vegetation species, Leaf area index, Mangrove, WorldView-2},

pages = {22--31},

file = {ScienceDirect Snapshot:files/307/S0303243417300983.html:text/html},

}

@article{vicente-serrano_diverse_2016,

title = {Diverse relationships between forest growth and the {Normalized} {Difference} {Vegetation} {Index} at a global scale},

volume = {187},

issn = {0034-4257},

url = {https://www.sciencedirect.com/science/article/pii/S003442571630373X},

doi = {10.1016/j.rse.2016.10.001},

abstract = {This study compared the densest available database of tree-ring growth with the longest Normalized Difference Vegetation Index (NDVI) information available at the global scale to quantify the relationship between annual forest growth and the NDVI across different forest types and regions and to characterize the patterns of response of forest growth to NDVI values at different temporal scales. We found a general positive relationship between the inter-annual NDVI variability and the annual tree growth in most of the analyzed forests. Nevertheless, there were strong differences in the tree growth responses to NDVI, given that the annual tree-ring records in each forest responded in a different way to the magnitude, seasonality and accumulation period of the NDVI values. Thus, we found eight main patterns of tree-ring response to the NDVI, which were related to the forest type and climate conditions of each corresponding site. The identified patterns may be useful for determining early-warning signals of changes in forest growth over large areas based on remote sensing information.},

urldate = {2024-09-09},

journal = {Remote Sensing of Environment},

author = {Vicente-Serrano, Sergio M. and Camarero, J. Julio and Olano, José M. and Martín-Hernández, Natalia and Peña-Gallardo, Marina and

Tomás-Burguera, Miquel and Gazol, Antonio and Azorin-Molina, Cesar and Bhuyan, Upasana and El Kenawy, Ahmed},

month = dec,

year = {2016},

keywords = {Dendrochronology, Forest growth, Normalized Difference Vegetation Index (NDVI), Tree rings},

pages = {14--29},

file = {ScienceDirect Snapshot:files/310/S003442571630373X.html:text/html;Versión enviada:files/309/Vicente-Serrano et al. - 2016 - Diverse relationships between forest growth and th.pdf:application/pdf},

}

@article{zhu_improving_2015,

title = {Improving forest aboveground biomass estimation using seasonal {Landsat} {NDVI} time-series},

volume = {102},

issn = {0924-2716},

url = {https://www.sciencedirect.com/science/article/pii/S0924271614002202},

doi = {10.1016/j.isprsjprs.2014.08.014},

abstract = {Spatially explicit knowledge of aboveground biomass (AGB) in large areas is important for accurate carbon accounting. Landsat data have

been widely used to provide efficient and timely estimates of forest AGB because of their long archive and relatively high spatial resolution. Previous studies have explored different empirical modeling approaches to estimate AGB, but most of them only used a single Landsat image in the peak season, which may cause a saturation problem and low accuracy. To improve the accuracy of AGB estimation using Landsat images, this study explored the use of NDVI seasonal time-series derived from Landsat images across different seasons to estimate AGB in southeast Ohio by six empirical modeling approaches. Results clearly show that NDVI in the fall season has a stronger correlation to AGB than in the peak season, and using seasonal NDVI time-series can result in a more accurate AGB estimation and less saturation than using a single NDVI. In comparing these different empirical approaches, it is difficult to decide which one is superior to the other because they have different strengths and their accuracy is generally similar, indicating that modeling methods may not be the key issue for improving the accuracy of AGB estimation from Landsat data. This study suggests that future research should pay more attention to seasonal time-series data, and especially the data from the fall season.},

urldate = {2024-09-09},

journal = {ISPRS Journal of Photogrammetry and Remote Sensing},

author = {Zhu, Xiaolin and Liu, Desheng},

month = apr,

year = {2015},

keywords = {NDVI, Aboveground biomass, Empirical model, Forest inventory and analysis, Landsat, Seasonal time-series},

pages = {222--231},

file = {ScienceDirect Snapshot:files/312/S0924271614002202.html:text/html},

}

@misc{pastor_remote_2015,

title = {Remote {Sensing} {\textbar} {Free} {Full}-{Text} {\textbar} {Spatiotemporal} {Variation} in {Mangrove} {Chlorophyll} {Concentration} {Using} {Landsat} 8},

url = {https://www.mdpi.com/2072-4292/7/11/14530},

abstract = {Existe la necesidad de desarrollar indicadores de la condición de los manglares utilizando datos de detección remota. Sin embargo, la estimación remota de las propiedades bioquímicas de las hojas y el dosel y la condición de la vegetación sigue siendo un desafío. En este documento, (i) probamos el desempeño de índices hiperespectrales y de banda ancha seleccionados para predecir la concentración de clorofila (CC) en hojas de manglares y (ii) mostramos el potencial de Landsat 8 para la estimación de CC de manglares a nivel de paisaje. La CC relativa de las hojas y la respuesta espectral de las hojas se midieron en 12 Unidades Elementales de Muestreo (ESU) distribuidas a lo largo de la costa noroeste de la Península de Yucatán, México. Se calcularon modelos de regresión lineal y coeficientes

de determinación para medir la asociación entre la CC y la respuesta espectral. A nivel de hojas, los índices de banda estrecha con la mayor correlación con la CC fueron los índices de Vogelmann y el MTCI (R 2 {\textgreater} 0,5). Los índices con bandas espectrales alrededor del borde rojo (705–753 nm) fueron más sensibles a la CC de las hojas de manglares. A nivel de ESU, el NDVI verde Landsat 8, que utiliza la banda verde en su formulación, explicó la mayor parte de la variación en CC (R 2 {\textgreater} 0,8). La evaluación de la precisión entre el CC estimado y el CC observado utilizando el método de validación cruzada de dejar uno fuera (LOOCV) arrojó un error cuadrático medio (RMSE) = 15 µg·cm −2 y R 2 = 0,703. Los mapas de CC que muestran la variación espaciotemporal de CC a escala del paisaje se crearon utilizando el modelo lineal. Nuestros resultados indican que el NDVI verde Landsat 8 se puede emplear para estimar el CC en grandes áreas de manglares donde no se pueden aplicar redes terrestres y son necesarias técnicas de mapeo basadas en datos satelitales. Además, el uso de tecnologías futuras que incluirán dos bandas alrededor del borde rojo, como Sentinel 2, mejorará el monitoreo de manglares a resoluciones espaciales y temporales más altas},

urldate = {2024-09-09},

author = {Pastor, Julio and Atkinson, Peter and Jadunandan, Tablero and Rioja, Rodolfo},

year = {2015},

file = {Remote Sensing | Free Full-Text | Spatiotemporal Variation in Mangrove Chlorophyll Concentration Using Landsat 8:files/314/14530.html:text/html},
}

@article{dutrieux_monitoring_2015,
series = {Multitemporal remote sensing data analysis},
title = {Monitoring forest cover loss using multiple data streams, a case study of a tropical dry forest in {Bolivia}},
volume = {107},
issn = {0924-2716},
url = {https://www.sciencedirect.com/science/article/pii/S0924271615000970},
doi = {10.1016/j.isprsjprs.2015.03.015},
abstract = {Automatically detecting forest disturbances as they occur can be extremely challenging for certain types of environments, particularly those presenting strong natural variations. Here, we use a generic structural break detection framework (BFAST) to improve the monitoring of forest cover loss by combining multiple data streams. Forest change monitoring is performed using Landsat data in combination with MODIS or rainfall data to further improve the modelling and monitoring. We tested the use of the Normalized Difference Vegetation Index (NDVI) from the Moderate Resolution Imaging Spectroradiometer (MODIS) with varying spatial aggregation window

sizes as well as a rainfall derived index as external regressors. The method was evaluated on a dry tropical forest area in lowland Bolivia where forest cover loss is known to occur, and we validated the results against a set of ground truth samples manually interpreted using the TimeSync environment. We found that the addition of an external regressor allows to take advantage of the difference in spatial extent between human induced and naturally induced variations and only detect the processes of interest. Of all configurations, we found the 13 by 13km MODIS NDVI window to be the most successful, with an overall accuracy of 87\%. Compared with a single pixel approach, the proposed method produced better time-series model fits resulting in increases of overall accuracy (from 82\% to 87\%), and decrease in omission and commission errors (from 33\% to 24\% and from 3\% to 0\% respectively). The presented approach seems particularly relevant for areas with high inter-annual natural variability, such as forests regularly experiencing exceptional drought events.},

urldate = {2024-09-09},

journal = {ISPRS Journal of Photogrammetry and Remote Sensing},

author = {Dutrieux, Loïc Paul and Verbesselt, Jan and Kooistra, Lammert and Herold, Martin},

month = sep,

year = {2015},

keywords = {MODIS, Landsat, Change detection, Deforestation, Spatial context, Time-series},

pages = {112--125},

file = {ScienceDirect Snapshot:files/316/S0924271615000970.html:text/html},
}

@article{chavez_50_2016,
title = {50 años de extracción de agua en la cuenca de la {Pampa} del {Tamarugal}: ¿{Pueden} los árboles \textit{de {Prosopis} tamarugo} sobrevivir en el hiperárido desierto de {Atacama} (norte de {Chile})?},
volume = {124},
issn = {0140-1963},
shorttitle = {50 años de extracción de agua en la cuenca de la {Pampa} del {Tamarugal}},
url = {https://www.sciencedirect.com/science/article/pii/S0140196315300537},
doi = {10.1016/j.jaridenv.2015.09.007},
abstract = {Groundwater-dependent ecosystems are threatened worldwide by unsustainable groundwater (GW) extraction. This is the case of the Prosopis tamarugo Phil forest in the hyper-arid Atacama Desert (Northern Chile), one of the most extreme ecosystems on Earth. Despite concerns about the conservation of this ecosystem, little research has been done to quantify the effects of the increasing GW depth (GWD) on the Tamarugo population. Here we provide a spatio-temporal assessment of the water condition of Tamarugo trees and propose GWD thresholds for their conservation. We

studied spatio-temporal changes of GWD and the water status of the forest using Landsat images and hydrogeological records (1988–2013). This was complemented with a digital inventory and estimation of the green canopy fraction (GCF) of all trees using fine resolution satellite images. Since Tamarugos are solar trackers, their canopy spectral reflectance changes on a diurnal and seasonal basis. Thus, novel remote sensing drought stress indicators were defined: the mean NDVI in winter (NDVIW) accounting for foliage loss and the NDVI difference between mean winter and summer (ΔNDVIW−S) accounting for canopy water loss. NDVIW and ΔNDVIW−S of the Tamarugo forest declined on average 19\% and 51\%, respectively, while GW depleted on average 3 m over the period 1988–2013. About 730,000 trees were identified in the study area, from which 5.2\% showed a GCF {\textless} 0.25 associated with severe drought stress. A GWD {\textgreater} 12 m increasingly limited the paraheliotropic leaf movement, leading to dehydration and foliage loss. Tamarugos at 12–16 m GWD suffered moderate drought stress while GWD of 16–20 m implied severe drought stress. We suggest 20 m GWD as a critical threshold for the survival of Tamarugo trees.},

urldate = {2024-09-09},

journal = {Journal of Arid Environments},

author = {Chávez, R. O. and Clevers, J. G. P. W. and Decuyper, M. and de Bruin, S. and Herold, M.},

month = jan,

year = {2016},

keywords = {Remote sensing, NDVI, Arid ecosystems, Drought stress, Time series, Water management},

pages = {292--303},

file = {ScienceDirect Snapshot:files/318/S0140196315300537.html:text/html},

}

@article{pettorelli_using_2005,

title = {Using the satellite-derived {NDVI} to assess ecological responses to environmental change},

volume = {20},

issn = {0169-5347},

url = {https://www.sciencedirect.com/science/article/pii/S016953470500162X},

doi = {10.1016/j.tree.2005.05.011},

abstract = {Assessing how environmental changes affect the distribution and dynamics of vegetation and animal populations is becoming increasingly important for terrestrial ecologists to enable better predictions of the effects of global warming, biodiversity reduction or habitat degradation. The ability to predict ecological responses has often been hampered by our rather limited understanding of trophic interactions. Indeed, it has proven difficult to discern direct and indirect effects of environmental change on animal populations

owing to limited information about vegetation at large temporal and spatial scales. The rapidly increasing use of the Normalized Difference Vegetation Index (NDVI) in ecological studies has recently changed this situation. Here, we review the use of the NDVI in recent ecological studies and outline its possible key role in future research of environmental change in an ecosystem context.},

number = {9},

urldate = {2024-09-09},

journal = {Trends in Ecology \& Evolution},

author = {Pettorelli, Nathalie and Vik, Jon Olav and Mysterud, Atle and Gaillard, Jean-Michel and Tucker, Compton J. and Stenseth, Nils Chr.},

month = sep,

year = {2005},

pages = {503--510},

file = {ScienceDirect Snapshot:files/320/S016953470500162X.html:text/html},

}

@article{matsushita_sensitivity_2007,

title = {Sensitivity of the {Enhanced} {Vegetation} {Index} ({EVI}) and {Normalized} {Difference} {Vegetation} {Index} ({NDVI}) to {Topographic} {Effects}: {A} {Case} {Study} in {High}-density {Cypress} {Forest}},

volume = {7},

copyright = {http://creativecommons.org/licenses/by/3.0/},

issn = {1424-8220},

shorttitle = {Sensitivity of the {Enhanced} {Vegetation} {Index} ({EVI}) and {Normalized} {Difference} {Vegetation} {Index} ({NDVI}) to {Topographic} {Effects}},

url = {https://www.mdpi.com/1424-8220/7/11/2636},

doi = {10.3390/s7112636},

abstract = {Vegetation indices play an important role in monitoring variations in vegetation.The Enhanced Vegetation Index (EVI) proposed by the MODIS Land Discipline Groupand the Normalized Difference Vegetation Index (NDVI) are both global-based vegetationindices aimed at providing consistent spatial and temporal information regarding globalvegetation. However, many environmental factors such as atmospheric conditions and soilbackground may produce errors in these indices. The topographic effect is another veryimportant factor, especially when the indices are used in areas of rough terrain. In thispaper, we theoretically analyzed differences in the topographic effect on the EVI and theNDVI based on a non-Lambertian model and two airborne-based images acquired from amountainous area covered by high-density Japanese cypress plantation were used as a casestudy. The results indicate that the soil adjustment factor “L” in the EVI makes it moresensitive to topographic conditions than is the NDVI. Based on these results, we stronglyrecommend that the topographic effect should be removed in the reflectance data beforethe EVI was calculated—as well as from other

vegetation indices that similarly include a term without a band ratio format (e.g., the PVI and SAVI)—when these indices are used in the area of rough terrain, where the topographic effect on the vegetation indices having only a band ratio format (e.g., the NDVI) can usually be ignored.},

language = {en},

number = {11},

urldate = {2024-09-10},

journal = {Sensors},

author = {Matsushita, Bunkei and Yang, Wei and Chen, Jin and Onda, Yuyichi and Qiu, Guoyu},

month = nov,

year = {2007},

note = {Number: 11
Publisher: Molecular Diversity Preservation International},

keywords = {NDVI, vegetation index, EVI, band ratio, topographic effect},

pages = {2636--2651},

file = {Full Text PDF:files/324/Matsushita et al. - 2007 - Sensitivity of the Enhanced Vegetation Index (EVI).pdf:application/pdf},

}

@article{paredes_uso_2018,

title = {Uso de índices de vegetación del sensor {MODIS}-{TERRA} en la estimación de biomasa aerea de pajonales altoandinos},

url = {https://repositorio.lamolina.edu.pe/bitstream/handle/20.500.12996/3351/paredes-choccemiguel-enrique.pdf?sequence=1&isAllowed=y},

abstract = {Se condujo un estudio en pajonales alto-andinos de la sierra central del Perú para evaluar
la relación entre la biomasa aérea y los índices de vegetación (IV): índice de vegetación
diferencial normalizada (NDVI) e índice de vegetación mejorado (EVI) del sensor
MODIS-TERRA. Las evaluaciones se realizaron durante los meses de Abril y Mayo del
2016 en las comunidades de Canchayllo, San Pedro de Racco y Tomas. Se utilizó una
grilla de 250 x 250 m (similar a un pixel de una imagen MODIS) y mapas de cobertura
vegetal para discriminar pixeles de pajonal de otros tipos de coberturas. La biomasa
disponible (Kg MS/a) se midió por el Método de Rendimientos Comparativos de
Haydock y Shaw (1975) en cuadrantes de 0.25 m2
a lo largo de transectas al paso en cada

pixel. Los IV se extrajeron de imágenes del producto MOD13Q1 de MODIS. Los
resultados muestran que las relaciones entre las variables NDVI – Biomasa y EVI –
Biomasa tuvieron coeficientes de determinación de 0.31 (n =46, p{\textless}0.01) y 0.22 (n=46,
p{\textless}0.01) respectivamente. La variabilidad y la baja correlación encontrada se atribuyó a
las diferencias propias de los pajonales de cada una de las tres zonas de evaluación; a lo
heterogéneo de la vegetación contenida en un pixel de MODIS (6.25 Ha); al número de
observaciones por pixel para el método utilizado para estimar la biomasa disponible; y a
la nubosidad propia de la época en la que se adquirió la información. Se recomienda el
uso de imágenes satelitales de sensores con una mayor resolución espacial o de otro tipo
como imágenes tomadas por DRONES, realizar experimentos similares con otros índices
de vegetación e incorporar variables que permitan modelar mejor el comportamiento de
la vegetación},

language = {es},

author = {Paredes, Miguel},

year = {2018},

file = {Chocce - TESIS PARA OPTAR EL GRADO DE INGENIERO ZOOTECNISTA.pdf:files/325/Chocce - TESIS PARA OPTAR EL GRADO DE INGENIERO ZOOTECNISTA.pdf:application/pdf},

}

@article{huete_comparison_1997,

title = {A comparison of vegetation indices over a global set of {TM} images for {EOS}-{MODIS}},

volume = {59},

issn = {0034-4257},

url = {https://www.sciencedirect.com/science/article/pii/S0034425796001125},

doi = {10.1016/S0034-4257(96)00112-5},

abstract = {A set of Landsat Thematic Mapper images representing a wide range of vegetation conditions from the NASA Landsat Pathfinder, global land cover test site (GLCTS) initiative were processed to simulate the Moderate Resolution Imaging Spectroradiometer (MODIS), global vegetation index imagery at 250 m pixel size resolution. The sites included boreal forest, temperate coniferous forest, temperate deciduous forest, tropical rainforest, grassland, savanna, and desert biomes. Differences and similarities in

sensitivity to vegetation conditions were compared among various spectral vegetation indices (VIs). All VIs showed a qualitative relationship to variations in vegetation. However, there were significant differences among the VIs over desert, grassland, and forested biomes. The normalized difference vegetation index (NDVI) was sensitive to and responded primarily to the highly absorbing red reflectance band, while other indices such (is the soil and atmosphere resistant vegetation index (SARVI) were more responsive to variations in the near-infrared (NIR) band. As a result, we found the NDVI to mimic red reflectances and saturate over the forested sites while the SARVI, by contrast, did not saturate and followed variations in NIR refleetances. In the arid and semiarid biomes, the NDVI was much more sensitive to canopy background variations than the SARVI. Maximum differences among vegetation index behavior occurred over the evergreen needleleaf forest sites relative to the deciduous broadleaf forests and drier, grassland, and shrub sites. These differences appear to be useful in complementing the NDVI for improved monitoring of vegetation, with the NDVI sensitive to fraction of absorbed photosynthetic active radiation and the SARVI more sensitive to structural canopy parameters such as leaf area index and leaf morphology.},

number = {3},

urldate = {2024-09-10},

journal = {Remote Sensing of Environment},

author = {Huete, A. and Liu, H. Q. and Batchily, K. and van Leeuwen, W.},

month = mar,

year = {1997},

pages = {440--451},

file = {ScienceDirect Snapshot:files/328/S0034425796001125.html:text/html},

}

@article{huete_development_1994,

title = {Development of vegetation and soil indices for {MODIS}-{EOS}},

volume = {49},

issn = {0034-4257},

url = {https://www.sciencedirect.com/science/article/pii/0034425794900183},

doi = {10.1016/0034-4257(94)90018-3},

abstract = {One of the primary interests of the NASA Earth Observing System (EOS) program is to study the role of vegetation in biospheric processes. Currently, the normalized difference vegetation index (NDVI) is utilized to study and monitor vegetation activity on an operational basis at global scales. Recently developed variants to the NDVI equation, based on improved knowledge of atmosphere, canopy background, and sensor-view geometry, are being considered for use with the EOS Moderate-Resolution Imaging Spectrometer (MODIS) sensor. A set of criteria is established to evaluate their performance with respect to the vegetation signal and

atmospheric and soil sources of noise. These include the vegetation signal-to-noise ratio (S/N), \% relative error, and vegetation equivalent noise (VEN), which form the basis for the evaluation and comparison of vegetation indices (VIs) across a wide range in vegetation covers. The NDVI variant equations outperformed the NDVI by minimizing atmospheric and/or soil background sources of contamination as well as increasing vegetation signal sensitivity. Preliminary estimates, based on the data sets tested here, indicate an overall level of uncertainty of ± 0.4 LAI (≈ 15\% cover) with the use of the soil adjusted and atmospherically resistant vegetation index (SARVI), compared with ± 0.8 LAI (30\% cover) for the NDVI. Eventually, the final evaluation and validation of VIs for MODIS will include a field campaign strategy, simulation studies, and a worldwide establishment of test sites that collectively cover a diverse range of biomes. Lastly, the retrieval of canopy biophysical information from these VIs are discussed.},

number = {3},

urldate = {2024-09-10},

journal = {Remote Sensing of Environment},

author = {Huete, A. and Justice, C. and Liu, H.},

month = sep,

year = {1994},

pages = {224--234},

file = {ScienceDirect Snapshot:files/330/0034425794900183.html:text/html},

}

@article{houborg_combining_2007,

title = {Combining vegetation index and model inversion methods for the extraction of key vegetation biophysical parameters using {Terra} and {Aqua} {MODIS} reflectance data},

volume = {106},

issn = {0034-4257},

url = {https://www.sciencedirect.com/science/article/pii/S003442570600280X},

doi = {10.1016/j.rse.2006.07.016},

abstract = {Accurate estimates of vegetation biophysical variables are valuable as input to models describing the exchange of carbon dioxide and energy between the land surface and the atmosphere and important for a wide range of applications related to vegetation monitoring, weather prediction, and climate change. The present study explores the benefits of combining vegetation index and physically based approaches for the spatial and temporal mapping of green leaf area index (LAI), total chlorophyll content (TCab), and total vegetation water content (VWC). A numerical optimization method was employed for the inversion of a canopy reflectance model using Terra and Aqua MODIS multi-spectral, multi-temporal, and multi-angle reflectance observations to aid the determination of vegetation-specific physiological and structural canopy parameters. Land cover and site-specific inversion modeling

was applied to a restricted number of pixels to build multiple species- and environmentally dependent formulations relating the three biophysical properties of interest to a number of selected simpler spectral vegetation indices (VI). While inversions generally are computationally slow, the coupling with the simple and computationally efficient VI approach makes the combined retrieval scheme for LAI, TCab, and VWC suitable for large-scale mapping operations. In order to facilitate application of the canopy reflectance model to heterogeneous forested areas, a simple correction scheme was elaborated, which was found to improve forest LAI predictions significantly and also provided more realistic values of leaf chlorophyll contents. The inversion scheme was designed to enable biophysical parameter retrievals for land cover classes characterized by contrasting canopy architectures, leaf inclination angles, and leaf biochemical constituents without utilizing calibration measurements. Preliminary LAI validation results for the Island of Zealand, Denmark (57°N, 12°E) provided confidence in the approach with root mean square (RMS) deviations between estimates and in-situ measurements of 0.62, 0.46, and 0.63 for barley, wheat, and deciduous forest sites, respectively. Despite the independence on site-specific in-situ measurements, the RMS deviations of the automated approach are in the same range as those established in other studies employing field-based empirical calibration. Being completely automated and image-based and independent on extensive and impractical surface measurements, the retrieval scheme has potential for operational use and can quite easily be implemented for other regions. More

validation studies are needed to evaluate the usefulness and limitations of the approach for other environments and species compositions.},

number = {1},

urldate = {2024-09-10},

journal = {Remote Sensing of Environment},

author = {Houborg, Rasmus and Soegaard, Henrik and Boegh, Eva},

month = jan,

year = {2007},

keywords = {MODIS, NDVI, EVI, Leaf area index, Canopy reflectance, Chlorophyll content, GI, Inverse modeling, NDWI, Satellite, Spectral reflectances, Vegetation water content},

pages = {39--58},

file = {ScienceDirect Snapshot:files/332/S003442570600280X.html:text/html},

}

@article{jiang_development_2008,

title = {Development of a two-band enhanced vegetation index without a blue band},

volume = {112},

issn = {0034-4257},

url = {https://www.sciencedirect.com/science/article/pii/S0034425708001971},

doi = {10.1016/j.rse.2008.06.006},

abstract = {The enhanced vegetation index (EVI) was developed as a standard satellite vegetation product for the Terra and Aqua Moderate Resolution Imaging Spectroradiometers (MODIS). EVI provides improved sensitivity in high biomass regions while minimizing soil and atmosphere influences, however, is limited to sensor systems designed with a blue band, in addition to the red and near-infrared bands, making it difficult to generate long-term EVI time series as the normalized difference vegetation index (NDVI) counterpart. The purpose of this study is to develop and evaluate a 2-band EVI (EVI2), without a blue band, which has the best similarity with the 3-band EVI, particularly when atmospheric effects are insignificant and data quality is good. A linearity-adjustment factor β is proposed and coupled with the soil-adjustment factor L used in the soil-adjusted vegetation index (SAVI) to develop EVI2. A global land cover dataset of Terra MODIS data extracted over land community validation and FLUXNET test sites is used to develop the optimal parameter (L, β and G) values in EVI2 equation and achieve the best similarity between EVI and EVI2. The similarity between the two indices is evaluated and demonstrated with temporal profiles of vegetation dynamics at local and global scales. Our results demonstrate that the differences between EVI and EVI2 are insignificant (within ±0.02) over a very large sample of snow/ice-free land cover types, phenologies, and scales when atmospheric influences are insignificant, enabling EVI2 as an acceptable and accurate substitute of EVI. EVI2 can be used for sensors without a blue band, such as the Advanced Very High

Resolution Radiometer (AVHRR), and may reveal different vegetation dynamics in comparison with the current AVHRR NDVI dataset. However, cross-sensor continuity relationships for EVI2 remain to be studied.},

number = {10},

urldate = {2024-09-10},

journal = {Remote Sensing of Environment},

author = {Jiang, Zhangyan and Huete, Alfredo R. and Didan, Kamel and Miura, Tomoaki},

month = oct,

year = {2008},

keywords = {MODIS, EVI, EVI2, Linearization, Vegetation indices},

pages = {3833--3845},

file = {ScienceDirect Snapshot:files/334/S0034425708001971.html:text/html},

}

@article{sudhanshu_application_2010,

title = {Application of {Vegetation} {Indices} for {Agricultural} {Crop} {Yield} {Prediction} {Using} {Neural} {Network} {Techniques}},

volume = {2},

copyright = {http://creativecommons.org/licenses/by/3.0/},

issn = {2072-4292},

url = {https://www.mdpi.com/2072-4292/2/3/673},

doi = {10.3390/rs2030673},

abstract = {Spatial variability in a crop field creates a need for precision agriculture. Economical and rapid means of identifying spatial variability is obtained through the use of geotechnology (remotely sensed images of the crop field, image processing, GIS modeling approach, and GPS usage) and data mining techniques for model development. Higher-end image processing techniques are followed to establish more precision. The goal of this paper was to investigate the strength of key spectral vegetation indices for agricultural crop yield prediction using neural network techniques. Four widely used spectral indices were investigated in a study of irrigated corn crop yields in the Oakes Irrigation Test Area research site of North Dakota, USA. These indices were: (a) red and near-infrared (NIR) based normalized difference vegetation index (NDVI), (b) green and NIR based green vegetation index (GVI), (c) red and NIR based soil adjusted vegetation index (SAVI), and (d) red and NIR based perpendicular vegetation index (PVI). These four indices were investigated for corn yield during 3 years (1998, 1999, and 2001) and for the pooled data of these 3 years. Initially, Back-propagation Neural Network (BPNN) models were developed, including 16 models (4 indices * 4 years including the data from the pooled years) to test for the efficiency determination of those four vegetation indices in corn crop yield prediction. The corn yield was best predicted using BPNN models that used the means and standard deviations of PVI grid images. In all three years, it provided higher prediction accuracies, coefficient of determination (r2), and lower standard error of

prediction than the models involving GVI, NDVI, and SAVI image information. The GVI, NDVI, and SAVI models for all three years provided average testing prediction accuracies of 24.26\% to 94.85\%, 19.36\% to 95.04\%, and 19.24\% to 95.04\%, respectively while the PVI models for all three years provided average testing prediction accuracies of 83.50\% to 96.04\%. The PVI pool model provided better average testing prediction accuracy of 94\% with respect to other vegetation models, for which it ranged from 89–93\%. Similarly, the PVI pool model provided coefficient of determination (r2) value of 0.45 as compared to 0.31–0.37 for other index models. Log10 data transformation technique was used to enhance the prediction ability of the PVI models of years 1998, 1999, and 2001 as it was chosen as the preferred index. Another model (Transformed PVI (Pool)) was developed using the log10 transformed PVI image information to show its global application. The transformed PVI models provided average corn yield prediction accuracies of 90\%, 97\%, and 98\% for years 1998, 1999, and 2001, respectively. The pool PVI transformed model provided as average testing accuracy of 93\% along with r2 value of 0.72 and standard error of prediction of 0.05 t/ha.},

language = {en},

number = {3},

urldate = {2024-09-10},

journal = {Remote Sensing},

author = {Sudhanshu, Panda and Ames, Daniel P. and Panigrahi, Suranjan},

month = mar,

year = {2010},

note = {Number: 3

Publisher: Molecular Diversity Preservation International},

keywords = {back propagation neural network (BPNN), data mining, green vegetation index (GVI), normalized difference vegetation index (NDVI), perpendicular vegetation index (PVI), soil adjusted vegetation index (SAVI), yield estimation},

pages = {673--696},

file = {Full Text PDF:files/336/Panda et al. - 2010 - Application of Vegetation Indices for Agricultural.pdf:application/pdf},

}

@article{miura_evaluation_2000,

title = {Evaluation of sensor calibration uncertainties on vegetation indices for {MODIS}},

volume = {38},

issn = {1558-0644},

url = {https://ieeexplore.ieee.org/abstract/document/843034?casa_token=s8N_EASMu1wAAAAA:ZSk3yFgbrEpvI86GJrpSOylbO1hvhw7H-lII_tzm-VTbVsJr96LeP0vFsjH5xaF3C4ClDibx},

doi = {10.1109/36.843034},

abstract = {The impact of reflectance calibration uncertainties on the accuracies of several vegetation indices (VIs) was evaluated for the Moderate Resolution Imaging Spectroradiometer (MODIS) sensor onboard the TERRA platform. A set of uncertainty propagation equations were designed to model the propagation of calibration uncertainties from top-of-atmosphere (TOA) reflectances to atmospherically-corrected VIs. The soil-adjusted vegetation index (SAVI), the atmospherically-resistant vegetation index (ARVI), and the enhanced vegetation index (EVI) were evaluated along with the normalized difference vegetation index (NDVI). The resultant VI uncertainties associated with calibration u/sub cal/(VI) varied with both surface reflectances and atmospheric conditions. Uncertainties in the NDVI and ARVI were highly dependent on pixel brightness, with the largest uncertainties occurring over dark targets with little or no vegetation. The SAVI uncertainties were nearly constant throughout a range of target brightness and vegetation abundance. The EVI uncertainties linearly increased with increasing EVI values. Atmosphere turbidities increased calibration uncertainties in all the VIs through their effect on TOA reflectances. The VI uncertainties were also found to decrease when the calibration errors were positively correlated between bands. Using field observational canopy reflectance data, the mean VI uncertainties were estimated to be /spl plusmn/0.01 VI units for the NDVI and SAVI, and /spl plusmn/0.02 VI units for the ARVI and EVI under normal atmosphere conditions (/spl ges/20 km visibility) and for a 2\% reflectance calibration uncertainty.},

number = {3},

urldate = {2024-09-10},

journal = {IEEE Transactions on Geoscience and Remote Sensing},

author = {Miura, T. and Huete, A.R. and Yoshioka, H.},

month = may,

year = {2000},

note = {Conference Name: IEEE Transactions on Geoscience and Remote Sensing},

keywords = {MODIS, Atmosphere, Atmospheric modeling, Brightness, Calibration, Equations, Image sensors, Reflectivity, Uncertainty, Vegetation mapping},

pages = {1399--1409},

file = {IEEE Xplore Abstract Record:files/338/843034.html:text/html},

}

@article{jayaraman_total_2000,

title = {Total solution approach using {IRS}-{1C} and {IRS}-{P3} data},

volume = {38},

issn = {1558-0644},

url = {https://ieeexplore.ieee.org/abstract/document/823953?casa_token=MfOKYoJG4K4AAAAA:QZfzDhN2GJAxegGgCZuNQdozXjcmcTWwcm1qMk9V_1M67q3kqSs4l-rNmto7jB6Raq0I0Cih},

doi = {10.1109/36.823953},

abstract = {High spectral (10 nm) and radiometric (16 bits) resolutions of IRS-P3:MOS-B coupled with moderate spatial resolution (188 m) of IRS-P3:WiFS provide unique solutions to many problems related to sustainable management of ecosystems. While the high spatial resolutions of IRS-1C PAN and IRS-1C LISS-3 help in identifying the structural attributes of the biosphere, a synthetic product of MOS-B and WiFS offers immense potential to address several crucial issues including improved classification accuracy in heterogeneous land covers, environmental stress, improved vegetation signal-to-noise ratio, etc. In this paper, the operational issues such as multisensor calibration and validation, registration and merging of multisensor data from different platforms, identification of red edge using IRS-P3:MOS-B data, resolving subpixel heterogeneity, scale anomalies and uncertainty in spectral estimates of biophysical variables are discussed. With the integration of parameters sensitive to atmospheric scattering and soil background reflectance into NDVI derived from the synthetic image, the spectral index called soil adjusted and atmospheric resistant vegetation index (SARVI) has been found to be more sensitive to biophysical variables such as leaf area index (LAI) and fraction of absorbed photosynthetically active radiation (FPAR). It has also reduced, up to certain extent, the uncertainty related to the spectral measurements of bio-physical variables. Further study, in this regard, aims at evaluating the changes in entropy with the fusion of high spectral, radiometric, spatial, and temporal data.},

number = {1},

urldate = {2024-09-10},

journal = {IEEE Transactions on Geoscience and Remote Sensing},

author = {Jayaraman, V. and Srivastava, S.K. and Kumaran Raju, D. and Rao, U.R.},

month = jan,

year = {2000},

note = {Conference Name: IEEE Transactions on Geoscience and Remote Sensing},

keywords = {Calibration, Vegetation mapping, Biosphere, Ecosystems, Radio spectrum management, Radiometry, Signal to noise ratio, Soil, Spatial resolution, Stress},

pages = {587--604},

file = {IEEE Xplore Abstract Record:files/341/823953.html:text/html},

}

@article{huete_soil-adjusted_1988-1,

title = {A soil-adjusted vegetation index ({SAVI})},

volume = {25},

issn = {0034-4257},

url = {https://www.sciencedirect.com/science/article/pii/003442578890106X},

doi = {10.1016/0034-4257(88)90106-X},

abstract = {A transformation technique is presented to minimize soil brightness influences from spectral vegetation indices involving red and near-infrared (NIR) wavelengths. Graphically, the transformation involves a shifting of the origin of reflectance spectra plotted in NIR-red wavelength space to account for first-order soil-vegetation interactions and differential red and NIR flux extinction through vegetated canopies. For cotton (Gossypium hirsutum L. var DPI-70) and range grass (Eragrosticslehmanniana Nees) canopies, underlain with different soil backgrounds, the transformation nearly eliminated soil-induced variations in vegetation indices. A physical basis for the soil-adjusted vegetation index (SAVI) is subsequently presented. The SAVI was found to be an important step toward the establishment of simple °lobal" that can describe dynamic soil-vegetation systems from remotely sensed data.},

number = {3},

urldate = {2024-09-10},

journal = {Remote Sensing of Environment},

author = {Huete, A.},

month = aug,

year = {1988},

pages = {295--309},

file = {ScienceDirect Snapshot:files/344/003442578890106X.html:text/html},

}

@article{bannari_review_1995,

title = {A review of vegetation indices},

volume = {13},

issn = {0275-7257},

url = {https://doi.org/10.1080/02757259509532298},

doi = {10.1080/02757259509532298},

abstract = {In the field of remote sensing applications, scientists have developed vegetation indices (VI) for qualitatively and quantitatively evaluating vegetative covers using spectral measurements. The spectral response of vegetated areas presents a complex mixture of vegetation, soil brightness, environmental effects, shadow, soil color and moisture. Moreover, the VI is affected by spatial-temporal variations of the atmosphere. Over forty vegetation indices have been developed during the last two decades in order to enhance vegetation response and minimize the effects of the factors described above. This paper summarizes, refers and discusses most of the vegetation indices found in the literature. It presents different existing classifications of indices and proposes to group them in a new classification.},

number = {1-2},

urldate = {2024-09-10},

journal = {Remote Sensing Reviews},

author = {Bannari, A. and Morin, D. and Bonn, F. and Huete, A.},

month = aug,

year = {1995},

note = {Publisher: Taylor \& Francis
_eprint: https://doi.org/10.1080/02757259509532298},
pages = {95--120},
}

@article{rodriguez-moreno_comparacion_2013,
title = {Comparación espacial y temporal de índices de la vegetación para verdor y humedad y aplicación para estimar {LAI} en el {Desierto} {Sonorense}},
volume = {4},
issn = {2007-0934},
url = {http://www.scielo.org.mx/scielo.php?script=sci_abstract&pid=S2007-09342013000400010&lng=es&nrm=iso&tlng=es},
abstract = {Se realizó una comparación multitemporal de cuatro índices de la vegetación en 50 sitios en una región árida subtropical con costa. Los índices de verdor (NDVI, SAVI y TSAVI) y de humedad (NDII) fueron evaluados. NDVI y SAVI estuvieron muy correlacionados mientras que TSAVI fluctuó menos y NDII mostró fuertes variaciones estacionales. La corrección topográfica (superficie iluminada) de los datos crudos causó un incremento en el valor de pendiente de la línea del suelo {\textgreater}20\%. Los índices, excepto NDII, se usaron para estimar el Índice de área foliar, y el análisis señal-

a-ruido evidenció que SAVI está muy cercano a NDVI, pero TSAVI tuvo mucha mayor señal en los meses secos.},

language = {es},

number = {4},

urldate = {2024-09-10},

journal = {Revista mexicana de ciencias agrícolas},

author = {Rodríguez-Moreno, Víctor M. and Bullock, Stephen H.},

month = jun,

year = {2013},

note = {Publisher: Instituto Nacional de Investigaciones Forestales, Agrícolas y Pecuarias},

pages = {611--623},

file = {Full Text PDF:files/347/Rodríguez-Moreno y Bullock - 2013 - Comparación espacial y temporal de índices de la v.pdf:application/pdf},

}

@article{xue_significant_2017,

title = {Significant {Remote} {Sensing} {Vegetation} {Indices}: {A} {Review} of {Developments} and {Applications}},

volume = {2017},

copyright = {Copyright © 2017 Jinru Xue and Baofeng Su.},

issn = {1687-7268},

shorttitle = {Significant {Remote} {Sensing} {Vegetation} {Indices}},

url = {https://onlinelibrary.wiley.com/doi/abs/10.1155/2017/1353691},

doi = {10.1155/2017/1353691},

abstract = {Vegetation Indices (VIs) obtained from remote sensing based canopies are quite simple and effective algorithms for quantitative and qualitative evaluations of vegetation cover, vigor, and growth dynamics, among other applications. These indices have been widely implemented within RS applications using different airborne and satellite platforms with recent advances using Unmanned Aerial Vehicles (UAV). Up to date, there is no unified mathematical expression that defines all VIs due to the complexity of different light spectra combinations, instrumentation, platforms, and resolutions used. Therefore, customized algorithms have been developed and tested against a variety of applications according to specific mathematical expressions that combine visible light radiation, mainly green spectra region, from vegetation, and nonvisible spectra to obtain proxy quantifications of the vegetation surface. In the real-world applications, optimization VIs are usually tailored to the specific application requirements coupled with appropriate validation tools and methodologies in the ground. The present study introduces the spectral characteristics of vegetation and summarizes the development of VIs and the advantages and disadvantages from different indices developed. This paper reviews more than 100 VIs, discussing their specific applicability and representativeness according to the vegetation of interest, environment, and implementation precision. Predictably, research, and development of VIs,

which are based on hyperspectral and UAV platforms, would have a wide applicability in different areas.},

language = {en},

number = {1},

urldate = {2024-09-23},

journal = {Journal of Sensors},

author = {Xue, Jinru and Su, Baofeng},

year = {2017},

note = {_eprint: https://onlinelibrary.wiley.com/doi/pdf/10.1155/2017/1353691},

pages = {1353691},

file = {Full Text PDF:files/351/Xue y Su - 2017 - Significant Remote Sensing Vegetation Indices A R.pdf:application/pdf;Snapshot:files/352/1353691.html:text/html},

}

@article{gitelson_optical_2001,

title = {Optical {Properties} and {Nondestructive} {Estimation} of {Anthocyanin} {Content} in {Plant} {Leaves}},

volume = {74},

issn = {1751-1097},

url = {https://onlinelibrary.wiley.com/doi/abs/10.1562/0031-8655%282001%290740038OPANEO2.0.CO2},

doi = {10.1562/0031-8655(2001)0740038OPANEO2.0.CO2},

abstract = {Absorption and reflectance spectra of maple (Acer platanoides), cotoneaster (Cotoneaster alaunica), dogwood (Cornus alba) and pelargonium (Pelargonium zonale) leaves with a wide range of pigment content and composition were studied in visible and near-infrared spectra in order to reveal specific anthocyanin (Anth) spectral features in leaves. Comparing absorption spectra of Anth-containing and Anth-free leaves with the same chlorophyll (Chl) content, absorption spectra of Anth in leaves were derived. The main spectral feature of Anth absorption in vivo was a peak around 550 nm; the peak magnitude was closely related to Anth content. A quantitative nondestructive technique was developed to subtract Chl contribution to reflectance in this spectral region and retrieve Anth content from reflectance over a wide range of pigment content and composition. Anth reflectance index in the form ARI = (R550)−1− (R700)−1, where (R550)−1 and (R700)−1 are inverse reflectances at 550 and 700 nm, respectively, allowed an accurate estimation of Anth accumulation, even in minute amounts, in intact senescing and stressed leaves.},

language = {en},

number = {1},

urldate = {2024-09-23},

journal = {Photochemistry and Photobiology},

author = {Gitelson, Anatoly and Merzlyak, Mark and Chivkunova, Olga},

year = {2001},

note = {_eprint: https://onlinelibrary.wiley.com/doi/pdf/10.1562/0031-8655\%282001\%290740038OPANEO2.0.CO2},

pages = {38--45},

file = {Snapshot:files/354/0031-8655(2001)0740038OPANEO2.0.html:text/html},

}

@article{zarco-tejada_assessing_2005,

title = {Assessing vineyard condition with hyperspectral indices: {Leaf} and canopy reflectance simulation in a row-structured discontinuous canopy},

volume = {99},

issn = {0034-4257},

shorttitle = {Assessing vineyard condition with hyperspectral indices},

url = {https://www.sciencedirect.com/science/article/pii/S0034425705002865},

doi = {10.1016/j.rse.2005.09.002},

abstract = {Methods for chlorosis detection and physiological condition monitoring in Vitis vinifera L. through accurate chlorophyll a and b content (Cab) estimation at leaf and canopy levels are presented in this manuscript. A total of 24 vineyards were identified for field and airborne data collection with the Compact Airborne Spectrographic Imager (CASI), the Reflective Optics System Imaging Spectrometer (ROSIS) and the Digital Airborne Imaging Spectrometer (DAIS-7915) hyperspectral sensors in 2002 and 2003 in northern

Spain, comprising 103 study areas of 10×10 m in size, with a total of 1467 leaves collected for determination of pigment concentration. A subsample of 605 leaves was used for measuring the optical properties of reflectance and transmittance with a Li-Cor 1800-12 Integrating Sphere coupled by a 200 μm diameter single mode fiber to an Ocean Optics model USB2000 spectrometer. Several narrow-band vegetation indices were calculated from leaf reflectance spectra, and the PROSPECT leaf optical model was used for inversion using the extensive database of leaf optical properties. Results showed that the best indicators for chlorophyll content estimation in V. vinifera L. leaves were narrow-band hyperspectral indices calculated in the 700–750 nm spectral region (r2 ranging between 0.8 and 0.9), with poor performance of traditional indices such as the Normalized Difference Vegetation Index (NDVI). Results for other biochemicals indicated that the Structure Insensitive Pigment Index (SIPI) and the Photochemical Reflectance Index (PRI) were more sensitive to carotenoids Cx+c and chlorophyll–carotenoid ratios Cab/Cx+c than to chlorophyll content Cab. Chlorophyll a and b estimation by inversion of the PROSPECT leaf model on V. vinifera L. spectra was successful, yielding a determination coefficient of r2=0.95, with an RMSE=5.3 μg/cm2. The validity of leaf-level indices for chlorophyll content estimation at the canopy level in V. vinifera L. was studied using the scaling-up approach that links PROSPECT and rowMCRM canopy reflectance simulation to account for the effects of vineyard structure, vine dimensions, row orientation and soil and shadow effects on the canopy reflectance. The index calculated as a combination of the

Transformed Chlorophyll Absorption in Reflectance Index (TCARI), and the Optimized Soil-Adjusted Vegetation Index (OSAVI) in the form TCARI/OSAVI was the most consistent index for estimating Cab on aggregated and pure vine pixels extracted from 1 m CASI and ROSIS hyperspectral imagery. Predictive relationships were developed with PROSPECT–rowMCRM model between Cab and TCARI/OSAVI as function of LAI, using field-measured vine dimensions and image-extracted soil background, row-orientation and viewing geometry values. Prediction relationships for Cab content with TCARI/OSAVI were successfully applied to the 103 study sites imaged on 24 fields by ROSIS and CASI airborne sensors, yielding r2=0.67 and RMSE=11.5 μg/cm2.},

number = {3},

urldate = {2024-09-23},

journal = {Remote Sensing of Environment},

author = {Zarco-Tejada, P. J. and Berjón, A. and López-Lozano, R. and Miller, J. R. and Martín, P. and Cachorro, V. and González, M. R. and de Frutos, A.},

month = nov,

year = {2005},

keywords = {Hyperspectral remote sensing, Optical index, Radiative transfer, RowMCRM, Scaling-up, Vine, Vineyards},

pages = {271--287},

file = {ScienceDirect Snapshot:files/356/S0034425705002865.html:text/html},

}

@article{zarco-tejada_fluorescence_2012,

series = {Remote {Sensing} of {Urban} {Environments}},

title = {Fluorescence, temperature and narrow-band indices acquired from a {UAV} platform for water stress detection using a micro-hyperspectral imager and a thermal camera},

volume = {117},

issn = {0034-4257},

url = {https://www.sciencedirect.com/science/article/pii/S0034425711003555},

doi = {10.1016/j.rse.2011.10.007},

abstract = {The remote detection of water stress in a citrus orchard was investigated using leaf-level measurements of chlorophyll fluorescence and Photochemical Reflectance Index (PRI) data, seasonal time-series of crown temperature and PRI, and high-resolution airborne imagery. The work was conducted in an orchard where a regulated deficit irrigation (RDI) experiment generated a gradient in water stress levels. Stomatal conductance (Gs) and water potential (Ψ) were measured over the season on each treatment block. The airborne data consisted on thermal and hyperspectral imagery acquired at the time of maximum stress differences among treatments, prior to the re-watering phase, using a miniaturized thermal camera and a micro-hyperspectral imager on board an unmanned aerial vehicle (UAV). The

hyperspectral imagery was acquired at 40cm resolution and 260 spectral bands in the 400-885nm spectral range at 6.4nm full width at half maximum (FWHM) spectral resolution and 1.85nm sampling interval, enabling the identification of pure crowns for extracting radiance and reflectance hyperspectral spectra from each tree. The FluorMOD model was used to investigate the retrieval of chlorophyll fluorescence by applying the Fraunhofer Line Depth (FLD) principle using three spectral bands (FLD3), which demonstrated that fluorescence retrieval was feasible with the configuration of the UAV micro-hyperspectral instrument flown over the orchard. Results demonstrated the link between seasonal PRI and crown temperature acquired from instrumented trees and field measurements of stomatal conductance and water potential. The sensitivity of PRI and Tc–Ta time-series to water stress levels demonstrated a time delay of PRI vs Tc–Ta during the recovery phase after re-watering started. At the time of the maximum stress difference among treatment blocks, the airborne imagery acquired from the UAV platform demonstrated that the crown temperature yielded the best coefficient of determination for Gs (r2=0.78; p{\textless}0.05) and Ψ (r2=0.34; p{\textless}0.001). Among the narrow-band indices calculated, the PRI515 index (reference band=515nm) obtained better results than PRI570, with r2=0.59 (p{\textless}0.01) for Gs, and r2=0.38 (p{\textless}0.001) for Ψ. The BGI1 index calculated from the blue (R400) and green (R550) bands resulted on the highest significance levels (p{\textless}0.001) for both Gs (r2=0.62) and Ψ (r2=0.49). Out of the structural indices assessed, RDVI, MTVI1 and TVI showed greater sensitivity for Gs

(r2=0.6; p{\textless}0.01) and Ψ (p{\textless}0.001) than NDVI. Chlorophyll fluorescence calculated from the micro-hyperspectral imagery with the FLD3 method tracked stress levels, obtaining r2=0.67 (p{\textless}0.05) with stomatal conductance, and r2=0.66 (p{\textless}0.001) with water potential. The work presented in this manuscript demonstrates the feasibility of thermal, narrow-band indices and fluorescence retrievals obtained from a micro-hyperspectral imager and a light-weight thermal camera on board small UAV platforms for stress detection in a heterogeneous tree canopy where very high resolution is required.},

urldate = {2024-09-23},

journal = {Remote Sensing of Environment},

author = {Zarco-Tejada, P. J. and González-Dugo, V. and Berni, J. A. J.},

month = feb,

year = {2012},

keywords = {UAV, Chlorophyll fluorescence, High resolution, Hyperspectral, Stress detection, Thermal},

pages = {322--337},

file = {ScienceDirect Snapshot:files/358/S0034425711003555.html:text/html},

}

@article{daughtry_discriminating_2001,

title = {Discriminating {Crop} {Residues} from {Soil} by {Shortwave} {Infrared} {Reflectance}},

volume = {93},

copyright = {© Published in Agron. J.93:125–131.},

issn = {1435-0645},

url = {https://onlinelibrary.wiley.com/doi/abs/10.2134/agronj2001.931125x},

doi = {10.2134/agronj2001.931125x},

abstract = {Quantifying crop residue cover on the soil surface is important for evaluating the effectiveness of conservation tillage practices. Current methods of measuring residue cover are inadequate in characterizing the spatial variability of residue cover over large fields. The objectives of this research were to determine the spectral reflectance of crop residues and soils as a function of water content and to evaluate the limits of discrimination that can be expected. Spectral reflectances of corn (Zea mays L.), soybean [Glycine max (L.) Merr.], and wheat (Triticum aestivum L.) residues plus five diverse soils were measured over the 400- to 2400-nm wavelength region at a wide range of moisture conditions in the laboratory. Reflectance factors for scenes with varying proportions of crop residues and soils were simulated. The spectra of dry crop residues displayed a broad absorption feature near 2100 nm, associated with lignin and cellulose, that was absent in spectra of soils. The relative depth of the cellulose–lignin absorption feature, defined as the cellulose absorption index (CAI), was positive for all crop residues, except

those saturated with water. In contrast, all soils had negative CAI values. Water significantly altered reflectance spectra of wet crop residues, but it did not prevent the discrimination of crop residues from the soils using the CAI. The wide range of CAI values expected for dry and moist conditions makes quantification of crop residue cover feasible. This reflectance technique appears promising for field- and regional-scale surveys of crop residue cover and conservation tillage practices.},

language = {en},

number = {1},

urldate = {2024-09-23},

journal = {Agronomy Journal},

author = {Daughtry, Craig S.T.},

year = {2001},

note = {_eprint: https://onlinelibrary.wiley.com/doi/pdf/10.2134/agronj2001.931125x},

pages = {125--131},

file = {Full Text PDF:files/360/Daughtry - 2001 - Discriminating Crop Residues from Soil by Shortwav.pdf:application/pdf;Snapshot:files/361/agronj2001.html:text/html},

}

@inproceedings{kim_use_1994,

title = {The {Use} of {High} {Spectral} {Resolution} {Bands} for {Estimating} {Absorbed} {Photosynthetically} {Active} {Radiation} ({A} {Par})},

url = {https://ntrs.nasa.gov/citations/19950010604},

abstract = {Most remote sensing estimations of vegetation variables such as Leaf Area Index (LAI), Absorbed Photosynthetically Active Radiation (APAR), and phytomass are made using broad band sensors with a bandwidth of approximately 100 nm. However, high resolution spectrometers are available and have not been fully exploited for the purpose of improving estimates of vegetation variables. A study directed to investigate the use of high spectral resolution spectroscopy for remote sensing estimates of APAR in vegetation canopies in the presence of nonphotosynthetic background materials such as soil and leaf litter is presented. A high spectral resolution method defined as the Chlorophyll Absorption Ratio Index (CARI) was developed for minimizing the effects of nonphotosynthetic materials in the remote estimates of APAR. CARI utilizes three bands at 550, 670, and 700 nm with bandwidth of 10 nm. Simulated canopy reflectance of a range of LAI were generated with the SAIL model using measurements of 42 different soil types as canopy background. CARI obtained from the simulated canopy reflectance was compared with the broad band vegetation indices (Normalized Difference Vegetation Index (NDVI), Soil Adjusted Vegetation Index (SAVI), and Simple Ratio (SR)). CARI reduced the effect of nonphotosynthetic background materials in the assessment of vegetation canopy APAR more effectively than broad band vegetation indices.},

urldate = {2024-09-23},

author = {Kim, Moon S. and Daughtry, C. S. T. and Chappelle, E. W. and Mcmurtrey, J. E. and Walthall, C. L.},

month = jan,

year = {1994},

note = {NTRS Author Affiliations: Maryland Univ., Agricultural Research Service (ARS), NASA Goddard Space Flight Center

NTRS Report/Patent Number: GSFC-E-DAA-TN72921

NTRS Document ID: 19950010604

NTRS Research Center: Goddard Space Flight Center (GSFC)},

keywords = {Earth Resources And Remote Sensing},

file = {19950010604.pdf:files/363/Kim et al. - 1994 - The Use of High Spectral Resolution Bands for Esti.pdf:application/pdf;Snapshot:files/364/19950010604.html:text/html},

}

@article{li_improving_2014,

title = {Improving estimation of summer maize nitrogen status with red edge-based spectral vegetation indices},

volume = {157},

issn = {0378-4290},

url = {https://www.sciencedirect.com/science/article/pii/S0378429013004322},

doi = {10.1016/j.fcr.2013.12.018},

abstract = {In recent decades, many spectral indices have been proposed to estimate crop nitrogen (N) status parameters. However, most of the indices based on red radiation lose their sensitivity under high aboveground biomass conditions. The objectives of this study were to (i) evaluate red-edge based spectral indices for estimating plant N concentration and uptake of summer maize (Zea mays L.) and (ii) study the influence of bandwidth and crop growth stage changes on the performance of various vegetation indices. Nitrogen rate experiments for maize were conducted in 2009 and 2010 at Quzhou Experimental Station of China Agricultural University in the North China Plain. The spectral indices were calculated from hyperspectral narrow bands, simulated Crop Circle ACS-470 active crop canopy sensor bands and simulated WorldView-2 satellite broad bands. The results indicated that red edge-based canopy chlorophyll content index (CCCI) performed the best across different bandwidths for estimating summer maize plant N concentration and uptake at the V6 and V7 and V10–V12 stages. The second best index was MERIS terrestrial chlorophyll index (MTCI). The four red edge-based indices, CCCI, MTCI, normalized difference red edge (NDRE) and red edge chlorophyll index (CIred edge), performed similarly better across bandwidths for estimating plant N uptake (R2=0.76–0.91) than normalized difference vegetation index (NDVI) and ratio vegetation index (RVI) (R2=0.54–0.80) at the V10–V12 and V6–V12 stages. More studies are needed to further evaluate these red edge-based vegetation indices using real Crop Circle ACS 470 sensor and satellite

remote sensing images for maize as well as other crops under on-farm conditions.},

urldate = {2024-09-23},

journal = {Field Crops Research},

author = {Li, Fei and Miao, Yuxin and Feng, Guohui and Yuan, Fei and Yue, Shanchao and Gao, Xiaowei and Liu, Yuqing and Liu, Bin and Ustin, Susan L. and Chen, Xinping},

month = feb,

year = {2014},

keywords = {Canopy chlorophyll content index, Crop Circle sensor, Nitrogen status, Precision nitrogen management, Red edge vegetation index, WorldView-2 satellite},

pages = {111--123},

file = {ScienceDirect Snapshot:files/366/S0378429013004322.html:text/html},

}

@article{broge_comparing_2001,

title = {Comparing prediction power and stability of broadband and hyperspectral vegetation indices for estimation of green leaf area index and canopy chlorophyll density},

volume = {76},

issn = {0034-4257},

url = {https://www.sciencedirect.com/science/article/pii/S0034425700001978},

doi = {10.1016/S0034-4257(00)00197-8},

abstract = {Hyperspectral reflectance data representing a wide range of canopies were simulated using the combined PROSPECT+SAIL model. The simulations were used to study the stability of recently proposed vegetation indices (VIs) derived from adjacent narrowband spectral reflectance data across the visible (VIS) and near infrared (NIR) region of the electromagnetic spectrum. The prediction power of these indices with respect to green leaf area index (LAI) and canopy chlorophyll density (CCD) was compared, and their sensitivity to canopy architecture, illumination geometry, soil background reflectance, and atmospheric conditions were analyzed. The second soil-adjusted vegetation index (SAVI2) proved to be the best overall choice as a greenness measure. However, it is also shown that the dynamics of the VIs are very different in terms of their sensitivity to the different external factors that affects the spectral reflectance signatures of the various modeled canopies. It is concluded that hyperspectral indices are not necessarily better at predicting LAI and CCD, but that selection of a VI should depend upon (1) which parameter that needs to be estimated (LAI or CCD), (2) the expected range of this parameter, and (3) a priori knowledge of the variation of external parameters affecting the spectral reflectance of the canopy.},

number = {2},

urldate = {2024-09-23},

journal = {Remote Sensing of Environment},

author = {Broge, N. H and Leblanc, E},

month = may,

year = {2001},

pages = {156--172},

file = {ScienceDirect Snapshot:files/368/S0034425700001978.html:text/html},

}

@article{gitelson_three-band_2006,

title = {Three-band model for noninvasive estimation of chlorophyll, carotenoids, and anthocyanin contents in higher plant leaves},

volume = {33},

issn = {1944-8007},

url = {https://onlinelibrary.wiley.com/doi/abs/10.1029/2006GL026457},

doi = {10.1029/2006GL026457},

abstract = {Leaf pigment content and composition provide important information about plant physiological status. Reflectance measurements offer a rapid, nondestructive technique to estimate pigment content. This paper describes a recently developed three-band conceptual model capable of remotely estimating total of chlorophylls, carotenoids and anthocyanins contents in leaves from many tree and crop species. We tuned the spectral regions used in the model in accord with pigment of interest and the optical

characteristics of the leaves studied, and showed that the developed technique allowed accurate estimation of total chlorophylls, carotenoids and anthocyanins, explaining more than 91\%, 70\% and 93\% of pigment variation, respectively. This new technique shows a great potential for noninvasive tracking of the physiological status of vegetation and the impact of environmental changes.},

language = {en},

number = {11},

urldate = {2024-09-23},

journal = {Geophysical Research Letters},

author = {Gitelson, Anatoly and Keydan, Galina and Merzlyak, Mark},

year = {2006},

note = {_eprint: https://onlinelibrary.wiley.com/doi/pdf/10.1029/2006GL026457},

file = {Snapshot:files/370/2006GL026457.html:text/html;Texto completo:files/371/Gitelson et al. - 2006 - Three-band model for noninvasive estimation of chl.pdf:application/pdf},

}

@article{idso_normalizing_1981,

title = {Normalizing the stress-degree-day parameter for environmental variability},

volume = {24},

issn = {0002-1571},

url = {https://www.sciencedirect.com/science/article/pii/0002157181900327},

doi = {10.1016/0002-1571(81)90032-7},

abstract = {Several experiments involving the measurement of foliage-air temperature differentials (TF—TA) and air vapor pressure deficits (VPD) were conducted on squash, alfalfa, and soybean crops at Tempe and Mesa, Arizona; Manhattan, Kansas; Lincoln, Nebraska; St. Paul, Minnesota; and Fargo, North Dakota. It is shown that throughout the greater portion of the daylight period, plots of TF—TA vs. VPD yield linear relationships for plants transpiring at the potential rate, irrespective of other environmental parameters except cloud cover. This fact is used to develop a crop water stress index that is reasonably independent of environmental variability. Examples of its application to stressed soybeans and alfalfa are provided.},

urldate = {2024-09-23},

journal = {Agricultural Meteorology},

author = {Idso, S and Jackson, R and Pinter, P and Reginato, R and Hatfield, J},

month = jan,

year = {1981},

pages = {45--55},

file = {ScienceDirect Snapshot:files/373/0002157181900327.html:text/html},

}

@article{buschmann_vivo_1993,

title = {In vivo spectroscopy and internal optics of leaves as basis for remote sensing of vegetation},

volume = {14},

issn = {0143-1161},

url = {https://doi.org/10.1080/01431169308904370},

doi = {10.1080/01431169308904370},

abstract = {In vivo reflection spectra of intact bean leaves (Phaseolus vulgaris) were measured between 400 and 800 nm under remote sensing conditions (illumination with white light, detection of a narrow angle of the reflected light) using the VIRAF spectrometer. The leaves with colours from yellow to green were chosen at different times during light-induced greening. The colours of the leaves were characterized by the chromaticity coordinates according to CIE 1931 calculated from the reflection spectra. The influence of the absorption of chlorophyll—the main pigment of green leaves—on the reflection spectrum of leaves is outlined. The shape of the in vivo reflection spectra is interpreted taking into account (a)the formation of pigment-protein complexes, (b) the sieve effect and the detour effect, as well as (c) the reflection, refraction and scattering of light inside the leaf tissue. Reflection signals at several distinct wavelengths and their ratios as well as the inflection point of the reflection rise from the far red towards the near-infrared were

checked for linear correlation with the chlorophyll content per leaf area. The normalized difference vegetation index (NDVI) exhibited a relatively bad correlation with the chlorophyll content. The best correlation was found for the logarithm of the ratio of the reflection signals at 800 and 550 nm. We suggest that this parameter is used, in combination with the detection of the inflection point, for remotely-detecting vegetation and for the estimation of its chlorophyll content.},

number = {4},

urldate = {2024-09-23},

journal = {International Journal of Remote Sensing},

author = {Buschmann, C. and Nagel, E.},

month = mar,

year = {1993},

note = {Publisher: Taylor \& Francis
_eprint: https://doi.org/10.1080/01431169308904370},

pages = {711--722},

}

@article{demetriades-shah_high_1990,

title = {High resolution derivative spectra in remote sensing},

volume = {33},

issn = {0034-4257},

url = {https://www.sciencedirect.com/science/article/pii/003442579090055Q},

doi = {10.1016/0034-4257(90)90055-Q},

abstract = {The use of derivative spectra is an established technique in analytical chemistry for the elimination of background signals and for resolving overlapping spectral features. Application of this technique for tackling analogous problems such as interference from soil background reflectance in the remote sensing of vegetation or for resolving complex spectra of several target species within individual pixels in remote sensing is proposed. Methods for generating derivatives of high spectral resolution data are reviewed. Results of experiments to test the use of derivatives for monitoring chlorosis in vegetation show that derivative spectral indices are superior to conventional broad-band spectral indices such as the near-infrared / red reflectance ratio. Conventional broad-band indices are sensitive to both leaf cover as well as leaf color. New derivative spectral indices which were able to monitor chlorosis unambiguously were identified. Potential areas for the application of this technique in remote sensing are considered.},

number = {1},

urldate = {2024-09-23},

journal = {Remote Sensing of Environment},

author = {Demetriades-Shah, Tanvir and Steven, Michael and Clark, Jeremy},

month = jul,

year = {1990},

pages = {55--64},

file = {ScienceDirect Snapshot:files/376/003442579090055Q.html:text/html},

}

@article{huete_overview_2002,

series = {The {Moderate} {Resolution} {Imaging} {Spectroradiometer} ({MODIS}): a new generation of {Land} {Surface} {Monitoring}},

title = {Overview of the radiometric and biophysical performance of the {MODIS} vegetation indices},

volume = {83},

issn = {0034-4257},

url = {https://www.sciencedirect.com/science/article/pii/S0034425702000962},

doi = {10.1016/S0034-4257(02)00096-2},

abstract = {We evaluated the initial 12 months of vegetation index product availability from the Moderate Resolution Imaging Spectroradiometer (MODIS) on board the Earth Observing System-Terra platform. Two MODIS vegetation indices (VI), the normalized difference vegetation index (NDVI) and enhanced vegetation index (EVI), are produced at 1-km and 500-m resolutions and 16-day compositing periods. This paper presents an initial analysis of the MODIS NDVI and EVI performance from both radiometric and biophysical

perspectives. We utilize a combination of site-intensive and regionally extensive approaches to demonstrate the performance and validity of the two indices. Our results showed a good correspondence between airborne-measured, top-of-canopy reflectances and VI values with those from the MODIS sensor at four intensively measured test sites representing semi-arid grass/shrub, savanna, and tropical forest biomes. Simultaneously derived field biophysical measures also demonstrated the scientific utility of the MODIS VI. Multitemporal profiles of the MODIS VIs over numerous biome types in North and South America well represented their seasonal phenologies. Comparisons of the MODIS-NDVI with the NOAA-14, 1-km AVHRR-NDVI temporal profiles showed that the MODIS-based index performed with higher fidelity. The dynamic range of the MODIS VIs are presented and their sensitivities in discriminating vegetation differences are evaluated in sparse and dense vegetation areas. We found the NDVI to asymptotically saturate in high biomass regions such as in the Amazon while the EVI remained sensitive to canopy variations.},

number = {1},

urldate = {2024-09-23},

journal = {Remote Sensing of Environment},

author = {Huete, A and Didan, K and Miura, T and Rodriguez, E. P and Gao, X and Ferreira, L. G},

month = nov,

year = {2002},

pages = {195--213},

file = {ScienceDirect Snapshot:files/378/S0034425702000962.html:text/html},

}

@article{woebbecke_color_1995,

title = {Color indices for weed identification under various soil, residue, and lighting conditions},

volume = {38},

abstract = {Color slide images of weeds among various soils and residues were digitized and analyzed for red, green, and blue (RGB) color content. Red, green, and blue chromatic coordinates (rgb) of plants were very different from those of background soils and residue. To distinguish living plant material from a nonplant background, several indices of chromatic coordinates were studied, tested, and were successful in identifying weeds. The indices included r-g, g-b, (g-b){\textbar}{\textbar}r-g{\textbar}, and 2g-r-b. A modified hue was also used to distinguish weeds from non-plant surfaces. The modified hue, 2g-r-b index, and the green chromatic coordinate distinguished weeds from a nonplant background (0.05 level of significance) better than other indices. However, the modified hue was the most computationally intense. These indices worked well for both nonshaded and shaded sunlit conditions. These indices could be used for sensor design for detecting weeds for spot spraying control.},

number = {1},

journal = {Transactions of the American Society of Agricultural Engineers},

author = {Woebbecke, D and Meyer, G and Von Bargen, K. and Mortensen, D},

year = {1995},

pages = {259--269},

annote = {Cited By :1149},

file = {Snapshot:files/381/display.html:text/html},

}

@article{zhang_application_2012,

title = {Application of hyperspectral remote sensing for environment monitoring in mining areas},

volume = {65},

issn = {1866-6299},

url = {https://doi.org/10.1007/s12665-011-1112-y},

doi = {10.1007/s12665-011-1112-y},

abstract = {Environmental problems caused by extraction of minerals have long been a focus on environmental earth sciences. Vegetation growing conditions are an indirect indicator of the environmental problem in mining areas. A growing number of studies in recent years made substantial efforts to better utilize remote sensing for dynamic monitoring of vegetation growth

conditions and the environment in mining areas. In this article, airborne and satellite hypersectral remote sensing data—HyMap and Hyperion images are used in the Mount Lyell mining area in Australia and Dexing copper mining area in China, respectively. Based on the analyses of biogeochemical effect of dominant minerals, the vegetation spectrum and vegetation indices, two hyperspectral indices: vegetation inferiority index (VII) and water absorption disrelated index (WDI) are employed to monitor the environment in the mining area. Experimental results indicate that VII can effectively distinguish the stressed and unstressed vegetation growth situation in mining areas. The sensitivity of VII to the vegetation growth condition is shown to be superior to the traditional vegetation index—NDVI. The other index, WDI, is capable of informing whether the target vegetation is affected by a certain mineral. It is an important index that can effectively distinguish the hematite areas that are covered with sparse vegetation. The successful applications of VII and WDI show that hyperspectral remote sensing provides a good method to effectively monitor and evaluate the vegetation and its ecological environment in mining areas.},

language = {en},

number = {3},

urldate = {2024-09-23},

journal = {Environmental Earth Sciences},

author = {Zhang, Bing and Wu, Di and Zhang, Li and Jiao, Quanjun and Li, Qingting},

month = feb,

year = {2012},

keywords = {Hyperspectral remote sensing, Environment monitoring, Environmental Chemistry, Mining, Spectral analysis, Vegetation index},

pages = {649--658},

file = {Full Text PDF:files/383/Zhang et al. - 2012 - Application of hyperspectral remote sensing for en.pdf:application/pdf},

}

@article{sripada_aerial_2005,

title = {Aerial {Color} {Infrared} {Photography} for {Determining} {Late}-{Season} {Nitrogen} {Requirements} in {Corn}},

volume = {97},

copyright = {© American Society of Agronomy},

issn = {1435-0645},

url = {https://onlinelibrary.wiley.com/doi/abs/10.2134/agronj2004.0314},

doi = {10.2134/agronj2004.0314},

abstract = {Fast and accurate methods of determining in-season corn (Zea mays L.) N requirements are needed to provide more precise and economical management and potentially decrease groundwater N contamination. The objectives of this study were (i) to determine if there is a response to late-season N applied to corn at pretassel (VT) under irrigated and nonirrigated conditions, and (ii) to develop a methodology for predicting in-

season N requirement for corn at the VT stage using aerial color infrared (CIR) photography. Field studies were conducted for 3 yr over a wide range of soil conditions and water regimes in the North Carolina Coastal Plain. Different fertilizer N rates were applied (i) at planting (NPL) to create a range of N supply, corn color, and near-infrared (NIR) radiance; and (ii) at VT (NVT) to measure yield response to NVT. Aerial CIR photographs were obtained for each site at VT before N application. Significant grain yield responses to NPL and NVT were observed. Economic optimum NVT rates ranged from 0 to 224 kg ha−1 with a mean of 104 kg ha−1. Better prediction of economic optimum NVT rates was obtained with spectral band combinations rather than individual bands, and improved when calculated relative to high-N reference strips measured at VT. The best predictor of economic optimum NVT (R 2 = 0.67) was a linear-plateau model based on corn color and NIR radiance expressed using the Green Difference Vegetation Index (GDVI) relative to high-N reference strips (Relative GDVI, RGDVI).},

language = {en},

number = {5},

urldate = {2024-09-23},

journal = {Agronomy Journal},

author = {Sripada, Ravi and Heiniger, Ronnie and White, Jeffrey and Weisz, Randy},

year = {2005},

note = {_eprint: https://onlinelibrary.wiley.com/doi/pdf/10.2134/agronj2004.0314},
pages = {1443--1451},
file = {Full Text PDF:files/385/Sripada et al. - 2005 - Aerial Color Infrared Photography for Determining .pdf:application/pdf;Snapshot:files/386/agronj2004.html:text/html},
}

@article{louhaichi_spatially_2001,
title = {Spatially {Located} {Platform} and {Aerial} {Photography} for {Documentation} of {Grazing} {Impacts} on {Wheat}},
volume = {16},
issn = {1010-6049},
url = {https://doi.org/10.1080/10106040108542184},
doi = {10.1080/10106040108542184},
abstract = {Goose populations that winter in Oregon's Lower Willamette Valley have increased from 25 000 to more than 250 000 birds in the last 25 years, resulting in heavy grazing of wheat and other crops. To map and document the extent and intensity of goose impacts on wheat fields, we combined rectified aerial photography with both globally positioned ground observations and vertical platform photographs. Aerial photos revealed areas of fields with sparse wheat cover while platform photos documented the cause. We estimated wheat cover in ground level photographs by ratioing red, green

and blue digital numbers. From platform photographs we recorded occurrence of grazing (from grazed leaf tips), intensity of grazing (from residual plant cover and leaf length), and other indicators of goose use (footprints and droppings). Because the ground photographs were spatially positioned, we could use this information to verify the cause of “thin” wheat. Crop damage from grazing/trampling, water submergence, and other factors was evident. Our results illustrate practical ways to combine aerial and ground-level image analysis, spectral observations, and global positioning systems to quantify field conditions in wheat.},

number = {1},

urldate = {2024-09-23},

journal = {Geocarto International},

author = {Louhaichi, Mounir and Borman, Michael and Johnson, Douglas},

month = mar,

year = {2001},

note = {Publisher: Taylor \& Francis _eprint: https://doi.org/10.1080/10106040108542184},

pages = {65--70},

file = {Full Text PDF:files/388/Louhaichi et al. - 2001 - Spatially Located Platform and Aerial Photography .pdf:application/pdf},

}

@article{gitelson_signature_1996,

title = {Signature {Analysis} of {Leaf} {Reflectance} {Spectra}: {Algorithm} {Development} for {Remote} {Sensing} of {Chlorophyll}},

volume = {148},

issn = {0176-1617},

shorttitle = {Signature {Analysis} of {Leaf} {Reflectance} {Spectra}},

url = {https://www.sciencedirect.com/science/article/pii/S0176161796802847},

doi = {10.1016/S0176-1617(96)80284-7},

abstract = {The goal of the study is to investigate the basic spectral properties of plant leaves to develop spectral indices more sensitive to chlorophyll concentration than the presently widely used Notmalized Difference Vegetation Index. These indices can serve as indicators of stress, senescence, and disease in higher plants. The spectral reflectance of senescing leaves of two deciduous species (maple and chestnut) as well as their pigment content were measured. Spectral indices were developed using reflectances corresponding to wavelengths with maximum and minimum sensitivity to variation in pigment concentration. The signature analysis of reflectance spectra indicated that, for a wide range of leaf greenness (completely yellow to dark green leaves), the maximum sensitivity of reflectance coincides with the maximum absorption of chlorophyll a at 670 nm. However, for yellow-green to green leaves (minimum chlorophyll a as low as 3-5 nmol/cm2), the reflectance near 670nm is not sensitive to chlorophyll concentration due to saturation

effects. Therefore, it seems inappropriate to use this spectral band for pigment estimation in yellow-green to green vegetation. The spectral bands ranging from 400 to 480 nm and above 730 nm are not sensitive to chlorophyll concentration as found for 670 nm. The reflectances at these wavelengths could be used as references in the vegetation indices. Maximum sensitivity to chlorophyll a concentration was found at 550-560 nm and 700-710 nm. Reflectances at 700 nm correlated very well with that at 550 nm for a wide range of chlorophyll concentrations for both plant species studied. The inverse reflectance, R550)-1 and (R700)-1 are proportional to chlorophyll a concentration; therefore indices R750/R550 and R750/R700 are directly proportional (correlation r2 {\textgreater} 0.95) to chlorophyll concentration. These indices were tested for a wide range of chlorophyll a concentration, using several independent data sets. The estimation error in the derivation of chlorophyll concentration from the indices is assessed to be less than 1.2 nmol/cm2.},

number = {3},

urldate = {2024-09-23},

journal = {Journal of Plant Physiology},

author = {Gitelson, Anatoly and Merzlyak, Mark},

month = jan,

year = {1996},

keywords = {remote sensing, vegetation indices, Reflectance spectra of leaves},

pages = {494--500},

file = {ScienceDirect Snapshot:files/390/S0176161796802847.html:text/html},

}

@article{smith_forecasting_1995,

title = {Forecasting wheat yield in a {Mediterranean}-type environment from the {NOAA} satellite},

volume = {46},

issn = {1444-9838},

url = {https://www.publish.csiro.au/ar/ar9950113},

doi = {10.1071/ar9950113},

abstract = {This paper reports the relationship between the spatial variation in mean wheat yield/ha of 50 Local Government Areas in Western Australia and satellite measures of the Normalized Difference Vegetation Index (NDVI). Yield/ha was based on estimates of the area harvested and actual grain received by the Cooperative Bulk Handling Ltd. The study area covered 16.3 million ha, in which 2.9 million ha of wheat were sown and 4.66 million tonnes of grain harvested. This was 78\% of the total Western Australian wheat crop. Spatial variations in NDVI in early July, at around stem elongation, accounted for 46\% of the spatial variation in final yield. This increased to 56\% of yield variance around the onset of anthesis at the end of August. It remained high until early November (48\%) when crops were senescing or senescent. A

combination of NDVI from late August and early November accounted for 70\% of the yield variance. In comparison, total rainfall during the 1992 growing season from April to October, the main determinant of yield variations, accounted for 28\% of the yield variation. The significant correlation of NDVI with final yield by the middle of the growing season 3 to 5 months before harvest indicates the feasibility of making useful yield forecasts from this time onwards. In addition, the NDVI could provide useful spatial information on the significance of the yield/canopy development/water use relationship which underlies this correlation.},

language = {en},

number = {1},

urldate = {2024-09-23},

journal = {Australian Journal of Agricultural Research},

author = {Smith, R. and Adams, J. and Stephens, D. and Hick, P. T.},

year = {1995},

note = {Publisher: CSIRO PUBLISHING},

pages = {113--125},

}

@article{lichtenthaler_detection_1996,

title = {Detection of {Vegetation} {Stress} {Via} a {New} {High} {Resolution} {Fluorescence} {Imaging} {System}},

volume = {148},

issn = {0176-1617},

url = {https://www.sciencedirect.com/science/article/pii/S0176161796800812},

doi = {10.1016/S0176-1617(96)80081-2},

abstract = {The UV-laser (λ 355 nm) induced fluorescence emission spectra of green leaves comprise the blue(F440) and green (F520) fluorescence bands as well as the red (F690) and far-red (F740) chlorophyll fluorescence emission bands. Based on the four UV-laser induced fluorescence bands blue, green, red and farred a high resolution fluorescence imaging system was established, which allows a fast and large scale screening of fluorescence gradients and local disturbances in fluorescence emission over the whole leaf surface. The new imaging method not only permits to screen leaves by means of images in four fluorescence bands (LIF images) but, in addition, via images of the fluorescence ratios blue/red (F440/F690), blue/farred (F440/F740), the chlorophyll fluorescence ratio red/far-red (F690/F740) and the ratio blue/green (F440/F520) (LIF ratio images). By fluorescence imaging we could prove that in aurea tobacco the major part of the leaves' blue and green fluorescence is emitted from the main and side leave veins, whereas the major part of the leaves' red and far-red chlorophyll fluorescence is emitted from the vein-free leaf regions, which also have the highest chlorophyll content. A smaller proportion of the aurea tobacco leaves' blue-green fluorescence emission is derived from the cell walls of epidermis cells. The fluorescence ratios blue/red and blue/far-red are very sensitive to

environmental changes, and thus permit early stress and strain detection in plants, and the evaluation of damage to the photosynthetic apparatus. Via monitoring the increase in chlorophyll fluorescence LIF images allow to detect differences in the time-dependent uptake of diuron and the progressing inhibition of photosynthetic electron transport in the treated leaf part. The novel fluorescence imaging technique sets a new dimension for early stress detection in the photosynthetic apparatus and in plants. It has many advantages over the previously applied point-data measurements of selected leaf points using conventional spectrofluorometers. The new fluorescence imaging system proved to be very suitable for remote sensing of plants in the near distance, and can be further developed for far distance remote sensing of the state of health of terrestrial vegetation. Some examples in the many possible ways of computer-aided fluorescence data processing (formation of different fluorescence ratios, screening of fluorescence profiles, histogramme plotting) are indicated.},

number = {5},

urldate = {2024-09-23},

journal = {Journal of Plant Physiology},

author = {Lichtenthaler, H. and Lang, M. and Sowinska, M. and Heisel, F. and Miehé, J. A.},

month = jan,

year = {1996},

keywords = {diuron, Fluorescence imaging blue-green fluorescence, fluorescence ratios blue/red blue/far-red, inhibitionof electron transport, LIF images, LIF ratio images, red and far-red chlorophyll fluorescence, red/far-red stress detection},

pages = {599--612},

file = {ScienceDirect Snapshot:files/393/S0176161796800812.html:text/html},

}

@misc{zhang_investigacion_2011,

title = {Investigación sobre inversión del índice de vegetación ambiental y del índice de área foliar basada en datos {CCD} de satélites ambientales},

url = {https://my.wanfangdata.com.cn/auth/user/alllogin.do?service=https%3a%2f%2foss.wanfangdata.com.cn%2fwww%2f%25E5%259F%25BA%25E4%25BA%258E%25E7%258E%25AF%25E5%25A2%2583%25E6%2598%259FCCD%25E6%2595%25B0%25E6%258D%25AE%25E7%259A%2584%25E7%258E%25AF%25E5%25A2%2583%25E6%25A4%258D%25E8%25A2%25AB%25E6%258C%2587%25E6%2595%25B0%25E5%258F%258A%25E5%258F%25B6%25E9%259D%25A2%25E7%25A7%25AF%25E6%258C%2587%25E6%2595%25B0%25E5%258F%258D%25E6%25BC%2594%25E7%25A0%2594%25E7%25A9%25B6.ashx%3fisread%3dtrue%26type%3dperio%26resourceId%3dgpxygpfx201110043},

abstract = {Utilizando el espectro del dosel vegetal simulado por el modelo directo PROSAIL, al construir el índice de vegetación se introdujeron las bandas canasta y verde para corregir la influencia de la atmósfera y el fondo del suelo, y se construyó un índice de vegetación ambiental (EVI) para evitar la saturación prematura. Basado en los datos de observación terrestre de múltiples períodos típicos de crecimiento del trigo de invierno, se estableció un modelo de inversión de series a largo plazo basado en EVI-LAI y el modelo se verificó de forma cruzada entre diferentes variedades. índice (LAI) establecido por EVI La precisión del modelo de inversión es mejor que la de modelos de índice de vegetación similares, tiene buena universalidad y se puede aplicar al monitoreo del crecimiento multitemporal por teledetección del trigo de invierno y a la inversión del LAI.},

urldate = {2024-09-23},

author = {Zhang, Ying and Meng, Qingyan and Wu, Jiali and Zhao, Feng},

year = {2011},

file = {2024-09-23晚上19-32-46@WanFangdata.txt:files/396/2024-09-23晚上19-32-46@WanFangdata.txt:text/plain;万方登录

:files/395/alllogin.html:text/html},

}

@article{mahlein_development_2013,

title = {Development of spectral indices for detecting and identifying plant diseases},

volume = {128},

issn = {0034-4257},

url = {https://www.sciencedirect.com/science/article/pii/S0034425712003793},

doi = {10.1016/j.rse.2012.09.019},

abstract = {Spectral vegetation indices (SVIs) have been shown to be useful for an indirect detection of plant diseases. However, these indices have not been evaluated to detect or to differentiate between plant diseases on crop plants. The aim of this study was to develop specific spectral disease indices (SDIs) for the detection of diseases in crops. Sugar beet plants and the three leaf diseases Cercospora leaf spot, sugar beet rust and powdery mildew were used as model system. Hyperspectral signatures of healthy and diseased sugar beet leaves were assessed with a non-imaging spectroradiometer at different developing stages and disease severities of pathogens. Significant and most relevant wavelengths and two band normalized differences from 450 to 950nm, describing the impact of a disease on sugar beet leaves were extracted from the data-set using the RELIEF-F algorithm. To develop hyperspectral indices for the detection of sugar beet diseases the best weighted combination of a single wavelength and a normalized wavelength difference was exhaustively searched testing all possible combinations. The optimized disease indices were tested for their ability to detect and to classify

healthy and diseased sugar beet leaves. With a high accuracy and sensitivity healthy sugar beet leaves and leaves, infected with Cercospora leaf spot, sugar beet rust and powdery mildew were classified (balanced classification accuracy: 89\%, 92\%, 87\%, 85\%, respectively). Spectral disease indices were also successfully applied on hyperspectral imaging data and on non-imaging data from a sugar beet field. Specific disease indices will improve disease detection, identification and monitoring in precision agriculture applications.},

urldate = {2024-09-23},

journal = {Remote Sensing of Environment},

author = {Mahlein, A. and Rumpf, T. and Welke, P. and Dehne, H. -W. and Plümer, L. and Steiner, U. and Oerke, E. -C.},

month = jan,

year = {2013},

keywords = {Band selection, Hyperspectral reflectance, leaf spot, Plant diseases, Powdery mildew, Precision crop protection, Spectral disease indices, Sugar beet, Sugar beet rust},

pages = {21--30},

file = {ScienceDirect Snapshot:files/398/S0034425712003793.html:text/html},

}

@article{musick_response_1988,

title = {Response to soil moisture of spectral indexes derived from bidirectional reflectance in thematic mapper wavebands},

volume = {25},

issn = {0034-4257},

url = {https://www.sciencedirect.com/science/article/pii/0034425788900995},

doi = {10.1016/0034-4257(88)90099-5},

abstract = {Laboratory reflectance measurements of 10 soils were used to determine the relationship between soil moisture and three spectral indices: the TM5/7 ratio and the WetnessR and BrightnessR features of the reflectance factor TM Tasseled Cap transformation. Response of the indices to dry mass water percentage was approximately linear for individual soils, except for WetnessR and BrightnessR at high moisture content. Soil differences in the slopes of the WetnessR- and Brithgness R-moisture content relationships were almost entirely eliminated by expressing water content as the percentage of water retained at 0.1 bar (10 kPa) tension (“relative water content”). The resultant soil lines were offset from one another by the differences in dry soil i index value. Slope of the TM5/7 response was not completely normalized by expressing moisture status as relative water content, because slope appeared to vary with dry soil ratio value. Sensitivity to the effects of illumination angle was negligible for the TM5/7 ratio, somewhat greater for WetnessR, and greatest for BrightnessR.},

number = {2},

urldate = {2024-09-23},

journal = {Remote Sensing of Environment},

author = {Musick, H. and Pelletier, Ramona},

month = jul,

year = {1988},

pages = {167--184},

file = {ScienceDirect Snapshot:files/400/0034425788900995.html:text/html},

}

@article{crippen_calculating_1990,

title = {Calculating the vegetation index faster},

volume = {34},

issn = {0034-4257},

url = {https://www.sciencedirect.com/science/article/pii/003442579090085Z},

doi = {10.1016/0034-4257(90)90085-Z},

abstract = {The near-infrared (NIR) versus red “infrared percentage vegetation index,” NIR/(NIR + Red), is functionally and linearly equivalent to the normalized difference vegetation index, (NIR-Red/(NIR + Red). Advantageously, it is both computationally faster and never negative.},

number = {1},

urldate = {2024-09-23},

journal = {Remote Sensing of Environment},

author = {Crippen, Robert},

month = oct,

year = {1990},

pages = {71--73},

file = {ScienceDirect Snapshot:files/402/003442579090085Z.html:text/html},

}

@article{daughtry_estimating_2000,

title = {Estimating {Corn} {Leaf} {Chlorophyll} {Concentration} from {Leaf} and {Canopy} {Reflectance}},

volume = {74},

issn = {0034-4257},

url = {https://www.sciencedirect.com/science/article/pii/S0034425700001139},

doi = {10.1016/S0034-4257(00)00113-9},

abstract = {Farmers must balance the competing goals of supplying adequate N for their crops while minimizing N losses to the environment. To characterize the spatial variability of N over large fields, traditional methods (soil testing, plant tissue analysis, and chlorophyll meters) require many point samples. Because of the close link between leaf chlorophyll and leaf N concentration, remote sensing techniques have the potential to evaluate the N

variability over large fields quickly. Our objectives were to (1) select wavelengths sensitive to leaf chlorophyll concentration, (2) simulate canopy reflectance using a radiative transfer model, and (3) propose a strategy for detecting leaf chlorophyll status of plants using remotely sensed data. A wide range of leaf chlorophyll levels was established in field-grown corn (Zea mays L.) with the application of 8 N levels: 0\%, 12.5\%, 25\%, 50\%, 75\%, 100\%, 125\%, and 150\% of the recommended rate. Reflectance and transmittance spectra of fully expanded upper leaves were acquired over the 400-nm to 1,000-nm wavelength range shortly after anthesis with a spectroradiometer and integrating sphere. Broad-band differences in leaf spectra were observed near 550 nm, 715 nm, and {\textgreater}750 nm. Crop canopy reflectance was simulated using the SAIL (Scattering by Arbitrarily Inclined Leaves) canopy reflectance model for a wide range of background reflectances, leaf area indices (LAI), and leaf chlorophyll concentrations. Variations in background reflectance and LAI confounded the detection of the relatively subtle differences in canopy reflectance due to changes in leaf chlorophyll concentration. Spectral vegetation indices that combined near-infrared reflectance and red reflectance (e.g., OSAVI and NIR/Red) minimized contributions of background reflectance, while spectral vegetation indices that combined reflectances of near-infrared and other visible bands (MCARI and NIR/Green) were responsive to both leaf chlorophyll concentrations and background reflectance. Pairs of these spectral vegetation indices plotted together produced isolines of leaf chlorophyll concentrations. The slopes of

these isolines were linearly related to leaf chlorophyll concentration. A limited test with measured canopy reflectance and leaf chlorophyll data confirmed these results. The characterization of leaf chlorophyll concentrations at the field scale without the confounding problem of background reflectance and LAI variability holds promise as a valuable aid for decision making in managing N applications.},

number = {2},

urldate = {2024-09-23},

journal = {Remote Sensing of Environment},

author = {Daughtry, C. S. T and Walthall, C. and Kim, M. S and de Colstoun, E. Brown and McMurtrey, J. E},

month = nov,

year = {2000},

pages = {229--239},

file = {ScienceDirect Snapshot:files/404/S0034425700001139.html:text/html},

}

@article{haboudane_hyperspectral_2004,

title = {Hyperspectral vegetation indices and novel algorithms for predicting green {LAI} of crop canopies: {Modeling} and validation in the context of precision agriculture},

volume = {90},

issn = {0034-4257},

shorttitle = {Hyperspectral vegetation indices and novel algorithms for predicting green {LAI} of crop canopies},

url = {https://www.sciencedirect.com/science/article/pii/S0034425704000264},

doi = {10.1016/j.rse.2003.12.013},

abstract = {A growing number of studies have focused on evaluating spectral indices in terms of their sensitivity to vegetation biophysical parameters, as well as to external factors affecting canopy reflectance. In this context, leaf and canopy radiative transfer models are valuable for modeling and understanding the behavior of such indices. In the present work, PROSPECT and SAILH models have been used to simulate a wide range of crop canopy reflectances in an attempt to study the sensitivity of a set of vegetation indices to green leaf area index (LAI), and to modify some of them in order to enhance their responsivity to LAI variations. The aim of the paper was to present a method for minimizing the effect of leaf chlorophyll content on the prediction of green LAI, and to develop new algorithms that adequately predict the LAI of crop canopies. Analyses based on both simulated and real hyperspectral data were carried out to compare performances of existing vegetation indices (Normalized Difference Vegetation Index [NDVI], Renormalized Difference Vegetation Index [RDVI], Modified Simple Ratio [MSR], Soil-Adjusted Vegetation Index [SAVI], Soil and Atmospherically Resistant Vegetation Index [SARVI], MSAVI, Triangular Vegetation Index [TVI],

and Modified Chlorophyll Absorption Ratio Index [MCARI]) and to design new ones (MTVI1, MCARI1, MTVI2, and MCARI2) that are both less sensitive to chlorophyll content variations and linearly related to green LAI. Thorough analyses showed that the above existing vegetation indices were either sensitive to chlorophyll concentration changes or affected by saturation at high LAI levels. Conversely, two of the spectral indices developed as a part of this study, a modified triangular vegetation index (MTVI2) and a modified chlorophyll absorption ratio index (MCARI2), proved to be the best predictors of green LAI. Related predictive algorithms were tested on CASI (Compact Airborne Spectrographic Imager) hyperspectral images and, then, validated using ground truth measurements. The latter were collected simultaneously with image acquisition for different crop types (soybean, corn, and wheat), at different growth stages, and under various fertilization treatments. Prediction power analysis of proposed algorithms based on MCARI2 and MTVI2 resulted in agreements between modeled and ground measurement of non-destructive LAI, with coefficients of determination (r2) being 0.98 for soybean, 0.89 for corn, and 0.74 for wheat. The corresponding RMSE for LAI were estimated at 0.28, 0.46, and 0.85, respectively.},

number = {3},

urldate = {2024-09-23},

journal = {Remote Sensing of Environment},

author = {Haboudane, Driss and Miller, John R and Pattey, Elizabeth and Zarco-Tejada, Pablo J and Strachan, Ian B},

month = apr,

year = {2004},

keywords = {Chlorophyll content, Hyperspectral, Green LAI, Precision agriculture, Prediction algorithms, Spectral indices},

pages = {337--352},

file = {ScienceDirect Snapshot:files/406/S0034425704000264.html:text/html},

}

@article{yang_impact_2008,

title = {{IMPACT} {OF} {BAND}-{RATIO} {ENHANCED} {AWIFS} {IMAGE} {TO} {CROP} {CLASSIFICATION} {ACCURACY}},

url = {https://www.asprs.org/a/publications/proceedings/pecora17/0041.pdf},

abstract = {Multispectral satellite images have been utilized in the National Agricultural Statistics Service (NASS) for crop cover classification and crop acreage estimation since the 1970's. Though ancillary data is utilized to enhance the classification accuracy, there are few applications that maximize the utilization of the feature information of the given multispectral images. Every multispectral image band directly provides the specific spectral response to a given land cover category. The different combinations of band ratios or vegetation indices enhance spectral characteristics of some crops while suppressing others. Therefore, various vegetation indices and image ratios of

Landsat images have been extensively studied and applied to identify various land cover and land use characteristics in the past. However, NASS began using the ResourceSat-1 AWIFS sensor for operational crop classification and acreage estimation in 2006. The AWIFS' bands are different from those of Landsat, and there is sparse literature published about research and applications of the spectral characteristics of AWIFS image band ratio and vegetation indices. In this paper, the impact of using band ratio and vegetation indices of the AWIFS images to the crop classification accuracy is empirically investigated via supervised classification. The classification results with respect to the additional vegetation index and band ratio are presented and compared in terms of the overall and crop only classification accuracy. The research indicates that appropriately used vegetation indices and image ratios can potentially improve crop classification accuracy though the gain may not be huge. It is concluded that further research is needed.},

language = {en},

author = {Yang, Zhengwei and Willis, Patrick and Mueller, Rick},

year = {2008},

file = {Yang et al. - 2008 - IMPACT OF BAND-RATIO ENHANCED AWIFS IMAGE TO CROP .pdf:files/407/Yang et al. - 2008 - IMPACT OF BAND-RATIO ENHANCED AWIFS IMAGE TO CROP .pdf:application/pdf},

}

@article{datt_new_1999,

title = {A {New} {Reflectance} {Index} for {Remote} {Sensing} of {Chlorophyll} {Content} in {Higher} {Plants}: {Tests} using \textit{{Eucalyptus}} {Leaves}},

volume = {154},

issn = {0176-1617},

shorttitle = {A {New} {Reflectance} {Index} for {Remote} {Sensing} of {Chlorophyll} {Content} in {Higher} {Plants}},

url = {https://www.sciencedirect.com/science/article/pii/S0176161799803149},

doi = {10.1016/S0176-1617(99)80314-9},

abstract = {The visible/near infrared reflectance properties of leaves from several Eucalyptus species were studied to determine appropriate indices for remote sensing of chlorophyll content. Reflectance near 710 nm wavelength showed a higher sensitivity to chlorophyll content than reflectance near 550nm. The near infrared band with the least sensitivity to chlorophyll content was located at 850 nm. The use of R710 nm as the sensitive band and R850 nm as the insensitive band, increased the correlation of the reflectance indices to chlorophyll content. Among several reflectance indices tested, the ratio (R850-R710)/(R850-R680) performed best, and is proposed as a new index for the remote estimation of chlorophyll content in higher plants. This new index is insensitive to the effects of leaf scattering on reflectance, and relates strongly to the variation in reflectance caused by chlorophyll absorption.},

number = {1},

urldate = {2024-09-23},

journal = {Journal of Plant Physiology},

author = {Datt, Bisun},

month = jan,

year = {1999},

keywords = {remote sensing, Chlorophyll content, Eucalyptus, leaf optical properties, reflectance index, reflectance spectra},

pages = {30--36},

file = {ScienceDirect Snapshot:files/410/S0176161799803149.html:text/html},

}

@article{chen_evaluation_1996,

title = {Evaluation of {Vegetation} {Indices} and a {Modified} {Simple} {Ratio} for {Boreal} {Applications}},

volume = {22},

issn = {0703-8992},

url = {https://doi.org/10.1080/07038992.1996.10855178},

doi = {10.1080/07038992.1996.10855178},

abstract = {Un ratio simple modifié (MSR) est proposé pour extraire les paramètres biophysiques des forêts boréales à l'aide de données de télédétection. Cet indice de végétation est formulé en fonction de l'évaluation de plusieurs indices de végétation dérivés de la combinaison de deux bandes

spectrales, dont les suivants : indice de végétation par différence normalisée ou indice d'activité végétale (NDVI), ratio simple (SR), indice de végétation ajusté en fonction des sols (SAVI, SAVI1, SAVI2), indice de végétation par différence pondérée (WDVI), indice de végétation zonale (GEMI), indice de végétation non linéaire (NLI) et indice de végétation par différence renormalisée (RDVI). Le ratio simple modifié est une version améliorée des indices de végétation par différence renormalisée et sert à délimiter les relations de ces derniers avec les paramètres biophysiques. Tous les indices ont été obtenus à partir d'images acquises par le capteur thématique de Landsat-5 dans les bandes 3 (visible) et 4 (proche infrarouge) après correction des effets de l'atmosphère (à l'exception de l'indice de végétation zonale). De plus, ils ont été corrélés avec des données de terrain obtenues dans vingt peuplements de pins de Banks (Pinus Banksiana) et d'épinettes noires (Picea mariana) au cours de l'expérience BOREAS menée en 1994. Ces mesures comprennent l'indice de surface foliaire (LAI) et la fraction du rayonnement photosynthétiquement utilisable (FPAR) absorbée par le couvert forestier. Parmi ces indices de végétation, les indices SR, MSR et NDVI présentaient la meilleure corrélation avec les indices LAI et FPAR, tant au printemps qu'en été. Tous les autres indices ont donné de piètres résultats. Les indices NDVI et MSR peuvent être exprimés comme une fonction de SR. Des erreurs de mesure se produisent souvent avec les données de télédétection en raison des variations de l'angle zénithal du soleil, des effets de recouvrement partiel des pixels par des nuages, des caractéristiques de surface dissemblables, des

variations de la topographie, ainsi que d'autres facteurs environnementaux. Ces erreurs entraînent généralement un accroissement ou une diminution simultanées des réflectances dans le rouge et le proche infrarouge; leurs effets peuvent être largement atténués en effectuant des rapports de bandes. Pour tous les autres indices impliquant des opérations mathématiques autres que des rapports de bandes, les erreurs peuvent être maintenues ou même amplifiées. Le principal problème que pose l'utilisation des indices de végétation obtenus à partir de données acquises dans les bandes rouges et infrarouges réside dans leur faible sensibilité aux conditions de végétation de l'étage dominant. Bien qu'un bon nombre des indices de végétation, tels que les indices SAVI, SAVI1 et SAVI2, soient développés afin de réduire au minimum les effets de l'arrière-plan sur l'extraction de l'information relative à la végétation, la sensibilité de ces indices aux changements de conditions de l'étage dominant est également réduite.},

number = {3},

urldate = {2024-09-23},

journal = {Canadian Journal of Remote Sensing},

author = {Chen, Jing},

month = sep,

year = {1996},

note = {Publisher: Canadian Aeronautics and Space Institute _eprint: https://doi.org/10.1080/07038992.1996.10855178},

keywords = {vegetation index, boreal forests, FPAR, LAI},

pages = {229--242},
}

@article{qi_modified_1994,
title = {A modified soil adjusted vegetation index},
volume = {48},
issn = {0034-4257},
url = {https://www.sciencedirect.com/science/article/pii/0034425794901341},
doi = {10.1016/0034-4257(94)90134-1},
abstract = {There is currently a great deal of interest in the quantitative characterization of temporal and spatial vegetation patterns with remotely sensed data for the study of earth system science and global change. Spectral models and indices are being developed to improve vegetation sensitivity by accounting for atmosphere and soil effects. The soil-adjusted vegetation index (SAVI) was developed to minimize soil influences on canopy spectra by incorporating a soil adjustment factor L into the denominator of the normalized difference vegetation index (NDVI) equation. For optimal adjustment of the soil effect, however, the L factor should vary inversely with the amount of vegetation present. A modified SAVI (MSAVI) that replaces the constant L in the SAVI equation with a variable L function is presented in this article. The L function may be derived by induction or by using the product of the NDVI and weighted difference vegetation index (WDVI). Results based on ground and

aircraft-measured cotton canopies are presented. The MSAVI is shown to increase the dynamic range of the vegetation signal while further minimizing the soil background influences, resulting in greater vegetation sensitivity as defined by a “vegetation signal” to “soil noise” ratio.},

number = {2},

urldate = {2024-09-23},

journal = {Remote Sensing of Environment},

author = {Qi, J. and Chehbouni, A. and Huete, A. R. and Kerr, Y. H. and Sorooshian, S.},

month = may,

year = {1994},

pages = {119--126},

file = {ScienceDirect Snapshot:files/413/0034425794901341.html:text/html},

}

@article{hunt_detection_1989,

title = {Detection of changes in leaf water content using {Near}- and {Middle}-{Infrared} reflectances},

volume = {30},

issn = {0034-4257},

url = {https://www.sciencedirect.com/science/article/pii/0034425789900461},

doi = {10.1016/0034-4257(89)90046-1},

abstract = {Detection of plant water stress by remote sensing has been proposed using indices of Near-Infrared (NIR, 0.7–1.3 μm) and Middle-Infrared (MIR, 1.3–2.5 μm) wavelengths. The first objective of this study was to test the ability of the Leaf Water Content Index (LWCI) to determine leaf Relative Water content (RWC) of different species with different leaf morphologies. The second objective was to determine how the Moisture Stress Index (MSI; MIR / NIR) varies with RWC and the Equivalent Water Thickness (EWT). Reflectance factors at 0.82 μm and 1.6 μm were measured on leaves of Quercus agrifolia (sclerophyllous leaves), Liquidambar styraciflua (hardwood deciduous tree leaves), Picea rubens and Picea pungens (conifer needles), and Glycine max (herbaceous dicot leaves) as they dried on a laboratory bench. RWC and EWT were measured concurrently with the reflectance measurements. The results showed that LWCI was equal to RWC for the species tested. However, the results of a sensitivity analysis indicated the reflectances at 1.6 μm for two different RWC must be known for accurate prediction of unknown RWC; thus the LWCI is impractical for field applications. MSI was linearly correlated to RWCwith each species having a different regression equation and to log10 EWT with data of all species falling on the same regression line. Because EWT is correlated with leaf area index, MSI should also be correlated with leaf area index. Assuming that the linear regression equation of MSI to EWT can be applied to canopies, then the minimum significant change of RWC that can be detected is 52\%. For most plants, the natural variation in RWC from water

stress is only about 20\%, so that we conclude that indices derived from NIR and MIR reflectances cannot be used to remotely-sense water stress.},

number = {1},

urldate = {2024-09-23},

journal = {Remote Sensing of Environment},

author = {Hunt, E. and Rock, Barrett},

month = oct,

year = {1989},

pages = {43--54},

file = {ScienceDirect Snapshot:files/415/0034425789900461.html:text/html},

}

@article{datt_visiblenear_1999,

title = {Visible/near infrared reflectance and chlorophyll content in {Eucalyptus} leaves},

volume = {20},

issn = {0143-1161},

url = {https://doi.org/10.1080/014311699211778},

doi = {10.1080/014311699211778},

abstract = {The visible/near infrared reflectance properties of leaves from several Eucalyptus species were studied to determine appropriate indices for remote sensing of chlorophyll content. A scatter correction technique was

applied to the reflectance spectra to reduce the additive and multiplicative scattering effects of leaf surface and internal structure. This method gave improved calibrations for the estimation of chlorophyll content. Reflectance near 710nm wavelength showed maximum sensitivity to chlorophyll content. Reflectance near 550nm was a less sensitive indicator of chlorophyll content. Among several reflectance indices tested, the ratio (R850-R710)/(R850-R680) performed best, and is proposed as a new index for the remote estimation of chlorophyll content in higher plants. From the first derivative of reflectance, the ratio D1(754)/D1(704) and the wavelength position of the red edge were best correlated to chlorophyll content. The ratio D2(712)/D2(688) from the second derivative of reflectance was also an equally good indicator of chlorophyll content.},

number = {14},

urldate = {2024-09-23},

journal = {International Journal of Remote Sensing},

author = {Datt, B.},

month = jan,

year = {1999},

note = {Publisher: Taylor \& Francis _eprint: https://doi.org/10.1080/014311699211778},

pages = {2741--2759},

file = {Full Text PDF:files/417/Datt - 1999 - Visiblenear infrared reflectance and chlorophyll .pdf:application/pdf},

}

@misc{vogelmann_red_1993,

title = {Red edge spectral measurements from sugar maple leaves: {International} {Journal} of {Remote} {Sensing}: {Vol} 14, {No} 8},

url = {https://www.tandfonline.com/doi/abs/10.1080/01431169308953986},

abstract = {Muchos rodales de arce azucarero en el noreste de los Estados Unidos sufrieron daños extensos por insectos durante la temporada de crecimiento de 1988. Se adquirieron datos de clorofila y datos de reflectancia de laboratorio de espectrómetro de alta resolución espectral para múltiples colecciones de hojas individuales desprendidas de arce azucarero afectadas de diversas maneras por el insecto durante la temporada de crecimiento de 1988. Los datos de reflectancia indicaron diferencias consistentes y diagnósticas en la porción del borde rojo (680-750 nm) del espectro entre las diversas muestras y poblaciones de hojas. Estas incluyeron diferencias en el punto de inflexión del borde rojo (REIP), una relación de reflectancia a 740-720 nm (RE3/RE2) y una relación de valores de primera derivada a 715-705 nm (D715/D705). Los tres parámetros del borde rojo estaban altamente correlacionados con la variación en el contenido total de clorofila. Otras medidas espectrales, incluido el índice de vegetación de diferencia normalizada (NDVI) y el índice de vegetación simple (VI), también variaron entre poblaciones y durante la temporada de crecimiento, pero no se

correlacionaron bien con el contenido total de clorofila. Los estudios de apilamiento de hojas sobre fondos claros y oscuros indicaron que REIP, RE3/RE2 y D715/D705 estaban mucho menos influenciados por las diferencias en la biomasa de las hojas verdes y la condición del fondo que el NDVI o el VI.},

urldate = {2024-09-23},

author = {Vogelmann, J. and Rock, B. and Moss, D.},

year = {1993},

file = {Red edge spectral measurements from sugar maple leaves\: International Journal of Remote Sensing\: Vol 14, No 8:files/419/01431169308953986.html:text/html},

}

@article{serrano_remote_2002,

title = {Remote sensing of nitrogen and lignin in {Mediterranean} vegetation from {AVIRIS} data: {Decomposing} biochemical from structural signals},

volume = {81},

issn = {0034-4257},

shorttitle = {Remote sensing of nitrogen and lignin in {Mediterranean} vegetation from {AVIRIS} data},

url = {https://www.sciencedirect.com/science/article/pii/S0034425702000111},

doi = {10.1016/S0034-4257(02)00011-1},

abstract = {Remote sensing estimates of vegetation nitrogen (N) and lignin concentration are central to assess ecosystem processes such as growth and decomposition. Although remote sensing techniques have been proven useful to assess N and lignin contents in continuous green canopies, more studies are needed to address their capabilities, particularly in low and sparsely vegetated ecosystems. We investigated the possibility of estimating canopy N and lignin concentrations in chaparral vegetation using Airborne Visible/Infrared Imaging Spectrometer (AVIRIS) reflectance acquired over an area around Point Dume in the Santa Monica Mountains (Los Angeles, CA, USA). Two approaches were tested: multiple stepwise regression based on first difference reflectance (FDR) and reflectance (R) indices. Multiple stepwise regressions (of three or fewer wavelengths) accounted for a large variance in canopy biochemical concentration (r2~0.9, P{\textless}0.01). Log transformed R indices [log (1/R)] formulated on the basis of previously known N and lignin absorption wavelengths also showed significant correlations (P{\textless}0.01) with canopy biochemical concentration (r2 ranging from 0.39 to 0.48). In addition, the contribution of structural and biochemical signals and background effects on the performance of these indices was evaluated. These indices accounted for a increased variance when adding information on canopy structural attributes (e.g., relative contribution of each species and biomass amount) to foliar biochemical concentration. The relative contributions of foliar biochemical concentration and canopy structure (biomass amount) on the

spectral signal were further evaluated by analyzing the residuals from linear regressions: foliar N concentration accounted for 42\% of the variance for a normalized difference index based on the 1510-nm N absorption feature, while the foliar lignin concentration accounted for 44\% of the variance for a normalized difference index based on the 1754 nm lignin absorption feature. These percentages increased to 58\% when stands with senescing vegetation were disregarded. We propose the two indices, Normalized Difference Nitrogen Index (NDNI=[log (1/R1510)−log (1/R1680)]/[log (1/R1510)+log (1/R1680)]) and Normalized Difference Lignin Index (NDLI=[log (1/R1754)−log (1/R1680)]/[log (1/R1754)+log (1/R1680)]) as indices to assess N and lignin in native shrub vegetation.},

number = {2},

urldate = {2024-09-23},

journal = {Remote Sensing of Environment},

author = {Serrano, Lydia and Peñuelas, Josep and Ustin, Susan L},

month = aug,

year = {2002},

pages = {355--364},

file = {ScienceDirect Snapshot:files/421/S0034425702000111.html:text/html},

}

@article{mcfeeters_use_1996,

title = {The use of the {Normalized} {Difference} {Water} {Index} ({NDWI}) in the delineation of open water features},

volume = {17},

issn = {0143-1161},

url = {https://doi.org/10.1080/01431169608948714},

doi = {10.1080/01431169608948714},

abstract = {The Normalized Difference Water Index (NDWI) is a new method that has been developed to delineate open water features and enhance their presence in remotely-sensed digital imagery. The NDWI makes use of reflected near-infrared radiation and visible green light to enhance the presence of such features while eliminating the presence of soil and terrestrial vegetation features. It is suggested that the NDWI may also provide researchers with turbidity estimations of water bodies using remotely-sensed digital data.},

number = {7},

urldate = {2024-09-23},

journal = {International Journal of Remote Sensing},

author = {McFeeters, S.},

month = may,

year = {1996},

note = {Publisher: Taylor \& Francis _eprint: https://doi.org/10.1080/01431169608948714},

pages = {1425--1432},

}

@article{verrelst_angular_2008,

series = {Earth {Observations} for {Terrestrial} {Biodiversity} and {Ecosystems} {Special} {Issue}},

title = {Angular sensitivity analysis of vegetation indices derived from {CHRIS}/{PROBA} data},

volume = {112},

issn = {0034-4257},

url = {https://www.sciencedirect.com/science/article/pii/S0034425707004683},

doi = {10.1016/j.rse.2007.11.001},

abstract = {View angle effects present in spectral vegetation indices can either be regarded as an added source of uncertainty for variable retrieval or as a source of additional information, enhancing the variable retrieval; however, the magnitude of these angular effects remains for most indices unknown or unquantified. We use the ESA-mission CHRIS-PROBA (Compact High Resolution Imaging Spectrometer onboard the Project for On-board Autonomy) providing spaceborne imaging spectrometer and multiangular data to assess the reflectance anisotropy of broadband as well as recently developed narrowband indices. Multiangular variability of Hemispherical Directional Reflectance Factor (HDRF) is a prime factor determining the indices´ angular response. Two contrasting structural vegetation types, pine forest and

meadow, were selected to study the effect of reflectance anisotropy on the angular response. Calculated indices were standardized and statistically evaluated for their varying HDRF. Additionally we employ a coupled radiative transfer model (PROSPECT/FLIGHT) to quantify and substantiate the findings beyond an incidental case study. Nearly all tested indices manifested a prominent anisotropic behaviour. Apart from the conventional broadband greenness indices [e.g. Simple Ratio Index (SRI), Normalized Difference Vegetation Index (NDVI)], light use efficiency and leaf pigment indices [e.g. Structure Insensitive Pigment Index (SIPI), Photochemical Reflectance Index (PRI) and Anthocyanin Reflectance Index (ARI)] did express significant different angular responses depending on the vegetation type. Following the quantification of the impact, we conclude that the angular-dependent fraction of non-photosynthetic material is of critical importance shaping the angular signature of these VIs. This work highlights the influence of viewing geometry and surface reflectance anisotropy, particularly when using light use efficiency and leaf pigment indices.},

number = {5},

urldate = {2024-09-23},

journal = {Remote Sensing of Environment},

author = {Verrelst, J. and Schaepman, M. E. and Koetz, B. and Kneubühler, M.},

month = may,

year = {2008},

keywords = {Vegetation indices, Coniferous canopy, Light use efficiency, Multiangular remote sensing, Narrowband indices, Photochemical Reflectance Index, Reflectance anisotropy},

pages = {2341--2353},

file = {ScienceDirect Snapshot:files/424/S0034425707004683.html:text/html},

}

@article{tucker_red_1979,

title = {Red and photographic infrared linear combinations for monitoring vegetation},

volume = {8},

issn = {0034-4257},

url = {https://www.sciencedirect.com/science/article/pii/0034425779900130},

doi = {10.1016/0034-4257(79)90013-0},

abstract = {In situ collected spectrometer data were used to evaluate and quantify the relationships between various linear combinations of red and photographic infrared radiances and experimental plot biomass, leaf water content, and chlorophyll content. The radiance variables evaluated included the red and photographic infrared (IR) radiance and the linear combinations of the IR/red ratio, the square root of the IR/red ratio, the IR-red difference, the vegetation index, and the transformed vegetation index. In addition, the

corresponding green and red linear combinations were evaluated for comparative purposes. Three data sets were used from June, September, and October sampling periods. Regression analysis showed the increased utility of the IR and red linear combinations vis-à-vis the same green and red linear combinations. The red and IR linear combinations had 7\% and 14\% greater regression significance than the green and red linear combinations for the June and September sampling periods, respectively. The vegetation index, transformed vegetation index, and square root of the IR/red ratio were the most significant, followed closely by the IR/red ratio. Less than a 6\% difference separated the highest and lowest of these four ER and red linear combinations. The use of these linear combinations was shown to be sensitive primarily to the green leaf area or green leaf biomass. As such, these linear combinations of the red and photographic IR radiances can be employed to monitor the photosynthetically active biomass of plant canopies.},

number = {2},

urldate = {2024-09-23},

journal = {Remote Sensing of Environment},

author = {Tucker, Compton},

month = may,

year = {1979},

pages = {127--150},

file = {ScienceDirect Snapshot:files/426/0034425779900130.html:text/html;Versión

enviada:files/427/Tucker - 1979 - Red and photographic infrared linear combinations .pdf:application/pdf},
}

@article{wang_nmdi_2007,
title = {{NMDI}: {A} normalized multi-band drought index for monitoring soil and vegetation moisture with satellite remote sensing},
volume = {34},
copyright = {Copyright 2007 by the American Geophysical Union.},
issn = {1944-8007},
shorttitle = {{NMDI}},
url = {https://onlinelibrary.wiley.com/doi/abs/10.1029/2007GL031021},
doi = {10.1029/2007GL031021},
abstract = {A new index, the Normalized Multi-band Drought Index (NMDI), is proposed for monitoring soil and vegetation moisture from space. NMDI is defined as , where R represents the apparent reflectance observed by a satellite sensor. Similar to the Normalized Difference Water Index, NMDI uses the 860 nm channel as the reference; instead of using a single liquid water absorption channel, however, it uses the difference between two liquid water absorption channels centered at 1640 nm and 2130 nm as the soil and vegetation moisture sensitive band. Analysis revealed that by combining information from multiple near infrared, and short wave infrared channels, NMDI has enhanced the sensitivity to drought severity, and is well suited to

estimate both soil and vegetation moisture. Typical soil reflectance spectra and satellite-acquired reflectances, are used to validate the usefulness of NMDI. Its application to areas with moderate vegetation coverage, however, needs further investigation.},

language = {en},

number = {20},

urldate = {2024-09-24},

journal = {Geophysical Research Letters},

author = {Wang, Lingli and Qu, John J.},

year = {2007},

note = {_eprint: https://onlinelibrary.wiley.com/doi/pdf/10.1029/2007GL031021},

keywords = {MODIS, remote sensing, drought monitoring, multi-band, NMDI, soil moisture},

file = {2024-09-23晚上22-46-52@WanFangdata.txt:files/484/2024-09-23晚上22-46-52@WanFangdata.txt:text/plain;Full Text PDF:files/429/Wang y Qu - 2007 - NMDI A normalized multi-band drought index for mo.pdf:application/pdf;Snapshot:files/430/2007GL031021.html:text/html},

}

@article{goel_influences_1994,

title = {Influences of canopy architecture on relationships between various vegetation indices and {LAI} and {Fpar}: {A} computer simulation},

volume = {10},

issn = {0275-7257},

shorttitle = {Influences of canopy architecture on relationships between various vegetation indices and {LAI} and {Fpar}},

url = {https://doi.org/10.1080/02757259409532252},

doi = {10.1080/02757259409532252},

abstract = {Vegetation Indices (VIs) are often used to estimate important biophysical parameters, like LAI and Fpar, from vegetation canopy reflectance data. In this study, a three-dimensional model (Diana) is utilized to generate architecturally realistic tree and crop canopies in various development stages and to calculate bidirectional reflectance factors in the principal plane. We investigate the influence of various factors like soil brightness, optical properties of canopy elements, leaf angle distribution, spacing distance between plants and solar and view geometries on relationships between VI and Fpar, LAI and percentage ground cover (GC) in order to determine optimal VI and viewing conditions for the estimation of Fpar and LAI/GC. These simulation studies suggest that: (1) in most cases, Vis using off-nadir reflectances are more informative and useful than those based on nadir reflectances; (2) the optimal VI and sun/view geometries are usually different for inferring different parameters, depending on canopy architecture; (3) LAI can be practically

estimated by VI only for homogeneous canopies while GC and Fpar can be inferred even for an inhomogeneous canopy; and (4) when optical properties of vegetation elements vary within a canopy, neither LAI/GC nor Fpar can be estimated by means of VI method with an acceptable accuracy.},

number = {4},

urldate = {2024-09-24},

journal = {Remote Sensing Reviews},

author = {Goel, Narendra and Qin, Wenhan},

month = oct,

year = {1994},

note = {Publisher: Taylor \& Francis _eprint: https://doi.org/10.1080/02757259409532252},

pages = {309--347},

}

@article{rondeaux_optimization_1996,

title = {Optimization of soil-adjusted vegetation indices},

volume = {55},

issn = {0034-4257},

url = {https://www.sciencedirect.com/science/article/pii/0034425795001867},

doi = {10.1016/0034-4257(95)00186-7},

abstract = {The sensitivity of the normalized difference vegetation index (NDVI) to soil background and atmospheric effects has generated an increasing interest in the development of new indices, such as the soil-adjusted vegetation index (SAVI), transformed soil-adjusted vegetation index (TSAVI), atmospherically resistant vegetation index (AR VI), global environment monitoring index (GEMI), modified soil-adjusted vegetation index (MSAVI), which are less sensitive to these external influences. These indices are theoretically more reliable than NDVI, although they are not yet widely used with satellite data. This article focuses on testing and comparing the sensitivity of NDVI, SAVI, TSAVI, MSAVI and GEMI to soil background effects. Indices are simulated with the SAIL model for a large range of soil reflectances, including sand, clay, and dark peat, with additional variations induced by moisture and roughness. The general formulation of the SAVI family of indices with the form VI = (NIR - R) / (NIR + R + X) is also reexamined. The value of the parameter X is critical in the minimization of soil effects. A value of X = 0.16 is found as the optimized value. Index performances are compared by means of an analysis of variance.},

number = {2},

urldate = {2024-09-24},

journal = {Remote Sensing of Environment},

author = {Rondeaux, Geneviève and Steven, Michael and Baret, Frédéric},

month = feb,

year = {1996},

pages = {95--107},

file = {ScienceDirect Snapshot:files/433/0034425795001867.html:text/html},

}

@article{gamon_narrow-waveband_1992,

title = {A narrow-waveband spectral index that tracks diurnal changes in photosynthetic efficiency},

volume = {41},

issn = {0034-4257},

url = {https://www.sciencedirect.com/science/article/pii/003442579290059S},

doi = {10.1016/0034-4257(92)90059-S},

abstract = {We present a new “physiological reflectance index” (PRI) isolated from narrow waveband spectral measurements of sunflower canopies. This index correlates with the epoxidation state of the xanthophyll cycle pigments and with the efficiency of photosynthesis in control and nitrogen stress canopies, but not in water stress canopies undergoing midday wilting. It is analogous in formulation to the broadband normalized difference vegetation index (NDVI) and uses reflectance at 531 nm and at a reference wavelength to minimize complications associated with diurnal sun angle changes. In

conjunction with other methods, this index may lead to improved remote and ground-based estimates of canopy photosynthetic function.},

number = {1},

urldate = {2024-09-24},

journal = {Remote Sensing of Environment},

author = {Gamon, J. and Peñuelas, J. and Field, C. B.},

month = jul,

year = {1992},

pages = {35--44},

file = {ScienceDirect Snapshot:files/435/003442579290059S.html:text/html},

}

@article{merzlyak_non-destructive_1999,

title = {Non-destructive optical detection of pigment changes during leaf senescence and fruit ripening},

volume = {106},

issn = {1399-3054},

url = {https://onlinelibrary.wiley.com/doi/abs/10.1034/j.1399-3054.1999.106119.x},

doi = {10.1034/j.1399-3054.1999.106119.x},

abstract = {Reflectance spectra in the visible and near infra-red range of the spectrum, acquired for maple (Acer platanoides L.), chestnut (Aesculus

hippocastanum L.), potato (Solanum tuberosum L.), coleus (Coleus blumei Benth.), leaves and lemon (Citrus limon L.) and apple (Malus domestica Borkh.) fruits were studied. An increase of reflectance between 550 and 740 nm accompanied senescence-induced degradation of chlorophyll (Chl), whereas in the range 400–500 nm it remained low, due to retention of carotenoids (Car). It was found that both leaf senescence and fruit ripening affect the difference between reflectance (R) near 670 and 500 nm (R678−R500), depending on pigment composition. The plant senescing reflectance index in the form (R678−R500)/R750 was found to be sensitive to the Car/Chl ratio, and was used as a quantitative measure of leaf senescence and fruit ripening. The changes in the index were followed during leaf senescence, and natural and ethylene-induced fruit ripening. This novel index can be used for estimating the onset, the stage, relative rates and kinetics of senescence/ripening processes.},

language = {en},

number = {1},

urldate = {2024-09-24},

journal = {Physiologia Plantarum},

author = {Merzlyak, Mark and Gitelson, Anatoly and Chivkunova, Olga and Rakitin, Victor},

year = {1999},

note = {_eprint: https://onlinelibrary.wiley.com/doi/pdf/10.1034/j.1399-3054.1999.106119.x},

pages = {135--141},

file = {Full Text PDF:files/437/Merzlyak et al. - 1999 - Non-destructive optical detection of pigment chang.pdf:application/pdf;Snapshot:files/438/j.1399-3054.1999.106119.html:text/html},

}

@article{blackburn_quantifying_1998,

title = {Quantifying {Chlorophylls} and {Caroteniods} at {Leaf} and {Canopy} {Scales}: {An} {Evaluation} of {Some} {Hyperspectral} {Approaches}},

volume = {66},

issn = {0034-4257},

shorttitle = {Quantifying {Chlorophylls} and {Caroteniods} at {Leaf} and {Canopy} {Scales}},

url = {https://www.sciencedirect.com/science/article/pii/S0034425798000595},

doi = {10.1016/S0034-4257(98)00059-5},

abstract = {An investigation was undertaken into the effectiveness of a range of hyperspectral approaches for estimating the concentrations of chlorophyll a, chlorophyll b, and the carotenoids at the plant canopy and leaf scales. Measurements of spectral reflectance, biophysical characteristics and pigment composition were made for a bracken (Pteridium aquilinum) canopy, and its components, throughout a growing season. The results indicate that

narrow-band reflectance indices, such as the pigment-specific simple ratio (PSSR), can be developed which have extremely strong relationships with the concentration per unit area of individual pigments at the canopy scale. Spectral derivative approaches, particularly those based on pseudo absorbance (Log 1/R), are also closely related to canopy pigment concentration per unit area, but are more useful for deriving estimates of the concentration per unit mass of photosynthetic pigments at both canopy and leaf scales.},

number = {3},

urldate = {2024-09-24},

journal = {Remote Sensing of Environment},

author = {Blackburn, George Alan},

month = dec,

year = {1998},

pages = {273--285},

file = {ScienceDirect Snapshot:files/440/S0034425798000595.html:text/html},

}

@article{chappelle_ratio_1992,

title = {Ratio analysis of reflectance spectra ({RARS}): {An} algorithm for the remote estimation of the concentrations of chlorophyll {A}, chlorophyll {B}, and carotenoids in soybean leaves},

volume = {39},

issn = {0034-4257},

shorttitle = {Ratio analysis of reflectance spectra ({RARS})},

url = {https://www.sciencedirect.com/science/article/pii/0034425792900893},

doi = {10.1016/0034-4257(92)90089-3},

abstract = {An algorithm utilizing reflectance spectra bands in the photosynthetically active radiation (PAR) region of the solar spectrum was developed for the remote estimation of the concentrations of chlorophyll a, chlorophyll b, and carotenoids in soybeans. The defining of specific bands in the reflectance spectrum that corresponded to absorption bands of the individual pigments was basic to the development of the algorithm. The detection of these bands was rendered difficult by the lack of detail in reflectance spectra. It was therefore necessary to manipulate the reflectance spectra so that absorption bands due to specific pigments could be detected and their spectral maxima defined. It was found that by dividing soybean reflectance spectra by an arbitrarily selected reference soybean reflectance spectrum, ratio spectra were obtained in which the absorption bands could be distinctly seen and their wavelength defined. These ratio spectra allowed the defining of those bands corresponding to the absorption bands of chlorophyll a chlorophyll b, and carotenoids. The strong linear relationships of certain combinations of the bands in the ratio spectra to the concentrations of the photosynthetic pigments made it possible to develop a ratio analysis of reflectance spectra algorithm (RARS) by which the concentrations of these

pigments could be calculated from the reflectance spectra. The measurements necessary for the development of RARS were made using soybeans which were grown at different nitrogen levels in order to obtain a range of reflectance spectra. A test of the RARS algorithm using other soybean plants showed very good agreement between measured pigment values and those calculated using RARS.},

number = {3},

urldate = {2024-09-24},

journal = {Remote Sensing of Environment},

author = {Chappelle, Emmett and Kim, Moon and McMurtrey, James},

month = mar,

year = {1992},

pages = {239--247},

file = {ScienceDirect Snapshot:files/442/0034425792900893.html:text/html},

}

@article{roujean_estimating_1995,

title = {Estimating {PAR} absorbed by vegetation from bidirectional reflectance measurements},

volume = {51},

issn = {0034-4257},

url =
{https://www.sciencedirect.com/science/article/pii/0034425794001143},

doi = {10.1016/0034-4257(94)00114-3},

abstract = {Satellite remote sensing allows estimation, at a global scale, of the photosynthetically active radiation absorbed (APAR) by the vegetation. Current estimates are based on retrieving the fraction (fAPAR) of PAR absorbed by the canopy from spectral vegetation indices (SVI) derived from combinations of spectral reflectance measurements. We show that currently used SVI are strongly affected by the soil reflectance as well as the sun/view geometry, which yields large uncertainties on the SVI-fAPAR statistical relationships. However, the errors can be reduced using optimal geometries and new SVI less affected by the soil reflectance. Such an approach yields an improvement of the fAPAR assessment down to less than 5\% of relative standard error. It is relevant for monitoring of the interannual variations of the net primary productivity (NPP) and its analysis to understand the climate sensitivity of the present ecosystems. These will permit more detailed studies of seasonal and regional biospheric carbon sources and sinks that affect the global distribution of atmospheric carbon dioxide.},

number = {3},

urldate = {2024-09-24},

journal = {Remote Sensing of Environment},

author = {Roujean, Jean-Louis and Breon, François-Marie},

month = mar,

year = {1995},

pages = {375--384},

file = {ScienceDirect Snapshot:files/444/0034425794001143.html:text/html},

}

@article{gamon_assessing_1999,

title = {Assessing leaf pigment content and activity with a reflectometer},

volume = {143},

issn = {1469-8137, 0028-646X},

url = {https://www.cambridge.org/core/journals/new-phytologist/article/assessing-leaf-pigment-content-and-activity-with-a-reflectometer/070BA29E75C935E961BABA4E1BA135D5},

doi = {10.1046/j.1469-8137.1999.00424.x},

abstract = {This study explored reflectance indices sampled with a ‘leaf reflectometer’ as measures of pigment content for

leaves of contrasting light history, developmental stage and functional type (herbaceous annual versus

sclerophyllous evergreen). We employed three reflectance indices: a modified normalized difference vegetation

index (NDVI), an index of chlorophyll content; the red/green reflectance ratio (RRED[ratio]RGREEN), an index of

anthocyanin content; and the change in photochemical reflectance index upon dark–light conversions (ΔPRI), an index of xanthophyll cycle pigment activity. In Helianthus annuus (sunflower), xanthophyll cycle pigment amounts were linearly related to growth light environment; leaves in full sun contained approximately twice the amount of xanthophyll cycle pigments as leaves in deep shade, and at midday a larger proportion of these pigments were in the photoprotective, de-epoxidized forms relative to shade leaves. Reflectance indices also revealed contrasting patterns of pigment development in leaves of contrasting structural types (annual versus evergreen). In H. annuus sun leaves, there was a remarkably rapid increase in amounts of both chlorophyll and xanthophyll cycle pigments along a leaf developmental sequence. This pattern contrasted with that of Quercus agrifolia (coast live oak, a sclerophyllous evergreen), which exhibited a gradual development of both chlorophyll and xanthophyll cycle pigments along with a pronounced peak of anthocyanin pigment content in newly expanding leaves. These temporal patterns of pigment development in Q. agrifolia leaves suggest that anthocyanins and xanthophyll cycle

pigments serve complementary photoprotective roles during early leaf development. The results illustrate the use
of reflectance indices for distinguishing divergent patterns of pigment activity in leaves of contrasting light history
and functional type.},
language = {en},
number = {1},
urldate = {2024-09-24},
journal = {The New Phytologist},
author = {Gamon, J. and Surfus, J.},
month = jul,
year = {1999},
keywords = {anthocyanins, chlorophyll, leaf development, leaf pigments, leaf reflectometer, photoprotection, reflectance indices, xanthophyll cycle},
pages = {105--117},
file = {Full Text PDF:files/447/Gamon y Surfus - 1999 - Assessing leaf pigment content and activity with a.pdf:application/pdf},
}

@article{gamon_assessing_1999-1,
title = {Assessing leaf pigment content and activity with a reflectometer},
volume = {143},
copyright = {http://onlinelibrary.wiley.com/termsAndConditions\#vor},

issn = {0028-646X, 1469-8137},

url = {https://nph.onlinelibrary.wiley.com/doi/10.1046/j.1469-8137.1999.00424.x},

doi = {10.1046/j.1469-8137.1999.00424.x},

abstract = {This study explored reflectance indices sampled with a ‘ leaf reflectometer ’ as measures of pigment content for leaves of contrasting light history, developmental stage and functional type (herbaceous annual versus sclerophyllous evergreen). We employed three reflectance indices : a modified normalized difference vegetation index (NDVI), an index of chlorophyll content ; the red{\textbackslash}green reflectance ratio (RRED : RGREEN), an index of anthocyanin content ; and the change in photochemical reflectance index upon dark–light conversions (∆PRI), an index of xanthophyll cycle pigment activity. In Helianthus annuus (sunflower), xanthophyll cycle pigment amounts were linearly related to growth light environment ; leaves in full sun contained approximately twice the amount of xanthophyll cycle pigments as leaves in deep shade, and at midday a larger proportion of these pigments were in the photoprotective, de-epoxidized forms relative to shade leaves. Reflectance indices also revealed contrasting patterns of pigment development in leaves of contrasting structural types (annual versus evergreen). In H. annuus sun leaves, there was a remarkably rapid increase in amounts of both chlorophyll and xanthophyll cycle pigments along a leaf developmental sequence. This pattern contrasted with that of Quercus agrifolia (coast live oak, a sclerophyllous evergreen), which exhibited a gradual development of both

chlorophyll and xanthophyll cycle pigments along with a pronounced peak of anthocyanin pigment content in newly expanding leaves. These temporal patterns of pigment development in Q. agrifolia leaves suggest that anthocyanins and xanthophyll cycle pigments serve complementary photoprotective roles during early leaf development. The results illustrate the use of reflectance indices for distinguishing divergent patterns of pigment activity in leaves of contrasting light history and functional type.},

language = {en},

number = {1},

urldate = {2024-09-24},

journal = {New Phytologist},

author = {Gamon, J. A. and Surfus, J. S.},

month = jul,

year = {1999},

pages = {105--117},

file = {assessing-leaf-pigment-content-and-activity-with-a-reflectometer.pdf:files/445/assessing-leaf-pigment-content-and-activity-with-a-reflectometer.pdf:application/pdf},

}

@article{huete_soil-adjusted_1988-2,

title = {A soil-adjusted vegetation index ({SAVI})},

volume = {25},

issn = {0034-4257},

url = {https://www.sciencedirect.com/science/article/pii/003442578890106X},

doi = {10.1016/0034-4257(88)90106-X},

abstract = {A transformation technique is presented to minimize soil brightness influences from spectral vegetation indices involving red and near-infrared (NIR) wavelengths. Graphically, the transformation involves a shifting of the origin of reflectance spectra plotted in NIR-red wavelength space to account for first-order soil-vegetation interactions and differential red and NIR flux extinction through vegetated canopies. For cotton (Gossypium hirsutum L. var DPI-70) and range grass (Eragrosticslehmanniana Nees) canopies, underlain with different soil backgrounds, the transformation nearly eliminated soil-induced variations in vegetation indices. A physical basis for the soil-adjusted vegetation index (SAVI) is subsequently presented. The SAVI was found to be an important step toward the establishment of simple °lobal" that can describe dynamic soil-vegetation systems from remotely sensed data.},

number = {3},

urldate = {2024-09-24},

journal = {Remote Sensing of Environment},

author = {Huete, A.},

month = aug,

year = {1988},

pages = {295--309},

file = {ScienceDirect Snapshot:files/450/003442578890106X.html:text/html},
}

@article{haboudane_integrated_2002,
title = {Integrated narrow-band vegetation indices for prediction of crop chlorophyll content for application to precision agriculture},
volume = {81},
issn = {0034-4257},
url = {https://www.sciencedirect.com/science/article/pii/S0034425702000184},
doi = {10.1016/S0034-4257(02)00018-4},
abstract = {Recent studies have demonstrated the usefulness of optical indices from hyperspectral remote sensing in the assessment of vegetation biophysical variables both in forestry and agriculture. Those indices are, however, the combined response to variations of several vegetation and environmental properties, such as Leaf Area Index (LAI), leaf chlorophyll content, canopy shadows, and background soil reflectance. Of particular significance to precision agriculture is chlorophyll content, an indicator of photosynthesis activity, which is related to the nitrogen concentration in green vegetation and serves as a measure of the crop response to nitrogen application. This paper presents a combined modeling and indices-based approach to predicting the crop chlorophyll content from remote sensing data

while minimizing LAI (vegetation parameter) influence and underlying soil (background) effects. This combined method has been developed first using simulated data and followed by evaluation in terms of quantitative predictive capability using real hyperspectral airborne data. Simulations consisted of leaf and canopy reflectance modeling with PROSPECT and SAILH radiative transfer models. In this modeling study, we developed an index that integrates advantages of indices minimizing soil background effects and indices that are sensitive to chlorophyll concentration. Simulated data have shown that the proposed index Transformed Chlorophyll Absorption in Reflectance Index/Optimized Soil-Adjusted Vegetation Index (TCARI/OSAVI) is both very sensitive to chlorophyll content variations and very resistant to the variations of LAI and solar zenith angle. It was therefore possible to generate a predictive equation to estimate leaf chlorophyll content from the combined optical index derived from above-canopy reflectance. This relationship was evaluated by application to hyperspectral CASI imagery collected over corn crops in three experimental farms from Ontario and Quebec, Canada. The results presented here are from the L'Acadie, Quebec, Agriculture and Agri-Food Canada research site. Images of predicted leaf chlorophyll content were generated. Evaluation showed chlorophyll variability over crop plots with various levels of nitrogen, and revealed an excellent agreement with ground truth, with a correlation of r2=.81 between estimated and field measured chlorophyll content data.},

number = {2},

urldate = {2024-09-24},

journal = {Remote Sensing of Environment},

author = {Haboudane, Driss and Miller, John R. and Tremblay, Nicolas and Zarco-Tejada, Pablo J. and Dextraze, Louise},

month = aug,

year = {2002},

pages = {416--426},

file = {ScienceDirect Snapshot:files/452/S0034425702000184.html:text/html},

}

@article{kauth_graphic_1976,

title = {A {Graphic} {Description} of the {Spectral}-{Temporal} {Development} of {Agricultural} {Crops} as {Seen} by {LANDSAT}},

url = {https://docs.lib.purdue.edu/cgi/viewcontent.cgi?article=1160&context=lars_symp},

abstract = {The time trajectories of agricultural data
points as seen in LANDSAT signal space form a pattern
suggestive of a tasselled woolly cap. Using this
easily visualized three dimensional construct most
of the important phenomena of crop development and

observation variables are pointed out, named, discussed and measured. The important crop phenomena
described are the distribution of signals from bare
soil, the processes of green development, of yellow
development, of shadowing and of harvesting. The
important external variables include view angle, sun
angle, atmospheric haze, and atmospheric water vapor.
The development of a quantitative picture of
the tasselled cap depends upon crop and atmosphere
effects modeling and upon empirical observation of
data signals. Quantitative data from a composite
of these sources is given. The tasselled cap structure is illustrated with cluster plots and diagrams.

The tasselled cap is a fertile source of ideas
for processing techniques. Examples discussed
include

a) A linear preprocessing transformation which
isolates green development, yellow development and soil brightness and allows the
reduction of the dimension of the feature
space.

b) The use of specific measurable pattern elements of the tasselled cap structure to

estimate and correct atmospheric haze and
moisture effects.},
language = {en},
author = {Kauth, R and Thomas, G},
year = {1976},
file = {Kauth y Thomas - The Tasselled Cap -- A Graphic Description of the .pdf:files/453/Kauth y Thomas - The Tasselled Cap -- A Graphic Description of the .pdf:application/pdf},
}

@article{richardson_distinguishing_1977,
title = {Distinguishing {Vegetation} from {Soil} {Background} {Information}},
url = {https://www.asprs.org/wp-content/uploads/pers/1977journal/dec/1977_dec_1541-1552.pdf},
abstract = {Landsat-1 and -2 multispectral scanner (MSS) data from six overpass dates (April 2, May 17,]une 4,]uly 10, October 17, and December 10, 1975) showed that MSS digital data for bare soil, cloud tops, and cloud shadows followed a highly predictable linear relation (soil background line) for MSS bands 5 and 7 (1'2=0.974) and bands 5 and 6 (1'2=0.986). Increasing vegetation development, documented by leaf area index (LAI) measurements, for 1973 and 1975 grain sorghum crops, was associated with displacement of sorghum MSS digital counts perpendicularly away from the soil background

line. Consequently, the perpendicular distance of a sorghum MSS measurement from the soil background line was tested as an index of plant vegetative development. Two perpendicular vegetation index models, the PVI and PVI6, yielded significant coefficients of determination (1'2) of 0.522 and 0.659, respectively, with LAI. SBL},

language = {en},

author = {Richardson, A and Weigand, C},

year = {1977},

file = {Richardson - Distinguishing Vegetation from Soil Background Inf.pdf:files/455/Richardson - Distinguishing Vegetation from Soil Background Inf.pdf:application/pdf},

}

@book{weng_advances_2011,

title = {Advances in {Environmental} {Remote} {Sensing}: {Sensors}, {Algorithms}, and {Applications}},

isbn = {978-1-4200-9181-6},

shorttitle = {Advances in {Environmental} {Remote} {Sensing}},

abstract = {Generating a satisfactory classification image from remote sensing data is not a straightforward task. Many factors contribute to this difficulty including the characteristics of a study area, availability of suitable remote sensing data, ancillary and ground reference data, proper use of variables and classification algorithms, and the analyst's e},

language = {en},

publisher = {CRC Press},

author = {Weng, Qihao},

month = feb,

year = {2011},

note = {Google-Books-ID: axxzZWiD9BMC},

keywords = {Science / Space Science / Astronomy, Technology \& Engineering / Remote Sensing \& Geographic Information Systems, Business \& Economics / Industries / Agribusiness, Mathematics / Geometry / General, Science / General, Science / Physics / Astrophysics, Technology \& Engineering / Environmental / General},

}

@book{danson_advances_1995,

address = {Chichester ; New York},

title = {Advances in environmental remote sensing},

isbn = {978-0-471-95464-4},

publisher = {Wiley},

editor = {Danson, F. Mark and Plummer, Stephen E.},

year = {1995},

keywords = {Remote sensing, Environmental sciences},

file = {Catálogo LC - Información del artículo (registro completo):files/460/search.html:text/html},

}

@article{birth_measuring_1968,
title = {Measuring the {Color} of {Growing} {Turf} with a {Reflectance} {Spectrophotometer}},
volume = {60},
copyright = {Copyright © American Society of Agronomy},
issn = {1435-0645},
url = {https://onlinelibrary.wiley.com/doi/abs/10.2134/agronj1968.00021962006000060016x},
doi = {10.2134/agronj1968.00021962006000060016x},
abstract = {A single−beam spectrophotometer was used to measure the spectral reflectance properties of growing turf. From the data a two−wavelength reflectance ratio R745/R675 was developed for an objective index of turf color. This ratio changed from 3.0 for light green turf color to 6.5 for dark green turf color. (visual rating of 4 to 10, respectively). A two−filter instrument (Ratiospect) was used to measure this index on eight samples of turf of three species. A correlation of 0.984 was obtained between the Ratiospect readings and a visual score of turf color.},
language = {en},
number = {6},
urldate = {2024-09-24},

journal = {Agronomy Journal},

author = {Birth, Gerald and McVey, George},

year = {1968},

note = {_eprint: https://onlinelibrary.wiley.com/doi/pdf/10.2134/agronj1968.00021962006000060016x},

keywords = {turf color, Windsor bluegrass},

pages = {640--643},

file = {Snapshot:files/462/agronj1968.html:text/html},

}

@article{jordan_derivation_1969,

title = {Derivation of {Leaf}-{Area} {Index} from {Quality} of {Light} on the {Forest} {Floor}},

volume = {50},

issn = {1939-9170},

url = {https://onlinelibrary.wiley.com/doi/abs/10.2307/1936256},

doi = {10.2307/1936256},

abstract = {Leaf—area index of a forest can be measured by determining the ratio of light at 800 μm to that at 675 μm on the forest floor. It is based on the principle that leaves absorb relatively more red than infrared light, and therefore, the more leaves that are present in the canopy, the greater will be the ratio.},

language = {en},

number = {4},

urldate = {2024-09-24},

journal = {Ecology},

author = {Jordan, Carl},

year = {1969},

note = {_eprint: https://onlinelibrary.wiley.com/doi/pdf/10.2307/1936256},

pages = {663--666},

file = {Snapshot:files/466/1936256.html:text/html},

}

@article{mcmurtrey_distinguishing_1994,

series = {Fluorescence {Measurements} of {Vegetation}},

title = {Distinguishing nitrogen fertilization levels in field corn ({Zea} mays {L}.) with actively induced fluorescence and passive reflectance measurements},

volume = {47},

issn = {0034-4257},

url = {https://www.sciencedirect.com/science/article/pii/0034425794901252},

doi = {10.1016/0034-4257(94)90125-2},

abstract = {Laser-induced fluorescence (LIF) is an active sensing technique capable of capturing immediate and specific indications of changes in plant physiology and metabolism as they relate to the concentration and photosynthetic activity of the plant pigments. Reflectance is a passive sensing technique that can capture differences in the concentration of the primary plant pigments. Fluorescence and reflectance were compared for their ability to measure levels of plant stress that are of agronomic importance in corn (Zea mays L.) crops. Laboratory LIF and reflectance spectra were made on excised leaves from field grown corn. Changes in the visible region of the spectrum were compared between groups of plants fertilized with seven different levels of nitrogen (N) fertilization. A pulsed nitrogen laser emitting photons at a wavelength of 337 nm was used as a fluorescence excitation source. Differences in maximum intensity of fluorescence occurred at 440 nm, 525 nm, 685 nm, and 740 nm. Significant separations were found between levels of N fertilization at several LIF wavelength ratios. Several reflectance algorithms also produced significant separations between certain levels of N fertilization.},

number = {1},

urldate = {2024-09-24},

journal = {Remote Sensing of Environment},

author = {McMurtrey, J. and Chappelle, E. and Kim, M. and Meisinger, J. and Corp, L.},

month = jan,

year = {1994},

pages = {36--44},

file = {ScienceDirect Snapshot:files/468/0034425794901252.html:text/html},

}

@article{datt_remote_1998,

title = {Remote {Sensing} of {Chlorophyll} a, {Chlorophyll} b, {Chlorophyll} a+b and {Total} {Carotenoid} {Content} in {Eucalyptus} {Leaves}},

volume = {66},

issn = {0034-4257},

url = {https://www.sciencedirect.com/science/article/pii/S0034425798000467},

doi = {10.1016/S0034-4257(98)00046-7},

abstract = {Algorithms based on reflectance band ratios have been developed for the remote estimation of chlorophyll a, chlorophyll b, chlorophyll a+b, and total carotenoid content of Eucalyptus leaves. Reflectance spectra over the 400–2500 nm range with a spectral resolution of 2 nm and the content of chlorophylls a, b, a+b, and total carotenoids were determined for leaves from several Eucalyptus species covering a wide range of chlorophyll a content (0.0121–0.0435 mg/cm2). Maximum sensitivity of reflectance to variation in pigment content was found in the green wavelength region at 550 nm and at 708 nm in the far-red wavelengths. The reflectance in the main pigment absorption regions in the blue (400–500 nm) and red (660–690 nm)

wavelengths proved to be insensitive to variation in pigment content. The ratio R672/(R550× R708) correlated best with chlorophyll a, chlorophyll a+b, and total carotenoid contents. The ratio R672/R550 correlated best with chlorophyll b content. Reflectance ratios involving near infrared bands such as R750/R550 and R750/R700 did not correlate well with pigment content. This was due to the differential scattering effects of the wide range of young and mature leaf samples. A method was developed for adjusting all spectra to the same level of scatter. The near-infrared-based reflectance ratios from the scatter adjusted spectra showed high sensitivity to pigment content. The ratio R860/(R550×R708) from the scatter adjusted spectra correlated best with chlorophyll a, chlorophyll a+b, and total carotenoid contents, while R860/R550 correlated best with chlorophyll b content. The newly developed algorithms were tested on a validation data set and allowed accurate estimates of leaf pigment content. The pigment contents estimated by the ratios from untransformed spectra, R672/(R550×R708) and R672/R550, were found to be not significantly different from the estimates obtained using the scatter-adjusted reflectance ratios, R860/(R550×R708) and R860/R550.},

number = {2},

urldate = {2024-09-24},

journal = {Remote Sensing of Environment},

author = {Datt, Bisun},

month = nov,

year = {1998},

pages = {111--121},

file = {ScienceDirect Snapshot:files/472/S0034425798000467.html:text/html},

}

@inproceedings{bannari_transformed_2002,

title = {Transformed difference vegetation index ({TDVI}) for vegetation cover mapping},

volume = {5},

url = {https://ieeexplore.ieee.org/abstract/document/1026867},

doi = {10.1109/IGARSS.2002.1026867},

abstract = {In this study, we present a new vegetation index, the TDVI: transformed difference vegetation index. This index shows the same sensitivity as the soil adjusted vegetation index (SAVI) to the optical proprieties of bare soil subjacent to the cover. It does not saturate like NDVI and SAVI and it shows an excellent linearity as a function of the rate of vegetation cover.},

urldate = {2024-09-24},

booktitle = {{IEEE} {International} {Geoscience} and {Remote} {Sensing} {Symposium}},

author = {Bannari, A. and Asalhi, H. and Teillet, P.M.},

month = jun,

year = {2002},

keywords = {Remote sensing, Vegetation mapping, Radiometry, Biomedical optical imaging, Linearity, Optical saturation, Optical sensors, Sensor phenomena and characterization, Soil measurements, Spectroradiometers},

pages = {3053--3055 vol.5},

file = {IEEE Xplore Abstract Record:files/475/1026867.html:text/html;IEEE Xplore Full Text PDF:files/474/Bannari et al. - 2002 - Transformed difference vegetation index (TDVI) for.pdf:application/pdf},

}

@techreport{rouse_monitoring_1974,

title = {Monitoring the {Vernal} {Advancement} and {Retrogradation} ({Green} {Wave} {Effect}) of {Natural} {Vegetation}},

url = {https://ntrs.nasa.gov/citations/19750020419},

abstract = {The author has identified the following significant results. The Great Plains Corridor rangeland project successfully utilized natural vegetation systems as phenological indicators of seasonal development and climatic effects upon regional growth conditions. An effective method was developed for quantitative measurement of vegetation conditions, including green biomass estimates, recorded in bands 5 and 6, corrected for sun angle, were used to compute a ratio parameter (TV16) which is shown to be highly correlated with green biomass and vegatation moisture content. Analyses

results of ERTS-1 digital data and correlated ground data are summarized. Attention was given to analyzing weather influences and test site variables on vegetation condition measurements with ERTS-1 data.},

number = {E75-10354},

urldate = {2024-09-24},

author = {Rouse, J. W. and Haas, R. H. and Deering, D. W. and Schell, J. A. and Harlan, J. C.},

month = nov,

year = {1974},

note = {NTRS Author Affiliations: Texas A\&M Univ.
NTRS Document ID: 19750020419
NTRS Research Center: Headquarters (HQ)},

keywords = {Earth Resources And Remote Sensing},

file = {19750020419.pdf:files/477/Rouse et al. - 1974 - Monitoring the Vernal Advancement and Retrogradati.pdf:application/pdf;Snapshot:files/478/19750020419.html:text/html},

}

@article{gitelson_novel_2002,

title = {Novel algorithms for remote estimation of vegetation fraction},

volume = {80},

issn = {0034-4257},

url = {https://www.sciencedirect.com/science/article/pii/S0034425701002899},

doi = {10.1016/S0034-4257(01)00289-9},

abstract = {Spectral properties of a wheat canopy with vegetation fraction (VF) from 0\% to 100\% in visible and near-infrared (NIR) ranges of the spectrum were studied in order to devise a technique for remote estimation of VF. When VF was {\textless}60\%, from emergence till middle of the elongation stage, four distinct, and quite independent, spectral bands of reflectance existed in the visible range of the spectrum: 400 to 500 nm, 530 to 600 nm, near 670 nm, and around 700 nm. When VF was between 60\% and 100\%, reflectance in the NIR leveled off or even decreases with an increase of VF. The decreased reflectance in the NIR, occurring at or near the midseason, can be a limiting factor in the use of that spectral region for VF estimation. It was found that for VF{\textgreater}60\%, the information content of reflectance spectra in visible range can be expressed by only two independent pairs of spectral bands: (1) the blue from 400 to 500 nm and the red near 670 nm; (2) the green around 550 nm and the red edge region near 700 nm. We propose using only the visible range of the spectrum to quantitatively estimate VF. The green (as well as a 700-nm band) and the red (near 670 nm) reflectances were used in developing new indices, which were linearly proportional to wheat VF ranging from 0\% to 100\%. The Atmospherically Resistant Vegetation Index (ARVI) concept was used to correct indices for atmospheric effects. Visible Atmospherically Resistant Index in the form

VARI=(Rgreen−Rred)/(Rgreen+Rred−Rblue) was found to be minimally sensitive to atmospheric effects allowing estimation of VF with an error of {\textless}10\% in a wide range of atmospheric optical thickness. Validation of the newly suggested technique was carried out using wheat independent data sets and reflectance data obtained for cornfields in Nebraska. Predicted green VF was compared with retrieved from digital images. Despite the fact that the reflectance contrast among the visible channels is much smaller than between the visible and NIR, the sensitivity of suggested indices to moderate to high values of VF is much higher than for the Normalized Difference Vegetation Index (NDVI), and the error in VF prediction did not exceed 10\%. Suggested indices will complement the widely used NDVI, ARVI, Soil Adjusted Vegetation Index (SAVI) and others, which are based on the red and the NIR bands in VF estimation, and also Green Atmospherically Resistant Index (GARI), which is based on the green and the NIR bands.},

number = {1},

urldate = {2024-09-24},

journal = {Remote Sensing of Environment},

author = {Gitelson, Anatoly A. and Kaufman, Yoram J. and Stark, Robert and Rundquist, Don},

month = apr,

year = {2002},

pages = {76--87},

file = {ScienceDirect Snapshot:files/480/S0034425701002899.html:text/html;Texto completo:files/481/Gitelson et al. - 2002 - Novel algorithms for remote estimation of vegetati.pdf:application/pdf},
}

@article{kogan_application_1995,
series = {Natural {Hazards}: {Monitoring} and {Assessment} {Using} {Remote} {Sensing} {Technique}},
title = {Application of vegetation index and brightness temperature for drought detection},
volume = {15},
issn = {0273-1177},
url = {https://www.sciencedirect.com/science/article/pii/027311779500079T},
doi = {10.1016/0273-1177(95)00079-T},
abstract = {In recent years the National Oceanic and Atmospheric Administration (NOAA) has designed a new AVHRR-based Vegetation Condition Index (VCI) that has showed to be useful for drought detection and tracking. Validations showed that the VCI has excellent ability to detect drought and to measure time of its onset, intensity, duration, and impact on vegetation. The VCI provides accurate drought information not only for well-defined, prolonged, widespread, and intensive droughts, but also for very localized,

short-term, and non well-defined droughts. In addition to the VCI, the AVHRR-based observations in thermal bands were used to develop the Temperature Condition Index (TCI). This index was used to determine temperature-related vegetation stress and also stress caused by an excessive wetness. This paper provides principles of these indices, describes data processing, and gives examples of VCI/TCI application in different ecological environments of the United States.},

number = {11},

urldate = {2024-09-24},

journal = {Advances in Space Research},

author = {Kogan, F.},

month = jan,

year = {1995},

pages = {91--100},

file = {ScienceDirect Snapshot:files/483/027311779500079T.html:text/html},

}

@article{wang_extraccion_2015,

title = {Extracción de información de vegetación basada en teledetección {UAV} en banda de luz visible.},

url = {https://d.wanfangdata.com.cn/periodical/ChlQZXJpb2RpY2FsQ0hJTmV3UzIwMjQwNzA0Eg9ueWdjeGIyMDE1MDUwMjIaCGx6enA3ZDJl},

author = {Wang, Xiaoqin and Wang, Miao and Wang, Shaoqiang and Wu, Yun},

year = {2015},

file = {2024-09-23晚上22-46-52@WanFangdata.txt:files/487/2024-09-23晚上22-46-52@WanFangdata.txt:text/plain},

}

@article{gitelson_wide_2004-1,

title = {Wide {Dynamic} {Range} {Vegetation} {Index} for {Remote} {Quantification} of {Biophysical} {Characteristics} of {Vegetation}},

volume = {161},

issn = {0176-1617},

url = {https://www.sciencedirect.com/science/article/pii/S0176161704705726},

doi = {10.1078/0176-1617-01176},

abstract = {The Normalized Difference Vegetation Index (NDVI) is widely used for monitoring, analyzing, and mapping temporal and spatial distributions of physiological and biophysical characteristics of vegetation. It is well documented that the NDVI approaches saturation asymptotically under

conditions of moderate-to-high aboveground biomass. While reflectance in the red region (ρred) exhibits a nearly flat response once the leaf area index (LAI) exceeds 2, the near infrared (NIR) reflectance (ρNIR) continue to respond significantly to changes in moderate-to-high vegetation density (LAI from 2 to 6) in crops. However, this higher sensitivity of the ρNIR has little effect on NDVI values once the ρNIR exceeds 30 \%. In this paper a simple modification of the NDVI was proposed. The Wide Dynamic Range Vegetation Index, WDRVI = (a * ρNIR-ρred)/(a * ρNIR+ρred), where the weighting coefficient a has a value of 0.1–0.2, increases correlation with vegetation fraction by linearizing the relationship for typical wheat, soybean, and maize canopies. The sensitivity of the WDRVI to moderate-to-high LAI (between 2 and 6) was at least three times greater than that of the NDVI. By enhancing the dynamic range while using the same bands as the NDVI, the WDRVI enables a more robust characterization of crop physiological and phenological characteristics. Although this index needs further evaluation, the linear relationship with vegetation fraction and much higher sensitivity to change in LAI will be especially valuable for precision agriculture and monitoring vegetation status under conditions of moderate-to-high density. It is anticipated that the new index will complement the NDVI and other vegetation indices that are based on the red and NIR spectral bands.},

number = {2},

urldate = {2024-09-24},

journal = {Journal of Plant Physiology},

author = {Gitelson, Anatoly},

month = jan,

year = {2004},

keywords = {leaf area index, reflectance, remote estimation, vegetation fraction, vegetation index},

pages = {165--173},

file = {ScienceDirect Snapshot:files/489/S0176161704705726.html:text/html},

}

@inproceedings{wolf_using_2012,

title = {Using {WorldView}-2 {Vis}-{NIR} multispectral imagery to support land mapping and feature extraction using normalized difference index ratios},

volume = {8390},

url = {https://www.spiedigitallibrary.org/conference-proceedings-of-spie/8390/83900N/Using-WorldView-2-Vis-NIR-multispectral-imagery-to-support-land/10.1117/12.917717.full},

doi = {10.1117/12.917717},

abstract = {Multispectral imagery (MSI) provides information to support decision making across a growing number of private and industrial applications. Among them, land mapping, terrain classification and feature extraction rank highly in the interest of those who analyze the data to produce information, reports, and intelligence products. The 8 nominal band centers of WorldView-2 allow us to use non-traditional means of measuring the differences which

exist in the features, artifacts, and surface materials in the data, and we can determine the most effective method for processing this information by exploiting the unique response values within those wavelength channels. The difference in responses across select bands can be sought using normalized difference index ratios to measure moisture content, indicate vegetation health, and distinguish natural features from man-made objects. The focus of this effort is to develop an approach to measure, identify and threshold these differences in order to establish an effective land mapping and feature extraction process germane to WorldView-2 imagery.},

urldate = {2024-09-24},

booktitle = {Algorithms and {Technologies} for {Multispectral}, {Hyperspectral}, and {Ultraspectral} {Imagery} {XVIII}},

publisher = {SPIE},

author = {Wolf, Antonio},

month = may,

year = {2012},

pages = {188--195},

}

@article{elvidge_comparison_1995,

title = {Comparison of broad-band and narrow-band red and near-infrared vegetation indices},

volume = {54},

issn = {0034-4257},

url = {https://www.sciencedirect.com/science/article/pii/003442579500132K},

doi = {10.1016/0034-4257(95)00132-K},

abstract = {An experiment has been conducted in which narrow-band field reflectance spectra were acquired of a rooted pinyon pine canopy with five different gravel backgrounds. Leaf area was successively removed as the measurements were repeated. From these reflectance spectra, narrow-band and broad-band (AVHRR, TM, MSS) red and near-infrared (NIR) vegetation index values were calculated. The performance of the vegetation indices was evaluated based on their capability to accurately estimate leaf area index (LAI) and percent green cover. Background effects were found for each of the tested vegetation indices. However, the background effects are most pronounced in the normalized difference vegetation index (NDVI) and ratio vegetation index (RVI). Background effects can be reduced using either the perpendicular vegetation index (PVI) or soil adjusted vegetation index (SAVI) formulations. The narrow-band versions of these vegetation indices had only slightly better accuracy than their broad-band counterparts. The background effects were minimized using derivative based vegetation indices, which measure the amplitude of the chlorophyll red-edge using continuous narrow-band spectra from 626 nm to 795 nm.},

number = {1},

urldate = {2024-09-24},

journal = {Remote Sensing of Environment},

author = {Elvidge, Christopher D. and Chen, Zhikang},

month = oct,

year = {1995},

pages = {38--48},

file = {ScienceDirect Snapshot:files/492/003442579500132K.html:text/html},

}

@article{danson_advances_2011,

title = {Advances in environmental remote sensing},

url = {https://cir.nii.ac.jp/crid/1130282268974869760},

language = {en},

urldate = {2024-09-24},

journal = {(No Title)},

author = {Danson, F. Mark},

year = {2011},

file = {Snapshot:files/494/1130282268974869760.html:text/html},

}

@article{giovos_remote_2021,

title = {Remote {Sensing} {Vegetation} {Indices} in {Viticulture}: {A} {Critical} {Review}},

volume = {11},

copyright = {http://creativecommons.org/licenses/by/3.0/},

issn = {2077-0472},

shorttitle = {Remote {Sensing} {Vegetation} {Indices} in {Viticulture}},

url = {https://www.mdpi.com/2077-0472/11/5/457},

doi = {10.3390/agriculture11050457},

abstract = {One factor of precision agriculture is remote sensing, through which we can monitor vegetation health and condition. Much research has been conducted in the field of remote sensing and agriculture analyzing the applications, while the reviews gather the research on this field and examine different scientific methodologies. This work aims to gather the existing vegetation indices used in viticulture, which were calculated from imagery acquired by remote sensing platforms such as satellites, airplanes and UAVs. In this review we present the vegetation indices, the applications of these and the spatial distribution of the research on viticulture from the early 2000s. A total of 143 publications on viticulture were reviewed; 113 of them had used remote sensing methods to calculate vegetation indices, while the rejected ones have used proximal sensing methods. The findings show that the most used vegetation index is NDVI, while the most frequently appearing applications are monitoring and estimating vines water stress and delineation of management zones. More than half of the publications use multitemporal analysis and UAVs as the most used among remote sensing platforms. Spain and Italy are the countries with the most publications on viticulture with one-

third of the publications referring to regional scale whereas the others to site-specific/vineyard scale. This paper reviews more than 90 vegetation indices that are used in viticulture in various applications and research topics, and categorized them depending on their application and the spectral bands that they are using. To summarize, this review is a guide for the applications of remote sensing and vegetation indices in precision viticulture and vineyard assessment.},

language = {en},

number = {5},

urldate = {2024-09-24},

journal = {Agriculture},

author = {Giovos, Rigas and Tassopoulos, Dimitrios and Kalivas, Dionissios and Lougkos, Nestor and Priovolou, Anastasia},

month = may,

year = {2021},

note = {Number: 5
Publisher: Multidisciplinary Digital Publishing Institute},

keywords = {spatial analysis, imagery, precision viticulture, spectral bands, vine},

pages = {457},

file = {Full Text PDF:files/498/Giovos et al. - 2021 - Remote Sensing Vegetation Indices in Viticulture .pdf:application/pdf},

}

@book{freden_third_1974,

title = {Third {Earth} {Resources} {Technology} {Satellite}-1 {Symposium}: {Section} {A}-{B}. {Technical} presentations},

shorttitle = {Third {Earth} {Resources} {Technology} {Satellite}-1 {Symposium}},

language = {en},

publisher = {Scientific and Technical Information Office, National Aeronautics and Space Administration},

author = {Freden, Stanley and Mercanti, Enrico and Becker, Margaret},

year = {1974},

note = {Google-Books-ID: cl42FB2_UEcC},

}

@article{liu_monitoring_1996,

title = {Monitoring regional drought using the {Vegetation} {Condition} {Index}},

volume = {17},

issn = {0143-1161},

url = {https://doi.org/10.1080/01431169608949106},

doi = {10.1080/01431169608949106},

abstract = {NDVI (Normalized Difference Vegetation Index) images generated from NOAA AVHRR GVI data were recently used to monitor large

scale drought patterns and their climatic impact on vegetation. The purpose of this study is to use the Vegetation Condition Index (VCI) to further separate regional NDVI variation from geographical contributions in order to assess regional drought impacts. Weekly NDVI data for the period of July 1985 to June 1992 were used to produce NDVI and VCI images for the South American continent. NDVI data were smoothed with a median filtering technique for each year. Drought areas were delineated with certain threshold values of the NDVI and VCI. Drought patterns delineated by the NDVI and VCI agreed quite well with rainfall anomalies observed from rainfall maps of Brazil. NDVI values reflected the different geographical conditions quite well. Seasonal and interannual comparisons of drought areas delineated by the VCI provided a useful tool to analyse temporal and spatial evolution of regional drought as well as to estimate crop production qualitatively. It is suggested that VCI data besides NDVI may be used to construct a large scale crop yield prediction model.},

number = {14},

urldate = {2024-09-24},

journal = {International Journal of Remote Sensing},

author = {Liu, W. and Kogan, F.},

month = sep,

year = {1996},

note = {Publisher: Taylor \& Francis

_eprint: https://doi.org/10.1080/01431169608949106},

pages = {2761--2782},
}

@article{zambrano_sixteen_2016,
title = {Sixteen years of agricultural drought assessment of the bio bio in {Chile} using a 250 m resolution vegetation condition index ({VCI})},
abstract = {Drought is one of the most complex natural hazards because of its slow onset and
long-term impact; it has the potential to negatively affect many people. There are several advantages
to using remote sensing to monitor drought, especially in developing countries with limited
historical meteorological records and a low weather station density. In the present study, we
assessed agricultural drought in the croplands of the BioBío Region in Chile. The vegetation
condition index (VCI) allows identifying the temporal and spatial variations of vegetation
conditions associated with stress because of rainfall deficit. The VCI was derived at a 250 m spatial
resolution for the 2000–2015 period with the Moderate Resolution Imaging Spectroradiometer

(MODIS) MOD13Q1product. Weevaluated VCI for cropland areas using the land cover MCD12Q1

version 5.1 product and compared it to the in situ Standardized Precipitation Index (SPI) for

six-time scales (1–6 months) from 26 weather stations. Results showed that the 3-month SPI (SPI-3),

calculated for the modifiedgrowingseason(November–April)insteadoftheregulargrowingseason

(September–April), has the best Pearson correlation with VCI values with an overall correlation of

0.63 and between 0.40 and 0.78 for the administrative units. These results show a very short-term

vegetation response torainfall deficit in September, whichisreflectedinthevegetationinNovember,

and also explains to a large degree the variation in vegetation stress. It is shown that for the

last 16 years in the BioBío Region we could identify the 2007/2008, 2008/2009, and 2014/2015

seasons as the three most important drought events; this is reflected in both the overall regional

and administrative unit analyses. These results concur with drought emergencies declared by the

regional government. Future studies are needed to associate the remote sensing values observed

at high resolution (250 m) with the measured crop yield to identify more detailed individual

crop responses.},

author = {Zambrano, Francisco and Lillo-Saavedra, Mario and Verbist, Koen and Lagos, Octavio},

year = {2016},

file = {remotesensing-08-00530.pdf:files/504/remotesensing-08-00530.pdf:application/pdf},

}

@inproceedings{meyer_machine_1999,

title = {Machine vision detection parameters for plant species identification},

volume = {3543},

url = {https://www.spiedigitallibrary.org/conference-proceedings-of-spie/3543/0000/Machine-vision-detection-parameters-for-plant-species-identification/10.1117/12.336896.full},

doi = {10.1117/12.336896},

abstract = {Machine vision based on classical image processing techniques has the potential to be a useful tool for plant detection and identification. Plant identification is needed for weed detection, herbicide

application or other efficient chemical spot spraying operations. The key to successful detection and identification of plants as species types is the segmentation of plants form background pixel regions. In particular, it would be beneficial to segment individual leaves form tops of canopies as well. The segmentation process yields an edge or binary image which contains shape feature information. Results indicate that red-green-blue formats might provide the best segmentation criteria, based on models of human color perception. The binary image can be also used as a template to investigate textural features of the plant pixel region, using gray image co-occurrence matrices. Texture features considers leaf venation, colors, or additional canopy structure that might be used to identify various type of grasses or broadleaf plants.},

urldate = {2024-09-24},

booktitle = {Precision {Agriculture} and {Biological} {Quality}},

publisher = {SPIE},

author = {Meyer, George and Hindman, Timothy and Laksmi, Koppolu},

month = jan,

year = {1999},

pages = {327--335},

}

@article{neto_enfoque_2004,

title = {Un enfoque combinado de computación estadística y soft para la clasificación sobre y mapeo de especies de malezas en sistemas de labranza mínima},

url = {https://digitalcommons.unl.edu/dissertations/AAI3147135},

abstract = {This dissertation describes a combined statistical-soft computing approach for classifying and mapping weeds species using color images in minimum-tillage systems. A new unsupervised separation index (ExGExR) is introduced to distinguish plant canopies from different soil/residue backgrounds. Results showed that ExGExR was significantly improved for all species and all three weeks over the previously published excess green (ExG). ExGExR performed very well for separating both pigweed and velvetleaf from bare soil and corn stalk backgrounds during the first and second week after crop emergence. A new algorithm for individual leaf extraction was introduced based on fuzzy color clustering and genetic algorithm. Images of green canopies were segmented into fragments of potential leaf regions using clustering algorithm. Fragments were then reassembled into individual leaves using genetic optimization algorithm. The algorithm performance was evaluated by comparing the actual number leaves automatically extracted with the number of potential leaves observed visually. An overall performance of 75\% for leaves correctly extracted was obtained. Elliptic Fourier method was next tested for characterizing the shape of hand selected young soybean, sunflower, red root pigweed, and velvetleaf leaves. Discriminant analysis of these shape coefficients suggested that the third week after emergence was

the best time to identify plant species with a correct classification average of 89.4\%. When leaves from the second and third week were analyzed a correct classification average of 89.2\% was reached. An unsupervised method for plant species identification was finally tested. Elliptic Fourier descriptors not only provided leaflet shape information, but also a lamina boundary template, controlling where textural features were computed. Each lamina shape extracted was corrected such that all leaflets had the same orientation for texture extraction. SAS PROC DISCRIM procedure was performed to build a species classification model using selected Fourier coefficients and local homogeneity and entropy texture features. An overall success rate of 86\% was obtained for plant species classification.},

journal = {Recolección ETD para la Universidad de Nebraska-Lincoln},

author = {Neto, Joao},

month = jan,

year = {2004},

pages = {1--170},

file = {"Un enfoque combinado de computación estadística y blanda para la clasificación y" por Joao Camargo Neto:files/507/AAI3147135.html:text/html},

}

@article{glenn_relationship_2008-1,

title = {Relationship {Between} {Remotely}-sensed {Vegetation} {Indices}, {Canopy} {Attributes} and {Plant} {Physiological} {Processes}: {What} {Vegetation} {Indices} {Can} and {Cannot} {Tell} {Us} {About} the {Landscape}},

volume = {8},

copyright = {http://creativecommons.org/licenses/by/3.0/},

issn = {1424-8220},

shorttitle = {Relationship {Between} {Remotely}-sensed {Vegetation} {Indices}, {Canopy} {Attributes} and {Plant} {Physiological} {Processes}},

url = {https://www.mdpi.com/1424-8220/8/4/2136},

doi = {10.3390/s8042136},

abstract = {Vegetation indices (VIs) are among the oldest tools in remote sensing studies. Although many variations exist, most of them ratio the reflection of light in the red and NIR sections of the spectrum to separate the landscape into water, soil, and vegetation. Theoretical analyses and field studies have shown that VIs are near-linearly related to photosynthetically active radiation absorbed by a plant canopy, and therefore to light-dependent physiological processes, such as photosynthesis, occurring in the upper canopy. Practical studies have used time-series VIs to measure primary production and evapotranspiration, but these are limited in accuracy to that of the data used in ground truthing or calibrating the models used. VIs are also used to estimate a wide variety of other canopy attributes that are used in Soil-Vegetation-Atmosphere Transfer (SVAT), Surface Energy Balance (SEB), and Global Climate Models (GCM). These attributes include fractional vegetation

cover, leaf area index, roughness lengths for turbulent transfer, emissivity and albedo. However, VIs often exhibit only moderate, non-linear relationships to these canopy attributes, compromising the accuracy of the models. We use case studies to illustrate the use and misuse of VIs, and argue for using VIs most simply as a measurement of canopy light absorption rather than as a surrogate for detailed features of canopy architecture. Used this way, VIs are compatible with "Big Leaf" SVAT and GCMs that assume that canopy carbon and moisture fluxes have the same relative response to the environment as any single leaf, simplifying the task of modeling complex landscapes.},

language = {en},

number = {4},

urldate = {2024-09-24},

journal = {Sensors},

author = {Glenn, Edward and Huete, Alfredo and Nagler, Pamela and Nelson, Stephen G.},

month = apr,

year = {2008},

note = {Number: 4
Publisher: Molecular Diversity Preservation International},

keywords = {NDVI, Evapotranspiration, EVI, Primary Production, Remote Sensing},

pages = {2136--2160},

file = {Full Text PDF:files/509/Glenn et al. - 2008 - Relationship Between Remotely-sensed Vegetation In.pdf:application/pdf},
}

@article{zambrano_sixteen_2016-1,
title = {Sixteen {Years} of {Agricultural} {Drought} {Assessment} of the {BioBío} {Region} in {Chile} {Using} a 250 m {Resolution} {Vegetation} {Condition} {Index} ({VCI})},
url = {https://www.mdpi.com/2072-4292/8/6/530},
abstract = {Drought is one of the most complex natural hazards because of its slow onset and
long-term impact; it has the potential to negatively affect many people. There are several advantages
to using remote sensing to monitor drought, especially in developing countries with limited
historical meteorological records and a low weather station density. In the present study, we
assessed agricultural drought in the croplands of the BioBío Region in Chile. The vegetation
condition index (VCI) allows identifying the temporal and spatial variations of vegetation
conditions associated with stress because of rainfall deficit. The VCI was derived at a 250 m spatial

resolution for the 2000–2015 period with the Moderate Resolution Imaging Spectroradiometer

(MODIS) MOD13Q1product. Weevaluated VCI for cropland areas using the land cover MCD12Q1

version 5.1 product and compared it to the in situ Standardized Precipitation Index (SPI) for

six-time scales (1–6 months) from 26 weather stations. Results showed that the 3-month SPI (SPI-3),

calculated for the modifiedgrowingseason(November–April)insteadoftheregulargrowingseason

(September–April), has the best Pearson correlation with VCI values with an overall correlation of

0.63 and between 0.40 and 0.78 for the administrative units. These results show a very short-term

vegetation response torainfall deficit in September, whichisreflectedinthevegetationinNovember,

and also explains to a large degree the variation in vegetation stress. It is shown that for the

last 16 years in the BioBío Region we could identify the 2007/2008, 2008/2009, and 2014/2015

seasons as the three most important drought events; this is reflected in both the overall regional

and administrative unit analyses. These results concur with drought emergencies declared by the

regional government. Future studies are needed to associate the remote sensing values observed

at high resolution (250 m) with the measured crop yield to identify more detailed individual

crop responses},

urldate = {2024-10-07},

author = {Zambrano, Francisco and Lillo-Saavedra, Mario and Verbist, Koen and Lagos, Octavio},

year = {2016},

file = {Sixteen Years of Agricultural Drought Assessment of the BioBío Region in Chile Using a 250 m Resolution Vegetation Condition Index (VCI):files/511/530.html:text/html},

}

@article{klisch_operational_2016,

title = {Operational {Drought} {Monitoring} in {Kenya} {Using} {MODIS} {NDVI} {Time} {Series}},

volume = {8},

copyright = {http://creativecommons.org/licenses/by/3.0/},

issn = {2072-4292},

url = {https://www.mdpi.com/2072-4292/8/4/267},

doi = {10.3390/rs8040267},

abstract = {Reliable drought information is of utmost importance for efficient drought management. This paper presents a fully operational processing chain for mapping drought occurrence, extent and strength based on Moderate Resolution Imaging Spectroradiometer (MODIS) normalized difference vegetation index (NDVI) data at 250 m resolution. Illustrations are provided for the territory of Kenya. The processing chain was developed at BOKU (University of Natural Resources and Life Sciences, Vienna, Austria) and employs a modified Whittaker smoother providing consistent (de-noised) NDVI “Monday-images” in near real-time (NRT), with time lags between zero and thirteen weeks. At a regular seven-day updating interval, the algorithm constrains modeled NDVI values based on reasonable temporal NDVI paths derived from corresponding (multi-year) NDVI “climatologies”. Contrary to other competing approaches, an uncertainty range is produced for each pixel, time step and time lag. To quantify drought strength, the vegetation condition index (VCI) is calculated at pixel level from the de-noised NDVI data and is spatially aggregated to administrative units. Besides the original weekly temporal resolution, the indicator is also aggregated to one- and three-monthly intervals. During spatial and temporal aggregations, uncertainty information is taken into account to down-weight less reliable observations. Based on the provided VCI, Kenya’s National Drought Management Authority (NDMA) has been releasing disaster contingency funds (DCF) to sustain counties in drought conditions since 2014. The paper illustrates the successful application of the drought

products within NDMA by providing a retrospective analysis applied to droughts reported by regular food security assessments. We also present comparisons with alternative products of the US Agency for International Development (USAID)'s Famine Early Warning Systems Network (FEWS NET). We found an overall good agreement (R2 = 0.89) between the two datasets, but observed some persistent (seasonal and spatial) differences that should be assessed against external reference information.},

language = {en},

number = {4},

urldate = {2024-10-08},

journal = {Remote Sensing},

author = {Klisch, Anja and Atzberger, Clement},

month = apr,

year = {2016},

note = {Number: 4
Publisher: Multidisciplinary Digital Publishing Institute},

keywords = {MODIS, Drought Contingency Funds, Kenya, NDMA, uncertainty, vegetation condition index, Whittaker smoother},

pages = {267},

file = {Full Text PDF:files/513/Klisch y Atzberger - 2016 - Operational Drought Monitoring in Kenya Using MODI.pdf:application/pdf},

}

@article{julien_comparison_2010,

title = {Comparison of cloud-reconstruction methods for time series of composite {NDVI} data},

volume = {114},

issn = {0034-4257},

url = {https://www.sciencedirect.com/science/article/pii/S0034425709003265},

doi = {10.1016/j.rse.2009.11.001},

abstract = {Land cover change can be assessed from ground measurements or remotely sensed data. As regards remotely sensed data, such as NDVI (Normalized Difference Vegetation Index) parameter, the presence of atmospherically contaminated data in the time series introduces some noise that may blur the change analysis. Several methods have already been developed to reconstruct NDVI time series, although most methods have been dedicated to reconstruction of acquired time series, while publicly available databases are usually composited over time. This paper presents the IDR (iterative Interpolation for Data Reconstruction) method, a new method designed to approximate the upper envelope of the NDVI time series while conserving as much as possible of the original data. This method is compared quantitatively to two previously applied methods to NDVI time series over different land cover classes. The IDR method provides the best profile reconstruction in most cases. Nevertheless, the IDR method tends to overestimate low NDVI values when high rates of change are present, although

this effect can be lowered with shorter compositing periods. This method could also be applied to data before compositing, as well as to reconstruct time series for other biophysical parameters such as land surface temperature, as long as atmospheric contamination affects these parameters negatively.},

number = {3},

urldate = {2024-10-08},

journal = {Remote Sensing of Environment},

author = {Julien, Yves and Sobrino, José A.},

month = mar,

year = {2010},

keywords = {NDVI, Atmospheric contamination, Data reconstruction, GIMMS, IDR},

pages = {618--625},

file = {ScienceDirect Snapshot:files/516/S0034425709003265.html:text/html},

}

@article{atkinson_inter-comparison_2012,

title = {Inter-comparison of four models for smoothing satellite sensor time-series data to estimate vegetation phenology},

volume = {123},

issn = {0034-4257},

url = {https://www.sciencedirect.com/science/article/pii/S0034425712001629},

doi = {10.1016/j.rse.2012.04.001},

abstract = {Several models have been fitted in the past to smooth time-series vegetation index data from different satellite sensors to estimate vegetation phenological parameters. However, differences between the models and fine tuning of model parameters lead to potential differences, uncertainty and bias between the results amongst users. The current research assessed four techniques: Fourier analysis, asymmetric Gaussian model, double logistic model and the Whittaker filter for smoothing multi-temporal satellite sensor observations with the ultimate purpose of deriving an appropriate annual vegetation growth cycle and estimating phenological parameters reliably. The research used Level 3 Medium Resolution Imaging Spectrometer (MERIS, spatial resolution {\textasciitilde}4.6km) Terrestrial Chlorophyll Index (MTCI) data over the years 2004 to 2006 composited at eight day intervals covering the Indian sub-continent. First, the four models were fitted to representative sample time-series of the major vegetation types in India, and the quality of the fit was analysed. Second, the effect of noise on model fitting was analysed by adding Gaussian noise to a standard profile. Finally, the four models were fitted to the whole study area to characterise variation in the quality of model fitting as a function of single and double vegetation seasons. These smoothed data were used to estimate the onset of greenness (OG), a major phenological parameter. The models were evaluated

using the root mean square error (RMSE), Akaike Information Criteria (AIC), and Bayesian Information Criteria (BIC). The first test (fitting to representative sample time series) revealed the consistently superior performance of the Whittaker and Fourier approaches in most cases. The second test (fitting after the addition of Gaussian noise) revealed the superior performance of the double logistic and Fourier approaches. Finally, when the approaches were applied to the whole study, thus, including vegetation with different phenological profiles and multiple growing seasons (third test), it was found that it was necessary to tune each of the models according to the number of annual growing seasons to produce reliable fits. The double logistic and asymmetric Gaussian models did not perform well for areas with more than one growing season per year. The mean absolute deviation in OG derived from these models was a maximum (3 to 4weeks) within the dry deciduous vegetation type and minimum (1week) in evergreen vegetation. All techniques yielded consistent results over the south-western and north-eastern regions of India characterised by tropical climate.},

urldate = {2024-10-08},

journal = {Remote Sensing of Environment},

author = {Atkinson, Peter M. and Jeganathan, C. and Dash, Jadu and Atzberger, Clement},

month = aug,

year = {2012},

keywords = {Phenology, Whittaker smoother, Asymmetric Gaussian, Double logistic, Filter techniques, Fourier, MERIS, MTCI},

pages = {400--417},

file = {ScienceDirect Snapshot:files/517/S0034425712001629.html:text/html},

}

@article{pearson_remote_1972,

title = {Remote mapping of standing crop biomass for estimation of the productivity of the shortgrass prairie, {Pawnee} {National} {Grasslands}, {Colorado}.},

url = {https://www.cabidigitallibrary.org/doi/full/10.5555/19740715986},

abstract = {In trials in 1968-71, the biomass of shortgrass prairie (main species Bouteloua gracilis) was estimated on small areas using a 2-channel spectral ratio method employing a small hand-held radiometer. Biomass estimation accuracy was {\textgreater}95\%. Large-area determinations were made using both a channel ratio technique and multispectral pattern recognition techniques using data from aerial photographs. Correlations between estimated values from the multispectral data and values taken from clipped plots in the same area were 80-90\%.},

author = {Pearson, R and Miller, L},

year = {1972},

}

@techreport{rouse_monitoring_1973,

title = {Monitoring the vernal advancement and retrogradation ({Green} wave effect) of natural vegetation},

url = {https://ntrs.nasa.gov/api/citations/19730017588/downloads/19730017588.pdf},

abstract = {Natural vegetation systems occupy broad areas of the Great Plains and their behavior provides a reliable indicator of seasonal drought and other bioclimatic influences which impact on the agricultural anagement and production activities of major economic importance to this region of the United States. The overall objective of this investigation is to determine the effectiveness of ERTStype data for monitoring these vegetation systems as phenological indicators and to assess the value of this new information source relative to rangeland management and agri-business decisions in the Great Plains.

The project employs an extensive test site network to monitor vegetation and climatic conditions from south Texas to North Dakota. Evaluation of hypotheses basic

to this endeavor involves analysis of spectral and temporal data, with primary emphasis on the use of quantitative MSS

measurements.

The initial effort has verified that the proposed project is viable and that stated objectives are obtainable with the available quality and quantity of ground observations,

aircraft imagery, and ERTS-1 data being received.

This activity has been responsible for development of related activities using ERTS-1 data from the Great Plains, especially for Texas. The spin-off projects have been user-generated, consequently, these ERTS data are impacting directly on established application efforts. It is recommended that these unscheduled demands for ERTS

data be recognized as an important avenue to high priority application areas.},

urldate = {2024-10-10},

author = {Rouse, John},

year = {1973},

file = {19730017588.pdf:files/522/19730017588.pdf:application/pdf},

}

@article{misra_kauth-thomas_1977,

title = {Kauth-{Thomas} brightness and greenness axes},

url = {https://cir.nii.ac.jp/crid/1572543024797184896},

urldate = {2024-10-10},

author = {Misra, P.},

year = {1977},

file = {Snapshot:files/525/1572543024797184896.html:text/html},

}

@inproceedings{ashburn_vegetative_1979,

title = {The vegetative index number and crop identification},

url = {https://ntrs.nasa.gov/citations/19800007243},

abstract = {A vegetative index number of numerical value was calculated from the digital values of the LANDSAT system to provide some measure of green growing vegetation. The usefulness of the green numbers for schemes in crop identification and acreage estimation is investigated and the Ashburn vegetation index (AVI) is compared with the Kauth-Thomas vegetation index (KVI) for crop identification schemes. Results of wheat acreage estimation using LACIE Procedure 1 and the AVI for eight sample segments are given. Tables show comparisons between the AVI and the KVI as well as visual results of the AVI.},

urldate = {2024-10-10},

author = {Ashburn, P.},

month = jul,

year = {1979},

note = {NTRS Author Affiliations: Department of Agriculture
NTRS Document ID: 19800007243
NTRS Research Center: Legacy CDMS (CDMS)},

keywords = {Earth Resources And Remote Sensing},

file = {Snapshot:files/527/19800007243.html:text/html},

}

@misc{hay_development_1979,

title = {Development of {AI} procedures for dealing with the effects of episodal events on crop temporal spectral response},

url = {https://ntrs.nasa.gov/api/citations/19800024310/downloads/19800024310.pdf},

abstract = {The primary objective of this task was to measure and quantitatively describe for the analyst the year-to-year variation in crop I{\textasciicircum} temporal - spectral response patterns due to any year-to-year variation

t

in the physical environment.

L' 4

A standard method for representing crop temporal-spectral response that was consistent among segments and years was developed in order to reliably measure and quantitatively describe year-to-year variation for the analyst. The method used discrete Landsat acquisitions to estimate a continuous ,function which represented a crop's spectral response pattern over its growing season. This method generated a consistent framework within which comparisons of temporal-spectral response characteristics among years, segments, and crops could be carried out.

Within any particular segment, the year-to-year variation in temporal-spectral response characteristics was in general highly significant relative to field-to-field variation. This observation underscored the need for the AI to calibrate labeling guidelines to the segment and year being analyzed. Table 1.7 summarizes both the observed year-to-year within-segment variation and the among segment-year variation in a useful way for the AI.

The nature and magnitude of field-to-field temporal-spectral variability, within each segment-year combination, was examined and statistically tested for year-to-year consistency. In one third of the cases, the field-to-field variation was found to be not constant from year to year.

Using Spring Wheat data only, all pairs of temporal and spectral variables were examined for significant correlation. There was no significant correlation between the spectral variable F Max (maximum GRABS amplitude) and any of the temporal variables. However, there were observed hi ghly si gnificant correlations among some of the temporal variables.

Multiple linear regression analyses were performed on Spring Wheat data, using temporal and spectral variables as dependent variables, and precipitation and temperature variables as independent variables.

The multiple regression models themselves offered little insight into the causal mechanism linking meteorological factors to spectral response pattern variation. However, two general types of relationships appeared consistently throughout the results. These were 1) a positive correlation between precipitation and temporal variables; and 2) a negative * correlation between temperature and spectral-temporal variables},

urldate = {2024-10-10},

author = {Hay, C. and Kuretz, C. and Odenweller, J. and Scheffner, E. and Wood, B.},

year = {1979},

file = {19800024310.pdf:files/529/19800024310.pdf:application/pdf},

}

@article{jackson_discrimination_1983,

title = {Discrimination of growth and water stress in wheat by various vegetation indices through clear and turbid atmospheres},

volume = {13},

issn = {0034-4257},

url = {https://www.sciencedirect.com/science/article/pii/0034425783900391},

doi = {10.1016/0034-4257(83)90039-1},

abstract = {Reflectance data were obtained over a drought-stressed and a well-watered wheat plot with a hand-held radiometer having bands similar to

the MSS bands of the Landsat satellites. Data for 48 clear days were interpolated to yield reflectance values for each day of the growing season, from planting until harvest. With an atmospheric path radiance model and Landsat 2 calibration data, the reflectances were used to simulate Landsat digital counts (not quantized) for the four Landsat bands for each day of the growing season, through a clear (≃100-km meteorological range) and a turbid (≃10-km meteorological range) atmosphere. Several ratios and linear combinations of bands were calculated using the simulated data, then assessed for their relative ability to discriminate vegetative growth and plant stress through the two atmospheres. The results showed that water stress was not detected by any of the indices until after growth was retarded, and the sensitivity of the various indices to vegetation depended on plant growth stage and atmospheric path radiance.},

number = {3},

urldate = {2024-10-10},

journal = {Remote Sensing of Environment},

author = {Jackson, R. D. and Slater, P. N. and Pinter, P. J.},

month = jul,

year = {1983},

pages = {187--208},

file = {ScienceDirect Snapshot:files/533/0034425783900391.html:text/html},

}

@misc{jackson_hand-held_1980,

title = {Hand-held radiometry: {A} set of notes developed for use at the {Workshop} of {Hand}-held radiometry - {NASA} {Technical} {Reports} {Server} ({NTRS})},

url = {https://ntrs.nasa.gov/citations/19810019958},

abstract = {A set of notes was developed to aid the beginner in hand-held radiometry. The electromagnetic spectrum is reviewed, and pertinent terms are defined. View areas of multiband radiometers are developed to show the areas of coincidence of adjacent bands. The amounts of plant cover seen by radiometers having different fields of view are described. Vegetation indices are derived and discussed. Response functions of several radiometers are shown and applied to spectrometer data taken over 12 wheat plots, to provide a comparison of instruments and bands within and among instruments. The calculation of solar time is reviewed and applied to the calculation of the local time of LANDSAT satellite overpasses for any particular location in the Northern Hemisphere. The use and misuse of hand-held infrared thermometers are discussed, and a procedure for photographic determination of plant cover is described. Some suggestions are offered concerning procedures to be followed when collecting hand-held spectral and thermal data. A list of references pertinent to hand-held radiometry is included.},

urldate = {2024-10-10},

author = {Jackson, R. and Pinter, P. and Paul, J. and Reginato, R. and Robert, J. and Idso, S.},

year = {1980},

}

@article{yazdani_vegetation_1982,

title = {Vegetation change detection in an agricultural area- {A} simple approach for use with geo-data base},

url = {https://scholar.google.es/scholar?hl=es&as_sdt=0%2C5&q=Yazdani%2C+R.%2C+Ryerson%2C+A.+R.+and+Derenyi%2C+E.+%281981%29+Vegetation+change+detection+in+an+area%E2%80%94a+simple+approach+for+use+with+geo-data+base.+Proceedings+of+the+7th+Canadian+Symposium+on+Remote+Sensing%2C+Winnipeg%2C+Manitoba%2C+Canada%2C+88-92&btnG=},

author = {Yazdani, R. and Derenyi, E. and Ryerson, R.},

year = {1982},

file = {scholar (1).enw:files/538/scholar (1).enw:application/x-endnote-refer;scholar (1).enw:files/539/scholar (1).enw:application/x-endnote-refer;scholar.enw:files/540/scholar.enw:application/x-endnote-refer},

}

@article{badhwar_use_1981,

title = {The use of parameters to separate and identify spring small grains},

url = {https://scholar.google.es/scholar?hl=es&as_sdt=0%2C5&q=Badhwar%2C+G.+D.+%281981%29+The+Use+of+Parameters+to+Separate+and+Identify+Spring+Small+Grains.+Quarterly+Technical+Interchange+Meeting%2C+NASA-JSC%2C+Houston%2C+TX%2C+USA.&btnG=},

author = {Badhwar, G.},

year = {1981},

}

@article{perry_functional_1984,

title = {Functional equivalence of spectral vegetation indices - {ScienceDirect}},

url = {https://www.sciencedirect.com/science/article/pii/0034425784900130},

abstract = {Numerous formulae, vegetation indices, have been developed to reduce multispectral scanner (MSS) data to a single number for assessing vegetation characteristics such as species, leaf area, stress, and biomass. Part I of this report gives the history and formulae of some four dozen vegetation indices. Studies investigating the empirical relationships among vegetation indices are summarized. Part II of this report develops the idea of two vegetation indices being functionally equivalent: Two vegetation indices

are taken to be equivalent for making a set of decisions, if the decisions made on the basis of one index could have been equally well made on the basis of the other index. The utility of these ideas is explored in the context of alarm models and graphical displays. Several widely used indices are shown to be equivalent.},

urldate = {2024-10-10},

author = {Perry, Charles and Lautenschalager},

year = {1984},

file = {Functional equivalence of spectral vegetation indices - ScienceDirect:files/543/0034425784900130.html:text/html},

}

@article{clevers_application_1986,

title = {The application of a vegetation index in correcting the infrared reflectance for soil background.},

url = {https://research.wur.nl/en/publications/the-application-of-a-vegetation-index-in-correcting-the-infrared-},

author = {Clevers, J.},

year = {1986},

}

@article{baret_tsavi_1989-1,

title = {{TSAVI} : {A} vegetation index which minimizes soil brightness effects on {LAI} and {APAR} estimation},

shorttitle = {{TSAVI}},

url = {https://cir.nii.ac.jp/crid/1573668926152004224},

urldate = {2024-10-10},

journal = {12th Canadian Symp. on Remote Sensing and IGARSS '90, Vancouver, Canada, 10-14 July 1989},

author = {Baret, F.},

year = {1989},

file = {TSAVI \: A vegetation index which minimizes soil brightness effects on LAI and APAR estimation Snapshot:files/552/1573668926152004224.html:text/html},

}

@inproceedings{courel_utilisation_1991,

address = {Sherbrooke, Canada},

title = {Utilisation des bandes spectrales du vert et du rouge pour une meilleure évaluation des formations végétales actives},

url = {https://hal.science/hal-00327879},

urldate = {2024-10-10},

booktitle = {Congrès {AUPELF}-{UREF}},

author = {Courel, Marie-Françoise and Chamard, Ph.C and Guenegou, M.C and Lerhun, Jeannine and Levasseur, J. and Togola, M.},

month = oct,

year = {1991},

keywords = {Bandes spectrales, Evaluation, Formations végétales},

file = {HAL Snapshot:files/554/hal-00327879.html:text/html},

}

@article{escadafal_etude_1991,

title = {Etude des propriétés spectrales des sols arides appliquée à l'amélioration des indices de végétation obtenus par télédétection},

volume = {312},

issn = {0764-4450},

number = {11},

journal = {Etude des propriétés spectrales des sols arides appliquée à l'amélioration des indices de végétation obtenus par télédétection},

author = {Escadafal, R and Huete, A.},

year = {1991},

note = {Place: Paris

Publisher: Gauthier-Villars},

pages = {1385--1391},

file = {Etude des propriétés spectrales des sols arides appliquée à l'amélioration des indices de végétation obtenus par télédétection:files/556/index.html:text/html},

}

@article{baret_potentials_1991,

title = {Potentials and limits of vegetation indices for {LAI} and {APAR} assessment},

volume = {35},

issn = {0034-4257},

url = {https://www.sciencedirect.com/science/article/pii/003442579190009U},

doi = {10.1016/0034-4257(91)90009-U},

abstract = {Most vegetation indices (VI) combine information contained in two spectral bands: red and near-infrared. These indices are established in order to minimize the effect of external factors on spectral data and to derive canopy characteristics such as leaf area index (LAI) and fraction of absorbed photosynthetic active radiation (P). The potentials and limits of different vegetation indices are discussed in this paper using the normalized difference (NDVI), perpendicular vegetation index (PVI), soil adjusted vegetation index (SAVI), and transformed soil adjusted vegetation index (TSAVI). The discussion is based on a sensitivity analysis in which the effect of canopy geometry (LAI and leaf inclination) and soil background are analyzed. The calculation is performed on data derived from the SAIL reflectance model. General semiempirical models, describing the relations between VI and LAI or P, are elaborated and used to derive the relative equivalent noise (REN) for the

determination of LAI and P. The performances of VIs are discussed on the basis of the REN concept.},

number = {2},

urldate = {2024-10-10},

journal = {Remote Sensing of Environment},

author = {Baret, F. and Guyot, G.},

month = feb,

year = {1991},

pages = {161--173},

file = {ScienceDirect Snapshot:files/558/003442579190009U.html:text/html},

}

@article{kaufman_atmospherically_1992-1,

title = {Atmospherically resistant vegetation index ({ARVI}) for {EOS}-{MODIS}},

volume = {30},

issn = {1558-0644},

url = {https://ieeexplore.ieee.org/abstract/document/134076},

doi = {10.1109/36.134076},

abstract = {An atmospherically resistant vegetation index (ARVI) is proposed and developed for remote sensing of vegetation from the Earth Observing System (EOS) MODIS sensor. The same index can be used for

remote sensing from Landsat TM and the EOS-HIRIS sensor. The index takes advantage of the presence of the blue channel (0.47.+or-0.01 mu m) in the MODIS sensor, in addition to the red (0.66+or-0.025 mu m) and the near-IR (0.865+or-0.02 mu m) channels that compose the present normalized difference vegetation index (NDVI). The resistance of the ARVI to atmospheric effects (in comparison to the NDVI) is accomplished by a self-correction process for the atmospheric effect on the red channel, using the difference in the radiance between the blue and the red channels to correct the radiance in the red channel. Simulations using radiative transfer computations on arithmetic and natural surface spectra, for various atmospheric conditions, show that ARVI has a similar dynamic range to the NDVI, but is, on average, four times less sensitive to atmospheric effects than the NDVI.{\textless}{\textgreater}},

number = {2},

urldate = {2024-10-10},

journal = {IEEE Transactions on Geoscience and Remote Sensing},

author = {Kaufman, Y.J. and Tanre, D.},

month = mar,

year = {1992},

note = {Conference Name: IEEE Transactions on Geoscience and Remote Sensing},

keywords = {MODIS, Remote sensing, Atmospheric modeling, Arithmetic, Computational modeling, Dynamic range, Earth Observing System, Satellites, Sensor systems, Vegetation},

pages = {261--270},

file = {IEEE Xplore Abstract Record:files/560/134076.html:text/html},

}

@misc{pinty_gemi_1992,

title = {{GEMI}: a non-linear index to monitor global vegetation from satellites},

url = {https://link.springer.com/article/10.1007/bf00031911},

abstract = {Knowledge about the state, spatial distribution and temporal evolution of the vegetation cover is of great scientific and economic value. Satellite platforms provide a most convenient tool to observe the biosphere globally and repetitively, but the quantitative interpretation of the observations may be difficult. Reflectance measurements in the visible and near-infrared regions have been analyzed with simple but powerful indices designed to enhance the contrast between the vegetation and other surface types, however, these indices are rather sensitive to atmospheric effects. The ‘correction’ of satellite data for atmospheric effects is possible but requires large data sets on the composition of the atmosphere. Instead, we propose a new vegetation index which has been designed specifically to reduce the

relative effects of these undesirable atmospheric perturbations, while maintaining the information about the vegetation cover.},

urldate = {2024-10-10},

author = {Pinty, B. and Verstraete, M.},

year = {1992},

file = {GEMI\: a non-linear index to monitor global vegetation from satellites | Plant Ecology:files/562/bf00031911.html:text/html},

}

@article{mcnairn_mapping_1993,

title = {Mapping {Corn} {Residue} {Cover} on {Agricultural} {Fields} in {Oxford} {County}, {Ontario}, {Using} {Thematic} {Mapper}},

volume = {19},

issn = {0703-8992},

url = {https://doi.org/10.1080/07038992.1993.10874543},

doi = {10.1080/07038992.1993.10874543},

abstract = {Une image du capteur thématique, obtenue en avril 1990, a été utilisée pour mesurer le pourcentage de résidu de maïs dans des cultures situées dans le comté d'Oxford, en Ontario. Cette étude avait un double objectif: 1) établir la relation entre la réflectance spectrale et la surface occupée par les résidus de cultures de maïs; 2) élaborer et mettre à l'essai une méthode permettant de prévoir le pourcentage de recouvrement par des résidus à partir de la réflectance spectrale. Les résultats montrent qu'il existe une relation

significative entre le pourcentage de la couverture du sol par des résidus de maïs et des variables liées à la réflectance. À l'aide d'un modèle linéaire simple utilisant l'indice d'activité végétale (NDI) formé du rapport du proche infrarouge sur l'infrarouge moyen, 65 pour cent (sols sablonneux), 86 pour cent (sols argileux), 92 pour cent (sols silteux) et 78 pour cent (toutes textures de sol confondues) des pixels ont été classifiés correctement dans l'une des trois catégories de résidus de cultures de maïs (0 à 20 pour cent, 21 à 45 pour cent et {\textgreater} 45 pour cent). L'ajout d'un deuxième NDI au modèle a permis d'augmenter à 72 pour cent la précision de la classification dans le cas des sols sablonneux. Lorsqu'on a réduit à deux catégories (0 à 20 pour cent et 21 à 100 pour cent) la couverture du sol par des résidus, on a ainsi accru la précision à plus de 90 pour cent. Pour toutes les valeurs obtenues, l'indice formé du rapport du proche infrarouge sur l'infrarouge moyen n'était pas sensible à la teneur des sols en matière organique, mais dépendait de la texture des sols.},

number = {2},

urldate = {2024-10-10},

journal = {Canadian Journal of Remote Sensing},

author = {McNairn, H. and Protz, R.},

month = apr,

year = {1993},

note = {Publisher: Canadian Aeronautics and Space Institute

_eprint: https://doi.org/10.1080/07038992.1993.10874543},

pages = {152--159},
}

@article{bannari_high_1994,
title = {High spatial and spectral resolution remote sensing for the management of the urban environment},
volume = {0},
url = {https://cir.nii.ac.jp/crid/1574231874657444352},
urldate = {2024-10-10},
journal = {First Int. Airborne Remote Sensing Conference and Exhibition, Strasburg, France},
author = {Bannari, A.},
year = {1994},
pages = {247--260},
file = {High spatial and spectral resolution remote sensing for the management of the urban environment Snapshot:files/565/1574231874657444352.html:text/html},
}

@misc{plummer_angular_1994,
title = {The angular vegetation index : an atmospherically resistant index for the second along track scanning radiometer ({ATSR}-2)},
url = {https://cir.nii.ac.jp/crid/1570854174936916736},

urldate = {2024-10-10},

author = {Plummer, S.},

year = {1994},

file = {The angular vegetation index \: an atmospherically resistant index for the second along track scanning radiometer (ATSR-2) | CiNii Research:files/569/1570854174936916736.html:text/html},

}

@article{zhang_approach_1996,

title = {Approach for a {Vegetation} {Index} {Resistant} to {Atmospheric} {Effect}},

url = {https://www.jipb.net/EN/abstract/abstract23925.shtml},

abstract = {Estimation of vegetation information at the regional scales using remo...},

language = {en},

urldate = {2024-10-10},

author = {Zhang, Ren-hua and Rao, N. and Liao, K.},

year = {1996},

}

@article{nijun_derivation_2024,

title = {Derivation of tasseled cap transformation coefficients for {SDGSAT}-1 {Multispectral} {Imager} at-sensor reflectance data},

volume = {17},

issn = {1753-8947},

url = {https://doi.org/10.1080/17538947.2024.2413885},

doi = {10.1080/17538947.2024.2413885},

abstract = {The tasseled cap transformation (TCT) is a widely used technique for reducing remote sensing multispectral data into three tasseled cap (TC) components – brightness, greenness, and wetness – while retaining essential information for various applications. We derived the TCT coefficients for 7-band SDGSAT-1 Multispectral Imager data for the first time by leveraging established Sentinel-2 TCT coefficients. This was achieved through Principal Component Analysis (PCA) for dimensional reduction of SDGSAT-1 data and the Procrustes Analysis (PA) method for aligning the principal components' eigenvectors with the directions of Sentinel-2 TC components. A comparison between the new SDGSAT-1 coefficients and those of Sentinel-2 and Landsat-8 revealed a strong correlation, demonstrating similar characteristics for brightness, greenness, and wetness components. Given the established applications of TCT, the SDGSAT-1 TCT could significantly facilitate the use of SDGSAT-1 Multispectral Imager data for vegetation monitoring, water body analysis, and change detection. This study not only presents the derivation of SDGSAT-1 TCT coefficients but also highlights the effectiveness of the PA method in deriving TC wetness component coefficients that are sensitive to water bodies and vegetation, even for multispectral data lacking the moisture-sensitive shortwave-infrared (SWIR) band.},

number = {1},

urldate = {2024-10-21},

journal = {International Journal of Digital Earth},

author = {Nijun, Jiang and Changyong, Dou and Yunwei, Tang and Galdies, Charles and Yan, Lin and Haifeng, Ding},

month = dec,

year = {2024},

note = {Publisher: Taylor \& Francis _eprint: https://doi.org/10.1080/17538947.2024.2413885},

keywords = {análisis de componentes principales, Análisis de Procusto, SDGSAT-1, Transformación de gorra con borlas},

pages = {2413885},

file = {Full Text PDF:files/572/Nijun et al. - 2024 - Derivation of tasseled cap transformation coeffici.pdf:application/pdf},

}

@article{almalki_monitoring_2022,

title = {Monitoring and {Mapping} {Vegetation} {Cover} {Changes} in {Arid} and {Semi}-{Arid} {Areas} {Using} {Remote} {Sensing} {Technology}: {A} {Review}},

volume = {14},

copyright = {http://creativecommons.org/licenses/by/3.0/},

issn = {2072-4292},

shorttitle = {Monitoring and {Mapping} {Vegetation} {Cover} {Changes} in {Arid} and {Semi}-{Arid} {Areas} {Using} {Remote} {Sensing} {Technology}},

url = {https://www.mdpi.com/2072-4292/14/20/5143},

doi = {10.3390/rs14205143},

abstract = {Vegetation cover change is one of the key indicators used for monitoring environmental quality. It can accurately reflect changes in hydrology, climate, and human activities, especially in arid and semi-arid regions. The main goal of this paper is to review the remote sensing satellite sensors and the methods used for monitoring and mapping vegetation cover changes in arid and semi-arid. Arid and semi-arid lands are eco-sensitive environments with limited water resources and vegetation cover. Monitoring vegetation changes are especially important in arid and semi-arid regions due to the scarce and sensitive nature of the plant cover. Due to expected changes in vegetation cover, land productivity and biodiversity might be affected. Thus, early detection of vegetation cover changes and the assessment of their extent and severity at the local and regional scales become very important in preventing future biodiversity loss. Remote sensing data are useful for monitoring and mapping vegetation cover changes and have been used extensively for identifying, assessing, and mapping such changes in different regions. Remote sensing data, such as satellite images, can be obtained from satellite-based and aircraft-based sensors to monitor and detect vegetation cover changes. By combining remotely sensed images, e.g., from satellites and aircraft, with ground truth data, it is possible to improve the accuracy of

monitoring and mapping techniques. Additionally, satellite imagery data combined with ancillary data such as slope, elevation, aspect, water bodies, and soil characteristics can detect vegetation cover changes at the species level. Using analytical methods, the data can then be used to derive vegetation indices for mapping and monitoring vegetation.},

language = {en},

number = {20},

urldate = {2024-10-22},

journal = {Remote Sensing},

author = {Almalki, Raid and Khaki, Mehdi and Saco, Patricia M. and Rodriguez, Jose F.},

month = oct,

year = {2022},

note = {Number: 20
Publisher: Multidisciplinary Digital Publishing Institute},

keywords = {remote sensing, multispectral, arid regions, GIS, hyperspectral, vegetation cover changes},

pages = {5143},

file = {Full Text PDF:files/574/Almalki et al. - 2022 - Monitoring and Mapping Vegetation Cover Changes in.pdf:application/pdf},

}

@article{fisher_ecostress_2020,

title = {{ECOSTRESS}: {NASA}'s {Next} {Generation} {Mission} to {Measure} {Evapotranspiration} {From} the {International} {Space} {Station}},

volume = {56},

copyright = {© 2020. The Authors.},

issn = {1944-7973},

shorttitle = {{ECOSTRESS}},

url = {https://onlinelibrary.wiley.com/doi/abs/10.1029/2019WR026058},

doi = {10.1029/2019WR026058},

abstract = {The ECOsystem Spaceborne Thermal Radiometer Experiment on Space Station (ECOSTRESS) was launched to the International Space Station on 29 June 2018 by the National Aeronautics and Space Administration (NASA). The primary science focus of ECOSTRESS is centered on evapotranspiration (ET), which is produced as Level-3 (L3) latent heat flux (LE) data products. These data are generated from the Level-2 land surface temperature and emissivity product (L2_LSTE), in conjunction with ancillary surface and atmospheric data. Here, we provide the first validation (Stage 1, preliminary) of the global ECOSTRESS clear-sky ET product (L3_ET_PT-JPL, Version 6.0) against LE measurements at 82 eddy covariance sites around the world. Overall, the ECOSTRESS ET product performs well against the site measurements (clear-sky instantaneous/time of overpass: r2 = 0.88; overall bias = 8\%; normalized root-mean-square error, RMSE = 6\%). ET uncertainty was generally consistent across climate zones, biome types, and times of day (ECOSTRESS samples the diurnal cycle), though temperate sites

are overrepresented. The 70-m-high spatial resolution of ECOSTRESS improved correlations by 85\%, and RMSE by 62\%, relative to 1-km pixels. This paper serves as a reference for the ECOSTRESS L3 ET accuracy and Stage 1 validation status for subsequent science that follows using these data.},

language = {en},

number = {4},

urldate = {2024-10-22},

journal = {Water Resources Research},

author = {Fisher, Joshua B. and Lee, Brian and Purdy, Adam J. and Halverson, Gregory H. and Dohlen, Matthew B. and Cawse-Nicholson, Kerry and Wang, Audrey and Anderson, Ray G. and Aragon, Bruno and Arain, M. Altaf and Baldocchi, Dennis D. and Baker, John M. and Barral, Hélène and Bernacchi, Carl J. and Bernhofer, Christian and Biraud, Sébastien C. and Bohrer, Gil and Brunsell, Nathaniel and Cappelaere, Bernard and Castro-Contreras, Saulo and Chun, Junghwa and Conrad, Bryan J. and Cremonese, Edoardo and Demarty, Jérôme and Desai, Ankur R. and De Ligne, Anne and Foltýnová, Lenka and Goulden, Michael L. and Griffis, Timothy J. and Grünwald, Thomas and Johnson, Mark S. and Kang, Minseok and Kelbe, Dave and Kowalska, Natalia and Lim, Jong-Hwan and Maïnassara, Ibrahim and McCabe, Matthew F. and Missik, Justine E.C. and Mohanty, Binayak P. and Moore, Caitlin E. and Morillas, Laura and Morrison, Ross and Munger, J. William and Posse, Gabriela and Richardson, Andrew D. and Russell, Eric S.

and Ryu, Youngryel and Sanchez-Azofeifa, Arturo and Schmidt, Marius and Schwartz, Efrat and Sharp, Iain and Šigut, Ladislav and Tang, Yao and Hulley, Glynn and Anderson, Martha and Hain, Christopher and French, Andrew and Wood, Eric and Hook, Simon},

year = {2020},

note = {_eprint: https://onlinelibrary.wiley.com/doi/pdf/10.1029/2019WR026058},

keywords = {eddy covariance, satellite, ECOSTRESS, evapotranspiration, latent heat flux, validation},

pages = {e2019WR026058},

annote = {e2019WR026058 2019WR026058},

file = {Full Text PDF:files/579/Fisher et al. - 2020 - ECOSTRESS NASA's Next Generation Mission to Measu.pdf:application/pdf;Snapshot:files/580/2019WR026058.html:text/html},

}

@article{guzman-alvarez_uso_2022,

title = {Uso de sensores remotos en la agricultura: aplicaciones en el cultivo del banano},

copyright = {https://creativecommons.org/licenses/by-nc-nd/4.0},

issn = {2215-3608, 1021-7444},

shorttitle = {Uso de sensores remotos en la agricultura},

url = {https://revistas.ucr.ac.cr/index.php/agromeso/article/view/48279},

doi = {10.15517/am.v33i3.48279},

abstract = {Introduction. Remote sensors offer the ability to observe an object without being in contact with it. They are widely used in agricultural applications and have large development potential in banana (Musa AAA) plantations.},

language = {es},

urldate = {2024-10-22},

journal = {Agronomía Mesoamericana},

author = {Guzman-Alvarez, Jose A. and González-Zuñiga, Miguel and Sandoval Fernandez, Jorge A. and Calvo-Alvarado, Julio Cesar},

month = aug,

year = {2022},

pages = {48279},

file = {Guzman-Alvarez et al. - 2022 - Uso de sensores remotos en la agricultura aplicac.pdf:files/581/Guzman-Alvarez et al. - 2022 - Uso de sensores remotos en la agricultura aplicac.pdf:application/pdf},

}

@article{haboudane_hyperspectral_2004-1,

title = {Hyperspectral vegetation indices and novel algorithms for predicting green {LAI} of crop canopies: {Modeling} and validation in the context of precision agriculture},

volume = {90},

issn = {0034-4257},

shorttitle = {Hyperspectral vegetation indices and novel algorithms for predicting green {LAI} of crop canopies},

url = {https://www.sciencedirect.com/science/article/pii/S0034425704000264},

doi = {10.1016/j.rse.2003.12.013},

abstract = {A growing number of studies have focused on evaluating spectral indices in terms of their sensitivity to vegetation biophysical parameters, as well as to external factors affecting canopy reflectance. In this context, leaf and canopy radiative transfer models are valuable for modeling and understanding the behavior of such indices. In the present work, PROSPECT and SAILH models have been used to simulate a wide range of crop canopy reflectances in an attempt to study the sensitivity of a set of vegetation indices to green leaf area index (LAI), and to modify some of them in order to enhance their responsivity to LAI variations. The aim of the paper was to present a method for minimizing the effect of leaf chlorophyll content on the prediction of green LAI, and to develop new algorithms that adequately predict the LAI of crop canopies. Analyses based on both simulated and real hyperspectral data were carried out to compare performances of existing vegetation indices (Normalized Difference Vegetation Index [NDVI], Renormalized Difference Vegetation Index [RDVI], Modified Simple Ratio [MSR], Soil-Adjusted Vegetation Index [SAVI], Soil and Atmospherically Resistant Vegetation Index [SARVI], MSAVI, Triangular Vegetation Index [TVI],

and Modified Chlorophyll Absorption Ratio Index [MCARI]) and to design new ones (MTVI1, MCARI1, MTVI2, and MCARI2) that are both less sensitive to chlorophyll content variations and linearly related to green LAI. Thorough analyses showed that the above existing vegetation indices were either sensitive to chlorophyll concentration changes or affected by saturation at high LAI levels. Conversely, two of the spectral indices developed as a part of this study, a modified triangular vegetation index (MTVI2) and a modified chlorophyll absorption ratio index (MCARI2), proved to be the best predictors of green LAI. Related predictive algorithms were tested on CASI (Compact Airborne Spectrographic Imager) hyperspectral images and, then, validated using ground truth measurements. The latter were collected simultaneously with image acquisition for different crop types (soybean, corn, and wheat), at different growth stages, and under various fertilization treatments. Prediction power analysis of proposed algorithms based on MCARI2 and MTVI2 resulted in agreements between modeled and ground measurement of non-destructive LAI, with coefficients of determination (r2) being 0.98 for soybean, 0.89 for corn, and 0.74 for wheat. The corresponding RMSE for LAI were estimated at 0.28, 0.46, and 0.85, respectively.},

number = {3},

urldate = {2024-09-23},

journal = {Remote Sensing of Environment},

author = {Haboudane, Driss and Miller, John R and Pattey, Elizabeth and Zarco-Tejada, Pablo J and Strachan, Ian B},

month = apr,

year = {2004},

keywords = {Chlorophyll content, Hyperspectral, Green LAI, Precision agriculture, Prediction algorithms, Spectral indices},

pages = {337--352},

}

@article{matsushita_sensitivity_2007-1,

title = {Sensitivity of the {Enhanced} {Vegetation} {Index} ({EVI}) and {Normalized} {Difference} {Vegetation} {Index} ({NDVI}) to {Topographic} {Effects}: {A} {Case} {Study} in {High}-density {Cypress} {Forest}},

volume = {7},

copyright = {http://creativecommons.org/licenses/by/3.0/},

issn = {1424-8220},

shorttitle = {Sensitivity of the {Enhanced} {Vegetation} {Index} ({EVI}) and {Normalized} {Difference} {Vegetation} {Index} ({NDVI}) to {Topographic} {Effects}},

url = {https://www.mdpi.com/1424-8220/7/11/2636},

doi = {10.3390/s7112636},

abstract = {Vegetation indices play an important role in monitoring variations in vegetation.The Enhanced Vegetation Index (EVI) proposed by the MODIS Land Discipline Groupand the Normalized Difference Vegetation Index (NDVI) are both global-based vegetationindices aimed at providing consistent

spatial and temporal information regarding globalvegetation. However, many environmental factors such as atmospheric conditions and soilbackground may produce errors in these indices. The topographic effect is another veryimportant factor, especially when the indices are used in areas of rough terrain. In thispaper, we theoretically analyzed differences in the topographic effect on the EVI and theNDVI based on a non-Lambertian model and two airborne-based images acquired from amountainous area covered by high-density Japanese cypress plantation were used as a casestudy. The results indicate that the soil adjustment factor “L” in the EVI makes it moresensitive to topographic conditions than is the NDVI. Based on these results, we stronglyrecommend that the topographic effect should be removed in the reflectance data beforethe EVI was calculated—as well as from other vegetation indices that similarly include a term without a band ratio format (e.g., the PVI and SAVI)—when these indices are used in the area of rough terrain, where the topographic effect on the vegetation indices having only a band ratio format (e.g., the NDVI) can usually be ignored.},

language = {en},

number = {11},

urldate = {2024-09-10},

journal = {Sensors},

author = {Matsushita, Bunkei and Yang, Wei and Chen, Jin and Onda, Yuyichi and Qiu, Guoyu},

month = nov,

year = {2007},

note = {Number: 11

Publisher: Molecular Diversity Preservation International},

keywords = {NDVI, vegetation index, EVI, band ratio, topographic effect},

pages = {2636--2651},

}

@misc{noauthor_figure_nodate,

title = {Figure 3. {Normalized} difference vegetation index ({NDVI}) maps of the {CMA}...},

url = {https://www.researchgate.net/figure/Normalized-difference-vegetation-index-NDVI-maps-of-the-CMA-in-a-1997-b-2007-and_fig3_317801699},

abstract = {Download scientific diagram {\textbar} Normalized difference vegetation index (NDVI) maps of the CMA in (a) 1997; (b) 2007; and (c) 2017. from publication: An Urban Heat Island Study of the Colombo Metropolitan Area, Sri Lanka, Based on Landsat Data (1997–2017) {\textbar} One of the major impacts associated with unplanned rapid urban growth is the decrease of urban vegetation, which is often replaced with impervious surfaces such as buildings, parking lots, roads, and pavements. Consequently, as the percentage of impervious surfaces continues... {\textbar} Urban Heat Island,

Normalized Difference Vegetation Index and Landsat {\textbar} ResearchGate, the professional network for scientists.},

language = {en},

urldate = {2024-11-05},

journal = {ResearchGate},

file = {Snapshot:files/591/Normalized-difference-vegetation-index-NDVI-maps-of-the-CMA-in-a-1997-b-2007-and_fig3_317801699.html:text/html},

}

@article{ranagalage_urban_2017,

title = {An {Urban} {Heat} {Island} {Study} of the {Colombo} {Metropolitan} {Area}, {Sri} {Lanka}, {Based} on {Landsat} {Data} (1997–2017)},

volume = {6},

doi = {10.3390/ijgi6070189},

abstract = {One of the major impacts associated with unplanned rapid urban growth is the decrease of urban vegetation, which is often replaced with impervious surfaces such as buildings, parking lots, roads, and pavements. Consequently, as the percentage of impervious surfaces continues to increase at the expense of vegetation cover, surface urban heat island (SUHI) forms and becomes more intense. The Colombo Metropolitan Area (CMA), Sri Lanka, is one of the rapidly urbanizing metropolitan regions in South Asia. In this study, we examined the spatiotemporal variations of land surface temperature (LST)

in the CMA in the context of the SUHI phenomenon using Landsat data. More specifically, we examined the relationship of LST with the normalized difference vegetation index (NDVI) and the normalized difference built-up index (NDBI) at three time points (1997, 2007 and 2017). In addition, we also identified environmentally critical areas based on LST and NDVI. We found significant correlations of LST with NDVI (negative) and NDBI (positive) (p {\textless} 0.001) across all three time points. Most of the environmentally critical areas are located in the central business district (CBD), near the harbor, across the coastal belt, and along the main transportation network. We recommend that those identified environmentally critical areas be considered in the future urban planning and landscape development of the city. Green spaces can help improve the environmental sustainability of the CMA.},

journal = {International Journal of Geo-Information},

author = {Ranagalage, Manjula and Estoque, Ronald and Murayama, Yuji},

month = jun,

year = {2017},

pages = {17},

file = {Texto completo:files/594/Ranagalage et al. - 2017 - An Urban Heat Island Study of the Colombo Metropol.pdf:application/pdf},

}

@article{velasco_lopez_estimacion_2010,

title = {Estimación del índice de área foliar en la {Reserva} de la {Biósfera} {Mariposa} {Monarca}},

url = {https://www.scielo.org.mx/scielo.php?script=sci_arttext&pid=S0187-73802010000200010},

urldate = {2024-11-05},

author = {Velasco López, Silvia and Champo, Omar and España, Ma Luisa and Baret, Frédéric},

year = {2010},

file = {Full Text PDF:files/596/Velasco López et al. - Estimación del índice de área foliar en la Reserva.pdf:application/pdf},

}

@article{ribeiro_adjusted_2016,

title = {Adjusted {Vegetation} {Index} to {Solo} ({SAVI}): state of the art and its potential},

volume = {9},

shorttitle = {Adjusted {Vegetation} {Index} to {Solo} ({SAVI})},

doi = {10.5935/1984-2295.20160144},

abstract = {A utilização do Sensoriamento Remoto para a avaliação do meio ambiente é cada vez mais aplicado em pesquisas. As imagens adquiridas pelos sensores acoplados aos satélites fornecem dados qualitativos e quantitativos do estado da vegetação através da aplicação dos índices de

vegetação. Os índices são obtidos pela combinação matemáticas das reflectâncias dos alvos nas faixas espectrais, principalmente do vermelho e infravermelho próximo e podem ser afetados por diferentes fatores tais como reflectância, irradiancia e o brilho do solo. Um dos índices comumente utilizados, principalmente em áreas semiáridas, onde se tem influencia do brilho do solo, é o índice de vegetação ajustado ao solo (IVAS). Este índice introduz um fator de ajuste (L) ao índice de vegetação normalizada (IVDN) para minimizar os efeitos da presença do solo. Porém para cada região deve-se estudar e determinar os melhores parâmetros para o mesmo. Portanto este trabalho tem como objetivo apresentar uma revisão de literatura em relação ao índice de vegetação ajustado ao solo em diferentes biomas brasileiro e outras aplicações.

A B S T R A C T

The use of remote sensing for environmental assessment is increasingly applied in research. The images acquired by the satellite sensors coupled to provide qualitative and quantitative information on the state of the vegetation by the application of vegetation indices. The indices are obtained by mathematical combination of the reflectance of the targets in the spectral bands, especially the red and near infrared and can be affected by different factors such as reflectance, irradiance and the brightness of the soil. One of the commonly used indices, especially in semi-arid areas where it has influence of soil brightness, is the vegetation index adjusted to the ground (UAI). This

index introduces an adjustment factor (L) normalized vegetation index (NDVI) to minimize the effects of soil present. However, for each region should study and determine the best parameters for the same. Therefore this work aims to present a literature review regarding the vegetation index adjusted to the soil in different Brazilian biomes and other applications.

Keywords : Remote Sensing; vegetation index; spectral analysis, biome.},

journal = {Revista Brasileira de Geografia Física},

author = {Ribeiro, Gabrielle and Silva, João and Silva, Janaina},

month = nov,

year = {2016},

}

@article{perea-ardila_estimacion_2021,

title = {Estimación de {Biomasa} {Aérea} y {Carbono} con {Teledetección} en {Bosques} {Alto}-{Andinos} de {Boyacá}, {Colombia}. {Estudio} de caso: {Santuario} de {Fauna} y {Flora} {Iguaque}},

copyright = {Derechos de autor 2021 Revista Cartográfica},

issn = {2663-3981},

shorttitle = {Estimación de {Biomasa} {Aérea} y {Carbono} con {Teledetección} en {Bosques} {Alto}-{Andinos} de {Boyacá}, {Colombia}. {Estudio} de caso},

url = {https://revistasipgh.org/index.php/rcar/article/view/821},

doi = {10.35424/rcarto.i102.821},

abstract = {Remote sensing tools are key for monitoring of biomass and carbon in forests, which are important to climate change mitigation. Aboveground biomass and carbon of the high-land andean forests of the Santuario de Fauna y Flora Iguaque (SFFI), Boyacá, Colombia was estimated through remote sensing techniques. A total of 23 temporal sampling plots of 250 m² were established and all individuals with diameter at breast height (dbh) \> 10 cm were measured. Aboveground biomass was estimated using an allometric equation and statically correlated with vegetation indexes (NDVI, SAVI AND EVI) obtained from LANDSAT 8 OLI in the dry and rainy season (2016). Lineal models were tested to estimated biomass based on vegetation index and carbon storage was estimated. The SFFI forests stored 30 t/ha of carbon in aboveground biomass and the best-fit model was based on NDVI in the dry season (adjR2 = 0.79). Maps of biomass and carbon distribution were developed. The forests of the SSFI have removed 164 Gg CO2 from atmosphere, which can be emitted in case of no conserve them. The areas with the greatest biomass and carbon were located in the southwest and north of the SFFI. With this study, a first approximation of the pattern of carbon and biomass distribution with a resolution of 30 m was carried out. It is tested that the use of remote sending data as a fundamental input for the monitoring of carbon projects in forestry ecosystems.},

language = {es},

number = {102},

urldate = {2024-11-05},

journal = {Revista Cartográfica},

author = {Perea-Ardila, Mauricio Alejandro and Andrade-Castañeda, Hernán J. and Segura-Madrigal, Milena A.},

month = jan,

year = {2021},

note = {Number: 102},

keywords = {Ecosistemas forestales, imágenes de satélite, índices de vegetación, LANDSAT 8, monitoreo},

pages = {91--123},

file = {Full Text PDF:files/600/Perea-Ardila et al. - 2021 - Estimación de Biomasa Aérea y Carbono con Teledete.pdf:application/pdf},

}

@misc{dutta_assessing_2020,

title = {Assessing {Forest} {Health} {Using} {Geographical} {Information} {System} {Based} {Analytical} {Hierarchy} {Process}: {Evidences} from {Southern} {West} {Bengal}, {India}},

url = {https://www.researchgate.net/publication/343601253_Assessing_Forest_Health_Using_Geographical_Information_System_Based_Analytical_Hierarchy_Process_Evidences_from_Southern_West_Bengal_India?_tp=eyJjb250ZXh0Ijp7ImZpcnN0UGFnZSI6Il9kaXJlY3QiLCJwYWdlIjoiX2RpcmVjdCJ9fQ},

urldate = {2024-11-05},

author = {Dutta, Shyamal and Rehman, Sufia and Sahana, Mehebub and Sajjad, Haroon},

year = {2020},

file = {Assessing Forest Health Using Geographical Information System Based Analytical Hierarchy Process\: Evidences from Southern West Bengal, India:files/602/343601253_Assessing_Forest_Health_Using_Geographical_Information_System_Based_Analytical_Hierar.html:text/html},

}

7.3. Detalle de las longitudes de banda de sensores satelitales analizados.

Tabla A 2. Sensores satelitales, número de bandas y sus respectivas longitudes.

Sensores	Número de bandas	Longitud de banda (nm)
Landsat MSS (Servicio Geológico de Estados Unidos, 2024)	4	Banda 1: 500-600 Banda 2: 600-700 Banda 3:700-800 Banda 4:800-1100
TM Landsat (Servicio Geológico de Estados Unidos, 2024)	7	Banda 1: 450-520 Banda 2: 520-600 Banda 3: 630-690 Banda 4: 760-900 Banda 5: 1550-1750 Banda 6: 10400-12500 Banda 7: 2080-2350

Continuación tabla anterior.

ETM+ Landsat (Servicio Geológico de Estados Unidos, 2024)	8	Banda 1: 450-520 Banda 2: 520-600 Banda 3: 630-690 Banda 4: 770-900 Banda 5: 1550-1750 Banda 6: 10400-12500 Banda 7: 2090-2350 Banda 8: 5200-900
Landsat OLI (Servicio Geológico de Estados Unidos, 2024)	11	Banda 1: 430-450 Banda 2: 450-510 Banda 3: 530-590 Banda 4: 640-670 Banda 5: 850-880 Banda 6: 1570-1650 Banda 7: 2110-2290 Banda 8: 500-680 (pancromática) Banda 9: 1360-1380 Banda 10: 10600-11190 Banda 11: 11500-12510
Sentinel-1 (EOS Data Analytics, 2021a)	Banda C	Longitud onda central Banda C: 5405
Sentinel-2 (EOS Data Analytics, 2021)	13	Longitud onda central Banda 1: 443 Longitud onda central Banda 2: 490 Longitud onda central Banda 3: 560 Longitud onda central Banda 4: 665 Longitud onda central Banda 5: 705

Continuación tabla anterior.

		Longitud onda central Banda 6: 740 Longitud onda central Banda 7: 783 Longitud onda central Banda 8: 842 Longitud onda central Banda 8A: 865 Longitud onda central Banda 9: 945 Longitud onda central Banda 10: 1375 Longitud onda central Banda 11: 1610 Longitud onda central Banda 12: 2190
MODIS (NASA Earth Data, s.f.b)	36	Banda 1: 620-670 Banda 2: 841-876 Bandas 3: 459-479 Banda 4: 545-565 Banda 5: 1230-1250 Banda 6: 1628-1652 Banda 7: 2105-2155 Banda 8: 405-420 Banda 9: 438-448 Banda 10: 483-493 Banda 11: 526-536 Banda 12: 546-556 Banda 13h: 662-672 Banda 13l: 662-672 Banda 14h: 673-683 Banda 14l: 673-683 Banda 15: 473-753 Banda 16: 862-877

Continuación tabla anterior.

		Banda 17: 890-920
		Banda 18: 931-941
		Banda 19: 915-965
		Banda 20: 3660-3840
		Banda 21: 3929-3989
		Banda 22: 3929-3989
		Banda 23: 4020-4080
		Banda 24: 4433-4498
		Banda 25: 4482-4549
		Banda 26: 1360-1390
		Banda 27: 6535-6895
		Banda 28: 7175-7475
		Banda 29: 8400-8700
		Banda 30: 9580-9880
		Banda 31: 10780-11280
		Banda 32: 11770-12270
		Banda 33: 13185-13485
		Banda 34: 13485-13785
		Banda 35: 13785-14085
		Banda 36: 14085-14385
AVHRR (Emery & Camps, 2017)	5	Banda 1: 580-680
		Banda 2: 725-1100
		Banda 3: 3550-3930
		Banda 4: 10700-12500
		Banda 5: 3550-3930
IKONOS (Gillian, s.f.a)	5	Banda 1: 445-516
		Banda 2: 506-595
		Banda 3: 632-698
		Banda 4: 757-853

Continuación tabla anterior.

		Pancromática: 526-929
MERIS (The European Space Agency, s.f.a)	15	Longitud onda central Banda 1: 412.5 Longitud onda central Banda 2: 442.5 Longitud onda central Banda 3: 490 Longitud onda central Banda 4: 510 Longitud onda central Banda 5: 560 Longitud onda central Banda 6: 620 Longitud onda central Banda 7: 665 Longitud onda central Banda 8: 681.25 Longitud onda central Banda 9: 708.75 Longitud onda central Banda 10: 753.75 Longitud onda central Banda 11: 760.625 Longitud onda central Banda 12: 778.75 Longitud onda central Banda 13: 865 Longitud onda central Banda 14: 885 Longitud onda central Banda 15: 900
QuickBird (Gillian, s.f.b)	5	Banda 1: 450-520 Banda 2: 520-600 Banda 3: 630-690 Banda 4: 760-900 Pancromática: 450-900
Rapid Eye (Satellite Imaging Corporation, 2022)	5	Banda 1: 440-510 Banda 2: 520-590 Banda 3: 630-685

Continuación tabla anterior.

		Banda 4: 690-730
		Banda 5: 760-850
SPOT (The European Space Agency, s.f.b)	4	Banda 1: 500-590
		Banda 2: 610-680
		Banda 3: 790-890
		Banda 4: 1580-1750
Worldwiew-2 (The European Space Agency, s.f.c)	8	Banda 1: 400-450
		Banda 2: 450-510
		Banda 3: 510-580
		Banda 4: 585-625
		Banda 5: 630-690
		Banda 6: 705-745
		Banda 7: 770-895
		Banda 8: 860-1040
ECOSTRESS (NASA Earth Data, s.f.a)	6	Longitud onda central Banda 1: 8280
		Longitud onda central Banda 2: 8790
		Longitud onda central Banda 3: 9060
		Longitud onda central Banda 4: 10500
		Longitud onda central Banda 5: 12050
		Longitud onda central Banda 6: 1600